TECHNISCHE UNIVERSITÄT MÜNCHEN

TUM SCHOOL OF NATURAL SCIENCES

Quantum phases of low-dimensional $\mathbb{Z}_2$ lattice gauge theories

---

Umberto Borla

Vollständiger Abdruck der von der
TUM School of Natural Sciences
der Technischen Universität München
zur Erlangung des akademischen Grades eines
Doktors der Naturwissenschaften (Dr. rer. nat.)
genehmigten Dissertation.

Vorsitz.: Prof. Dr. Christian Back

Prüfer der Dissertation: 1. Prof. Dr. Sergej Moroz
2. Prof. Dr. Johannes Knolle

Die Dissertation wurde am 24.10.2022 bei der Technischen Universität München
eingereicht und durch die TUM School of Natural Sciences am 9.11.2022
angenommen.

Abstract

We study a variety of quantum many body systems characterized by local $\mathbb{Z}_2$ gauge invariance. In one spatial dimension we focus on quantum phases of single-component fermions, with particular attention to confinement of $U(1)$ symmetric matter and edge physics of a $\mathbb{Z}_2$ gauged version of Kitaev's chain. In certain strongly coupled limits these systems are described by an emergent constrained integrable model, which we study in great detail. The same model emerges as a particular integrable sector of the Ising chain in a weakly tilted field, which allows to obtain exact results about its late times dynamics by means of the generalized hydrodynamics. In two spatial dimensions we discover that the interplay between spinless fermions and $\mathbb{Z}_2$ gauge fields results in an intricate quantum phase diagram. This includes a dimerized Mott insulating state, a Dirac-deconfined phase and a regime where all the particles combine into large, slowly moving clusters. At half filling we find signatures of a novel type of quantum criticality, where confinement and translational symmetry breaking occur simultaneously. From the methodological point of view, in this thesis we develop a local mapping between $\mathbb{Z}_2$ gauge theories with matter and gauge-invariant spin $1/2$ systems. This provides new conceptual insight and significant computational advantages. The models that we study have relevant applications in the rapidly evolving field of digital and analog quantum simulation.

Kurzfassung

Wir untersuchen eine Vielzahl von Quantenvielteilchensystemen, die durch lokale $\mathbb{Z}_2$-Eichinvarianz gekennzeichnet sind. In einer Raumdimension konzentrieren wir uns auf Quantenphasen von Einkomponenten-Fermionen, mit besonderem Augenmerk auf den Einschluss von $U(1)$-symmetrischer Materie und die Randphysik einer $\mathbb{Z}_2$-geeichten Version der Kitaev-Kette. In bestimmten, stark gekoppelten Grenzfällen werden diese Systeme durch ein emergentes, beschränkt integrables Modell beschrieben, das wir sehr detailliert untersuchen. Dasselbe Modell taucht als ein besonderer integrabler Sektor der Ising-Kette in einem schwach geneigten Feld auf. Dies ermöglicht es, mit Hilfe der verallgemeinerten Hydrodynamik, exakte Ergebnisse über seine Spätzeitdynamik zu erhalten. In zwei Raumdimensionen entdecken wir, dass das Zusammenspiel zwischen spinlosen Fermionen und $\mathbb{Z}_2$-Eichfeldern zu einem komplizierten Quantenphasendiagramm führt. Dazu gehören ein dimerisierter Mott-Isolatorzustand, eine Dirac-Deconfinement Phase und ein Zustand, in dem sich alle Teilchen zu großen, sich langsam bewegenden Clustern zusammenschließen. Bei halber Füllung finden wir Anzeichen für eine neuartige Quantenkritikalität, bei der Confinement und Translationssymmetriebrechung gleichzeitig auftreten. Aus methodischer Sicht entwickeln wir in dieser Arbeit ein lokales Mapping zwischen $\mathbb{Z}_2$-Eichtheorien mit Materie und eichinvarianten Spin-1/2 Systemen. Dies bietet neue konzeptionelle Einsichten und erhebliche rechnerische Vorteile. Die von uns untersuchten Modelle haben relevante Anwendungen auf dem sich schnell entwickelnden Gebiet der digitalen und analogen Quantensimulation.

Publications

This thesis aims at providing a self-contained account of recent results in $\mathbb{Z}_2$ lattice gauge theories and related models. The original results, to which the author has contributed, are contained in peer-reviewed publications or preprints. The chapters of this thesis are not in one-to-one correspondence with the publications, but are rather divided by theme in order to follow a coherent conceptual flow. The following publications constitute the backbone of this thesis:

- **Umberto Borla**, Ruben Verressen, Fabian Grusdt, Sergej Moroz:
  "Confined phases of one-dimensional spinless fermions coupled to $\mathbb{Z}_2$ gauge theory", *Phys. Rev. Lett.*, 124(12):120503, 2020

  This work constitutes the core of section 2.2. Results concerning the Alcaraz-Bariev model are reviewed in more detail in Chapter 3, in the context of emerging constraints. The mapping between $\mathbb{Z}_2$ gauged fermions and spins in one dimension is the subject of section 5.1.

- **Umberto Borla**, Ruben Verressen, Jeet Shah, Sergej Moroz:
  "Gauging the Kitaev chain", *SciPost Physics*, 10(6):148, 2021.

  This work constitutes the core of section 2.3. Subtleties related to the aforementioned mapping are expanded upon in section 5.1.

- **Umberto Borla**, Bhilahari Jeevanesan, Frank Pollmann, Sergej Moroz:
  "Quantum phases of two-dimensional $\mathbb{Z}_2$ gauge theory coupled to single-component fermion matter ", *Phys. Rev. B* 105, 075132, 2022.

  This work constitutes the core of section 4.3. The 2d mapping between gauged fermions and spins is the subject of section 5.2.

- Alvise Bastianello, **Umberto Borla**, Sergej Moroz:
  "Fragmentation and Emergent Integrable Transport in the Weakly Tilted Ising Chain", *Phys. Rev. Lett.* 128, 196601 (2022).

  This work constitutes the core of section 3.3. Technical results concerning the hydrodynamics and thermodynamics of the constrained XXZ chain are split between section 3.1 and the Appendix. For this publication I focused almost entirely on the numerics, while Alvise Bastianello focused on integrability and GHD.

Besides the peer-reviewed publications above, the following preprints contain material which is included in this thesis:

- Aritra Das, **Umberto Borla**, Sergej Moroz:
  "Fractionalized holes in one-dimensional $\mathbb{Z}_2$ gauge theory coupled to fermion matter - deconfined dynamics and emergent integrability", arXiv:2111.13205.

  The results contained in this paper are summarized in section 2.2.4.

- Matjaž Kebrič, **Umberto Borla**, Ulrich Shollwöck, Sergej Moroz, Luca Barbiero, Fabian Grusdt:
  "Confinement Induced Frustration in a (1+1)D $\mathbb{Z}_2$ Lattice Gauge Theory", arXiv:2206.13487.

  The main results of this paper are summarized in section 2.2.6.

Contents

1 Introduction 1

1.1 Overview 1

1.2 Gauge theories: development and generalities 3

1.2.1 Gauge invariance in classical electrodynamics 3

1.2.2 Quantum electrodynamics 4

1.2.3 Non-Abelian gauge theories 5

1.2.4 Gauge theories on the lattice 6

1.3 Development of $\mathbb{Z}_2$ lattice gauge theories 7

1.3.1 $\mathbb{Z}_2$ lattice gauge theories coupled to matter fields 8

1.4 Quantum simulation of $\mathbb{Z}_2$ lattice gauge theories 10

1.4.1 Analog quantum simulation 10

1.4.2 Digital quantum simulation 11

2 $\mathbb{Z}_2$ gauge theories in one spatial dimension 13

2.1 Gauge invariance 14

2.1.1 $U(1)$ gauge fields on the lattice 14

2.1.2 Gauging fermionic parity 15

2.1.3 Gauge invariant Hamiltonians 18

2.1.4 Gauge invariant observables 18

2.1.5 Confinement 19

2.2 Fermionic matter with a global $U(1)$ symmetry 20

2.2.1 Free fermions at $h = 0$ 20

2.2.2 Confinement at finite h 21

2.2.3 The effective model at large h 23

2.2.4 Dynamics of holes: fractionalization and deconfinement 26

2.2.5 Field-theoretical perspective: Luttinger Liquid and the lattice-continuum correspondence 30

2.2.6 Models with repulsive interactions 31

2.3 Gauged Kitaev chain 34

2.3.1 The Kitaev chain 35

2.3.2 The Gauged Kitaev chain 37

2.3.3 Bulk Phase diagram 37

2.3.4 Edge physics: the Higgs phase is an SPT 39

2.3.5 Gentle gauging 42

3 Emergent integrability and extended constraints 51
3.1 The Alcaraz-Bariev model 52
3.1.1 The model 52
3.1.2 Transport in the Alcaraz-Bariev model 53
3.2 Constrained XXZ chain from $\mathbb{Z}_2$ lattice gauge theories 58
3.2.1 AB model from constrained hole dynamics at large h 59
3.2.2 Extended constraints from density-density repulsive interactions 60
3.3 Constrained XXZ chain as a limit of the tilted-field Ising model 61
3.3.1 Effective Hamiltonian from perturbation theory 62
3.3.2 Integrable transport of isolated magnons 66
3.3.3 Beyond isolated magnons 69

4 $\mathbb{Z}_2$ gauge theories in two spatial dimensions 77
4.1 Pure $\mathbb{Z}_2$ lattice gauge theories 78
4.1.1 Wegner's $\mathbb{Z}_2$ LGT and the toric code 78
4.1.2 Odd $\mathbb{Z}_2$ LGT 83
4.2 Coupling to matter fields: notable examples 85
4.2.1 Ising matter 85
4.2.2 Spinful fermionic matter 90
4.3 $\mathbb{Z}_2$ lattice gauge theory with spinless fermionic matter 93
4.3.1 Symmetries of the model 94
4.3.2 Free fermions in a static $\mathbb{Z}_2$ gauge field at $h \to 0$ 97
4.3.3 Quantum dimers at $h \to \infty$ 101
4.3.4 Half filling phase diagram and exotic quantum criticality 107

5 $\mathbb{Z}_2$ gauge theories with spinless fermionic matter as spin $1/2$ systems 111
5.1 The mapping in one dimension 112
5.1.1 Gauge invariant spins 112
5.1.2 Mapping of Hamiltonians 113
5.1.3 Notable examples 114
5.1.4 Constrained Hilbert space and emergent PXP model 117
5.1.5 Mapping of Ising matter 118
5.2 The mapping in two dimensions 121
5.2.1 Gauge invariant spins 122
5.2.2 Mapping of Hamiltonians 122
5.2.3 Mapping of observables 127

6 Conclusions and outlook 133

Appendix 137
A Numerical Methods 137
A.1 DMRG 137
A.2 TEBD 139
A.3 Exact Diagonalization 140
B Luttinger liquids 140
C Details on integrability results and generalized hydrodynamics 141
C.1 Summary of XXZ thermodynamics 141

- C.2 The AB model as the XXZ chain in reduced volume 143
- C.3 Thermal states in the presence of an external magnetic field . . 144

D Free fermions on an infinite cylinder in a π flux. 145

Chapter 1

Introduction

1.1 Overview

This thesis revolves for the most part around a specific type of many-body quantum systems, namely $\mathbb{Z}_2$ lattice gauge theories[1] (LGT) in one and two spatial dimensions. Depending on their background, the reader might find the subject somewhat mundane at first sight. Why even consider the $\mathbb{Z}_2$ group, when our universe is understood in terms of the intricate non-abelian gauge groups that underlie the Standard Model of particle physics? To our luck, years of research revealed that models with $\mathbb{Z}_2$ gauge symmetry are far from trivial, and can be of interest to a very broad audience. To the high energy physicist elementary examples of gauge theories -with simpler gauge groups or in lower dimensions- can provide useful insight into mechanisms of confinement, that resemble the phenomenology of quantum chromodynamics (QCD). From the condensed matter physicist point of view these models find applications in the theory of high-T_c superconductors and, more in general, in the description of fractionalized phases of matter where the $\mathbb{Z}_2$ gauge redundancy can be attributed to the splitting of the constituents into partons that behave independently. More recently, $\mathbb{Z}_2$ LGT emerged as paradigmatic examples of systems exhibiting quantum topological order, a discovery that deeply influenced our way of classifying quantum phases of matter. In this context, they emerge naturally as a description of the low-energy properties of gapped $\mathbb{Z}_2$ spin liquids. Together with a number of exotic phenomena that characterize strongly-correlated quantum systems, topological order is manifestation of *emergence* [1]. This fascinating concept is the statement that the behavior of a large number of interacting particles[2] cannot be traced back in any meaningful way to the constituents, but rather exhibits entirely new phenomenology that arises from their interplay. Popular examples of this principle are Bose-Einstein condensates, superfluids/superconductors and the fractional quantum Hall effect.

Another connection to a thriving area of research is given by the emergence of quantum integrable models as limits of one dimensional $\mathbb{Z}_2$ lattice gauge theories. This allows to extract an unexpected amount of exact results and apply powerful analytical tools to obtain physically relevant information about quantum dynamics. The modern understanding of many-body systems relies heavily on their rich entanglement structure. Indeed, a now ubiquitous perspective that originates form quantum information theory aims at representing quantum states as tensor networks (TN), i.e. graphs of tensors that encode symmetries and local degrees of freedom. Besides its conceptual relevance this representation proved to be an exceptional computational tool, and it is at the heart of many numerical algorithms which enormously increased our ability to tackle many-body systems. Even in this context, $\mathbb{Z}_2$ lattice gauge theories are in the spotlight. Due to their discrete nature and small local Hilbert space, they are natural candidates to test theoretical and numerical advances of tensor network based techniques. While in this thesis details about numerical methods are relegated to the appendix, many of the results that we present would not be possible without the tremendous progress made by the community in the recent years.

---

[1] These are often referred to as Ising lattice gauge theories in the literature, for reasons that will soon become apparent.

[2] Of the order of the Avogadro number $N_A \approx 6 \cdot 10^{23}$.

Having conveyed to the reader the theoretical importance of such models, we now turn to their experimental realizations. At the present time a considerable effort is directed towards the analog simulation of condensed matter systems. This has rapidly evolved into an extremely rich experimental field, which employs a wide array of ingenious methods to reproduce specific interacting quantum systems in the controlled environment of a laboratory. The most successful implementations involve ultracold atoms in optical lattices, trapped ions or Rydberg atoms. While quantum simulation is by no means limited to LGT, one of its most ambitious goals is to simulate gauge theories which are relevant to the Standard Model of particle physics. Such goal can only be achieved step by step, and a successful implementation of $\mathbb{Z}_2$ lattice gauge theories in more than one dimension can constitute a significant breakthrough.

A bird's-eye view of this thesis

The rest of this introductory chapter aims at giving the reader some necessary background information, so that our results can be understood under a more general perspective. We first provide some relevant historical information, starting with how gauge theories developed in the context of fundamental interactions and then focusing on their condensed matter applications. Chapter 2 is dedicated to one-dimensional $\mathbb{Z}_2$ lattice gauge theories, and it includes an introduction to the most relevant technical aspects. Chapter 3 can be seen as a slight detour from the main theme of the thesis, since it focuses on a particular integrable model, a constrained version of the celebrated XXZ chain. This model plays a prominent role in our research, since it emerges in certain limits of $\mathbb{Z}_2$ lattice gauge theories but also as an integrable sector of the Ising chain in a tilted field. In Chapter 4 we move on to two dimensions. Here we introduce some of the most relevant models in the literature, including Franz Wegner's pure $\mathbb{Z}_2$ LGT and systems where the $\mathbb{Z}_2$ gauge fields mediate interactions between (hardcore) bosonic and fermionic matter fields. In the last section of the chapter, we give an account of our original results and unveil the intricate phase diagram of a model which was unexplored until now. To conclude, Chapter 5 is dedicated to a powerful and fascinating analytical tool, i.e. the duality between $\mathbb{Z}_2$ LGT and spin 1/2 systems. We provide details on such mapping, and highlight its usefulness in a number of contexts.

1.2 Gauge theories: development and generalities

It is safe to say that gauge theories are a cornerstone in our understanding of Nature. The Standard Model of particle physics, which describes to unprecedented accuracy the electromagnetic, weak and strong interactions, is the prime example of gauge theory [2–4]. Local gauge invariance appears, in a different guise, in Einstein's theory of gravity, the General Relativity [5]. It is therefore no surprise that the concept plays a key role in the frontiers of research, which try to combine what we know about phenomena that occur on infinitely small and infinitely large length scales. Such "theories of everything" include String Theory [6] and Loop Quantum Gravity [7]. While gauge theories can be regarded as the undisputed protagonists of 20th century physics, they roots are even older and can be traced back already to Maxwell's equations.

1.2.1 Gauge invariance in classical electrodynamics

The first instance of gauge invariance appeared historically in the context of classical electrodynamics [8]. It follows from this observation: the equations expressing the electric and magnetic fields in terms of potentials,

$$\mathbf{E} = -\nabla\phi - \frac{\partial \mathbf{A}}{\partial t} \qquad \mathbf{B} = \nabla \times \mathbf{A}, \tag{1.1}$$

are invariant under the *local* transformation

$$\mathbf{A} \to \mathbf{A} + \nabla f \qquad \phi \to \phi - \frac{\partial f}{\partial t} \tag{1.2}$$

where f is an arbitrary scalar function of coordinates and time (hence the local character of the transformation). In the four-dimensional Lorentz invariant notation, where the scalar and vector potentials are combined into a four-vector $A^\mu = (\phi, \mathbf{A})$, this reads $A_\mu \to A_\mu + \partial_\mu f$, i.e. the electromagnetic potential is defined up to a total divergence.

Understandably, at this stage it is hard to see gauge invariance as something more than a mathematical curiosity characterizing the solutions of Maxwell's equations. Indeed, it took a long time to appreciate how this innocuous transformation provides an extremely powerful guiding principle in the formulation of the most successful theories of fundamental interactions. A first application of this principle in a broader context was made by Hermann Weyl, in an unsuccessful attempt to unify electromagnetism with gravity [9].[3] The picture started to become clearer in the context of Lagrangian field theory, where symmetries are operations that leave the action of the system invariant. Since the subsequent quantum theories rely on this approach, let us quickly review it in its classical version.[4] The electric and magnetic fields can be combined into the rank two antisymmetric space-time tensor

---

[3] This is also where the expression *gauge* is first used.

$$F_{\mu\nu} = \partial_\mu A_\nu - \partial_\nu A_\mu \tag{1.3}$$

whose components correspond to different spatial components of $\mathbf{E}$ and $\mathbf{B}$.[5] The Lagrangian for the pure Maxwell theory (without any sources) reads

$$\mathcal{L}_{EM} = -\frac{1}{4} F_{\mu\nu} F^{\mu\nu} = \frac{\mathbf{E}^2 - \mathbf{B}^2}{2}. \tag{1.4}$$

From this, the celebrated Maxwell's equations can be derived using the principle of least action. The gauge invariance of $\mathcal{L}_{EM}$ follows from the manifest gauge invariance of (1.3). A crucial point is to be made here. While it is perfectly possible to express $\mathcal{L}_{EM}$ in terms of the *physical* fields $\mathbf{E}$ and $\mathbf{B}$, we choose to give more importance to the most elegant and compact description in terms of the potential A_μ, which we refer to as a *gauge* field. While here this choice appears to be merely aesthetic, it turns out that A^μ is the object that naturally couples to matter fields[6] and it is in this sense to be preferred. This has deep implications: the "best" description of Nature we can think of is not directly in terms of the electric and magnetic fields that we experience everyday, but rather of the unphysical object A_μ. But gauge field configurations related by the transformations (1.2) are physically equivalent: in exchange for formal simplicity, we have accepted to describe our universe with redundant degrees of freedom.

1.2.2 Quantum electrodynamics

The advent of quantum physics brought up the revolutionary idea that particles can sometimes have wave-like character and vice-versa. For instance, by zooming in sufficiently, one will see that electromagnetic radiation is constituted by elementary quanta, the photons. Indeed, the modern understanding is that all elementary forces are mediated by bosonic particles which are quanta of the corresponding gauge fields. These are the photons for electromagnetism, the $W^\pm$ and Z bosons for the weak interactions and gluons for the strong interactions [2, 4].[7] How to fit the wave-particle duality of quantum mechanics into the relativistic setup that electromagnetism entails was however far from clear. After considerable efforts it was understood how to correctly quantize free photons and electrons [10], but a theory describing the interactions between light and matter was still plagued by serious theoretical problems. While systematic methods were developed [11] to "canonically" quantize Lagrangian theories by going through the Hamiltonian formalism first, the resulting models did not seem to make physical sense. In particular, they returned divergent results for many relevant observables such as scattering amplitudes. This so called “problem of infinities” was resolved (and just partially understood) only later, with the development of a perturbative scheme able to handle the aforementioned divergences [12–15].

---

[4] The following review is by no means exhaustive, and serves the sole purpose of making the historical discussion less abstract. In particular we will be very cavalier when it comes to prefactors and indexes. The reader should refer to the cited literature for details.

[5] One can easily verify this by using equations (1.1). For instance $F_{tx} = \partial_t A_x - \partial_x \phi = E_x$.

[6] For instance, the coupling to a classical current j^μ takes the form $\delta\mathcal{L} = A_\mu j^\mu$.

[7] Matter fields, on the other hand are all described by fermionic fields. These are the leptons and quarks.

The modern, textbook approach is to introduce quantum electrodynamics (QED) as the quantum field theory described by the Lagrangian [2, 3]

$$\mathcal{L}_{QED} = -\frac{1}{4}F^{\mu\nu}F_{\mu\nu} + \bar{\psi}\left(i\gamma^{\mu}\partial_{\mu} - \gamma^{\mu}A_{\mu} - m\right)\psi \tag{1.5}$$

where ψ is a spinor field representing fermionic matter (electrons), m is the mass of the electron and γ a set of Dirac matrices. We can recognize in it terms for the free photons and electrons, i.e. the Maxwell and Dirac Lagrangians. As anticipated, interactions are described by the coupling of the fermionic current $j^{\mu} = \bar{\psi}\gamma^{\mu}\psi$ to the gauge field A_{μ}. If we insist on maintaining the gauge invariance of the model, we must specify how a local gauge transformation acts on the matter fields. It can be verified that the Lagrangian (1.5) is invariant under

$$A_{\mu} \to A_{\mu} + \partial_{\mu}f(x), \qquad\qquad \psi \to e^{if(x)}\psi, \tag{1.6}$$

i.e. a *local* change in the phase of the matter fields does not affect the physics. This brings up a different, fascinating way of interpreting gauge transformations. The original theory describing free fermions[8] enjoys a *global* $U(1)$ symmetry, corresponding to the conservation of total particle number.[9] In QED this global symmetry is “promoted” to a local one, and this can only be done by coupling it to new degrees of freedom - the gauge fields.[10] This is precisely the guiding principle that inspired the development of non-Abelian gauge theories. It is however far from clear why Nature behaves this way. So far, nobody has been able come up with a good physical reason why the fundamental equations ruling our universe should be invariant under specific local transformations. Before moving to the next section, let us make one more observation. A fundamental requirement for a sensible theory of electrodynamics is that it must predict the masslessness of photons, which is tested experimentally to great accuracy. A mass term for the photon would take the form $m_p^2 A^{\mu}A_{\mu}$, and it is not forbidden by general principles[11] unless we also introduce gauge invariance as a requirement.

1.2.3 Non-Abelian gauge theories

Given the spectacular success of QED in describing electromagnetic interactions at the quantum level, it is no surprise that gauge theories were natural candidates for capturing the remaining fundamental interactions. While conceptually similar, gauge theories with non-Abelian gauge groups pose significant mathematical challenges. Their structure was clarified by Yang and Mills in 1954 [17], who paved the way for the Standard Model as we know it today. The path in this direction was however far from linear. As a first obstacle, it was long known that the weak interaction must be mediated by massive particles[12], while the gauge fields of Yang-Mills theories are necessarily massless -for the same reasons outlined above in the context of QED. The solution to this conundrum came by adapting the concept of spontaneous symmetry breaking (SSB) to gauge theories. While models with global continuous symmetries can exhibit proper spontaneous symmetry breaking, which leads to massless Goldstone bosons in the spectrum of the theories, this cannot happen in gauge theories. However, if an additional scalar (Higgs) field is present, SSB in this sector of the model can result in the absence of Goldstone bosons and in the gauge fields acquiring a mass instead [18–21]. This phenomenon, known as the Higgs mechanism, finds applications well outside the realm of high energy physics and it is used -most notably- to explain superconductivity.[13] Yang-Mills theories, on the other hand, provided a natural solution to the problem of asymptotic freedom of the strong interactions, i.e. the fact that the strong interaction between quarks actually becomes weak at large enough energies [22, 23]. After the smoke cleared up, a surprisingly elegant description emerged. The electromagnetic and weak interactions are combined into a model with gauge group $U(1) \times SU(2)$, the electroweak theory. The strong interaction is captured by quantum chromodynamics, an $SU(3)$ gauge theory. These models, together with the Higgs field that gives mass to the W and Z bosons of the weak interactions, form the Standard Model of particle physics.

---

[8] We can also include density-density interactions between fermions.

[9] This is a consequence of Noether’s theorem [16], which we will not review here.

[10] In section 2.1.1 we will see how this works concretely, by applying these ideas to the simple case of 1d QED on the lattice.

[11] These general principles are Lorentz invariance and renormalizability.

1.2.4 Gauge theories on the lattice

This thesis deals for the most part with gauge theories which are defined on a lattice. While this approach is to some extent natural when dealing with condensed matter applications where a real lattice exists, the same is not true for the models describing the fundamental interactions. To the best of our knowledge, the spacetime in which we live is not discretized and a lattice is only introduced for computational purposes. In the '70s the Standard Model was laid out and has not evolved significantly since then. While the theory gave fantastic agreement with experiments whenever perturbative results were available, little was known about the strongly coupled regime where -for instance- quarks are confined into mesons and baryons. In was in this context that the lattice approach was developed, first as a tool to perform systematically some analytical calculations and then as a powerful computational method [24, 25]. Indeed, since in LGT the models are naturally regularized by discretizing the path integral, they are extremely suitable for numerical simulations. The ability to run such calculations improved immensely with the development of quantum Monte Carlo algorithms, that exploit the formal analogy between path integrals and partition functions to evaluate observables through random sampling.

---

[12] Vector bosons, in the gauge theory language.

[13] The subject of spontaneous symmetry breaking in the context of superconductivity is a subtle one. The first theories of superconductivity did not emphasize this point of view, and even now it is often explained in terms of SSB of a global $U(1)$ symmetry leading to a Landau order parameter.

The success of these methods is testified for instance by precise computation of masses of mesons and baryons, but several challenges remain unsolved [26, 27]. In general, discretization of spacetime -which makes the number of degrees of freedom finite- is a necessary step for most numerical methods, including exact diagonalization and tensor networks. Lattice gauge theories are a complex subject that presents many subtleties that are beyond the scopes of this thesis. Among other things meaningful comparison with high-energy physics experiments requires taking the continuum limit, which involves a complicated renormalization group analysis. Besides, the choice of fermionic matter fields brings up the notorious problem of fermion doubling, that occurs when putting chiral fermions on the lattice [28, 29]. Workarounds are required if one is interested in recovering the Dirac equation in the continuum, as it is the case for example in the study of the lattice Schwinger model. This is usually achieved by the "staggered fermions" method [24],[14], although alternative approaches exists [27]. To our luck, none of this is necessary from our perspective. The models that we study are mostly motivated by condensed matter applications where the lattice formulation, and not its continuum limit, is regarded as fundamental.

1.3 Development of $\mathbb{Z}_2$ lattice gauge theories

While lattice gauge theories rose to prominence in the mid-'70s, the model which is most relevant to our purposes was discovered already in 1971 by Franz Wegner [30] in a context which had little to do with high-energy physics. In the attempt of generalizing the self-duality of the classical 2d Ising model to three dimensions, Wegner realized that the dual model exhibited invariance under a set of *local* transformations. While he did not use the term "gauge theory", what he discovered is exactly the $\mathbb{Z}_2$ model that lays the foundations of this thesis. Although the $\mathbb{Z}_2$ lattice gauge theory was initially deemed too elementary to be of broader interest, it turned out to be relevant for an unexpected reason. A cornerstone in the understanding of continuous (i.e. second order) phase transitions is Landau's theory [31]. According to this paradigm, such transitions are characterized by the spontaneous breaking of some symmetry, which leads to the non-zero expectation value of a *local* order parameter in the ordered phase [32–34]. Examples of systems which are accurately described in this way are ferromagnets and superfluids. Wegner's $\mathbb{Z}_2$ gauge theory, on the other hand, escapes this classification and exhibits a continuous confinement transition between weakly and strongly coupled regimes that is not characterized by a local order parameter. While this important fact went under the radar for quite some time, it is now regarded as a fundamental example of topological phase transition. Topology-related phenomena are now ubiquitous in many-body physics, and the term "topological" itself is used at the present time to refer to a number of distinct concepts. In this specific example, the deconfined phase of Wegner's $\mathbb{Z}_2$ lattice gauge theory is said to exhibit *topological*

---

[14] This amounts to introducing a mass term with alternating sign, and regarding particles (antiparticles) as living on even (odd sites) of the chain. The models that we study can be easily adapted to this approach, but the results and their interpretation may differ substantially.

order [35]. This feature manifests itself in a degeneracy of the ground state on manifolds with non-trivial topology (e.g. on a torus) and in the presence of fractionalized anyonic excitations [33, 36]. In modern times, the list of systems exhibiting quantum topological order has grown substantially and includes Kitaev's toric code [37] and several examples of quantum spin liquids [36, 38].

1.3.1 $\mathbb{Z}_2$ lattice gauge theories coupled to matter fields

As just discussed, the pure[15] $\mathbb{Z}_2$ LGT is relevant on its own. However, as expected, even richer phenomenology emerges when the model is coupled to matter fields. Unsurprisingly, the first notable results in this direction came from the high-energy community. The surge of interest in gauge theories defined on a lattice resulted in a systematic study of different models. In a seminal paper Fradkin and Shenker investigated in great generality lattice gauge theories with scalar Higgs matter [39]. Their results included a variety gauge group and representations of the matter fields, and covered generic spacetime dimensions, including the $\mathbb{Z}_2$ model in $d = 2$ which is relevant for us.[16] In this case, a Higgs field transforming in the fundamental representation of the gauge group[17] is nothing but a two-state bosonic field, i.e. an Ising spin. Since the results contained in this paper are of fundamental importance to the field, we review them in detail in Section 4.2.1 of this thesis. Despite these early success, extensions including fermionic matter fields were not pursued for a long period of time. On the one hand, from the numerical point of view, the presence of fermionic fields was problematic for the quantum Monte Carlo algorithms which were plagued by the infamous sign problem. On the other hand, such models did not yet have an application in condensed matter theory and the interest of high-energy physicists was concentrated elsewhere. This changed drastically in the '90s, when the struggle to explain exotic phenomena such as high-T_c superconductivity [40, 41] paved the way to the exploration of new theoretical models. In particular, $\mathbb{Z}_2$ gauge invariance showed up naturally in the description of deconfined excitations carrying fractional quantum numbers. This can be understood in the following way: we can indeed imagine splitting a fermionic operator $f_s^\dagger$ into two separate parts

$$f_s^\dagger = b_s^\dagger \, c^\dagger, \tag{1.7}$$

where $b_s^\dagger$ creates a neutral boson with spin 1/2 while $c^\dagger$ creates a spinless fermion with unit charge.[18] This approach explains why gauge theories emerge naturally in this context. In Eq. 1.7 one can *locally* change the sign of both $b^\dagger$ and $c^\dagger$ simultaneously without affecting the physical f-fermions. In certain contexts the electrons are believed to fractionalize, in the sense that spin and charge degrees of freedom behave independently. Since a theory for the charge degrees of freedom only should inherit the local sign flip invariance from the parent model, it must take the form of a gauge theory. In 1999, Senthil and Fisher published a paper showing how one such model captures the transition between an antiferromagnetic Mott insulator and a conventional d-wave superconductor [42]. It was also shown that similar models can be used to describe a number of exotic superconducting and insulating phases.

---

[15] We will use the term "pure" to refer to a gauge theory not coupled to matter fields throughout this thesis.

[16] Throughout this thesis, we use d to denote the number of spatial dimensions. The spacetime dimension is $D = d + 1$.

[17] Which for the group $\mathbb{Z}_2$ is the only representation.

[18] This also serves as a possible justification to investigate systems with spinless fermions, which become the relevant low energy degrees of freedom when the b-particles are gapped out. Note that the splitting (1.7) is a choice, since the fermionic statistics can be attributed to either particle.

Not long after, the already exciting classification of unconventional phases of matter was further enriched by the introduction of new ideas. The exotic phase diagram of the pure $\mathbb{Z}_2$ gauge theory forced a paradigm shift in the community, and brought concepts such as topological order and anyonic excitations into the game. The so-called orthogonal fermions, forming a fractionalized non-Fermi liquid, provided another example of dynamical $\mathbb{Z}_2$ gauge fields coupled to fermionic and Ising matter [43]. Substantial progress in our understanding of the quantum phase diagram of a Fermi sea of spin 1/2 fermions interacting with dynamical $\mathbb{Z}_2$ gauge fields has been achieved by Gazit and collaborators thanks to sign-problem free determinant quantum Monte Carlo studies [44–46]. Much like Fradkin and Shenker's, this work was of great inspiration for the research behind this thesis, and is therefore reviewed in some detail in Section 4.2.2. In addition, in the absence of a confining electric term, the interpolation between the gauged and ungauged versions of this fermionic model has been studied recently in [47].[19] The phase diagram of the $\mathbb{Z}_2$ gauge theory interacting with gapless fermions, where the Gauss law constraint is not imposed but emerges dynamically, was mapped out in [48]. Other works include the study of exactly solvable deformations of the two-dimensional Ising gauge theory coupled to fermions [49, 50], spinless fermion matter interacting with dynamical $\mathbb{Z}_2$ gauge fields on a cross-linked Creutz-Ising ladder [51], and isolated visons in a Fermi sea of $\mathbb{Z}_2$-charged anyons [52]. Even more recent publications include [53] and [54].

The discussion so far has focused on $\mathbb{Z}_2$ LGTs in two spatial dimensions. Historically, this is not a coincidence. While one-dimensional models with continuous gauge groups -such as the celebrated Schwinger model (QED_2)- were studied by the high-energy community since the beginning [55–66], $\mathbb{Z}_2$ gauge theories were regarded as too trivial to be of interest, even from a purely theoretical point of view.[20] At the same time the physics of one-dimensional systems, such as the spin chains which are so popular in the condensed matter community, was generally well understood in terms of the Luttinger liquid paradigm [34, 67]. For this reason, there was little need to resort to $\mathbb{Z}_2$ LGTs to explain phenomena of the real world. This point of view has changed in the recent years. Somewhat curiously, while from the high-energy physics perspective 1d LGTs are usually studied as toy models of confinement, their interest for the condensed matter community is mostly related to the deconfined phase [68–71]. On one side, some developments in the classification of quantum phases of matter brought $\mathbb{Z}_2$ gauge theories into play, showing for instance how they fit into an intricate web of dualities [72, 73] or emerge at deconfined quantum critical points [74]. Then, $\mathbb{Z}_2$ gauged model turned out to be a fertile playground for some new ideas in quantum dynamics, such as disorder-free localization [75] and quantum scars [76–83]. Related to this, quantum integrable models are found to emerge as particular limits of $\mathbb{Z}_2$ lattice gauge theories, creating an unexpected bridge between two apparently distant communities [70, 84]. Last but not least, the rising interest in low dimensional models is now motivated by experimental efforts in the field of quantum simulation. We will have a glimpse at this vast area of research in the following section.

---

[19] This is partially analogous to the investigation that we present in section 2.3.5, where we interpolate between gauged and ungauged Kitaev chains.

[20] One of the reasons is that in 1d the Gauss law can be used to eliminate the gauge degrees of freedom, at the price of introducing non-local interactions between matter fields. An example of this is given in section 2.2.5.

1.4 Quantum simulation of $\mathbb{Z}_2$ lattice gauge theories

As we just saw, historically the interest in $\mathbb{Z}_2$ lattice gauge theories coupled to matter fields was mainly motivated by the investigation of fractionalized phases of matter. In the recent years, however, a new surge of interest came from an entirely different direction: quantum simulation [85–91]. Indeed, a remarkable effort is being made to realize simple condensed matter models -including gauge theories- in a number of different experimental platforms using quantum technologies. An ultimate goal of such simulations is to realize in a controlled environment the gauge theories which are most relevant to our understanding of the universe, such as the Standard Model itself. Considerable technical challenges, however, make it desirable to start from the simplest scenarios. This is where $\mathbb{Z}_2$ lattice gauge theories in low dimensions come into play. Despite the inevitable simplifications implied by the use of the simplest discrete gauge group, such models offer valuable insight into phenomena such as confinement and fractionalization. Quantum simulation schemes can be divided in two big families: analog and digital. Below, we give a brief account of both approaches.

1.4.1 Analog quantum simulation

The idea that underlies analog quantum simulation is to map the Hamiltonian of the physical system that one wants to investigate to a “simulator Hamiltonian”. The latter describes a real quantum system that is implemented in the lab using one of many schemes and whose parameters are to some extent controllable. An analog quantum simulator is a dedicated device, in the sense that it is built with the idea to simulate a specific quantum system. The most popular platform for analog quantum simulation are ultracold atoms in optical lattices [92, 93]. Optical lattices are spatially periodic structures created by the interference of laser beams. The maxima and minima of the potential can be used to trap neutral atoms exploiting the Stark effect, while tunneling and interactions between different sites are achieved in a problem-dependent manner. Recent advances in laser technology and quantum gas microscopy allowed significant progress in the field, which resulted for instance in the successful simulation of the Bose-Hubbard [94, 95] and Hofstadter [96] models. While simulation of gauge theories -as opposed to e.g. spin systems- is harder to achieve due to the additional degrees of freedom and interactions, significant progress has been made [86, 97–99]. For instance, pioneering experimental work [100] has led to the first simulation of string breaking in the Schwinger model [55]. Particularly relevant to the subject of this thesis is the proposal of a Floquet implementation for $\mathbb{Z}_2$ lattice gauge theories coupled to dynamical matter [101–103]. Proof of principle experiments on a two component mixture of ultracold atoms, simulating two hardcore bosons interacting through a $\mathbb{Z}_2$ gauge field, have been performed [101]. Combining several of these structures allows to simulate $\mathbb{Z}_2$ gauge theories on 1d chains or ladders, although control of the parameters and the implementation of a plaquette term remains a challenge. This field of research in in constant evolution, with proposals of new simulation schemes and models to implement [102, 104, 105], and serves as an additional motivation to our research.

1.4.2 Digital quantum simulation

Digital quantum simulation [106], on the other hand, consists in the simulation of a system (for instance of its quantum dynamics) on a potentially universal quantum computer. The latter is a machine that is capable of applying a certain set of quantum gates[21] to an arbitrary initial quantum state. For concreteness, one can think of the initial state as a certain quantum state of a spin system[22]. Then, in a typical digital quantum simulation, the machine modifies this state by applying a sequence of local unitary operators. This corresponds usually, but not exclusively, to a “discrete” time evolution governed by some Hamiltonian.[23] While current experimental efforts are limited by the small number of effective qubits that even the most advanced quantum computers can sport, improvements are expected in the near future. Research connected to the $\mathbb{Z}_2$ gauge theories which are relevant for us is presented for example in [107–112].

---

[21] I.e. -for our purposes- one or two sites unitary operators.

[22] This is especially natural, since spins are the simplest example of qubits.

[23] The Hamiltonian evolution reads $|\psi(t)\rangle = e^{iHt}|\psi(0)\rangle$, and so the time evolution operator is generally non-local. A procedure known as “Trotterization”, however, approximates it with a product of local operators.

Chapter 2

$\mathbb{Z}_2$ gauge theories in one spatial dimension

This chapter is devoted to $\mathbb{Z}_2$ lattice gauge theories in $1+1$ dimensions. Unlike their two dimensional counterparts, in the absence of coupling to matter fields a pure $\mathbb{Z}_2$ lattice gauge theory on the line can only be trivial, due to the absence of a local Wilson loop.[1] For this reason, we immediately jump to the formulation of models where the gauge fields mediate interactions between particles, similarly to the vector bosons of the Standard Model. Since the original results of this thesis mostly concern theories with spinless fermionic matter, this will be the natural choice throughout the discussion. While in relativistic quantum field theories fermions are forced to have half-integer spin as a consequence of the spin-statistics theorem [2], this is not the case in the non-relativistic framework typical of condensed matter physics.[2] In particular, in one dimension spinless fermions are a ubiquitous computational tool due to the Jordan-Wigner transformation, but also arise physically in contexts where the charge and spin degrees of freedom separate and the latter are gapped out. A recurrent theme of our research work is the duality between $\mathbb{Z}_2$ lattice gauge theories coupled to spinless fermions and spin 1/2 systems. As a matter of fact, this is so ubiquitous that we decided to devote chapter 5 entirely to an in-depth analysis of the subject. While in the original papers [70, 113–116], the two formulations are intertwined, in the present chapter we stick to the gauge-theory perspective exclusively. This serves a dual purpose: on the one hand it gives the reader a unified picture of our research, while on the other hand it offers a slightly different take on the subject compared to the papers to which we refer.

---

[1] This is also true for electrodynamics, and it corresponds to the known fact that there is no magnetic field in one dimension. On the circle, a non-local Wilson loop can be defined, and it measures the magnetic flux threading it.

[2] To our purpose, the statistics in encoded in the canonical anticommutation relations while the (non-relativistic) spin is simply an internal degree of freedom. The two concepts are entirely independent.

Structure

This chapter is structured as follows: in section 2.1 we introduce gauge fields in the familiar context of electrodynamics using the Hamiltonian formalism, and then we specialize to the $\mathbb{Z}_2$ case. We omit general aspects that are already discussed in the introduction to focus on the details that are more relevant to our scopes. After introducing some key concepts, we move to a discussion of original research. This includes in particular the comprehensive study of two specific models. Section 2.2 is dedicated to hopping fermions with a global $U(1)$ symmetry coupled to $\mathbb{Z}_2$ gauge fields, and includes detailed discussions of perturbative results, field theoretical subtleties and the inclusion of repulsive interactions. In section 2.3, on the other hand, we study a model that includes a pairing term and can be seen as a $\mathbb{Z}_2$ gauged version of the Kitaev chain. In this case, the original results concern the presence of a topologically non-trivial phase of matter that -similarly to the regular Kitaev chain- manifests itself in the presence of edge modes.

2.1 Gauge invariance

As argued in the introduction, one way of understanding gauge theories is that they can be obtained by taking a model which exhibits a global symmetry and promoting such symmetry to a local one. Here we will see how this works in the concrete case of 1d electrodynamics on the lattice, and then we will focus on $\mathbb{Z}_2$ gauge fields by restricting the $U(1)$ symmetry to its parity subgroup.

2.1.1 $U(1)$ gauge fields on the lattice

We consider spinless fermionic matter, although the principles outlined below are easily generalized to spinful or bosonic fields. Fermions live on the sites of a chain and, in the simplest scenario, can hop from one site to the other following a tight binding model described by the quantum Hamiltonian

$$H_{TB} = -t \sum_i \left(\hat{c}_i^\dagger \hat{c}_{i+1} + h.c \right) - \mu \sum_i \hat{c}_i^\dagger \hat{c}_i . \tag{2.1}$$

This model is non-interacting and enjoys a global $U(1)$ symmetry

$$\hat{c}_i \to \hat{c}_i \, e^{i\alpha} \tag{2.2}$$

which corresponds to particle number[3] conservation. Can this symmetry be promoted to a local one, meaning that the transformation (2.2) leaves the Hamiltonian invariant even if the parameter α is site-dependent? The task turns out to be non-trivial and requires the introduction of additional degrees of freedom, the so-called "gauge fields". These are operators which are defined on the links connecting two sites, of the form

$$U_{i+\frac{1}{2}} = e^{iA_{i+1/2}}, \tag{2.3}$$

---

[3] Or electric charge.

where we have introduced the notation $i + 1/2$ to denote the link between sites i and $i + 1$. Under the local transformation the gauge fields transform[4] as

$$A_{i+\frac{1}{2}} \rightarrow A_{i+\frac{1}{2}} + \alpha_i - \alpha_{i+1}, \tag{2.4}$$

so that the local phase factors from the matter and gauge fields cancel each other and the interacting Hamiltonian

$$H_{U(1)} = -t \sum_i \left(\hat{c}_i^\dagger \, U_{i+\frac{1}{2}} \, \hat{c}_{i+1} + h.c \right) - \mu \sum_i \hat{c}_i^\dagger \hat{c}_i . \tag{2.5}$$

is left invariant. As the notation suggests, the field A corresponds to the electromagnetic potential, and we have recovered the standard way to couple charged particles to a static external source, known as the Peierls substitution. In general, however, the gauge degrees of freedom are fluctuating quantum fields whose dynamics is determined by appropriate terms in the Hamiltonian.

2.1.2 Gauging fermionic parity

In the following we will be interested in the gauge group $\mathbb{Z}_2$. This can be easily obtained by restricting the phases (2.3) to take the values ± 1, i.e. $A \in \{0, \pi\}$. With this in mind, one can identify the U operator with the Pauli matrix σ^z. In a similar way, σ^x can be seen as the equivalent to e^{iE} which corresponds to the energy of the electric field.[5] A $\mathbb{Z}_2$ gauge transformation is parametrized by the sign $s_i = e^{i\alpha_i} \in \{-1, 1\}$ such that

$$\hat{c}_i \rightarrow s_i \, \hat{c}_i \qquad\qquad \sigma^z_{i+\frac{1}{2}} \rightarrow s_i \, \sigma^z_{i+\frac{1}{2}} \, s_{i+1} . \tag{2.6}$$

Since

$$\left[(-1)^{\hat{n}_i}, \hat{c}_i \right] = -\hat{c}_i \qquad\qquad \{\sigma^z_i, \sigma^x_i\} = 0, \tag{2.7}$$

where $\hat{n}_i = \hat{c}_i^\dagger \hat{c}_i$, the local gauge transformation can be generated by the Gauss operator

$$G_i = \sigma^x_{i-\frac{1}{2}} \, (-1)^{\hat{n}_i} \, \sigma^x_{i+\frac{1}{2}}, \tag{2.8}$$

in the sense that the conjugation $O \rightarrow G^{-1} \, O \, G$ flips the sign of $\hat{c}$ or σ^z operators which share a link or site with G, and leaves the others invariant. Since the action of G always affects an even number of such operators, this guarantees gauge invariance, i.e. that

$$[G_i, H_G] = 0 \quad \forall \, i. \tag{2.9}$$

---

[4] The reader can recognize on the right hand side of Eq. (2.4) the discrete divergence $\delta\alpha = \alpha_{i+1} - \alpha_i$, so that this is the equivalent to the continuum transformation $A_\mu \rightarrow A_\mu + \partial_\mu \alpha$ mentioned in the introduction.

[5] Note however that due to the finite dimension of the Hilbert space, E and A do not satisfy the usual commutation relations of QED.

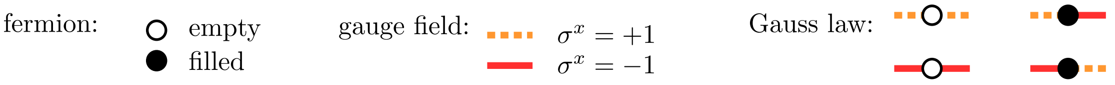

Figure 2.1: Pictorial depiction of the local Hilbert space of a $\mathbb{Z}_2$ gauge theory with single-component fermionic matter, in the basis where $\hat{n}$ and σ^x are diagonal. On the right, we show the four physical states that are selected by the Gauss law (2.8). $\mathbb{Z}_2$ charged fermions (black dots) are sources of electric lines.

The Hilbert space

Equation (2.9) shows that a gauge invariant Hamiltonian enjoys an extensive number of conservation laws, one for each site of the chain. Since $G^2 = 1$, the Gauss operator has eigenvalues ± 1. As a result, the Hilbert space is separated into an exponentially large number of sectors, each corresponding to a choice $\{G_i = \pm 1\}$. Once a sector is chosen, a gauge invariant Hamiltonian operates within that sector, which is consequently referred to as the *physical Hilbert space*. In the rest of this thesis the physical Hilbert space is determined by the choice $G_i = 1\,\forall i$, unless otherwise stated.

As the name suggests, the Gauss law can be interpreted analogously to the one of electrodynamics. By rewriting the gauge constraint as

$$\sigma^x_{i-\frac{1}{2}}\,\sigma^x_{i+\frac{1}{2}} = (-1)^{\hat{n}_i}, \quad \text{i.e.} \quad E_{i+\frac{1}{2}} - E_{i-\frac{1}{2}} = \begin{cases} \pi & \text{if there is a } \mathbb{Z}_2 \text{ charge} \\ 0 & \text{otherwise} \end{cases} \tag{2.10}$$

we learn that the $\mathbb{Z}_2$ charge corresponding to the fermion parity on a given site[6] determines the divergence of the electric field, i.e. the difference in its value across the two neighboring links. While the local Hilbert space of a link-site-link subsystem consists of $2^3 = 8$ states, the Gauss law constrains it to the four physical states shown in Fig. 2.1.2. In the following, we will often operate in a basis where σ^x is diagonal. We will generally refer to the state with $\sigma^x = +1$ as the "electric vacuum", while links where $\sigma^x = -1$ constitute "electric strings".[7] In this language, we can say that $\mathbb{Z}_2$ charges are sources for electric strings (flux lines). Unless the electric string extends to infinity, it has to terminate on a second $\mathbb{Z}_2$ charge, forming a flux tube. A basis for the many body Hilbert space, therefore, consists of states containing a certain number of pairs of fermions sitting at an arbitrary distance from each other, connected by electric lines. One can also look at this in a different way: the bare fermionic creation operator $\hat{c}^\dagger$ is not gauge invariant, and therefore it has no physical meaning. It can be made invariant by the attachment of a string:

$$\hat{c}^\dagger_i \to \hat{f}^\dagger_i = \left(\prod_{j\le i} \sigma^z_{j-\frac{1}{2}}\right) \hat{c}^\dagger_i. \tag{2.11}$$

---

[6] Which for spinless fermions is in one to one correspondence to the electric charge/particle number: $(-1)^{\hat{n}} = 1 - 2\hat{n}$.

[7] This choice is conventional and corresponds to taking positive values of h. As we discuss at the beginning of section 2.2, we do not lose generality by doing so.

When acting on the fermion and electric vacuum, not only does the newly introduced $\hat{f}_i^\dagger$ create a particle at site i, but it also flips the state of the electric field on each link to its left, effectively attaching a semi-infinite electric string to it. As a matter of fact, the replacement (2.11) is another recipe to obtain a gauged model from an ungauged one.[8] This highlights the fact that gauging a model is an invasive procedure, and deeply non-local in nature.

The fate of fermion parity

We conclude this subsection by addressing some technicalities related to boundary conditions. From the discussion above it is clear that on a closed chain only an even number of $\mathbb{Z}_2$ charges is allowed, since the electric string originating from one charge can only terminate on another charge. On a finite open chain, on the other hand, electric lines can stretch all the way to the edge. In principle one can consider two different types of boundaries, depending on whether the chain ends with a link or with a site. We will always consider the first option, since it does not require a redefinition of the Gauss law (2.8)[9]. In this setup the total fermion parity P can be related to the values of σ^x at the boundary: from multiplying together all Gauss operators one gets

$$1 = \prod_i G_i = \sigma^x_{\frac{1}{2}} \left(\prod_{i=0}^{L} (-1)^{n_i} (\sigma^x_{i+\frac{1}{2}})^2 \right) \sigma^x_{L+\frac{1}{2}} = \sigma^x_{\frac{1}{2}} \; P \; \sigma^x_{L+\frac{1}{2}}, \tag{2.12}$$

from which we learn that

$$P = \sigma^x_{\frac{1}{2}} \sigma^x_{L+\frac{1}{2}}. \tag{2.13}$$

On an infinite chain the total fermionic parity is determined by the value of the $\mathbb{Z}_2$ electric field at infinity, and we will normally assume it to be even.

An excursus: quantum link models

In this section, we have introduced the $\mathbb{Z}_2$ lattice gauge theory as a "discretization" of the $U(1)$ gauge group. In a similar fashion we could have restricted the phase (2.3) to take n values around the circle instead of just two, which leads to a $\mathbb{Z}_n$ lattice gauge theory. Since in the limit $n \to \infty$ one expects to recover the physics of a $U(1)$ gauge theory, $\mathbb{Z}_n$ models can be seen as one way to approximate QED. Finding a proper way of truncating the local Hilbert space is indeed a must to perform numerical calculations on systems with a bosonic local Hilbert space. A different way to achieve such truncation is given by the so-called quantum link models [117]. In the $U(1)$ case on which we focus, the idea is to replace the link variables (2.3) with spin S operators, thus truncating the local Hilbert space to $2S + 1$ states. In the limit $S \to \infty$ the Kogut-Susskind formulation [24] of a Hamiltonian $U(1)$ LGT is recovered. Conventionally, the third component of the spin $\hat{S}_z$ corresponds to the electric field, whose quanta are created and destroyed by the raising and lowering operators $\hat{S}^+$ and $\hat{S}^-$. Quantum link models are an active area of research in the field of Hamiltonian lattice gauge theory, and several studies have shown that such models can capture important features of $U(1)$ gauge theories even for small values of the spin S [118–120].

---

[8] This is equivalent to the construction adopted for QED in the continuum, where a fermionic field $\Psi(x)$ is replaced by the non-local object $e^{i\int_{-\infty}^{x} A(x')\,dx'}\Psi(x)$.

[9] It may require a redefinition of the Hamiltonian at the boundaries.

2.1.3 Gauge invariant Hamiltonians

Having established the form of the physical Hilbert space and of the gauge generators starting from general principles, it is now time to figure out how a generic $\mathbb{Z}_2$ invariant Hamiltonian looks like. The global symmetry that is gauged is nothing but the fermionic parity $P : \hat{c}_i \to -\hat{c}_i$. Since this symmetry is automatically satisfied by any local fermionic Hamiltonian, there are no particular restrictions on the type of fermion bilinears that we can consider. In particular, we can also include "anomalous" terms of the form $\hat{c}_i\hat{c}_{i+1} + h.c.$, which violate particle number conservation and would not be allowed in a $U(1)$ theory. Such terms can be made gauge-invariant through the very same procedure outlined above for the hopping. Besides, any term that does not change under the gauge transformation (2.8) can be added to the Hamiltonian without spoiling its gauge invariance. Obvious choices are Hubbard-like interactions that depend only on the fermion densities $\hat{n}_i$, and terms that involve any combination of σ^x.[10] Of the latter, the simplest and most relevant one has the form $\sum_i \sigma^x_{i+\frac{1}{2}}$, which plays the role of $\mathbb{Z}_2$ electric field energy.[11] More complicated terms can be constructed by taking combinations of fermion bilinears and σ^z, but we will not consider them here.

After putting everything together, a general Hamiltonian describing the interaction between spinless fermions and $\mathbb{Z}_2$ gauge fields reads:

$$\begin{aligned} H_G = &- t\sum_i \left(\hat{c}_i^\dagger\, \sigma^z_{i+\frac{1}{2}}\, \hat{c}_{i+1} + h.c\right) - \Delta \sum_i \left(\hat{c}_i^\dagger\, \sigma^z_{i+\frac{1}{2}}\, \hat{c}_{i+1}^\dagger + h.c\right) - \mu\sum_i \hat{n}_i \\ &- \sum_k\sum_i U_k\, \hat{n}_i\hat{n}_{i+k} - \sum_i h_1\, \sigma^x_{i+\frac{1}{2}} - \sum_i h_2\, \sigma^x_{i-\frac{1}{2}}\, \sigma^x_{i+\frac{1}{2}} + \dots \end{aligned}$$

with the dots indicating that we omitted density-density interactions involving more that two sites and and more complicated terms involving combinations of σ^x.

2.1.4 Gauge invariant observables

In a gauge theory, only gauge invariant quantities are considered physical. As a matter of fact, Elitzur's theorem [121] ensures that the expectation value of any non gauge invariant operator - evaluated on a physical (gauge invariant) many-body state - needs to vanish. This is often stated as the fact that a gauge symmetry cannot be spontaneously broken,[12] although this is a trivial statement if we adopt the perspective of the introduction, i.e. that gauge symmetry is not an actual symmetry but a mere redundancy in our description of Nature.[13]

---

[10] The Gauss operator G is diagonal in the basis where both σ^x and $\hat{n}$ are diagonal.

[11] This can be seen by following up on the analogy with electrodynamics. Since $\sigma^x \approx e^{iE} \approx \cos E$, in the continuum generates a term proportional to E^2. Similarly, the term $\sigma^x_{i-\frac{1}{2}}\, \sigma^x_{i+\frac{1}{2}}$ corresponds to $(\nabla E)^2$.

[12] In that case, the non-vanishing expectation value would play the role of the condensate.

In the previous subsection, we saw how to construct gauge invariant Hamiltonians. The same principles can be applied to the construction of observables. In particular, all observables involving fermionic operators are made invariant by the replacement $\hat{c} \to \hat{f}$, which amounts to the insertion of a string of σ^z on the links between pairs of fermionic operators. A few examples are given below:

- Fermion-fermion correlator (single particle Green's function):

$$\mathcal{G}_{ij} = \hat{f}_i^\dagger \hat{f}_j = \hat{c}_i^\dagger \left(\prod_{i \le l < j} \sigma^z_{l+\frac{1}{2}} \right) \hat{c}_j. \tag{2.14}$$

- Dimer creation operator:

$$\hat{b}^\dagger_{i+\frac{1}{2}} = \hat{f}_i^\dagger \hat{f}_{i+1}^\dagger = \hat{c}_i^\dagger \sigma^z_{i+\frac{1}{2}} \hat{c}_{i+1}^\dagger \tag{2.15}$$

- Dimer-dimer correlator:

$$\mathcal{F}_{ij} = \hat{b}^\dagger_{i+\frac{1}{2}} \hat{b}_{j+\frac{1}{2}} = \hat{f}_i^\dagger \hat{f}_{i+1}^\dagger \hat{f}_j \hat{f}_{j+1} = \hat{c}_i^\dagger \sigma^z_{i+\frac{1}{2}} \hat{c}_{i+1}^\dagger \hat{c}_j \sigma^z_{j+\frac{1}{2}} \hat{c}_{j+1} \tag{2.16}$$

As for the gauge sector, anything that depends on σ^x only is a gauge invariant observable. Strings of σ^z, on the other end, must have $\mathbb{Z}_2$ charged endpoints,[14] and so the only possibility that does not involve other operators is the closed Wilson line

$$W = \prod_i \sigma^z_{i+\frac{1}{2}} \tag{2.17}$$

on a periodic chain.

2.1.5 Confinement

Before turning to the phenomenology of specific models, we focus on a general feature of one-dimensional $\mathbb{Z}_2$ lattice gauge theories, i.e. the confining nature of the electric field.[15] For $h > 0$ the term $-h \sum_i \sigma^x_{i+\frac{1}{2}}$ introduces an energy cost for the electric strings which is equal to

$$\Delta E = 2hL, \tag{2.18}$$

where L is the length of the string. Therefore, static probe charges which are connected by a flux tube need to stay as close as possible in order to minimize their potential energy. In the presence of dynamics and other types of interactions, there is an interplay between different effects competing with the confining potential, which can delocalize the charges. We expect however to observe confinement whenever the "field strength" h is significantly larger than all other energy scales in the game. On a lattice, it is easy to see how the consequences of confinement depend significantly on the type of matter involved: whenever a site can be occupied by multiple charges, e.g. in the case of bosons or spinful fermions, the charges simply sit on top of each other and the electric strings vanish. In the relevant case of single-species fermions, however, the Pauli exclusion principle forbids double occupancy on a single site, and therefore two $\mathbb{Z}_2$ charges must be at least one lattice spacing apart. The effect of confinement, in this case, is the formation of extended dimers consisting of two particles connected by an electric string of unit length[16]. Such objects play a central role in the models that we investigate, as their dynamics determines very nontrivial phenomenology in the large h regime, where they are the appropriate emergent degrees of freedom.

---

[13] Symmetry breaking can occur in a different guise, the Higgs mechanism. The resulting model appears to exhibit SSB once a specific gauge is fixed.

[14] An example of this is the fermion-fermion correlator (2.14).

[15] This not specific to $\mathbb{Z}_2$, the same is true for $U(1)$ electrodynamics.

2.2 Fermionic matter with a global $U(1)$ symmetry

We consider now the simple model described by the Hamiltonian

$$H = -t \sum_i \left(\hat{c}_i^\dagger \, \sigma^z_{i+\frac{1}{2}} \, \hat{c}_{i+1} + h.c \right) - \mu \sum_i \hat{c}_i^\dagger \hat{c}_i - h \sum_i \sigma^x_{i+\frac{1}{2}}, \tag{2.19}$$

restricted to the physical Hilbert space where $G_i = +1$, with the Gauss operator as in Eq. (2.8). The Hamiltonian (2.19) is invariant under a global $U(1)$ transformation $\hat{c} \to \hat{c}\, e^{i\alpha}$, corresponding to particle number conservation. Therefore we can either consider sectors with a fixed number of particles or tune the filling "by hand" through the chemical potential μ.[17] The energy spectrum is invariant under $t \to -t$, since this is equivalent to a global unitary transformation that flips the sign of σ^y and σ^z, leaving σ^x invariant. With a similar argument, one can show that the spectrum is also invariant under $h \to -h$, so that we can restrict ourselves to the cases h, $t > 0$ without loss of generality.[18]

2.2.1 Free fermions at $h = 0$

We consider first the case $h = 0$, where the gauge fields have no dynamics and only determine the phase (sign) of the hopping term. On a closed chain, in the absence of the electric term the Hamiltonian has an additional *magnetic* symmetry, corresponding to the gauge-invariant closed Wilson line (2.17). This will play a central role in section 2.3, where we investigate edge physics and symmetry protected topological (SPT) phases. Here we just notice that $W = +1$

---

[16] When appropriate, we will refer to these objects as "mesons". This emphasizes the analogy with the strong interaction of the Standard Model, that binds quarks into mesons.

[17] In a certain sense, the inclusion of a chemical potential is redundant since it only shifts the energy by a constant in each sector with a given number of particles. However, it is needed for some numerical applications where particle number conservation cannot be enforced directly.

[18] This corresponds indeed to defining the electric vacuum as $\sigma^x = +1$ on every link, as assumed earlier.

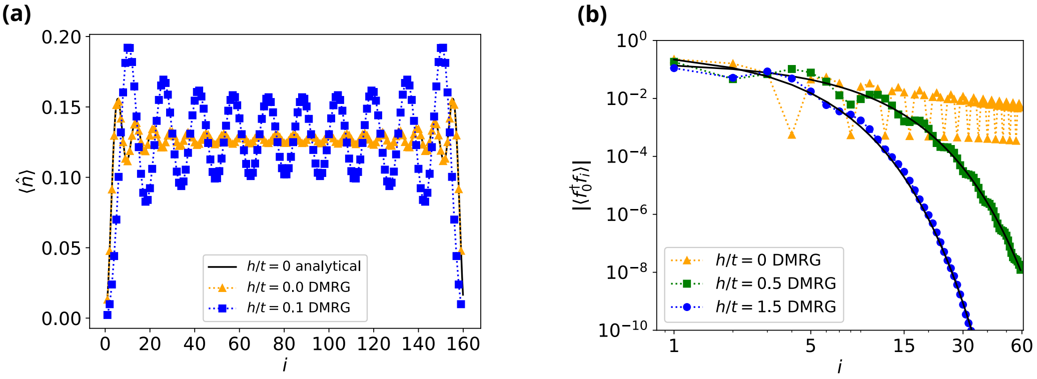

Figure 2.2: DMRG results for the system described by the Hamiltonian (2.19) at filling 1/8, on an open chain of length $L = 160$. (a) The period of the Friedel oscillations is doubled for small finite values of h, hinting at a halving of the effective density of the constituents. (b) Fermion-fermion correlators decay exponentially for any finite value of h, hinting at the confinement of the $\hat{f}$ fermions. At $h = 0$, they decay as a power law with the characteristic free-fermion exponent.

(-1) corresponds to choosing periodic (antiperiodic) boundary conditions for the fermions.[19]

By introducing the gauge-invariant $\hat{f}$ operators (2.11), one obtains a Hamiltonian of free fermions

$$H = -t \sum_i \left(\hat{f}_i^\dagger \hat{f}_{i+1} + h.c \right) - \mu \sum_i \hat{f}_i^\dagger \hat{f}_i \,, \tag{2.20}$$

which is diagonalized by going to momentum space. The system is therefore a Fermi gas, whose ground state is obtained by filling up the energy bands $E(k)$ with single particle states up to the Fermi level [122]. On a closed chain, the spectrum of the Hamiltonian (2.19) differs from the one of free fermions in that it only includes states with an even number of particles, while both periodic and antiperiodic boundary conditions are accounted for.[20]

2.2.2 Confinement at finite h

In the presence of h, the fermions are not free anymore, but they interact through a confining potential. Following the arguments of subsection 2.1.5, we expect fermions to combine into dimers. What is interesting is that this confinement happens as soon as a finite h is introduced, which can be detected in a number

---

[19] This can be seen by fixing the gauge. Choosing $\sigma^z = +1$ everywhere corresponds to periodic boundary conditions, since a particle acquires no phase when hopping all the way around the chain. If we choose $\sigma^z = -1$ on one single link, on the other hand, the particle acquires a π phase.

[20] The latter can be avoided by working in a sector where W is fixed to a specific value ±1.

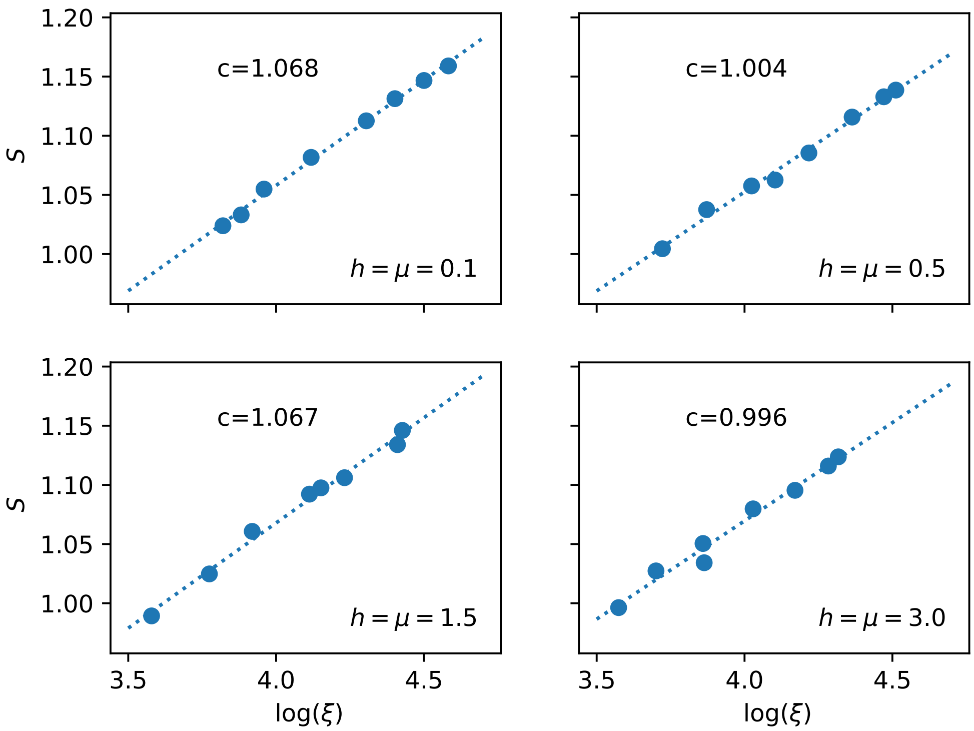

Figure 2.3: The central charge of the system is calculated numerically with iDMRG for different values of the parameters by using the scaling relation between entanglement entropy S and correlation length ξ, see Appendix A for details. The result $c = 1$ is consistent with the fact that the system is a Luttinger liquid, described by a compact boson CFT.

of ways. First, we look at the behavior of the gauge invariant fermion-fermion correlators. At $h = 0$ these decay as a power law, with the exponent given by the well known result for the fermionic Green's function in one dimension:

$$\mathcal{G}_{ij}^{\text{free fermions}} \approx \frac{1}{|i-j|}. \tag{2.21}$$

Even for small finite values of h, however, this is modified to an exponential decay that hints at the confinement of the $\hat{f}$-fermions. Results are shown in Fig. 2.2(b).

A second signature of confinement comes from the doubling of the period of the Friedel oscillations. These modulations of the density, that we observe numerically and show in Fig. 2.2(a), occur in chains with open boundary conditions and have a periodicity that is inversely proportional to the density of the constituents itself.[21] For finite values of h we observe that the period is doubled, meaning that the effective density of the system is halved. This is consistent with the fact that we now have to regard the dimers as fundamental constituents; since one dimer is composed of two fermions, the dimer density is half of the fermion density.

---

[21] Which is proportional to the Fermi momentum k_F, but the latter is not a well defined quantity for the dimers, because they are bosons.

Up to this point, our analysis has led to the conclusion that the gauge invariant $\hat{f}$-fermions are confined. It is however incorrect to assume the presence of a mass gap. By looking into the pair-pair correlators (2.16) we observe that they decay as a power-law, indicating the existence of gapless excitations. We have to conclude that the system remains gapless throughout the whole phase diagram, and can be classified as a Luttinger liquid [67, 123, 124]. This is a standard theoretical framework that describes the low energy properties of interacting fermionic systems in one dimension, where the Fermi liquid paradigm breaks down.[22] In this case, our interpretation is that the "elementary constituents" of the Luttinger liquid are the deconfined bosonic dimers, as will become clear in the next section. Such interplay between confinement and Luttinger liquid properties is interesting by itself, and it hides a number of subtleties that will be the subject of section 2.2.5. In Fig. 2.3 we show the numerical results for the central charge of the system. The value $c = 1$ is consistent with the idea that the system is a Luttinger liquid described by the compact boson conformal field theory (CFT).

2.2.3 The effective model at large h

The model (2.19) exhibits interesting features in the limit of large $\mathbb{Z}_2$ string tension, i.e. when $h \gg t$. Here, the dimers can be thought of as compact objects that extend over two sites only. In this limit we can consider a reduced gauge invariant Hilbert space where the dimers are bosons living on the "dual" lattice formed by the links of the chain. As a consequence of Pauli's principle for the underlying fermions, the presence of two dimers on the same link and also on neighboring links is forbidden. Therefore, we identify the fundamental degrees of freedom of the problem as hardcore bosons with an extended hardcore constraint.

We develop an effective theory that governs the dynamics of such dimers. While this can be done formally with a Schrieffer-Wolff transformation [125], it is instructive to adopt here a more intuitive approach, by considering directly the processes that contribute to the effective Hamiltonian at second order.[23] These are "virtual" processes that are allowed by the original Hamiltonian (2.19), and occur in two steps. Starting from a generic state in the reduced Hilbert space, the first process brings it to a high-energy state that lies out of that space, while the second one brings it back.[24] In this case there are two such processes, both involving the hopping of the original fermions:

- **Dimer hopping:** one of the fermions in the dimer hops to a neighboring (empty) site, extending the electric line that connects it to the other fermion by one unit. This creates an intermediate virtual state containing a dimer of length two. Then, the other fermion hops along in the same direction,

---

[22] A comprehensive account of Luttinger liquids is beyond the scope of this thesis, and we refer the reader to the literature [34, 36, 67]. In Appendix B we give an account of the most relevant results, which also serves the purpose of fixing a convention for the notation.

[23] A more systematic display of the Schrieffer-Wolff transformation is given in section 3.3.1, where a complicated effective Hamiltonian is derived.

[24] As it is the case here, the final state can be either the same state as the initial, or a different one.

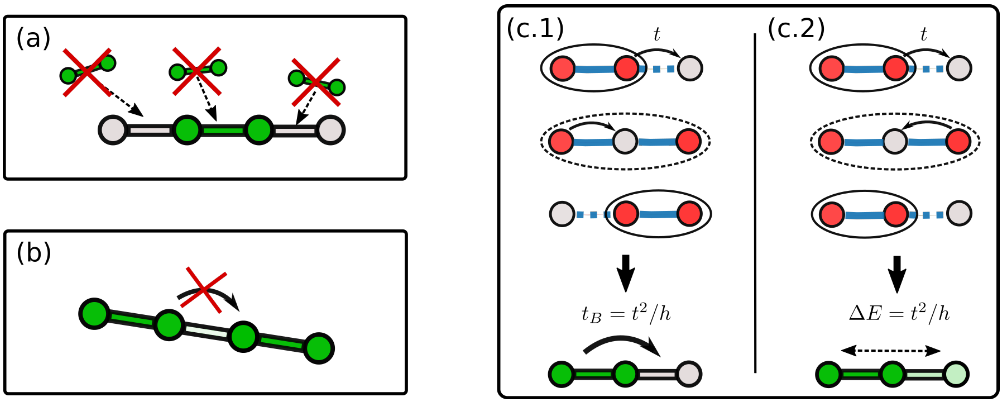

Figure 2.4: Schematic depiction of the hardcore constraints of the effective dimer model (a), of the inhibition of length fluctuations for packed dimers (b) and of the second order perturbation theory processes described in the main text (c).

and the electric string is shortened back. As a result, the initial dimer has hopped to the neighboring link.

- **Length fluctuation:** the first fermion hops by one site as described above, but successively it hops back and the initial state is restored. Naively, this contributes only a diagonal term to the effective Hamiltonian. However, this is not the case since such process is inhibited if a neighboring site is already occupied. Intuitively, since this process reduces the energy of the system,[25] the dimers prefer to stay away from each other to make it possible, which manifests itself in a repulsive interaction.

The amplitude for these processes can be inferred from the general perturbation theory expression

$$H^{\text{eff},2}_{mm'} = \sum_k \frac{\langle m|H|k\rangle\langle k|H|m'\rangle}{E_m - E_k}, \tag{2.22}$$

where the sum is over the intermediate "virtual" states $|k\rangle$. In our case all the matrix elements in the numerator are simply equal to t and the energy denominator is $2h$, the cost of flipping the $\mathbb{Z}_2$ electric field on one link. With all this in mind, we can write down the expression for the effective Hamiltonian:

$$H^{\text{eff}} = \sum_{j^*} \mathcal{P}_1 \left[-t_B \left(b^\dagger_{j^*} b_{j^*+1} + h.c. \right) + U_B \, n^B_{j^*} n^B_{j^*+2} \right] \mathcal{P}_1. \tag{2.23}$$

Here we have introduced the notation $j^* := j + 1/2$ to label the links of the lattice, the $b^\dagger$ are the dimer operators (2.15) and the projector $\mathcal{P}_1$ enforces the hardcore constraints described above. The dimer hopping and repulsion are given by

$$t_B = \frac{t^2}{2h}, \qquad U_B = \frac{t^2}{h} = 2t_B, \tag{2.24}$$

---

[25] All second order perturbation theory contributions have negative sign, as one can see from Eq. (2.22).

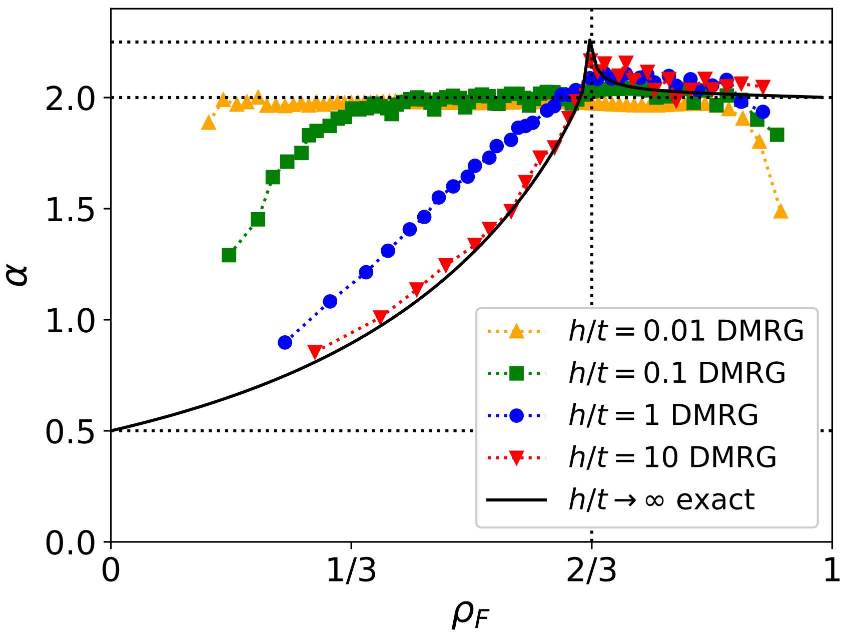

Figure 2.5: Exponent of the power-law decay of the dimer-dimer correlator, calculated using iDMRG. Data at low filling is difficult to obtain due to numerical instabilities. As $h \to 0$, $\alpha \to 2$ which is the free-fermions result, while for low fillings and $h \neq 0$ we converge to the result $\alpha = 1/2$ of non-interacting hardcore bosons. At large h the results match the analytical prediction from the effective AB model.

with the factor of two in U_B coming from the fact that the length fluctuation happens on both sides of the dimer. The extended hardcore constraints and second order virtual processes are represented pictorially in Fig. 2.2.3.

Since hardcore bosons can be effectively treated as spins,[26] the effective Hamiltonian (2.23) is a constrained version of the celebrated XXZ chain. This model was studied by Alcaraz and Bariev [126], who showed that it is integrable exactly like its unconstrained version. A detailed discussion of the AB model is presented in Chapter 3, where we unveil some unexplored features and explore certain aspects of its dynamics. Here, we limit ourselves to a comparison of the analytical results in the original paper [126] with our numerical simulations performed on the full model (2.19) at large h. In this limit, one can compute the exponent for the power-law decay of the dimer-dimer correlator as a function of the filling, and compare it with the exact result from integrability.[27] As shown in Fig. 2.5, the numerical result is in excellent agreement with the analytical prediction, confirming the correctness of our analysis. As explained above, the system is a Luttinger liquid whose elementary constituents are bosons. The results of this subsection

---

[26] One just needs to identify $b^\dagger$ with σ^+ and $\hat{n}$ with $\frac{1+\sigma^z}{2}$. This is not to be confused with the Jordan-Wigner duality between the XXZ chain and the 1D spinless Fermi-Hubbard model, which is non-local.

[27] This is straightforward, since dimer operators corresponds to primary field of the compact boson CFT for which the conformal dimensions are known.

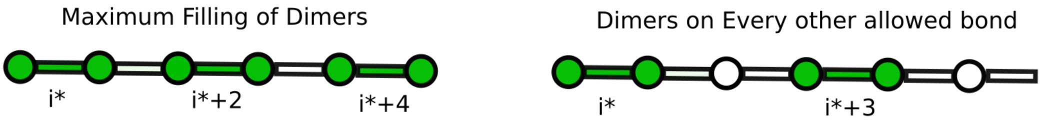

Figure 2.6: Left: A lattice fully filled with fermions hosts one dimer every two links. This shows that half-filling is the maximum possible filling for the effective dimer model. Right: A Mott state with one dimer every three links, corresponding to a density of fermions $\rho_F = 2/3$.

clarify the microscopic properties of the underlying bosonic dimers, beyond the low energy limit. For this reason we can interpret the dimer-dimer correlators as single particle Green's functions, from which the Luttinger parameter K can be computed from the exponent of the power-law decay as [67]

$$K = \frac{1}{2\alpha}. \tag{2.25}$$

This value completely determines the low energy properties of the system and, once computed, it allows to make a number of further analytical predictions.

Interestingly, our results from perturbation theory fix the ratio between the repulsion and the hopping to 2. This is exactly the isotropic (Heisenberg) point of the XXZ chain, where the Hamiltonian exhibits an enhanced $SU(2)$ symmetry and at half filling is at the transition between the gapless XY phase and the Mott insulator. This is still valid for the constrained version of the model, where $\rho_F = 2/3$ plays the role of half-filling, which we will justify in Chapter 3 (See Eq. (3.4)). This means that for this value of the density any repulsive interaction between dimers can open up a gap and stabilize a Mott state with one dimer every three links, as shown in Fig. 2.6. We postpone a more detailed analysis to section 2.2.6.

To conclude, we note the following intriguing fact: while the system is in general non integrable, both the $h = 0$ and the $h \to \infty$ limits are indeed integrable systems which very much differ from each other: free fermions on one side and the constrained XXZ chain on the other. Some dimer states have been found to be quantum scars of the system for generic values of h [82]. Interestingly, our analysis reveals that in the large h limit these states do not fall into an arbitrary region of the spectrum but rather belong to the effective low-energy Hilbert space. The subject of scarred states and weak ergodicity breaking is a very active one, and its connection to lattice gauge theories is emerging as a promising direction of research [76–81, 83].

2.2.4 Dynamics of holes: fractionalization and deconfinement

Up until now we have studied the system at generic filling, coming to the conclusion that it is described by a Luttinger liquid with interaction dependent Luttinger parameter. While the interpretation in terms of elementary dimers is suggestive and very intuitive at moderate fillings, where they can be seen as separate interacting entities, it is less enlightening when we are close to full filling. Here, as we will see, a description in terms of holes seems more appropriate. To this purpose, we introduce the hole creation and annihilation operators

$$h_i^\dagger = c_i \prod_{j\geq i} \sigma^z_{j+1/2}, \quad h_i = c_i^\dagger \prod_{j\geq i} \sigma^z_{j+1/2}, \tag{2.26}$$

in terms of which the Hamiltonian reads

$$\mathcal{H} = -t\sum_i (h_i h_{i+1}^\dagger + \text{h.c.}) - h\sum_i (-1)^{\sum_{j>i} 1-n_j^h}. \tag{2.27}$$

The last term in the Hamiltonian mediates an infinite-range potential between two holes. The potential has a zig-zag form which alternates between the values -$2h$ and 0 for the odd and even distances, respectively. As a result, the two holes are deconfined and free to spread far away from each other in the absence of other holes. This is in stark contrast to the original fermionic particles which are confined due to an attractive potential that scales linearly with distance. The deconfinement of holes is intimately related to the spontaneous breaking of translational symmetry. Indeed, there are two degenerate hole vacua[28] which are distinguished by the position of the $\mathbb{Z}_2$ electric strings. In other words, the gauge sector lies in one of the two antiferromagnetic ground states in the σ^x basis. The creation of a hole through the operator (2.26) flips the electric field on each link to its right, effectively creating a domain wall between two different vacua. Since these are degenerate, the hole can move freely with no energy cost.

Hole dynamics

We now turn our attention to the time evolution of a quantum state in which a single hole is fully localized at site $m = 0$ at time $T = 0$. A general single-hole state may be written as

$$|\Psi\rangle = \sum_m \psi_m h_m^\dagger |0\rangle \equiv \sum_m \psi_m |m\rangle, \tag{2.28}$$

where $|0\rangle$ denotes a vacuum of holes, i.e. a state fully filled with fermions. In order to follow the time evolution of this state, one needs to solve the time-dependent Schrödinger equation, which for this case reads

$$i\partial_T \psi_m = -t(\psi_{m+1} + \psi_{m-1}) + h(1 + (-1)^{m+1})\psi_m. \tag{2.29}$$

At $h = 0$ the hole is free with the dispersion relation

$$E(k) = -2t\cos k, \tag{2.30}$$

so that the time-evolved state is simply given by

$$\psi_m(T) = \int_{-\pi}^{\pi} e^{2itT\cos k} e^{ikm} dk/(2\pi) = J_m\left(\frac{T}{T_0}\right), \tag{2.31}$$

---

[28] I.e. the states fully occupied by fermions.

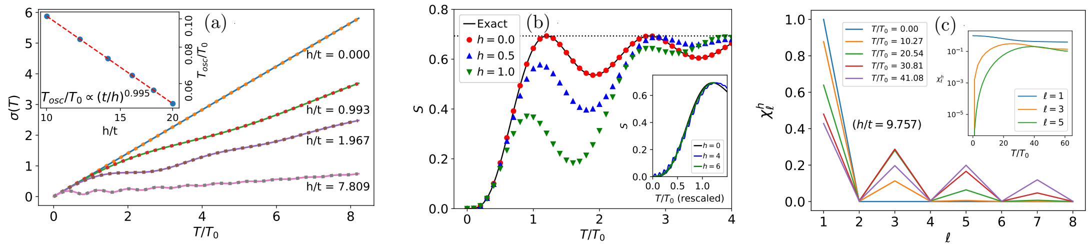

Figure 2.7: (a) Dynamics of a hole : The solid lines denote the standard deviation obtained from the ED while the dotted lines were computed by solving numerically Eq. (2.29). For $h = 0$, we obtain an excellent agreement with (2.32). As h is increased, we observe an oscillatory behavior on top of the overall linear growth. In the inset, the time period of the oscillations is plotted (blue dots), which decays as h^{-1} for large h. (b) The hole entanglement entropy under a bipartition from TEBD: The solid black line is the analytical result at $h = 0$. The dotted line represents $S = \ln 2$. The inset shows that under rescaling time T by $t/(2h)$ the curves for $h \gg t$ collapse onto the one for $h = 0$ as expected from arguments in the main text. (c) The density-density correlator χ_l^h of a state with two holes localized nearby at $T = 0$.When $h \gg t$, the holes prefer to remain odd distance apart. Inset : $\chi_\ell^h(T)$ for fixed ℓ. The likelihood at $\ell = 1$ progressively decreases while that of other odd ℓ's increase, untill they saturate. ED performed on chain with 19 sites.

where $J_m(x)$ denotes the Bessel function of the first kind and $T_0 = (2t)^{-1}$. One can quantify the spreading of the hole in time by computing the standard deviation of the hole from its original site:

$$\sigma(T) = \sqrt{\langle x^2 \rangle - \langle x \rangle^2} = \frac{T}{\sqrt{2}T_0}. \tag{2.32}$$

We learn that the hole spreads linearly in time with the rate controlled by the hopping parameter t. The numerical results shown in Fig. 2.7a reveal that the dynamics slows down as the string tension h is increased. Moreover, on top of the linear growth we observe damped oscillations whose frequency increases as h grows.

The salient features can be understood analytically in the limit $h \gg t$. First, the spectrum of the Schrödinger equation (2.29) forms two bands in the halved Brillouin zone with energies

$$E_\pm(k) = h \pm \sqrt{(2t\cos k)^2 + h^2}. \tag{2.33}$$

The wave function at site n can be expressed as

$$\Psi_n(T) = \int_{-\pi/2}^{\pi/2} \frac{dk}{2\pi} (c_k^- \phi_-(k,n) e^{-iE_- T} + c_k^+ \phi_+(k,n) e^{-iE_+ T}), \tag{2.34}$$

where $\phi_\pm(k)$ are the eigenfunctions and the coefficients $c_k^\pm$ are chosen to ensure that the hole is localized at $n = 0$ at $T = 0$. In the limit of large h, we have

$$E_- \approx -2T_s^{-1}\cos^2 k, \qquad E_+ \approx 2h + 2T_s^{-1}\cos^2 k, \tag{2.35}$$

where we introduced a slow time scale $T_s = h/t^2$. Thus the wave function becomes

$$\Psi_n(T) = f_n(T/T_s) + e^{2ihT} g_n(T/T_s). \tag{2.36}$$

This form makes it manifest that the rapidly-oscillating factor e^{2ihT} is responsible for the oscillations observed in Fig. 2.7 (a). As a result, in the large-h regime, the time scale of these oscillations scales as h^{-1}. The inset of Fig. 2.7 (a) confirms this prediction.

Entanglement spreading

We now study the time evolution of the entanglement entropy (EE) of the single-hole state investigated above under a bipartition cut at the site, where the hole is initially localized. At time $T = 0$ we start from a product state, so that the EE is vanishing. Since the hole is a single particle excitation, the corresponding EE is bounded by $\ln 2$ [127]. As shown in Fig. 3 (b), numerical TEBD results confirm that the hole entanglement growth slows down as h/t increases. Under rescaling the time T by a factor of $t/2h$ the EE growth at $h \gg t$ collapses to the $h = 0$ curve. This is because the $h \gg t$ limit is governed by an effective model[29] which describes the pure hopping of a single hole with the typical second-order perturbation theory time scale $T_s = h/t^2$.

Density-density correlators

The time evolution of a pair of holes sheds more light on their deconfined nature. The density-density correlator

$$\chi^h_\ell = \sum_k \langle n^h_k n^h_{k+\ell} \rangle \tag{2.37}$$

measures the likelihood of the separation between the two holes, initially localized at neighbouring sites at $T = 0$ (Fig. 2.7c). As expected, holes spread away from each other and in the large h limit they prefer to be an odd distance apart. In contrast, the corresponding computations of the fermionic density-density correlator

$$\chi^f_\ell = \sum_k \langle n^f_k n^f_{k+\ell} \rangle \tag{2.38}$$

for a pair of fermions reveals that they remain closely confined together.

Above arguments illustrate the deconfined nature of the lattice holes on top of the quantum vacuum fully filled with fermions. At finite density of holes, however, at $h \neq 0$ one observes that the hole-hole correlation function decays exponentially. As a result, at any finite hole filling the lattice operator creating a hole does not coincide with the annihilation operator of the emergent deconfined fermionic excitation of the Luttinger liquid field theory discussed in [70].

---

[29] See section 3.2.1 for more details.

2.2.5 Field-theoretical perspective: Luttinger Liquid and the lattice-continuum correspondence

Having established that the system (2.19) is a Luttinger liquid for all values of h, we can look concretely into the effective low energy continuum model and check its consistency with our results. In particular, there are a couple of question that can be raised:

- Luttinger liquids have deconfined fermionic excitations. How is this consistent with the confinement of *lattice* fermions?
- How can the confining potential not be an RG-relevant perturbation, that would gap the whole system?

To answer the first question, we need to understand how the lattice-continuum correspondence works. At $h = 0$, i.e. for free fermions, it is well known that there is a direct matching between lattice fermionic operators and fields of the compact boson CFT:

$$\hat{f} \to e^{i(\phi+\theta)}. \tag{2.39}$$

Such correspondence holds, for instance, even after the introduction of quartic interactions so that their effect is entirely captured by a renormalization of the Luttinger parameter.[30] In the gauged model, however, a novel type of interactions (i.e. $h\,\sigma^x$) is allowed and its effects are not known *a priori*. As a guiding principle, we can use the symmetries of the two models. At $h = 0$ the system enjoys a global magnetic $\mathbb{Z}_2$ symmetry generated by $\prod \sigma^z$, which in the continuum corresponds to $\theta \to -\theta$. At $h \neq 0$, on the other hand, the global $\mathbb{Z}_2$ symmetry is explicitly broken and there is no reason why this identification should still hold. The field theory operators correspond instead to new, deconfined fermionic excitations whose expression on the lattice is not known, and only in the limit $h \to 0$ coincide with the $\hat{f}$-fermions.

Let us now try to understand the effect of a small electric perturbation near the free fermion point. Resolving the Gauss' law, the h-term can be turned into a non-local interaction:[31]

$$\sigma^x_{i-1/2} = (-1)^{\sum_{j\geq i} n^f_j} = e^{i\pi \sum_{j\geq i} n^f_j} \tag{2.40}$$

By taking the continuum limit and using the bosonization recipe $\rho_F(x) \to \rho_F^0 - \partial_x\phi(x)/\pi$, we obtain that

$$-h\sum_i \sigma^x_i \approx -h\int dx\, e^{i\pi\int_{x>x_i}\rho_F(x)} \approx -h\int dx\, \cos\left(k_F x - \phi(x)\right), \tag{2.41}$$

where we have defined the Fermi momentum $k_F = \pi\rho_F^0$. Since a fermion corresponds to a π-kink in the ϕ field, Eq. (2.41) seems to suggest that isolated fermions are energetically punished while tightly bound dimers are favored. This naive observation, however, has to be complemented with the fact that the perturbation is not RG-relevant. Near the free fermion point, indeed, the only relevant perturbations are $\cos(\phi)$ and $\cos(2\phi)$ which cannot be generated without breaking the lattice translation symmetry of the Hamiltonian [128].[32] Therefore, despite the appearance, the effect of the electric term has to be encoded into the marginal deformation $(\partial\phi)^2$ which renormalizes the Luttinger parameter.

---

[30] See Appendix B for a brief introduction to Luttinger Liquids and for an explanation fo the notation that we use.

[31] This is general to gauge theories in one dimension.

Finally, we consider the large h regime. From the analysis above it is clear that the system is still described by the compact boson CFT, with a Luttinger parameter that depends both on h and ρ_F and can be calculated from Eq. (2.25). We found that the effective constrained XXZ model that describes this limit lies exactly at the antiferromagnetic Heisenberg point, and so at the "half filling" $\rho_F = 2/3$ we are at the edge of a Mott lobe. Here the Luttinger parameter (as a function of ρ_F) has a cusp where it hits the value $K^* = 1/9$. For such value perturbations of the form $\cos(6\,\phi)$ become RG-relevant, inducing a mass term which drives a Mott transition into a phase of commensurability three.

To summarize, we have shown that the low-energy Luttinger liquid model describes well our lattice results for all values of h and of ρ. This is consistent with the fact that a $\mathbb{Z}_2$ gauged Dirac fermion is a compact boson, as shown in reference [73].

2.2.6 Models with repulsive interactions

As explained in section 2.1, all sorts of density-density interactions are gauge invariant and can be included into the model discussed above without any modification. The possibilities are many and in the following we only consider the simple case of nearest-neighbor repulsive interactions, which add an interesting twist to the ground state physics of the one-dimensional $\mathbb{Z}_2$ LGT studied above. The modified Hamiltonian reads

$$H_V = H + V \sum_i \hat{n}_i \hat{n}_{i+1}, \tag{2.42}$$

where H is given by Eq. (2.19).

In the absence of electric coupling, or when $t, V \gg h$, the interplay between hopping and repulsion determines the physics of the system, and the gauge fields do not play a significant role. In particular, at $h = 0$ when the system is at half-filling it enters a conventional Mott phase for large values of V. The quantum critical point is located at $V = 2t$, which is the $SU(2)$-symmetric Heisenberg point of the dual XXZ chain.[33] In the following, we focus on more interesting scenarios where the interplay between repulsion and confining $\mathbb{Z}_2$ gauge fields plays a central role.

---

[32] In our notation, one site translations act on the ϕ field as $\phi \to \phi + k_F$. At half filling $k_F = \pi/2$ and the first invariant term is $\cos(4\pi)$ which is not RG relevant at the free fermion point.

[33] In [115, 129] hardcore bosons are considered instead of spinless fermions. In this case the mapping to the XXZ chain is a simple relabeling of the operators. The subtle differences between the two (in 1d) do not play a role for our purposes, and we treat them as essentially interchangeable.

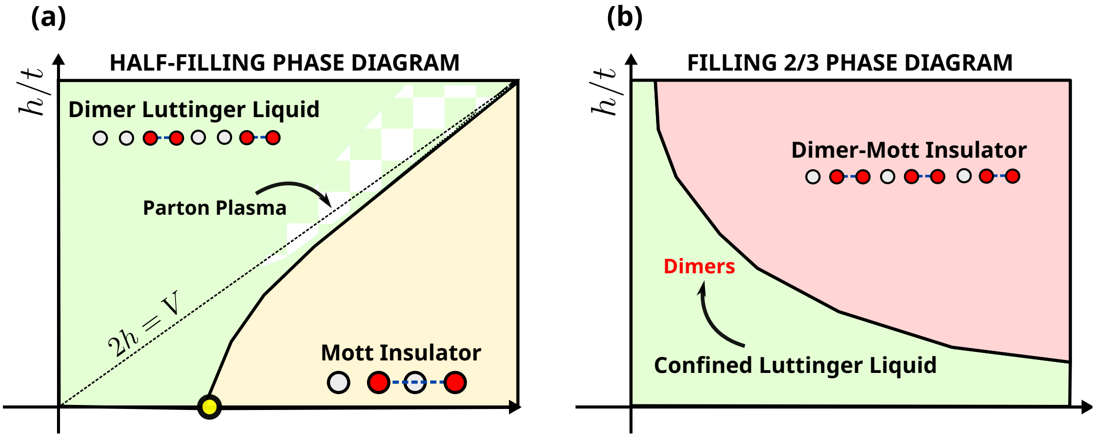

Figure 2.8: A sketch of the phase diagram of the $\mathbb{Z}_2$ LGT model with the repulsive interaction (2.42) at half-filling (a) and filling 2/3 (b). At half filling the repulsive interactions stabilize a Mott state (yellow region) which is destroyed by a sufficiently large h, that triggers the formation of dimers (green region). On the line $2h = V$, dimers of different length are degenerate and deconfined on short-to-intermediate length scales, giving a parton plasma. At filling 2/3, on the contrary, the repulsion alone cannot stabilize a Mott state. As h is introduced, however, the resulting dimers experience repulsive interactions of strength V, causing the Mott pattern shown in the figure (red).

Stabilizing a dimer-Mott state at filling 2/3

As discussed in section 2.2.3, at large h the emergent dimer-dimer repulsive interactions are on the verge of stabilizing the dimer-Mott state shown in Fig. 2.6 at filling 2/3. Indeed the system lies exactly at the critical point where the gap vanishes, and any additional small repulsion would trigger the transition. It is easy to verify that introducing a finite V does the trick, i.e. that the repulsion between the elementary constituents is converted, in the large h limit, into an additional repulsion between dimers:

$$t_D = \frac{t^2}{h} \to t_D + V, \qquad h \to \infty, \quad V \ll h. \tag{2.43}$$

In [129] it is shown that such transition survives well below the large h limit, i.e. that a Mott gap opens for small finite values of h when $t \approx V$. The complete phase diagram for the model is shown in Fig. 2.8(b).

Resonating quantum dimers at half-filling

Having established the effects of the repulsive interactions at filling 2/3, we now focus on half filling. Consider first the case of zero hopping $t = 0$. Here it is easy to see that the straight line $2h = V$ plays a special role: although so far we thought of dimers of length one as the fundamental constituents in the large h limit, in this case they are allowed to fluctuate in length and are indeed energetically degenerate

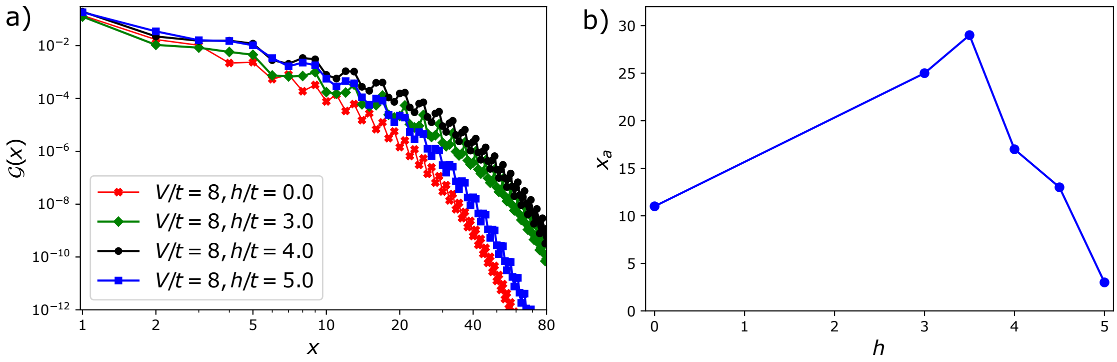

Figure 2.9: (a) Green's function in the Mott state (red), around the transition line at $2h = V = 8t$ (black), above the transition line $2h = 5t, V = 8t$ (green) and below the transition line $2h = 3t, V = 8t$ in the Mott state (blue). We observe strong exponential decay when $2h > V$ and a slower exponential decay when $2h < V$. This is to be contrasted with the case $2h = V$ where the initial, slow, power-law decay eventually turns into a uniform exponential decay for longer distance. On the other hand a steady exponential decay is observed deep in the Mott state when $V = 8t$ and $h = 0$. (b) Distance x_a where the Green's function behaviour changes from algebraic to exponential decay as a function of h, for $V = 8t$.

with dimers of length two. This is because the cost $\Delta E = 2h$ of extending the dimer is compensated by the fact that for extended dimers there is no V repulsion between its partons. This is possible for all fillings $n \leq 1/2$. For higher fillings extending a dimer will necessarily bring a parton close to another one, neutralizing the energy gain. Away from this line, it is clear that the degeneracy is lifted and one or the other configuration is privileged.

For finite t, there is instead an extended region around the line $2V = h$ where the system is characterized by strong fluctuations between tight and extended dimers. We refer to this part of the phase diagram as a "pre-formed parton plasma". Here, although the constituents are confined, they are allowed to fluctuate over length-scales which are comparable to the interparticle spacing. This means that they are effectively deconfined over such length scales, as one can detect by looking for instance into the parton-parton Green's function. While this normally exhibits an exponential decay, in this case it follows a power law behavior over short-to-medium length scales as shown in Fig. 2.9. The system exhibits Luttinger liquid behavior on the whole critical line, although in this case it is not straightforward to associate it with a microscopical picture. Following the logic of section 2.2.3, the Luttinger parameter K can be computed from the pair-pair correlator. One finds that it reaches very small values, which testify the presence of very strong repulsive interactions.

Further away from this line, the region $2V > h$ where length two dimers are favored transitions into the conventional Mott state that exhibits the same alternating density pattern shown in Fig. 2.8(a). Here fluctuations are completely suppressed and a gap opens. In the opposite limit $2V < h$ we can think again of tight dimers as the undisturbed fundamental constituents, which form a Luttinger liquid. In agreement with the results of sections 2.2.3 and 2.2.5, at half filling the

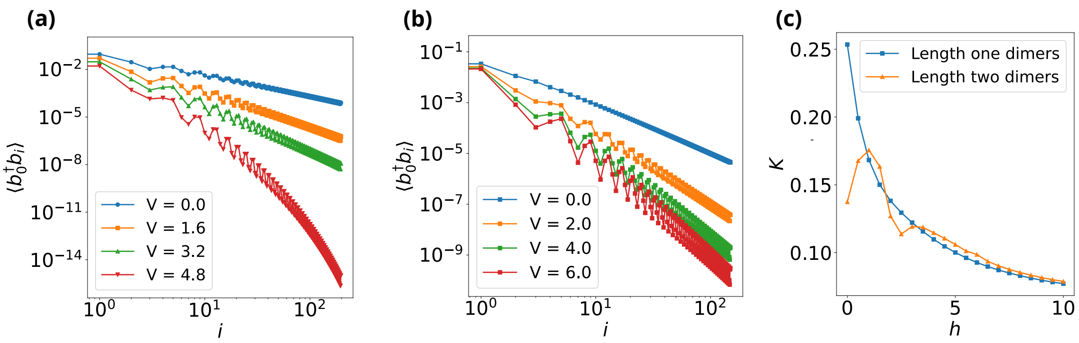

Figure 2.10: Pair-pair correlators at a fixed value of $h = 2t$ (a) and on the $2h = V$ line (b), for several values of V. In the first case, the crossover from power-law to exponential decay indicates that the system becomes a Mott insulator for large enough V. In the second case, the correlators exhibit a power-law decay on the whole line, with an exponent that increases monotonically with h as shown in (c). The same behaviour is also observed if we consider extended dimers of length two ($l = 1$). This hints at a gapless Luttinger liquid phase with strong repulsive interactions.

repulsion is not large enough to stabilize a dimer-Mott state, and it simply lowers the Luttinger parameter of the system. In Fig 2.10 we show numerical results for the pair-pair correlators, that fully agree with the analysis presented above.

2.3 Gauged Kitaev chain

The second model that we consider in this chapter is a gauged version of the celebrated Kitaev's chain. This is a free fermionic theory which includes a pairing term that breaks the global $U(1)$ particle number symmetry. It is renowned as a simple solvable example of model that falls into the SPT paradigm [130–134] and exhibits edge modes. Compared to the $U(1)$ conserving Hamiltonians discussed in the previous section, here we focus less on the bulk phenomenology of the model and more on edge physics. In particular we try to find an answer to the following questions:

- What is left of the peculiar edge physics of the Kitaev chain after gauging fermion parity?
- Is there a unified framework, from which both the ungauged and gauged models can emerge? If so, how are they related?

Through the course of this section, we also introduce the interesting idea that the Higgs phase of a gauge theory is an SPT. After reminding the reader of some salient features of the Kitaev chain, we move on to the gauged model and we focus on its phase diagram, where we put particular emphasis on the subtleties related to boundary phenomena. Finally, in the attempt to give answer to the second question formulated above, we introduce the concept of "gentle gauging". We also want to mention some possible experimental relevance of our work: according to [135], the gauged Kitaev model (2.54) -without the Gauss constraint (2.8)- can be realized in a helical quantum wire proximity coupled to a superconductor with quantum phase slips. That model exhibits an interesting relation between thermal conductance and confinement.

2.3.1 The Kitaev chain

The Kitaev chain is a tight-binding model of spinless fermions living on the sites of a lattice with nearest neighbor hopping and pairing,[34] described by the quadratic Hamiltonian [136, 137]

$$\begin{aligned} H &= -t\sum_j \left(c_j^\dagger - c_j\right)\left(c_{j+1}^\dagger + c_{j+1}\right) - \mu\sum_j \left(c_j^\dagger c_j - \frac{1}{2}\right) \\ &= it\sum_j \tilde{\gamma}_j\gamma_{j+1} + \frac{i\,\mu}{2}\sum_j \tilde{\gamma}_j\gamma_j. \end{aligned} \tag{2.44}$$

In the second line, we have introduced the convenient Majorana operators

$$\gamma_i = c_i^\dagger + c_i \qquad \text{and} \qquad \tilde{\gamma}_i = i\left(c_i^\dagger - c_i\right) \tag{2.45}$$

which satisfy the hermiticity condition $\gamma_i^\dagger = \gamma_i$ and the anticommutation relations

$$\{\gamma_i, \gamma_j\} = 2\delta_{ij}, \qquad \{\tilde{\gamma}_i, \tilde{\gamma}_j\} = 2\delta_{ij}, \qquad \{\gamma_i, \tilde{\gamma}_j\} = 0 \tag{2.46}$$

This simple Hamiltonian has been studied extensively, and it is the paradigmatic example of a system exhibiting two quantum phases which are not distinguishable by a local order parameter. For $\left|\frac{t}{\mu}\right| > \frac{1}{2}$ (weak pairing), the chain is in the topological phase, characterized by the presence of robust Majorana edge modes which are protected by the $\mathbb{Z}_2^f$ fermionic parity symmetry. These edge modes can be constructed exactly for a half-infinite chain: if we define

$$\gamma_l := \sum_{j=1}^{\infty} \left(-\frac{\mu}{2t}\right)^{j-1} \gamma_j, \tag{2.47}$$

then it is straightforward to show that $[\gamma_l, H] = 0$. Hence, if $|\mathrm{gs}\rangle$ is a ground state, then so is $\gamma_l|\mathrm{gs}\rangle$. Since these two states have opposite fermion parity $P = (-1)^{\sum_j n_j}$, they cannot be linearly dependent. The ground state is thus twofold degenerate with boundaries, whereas it can be shown to be unique in the absence of boundaries.

The edge mode in Eq. (2.47) is only localized for $\left|\frac{t}{\mu}\right| > \frac{1}{2}$. Indeed, for $\left|\frac{t}{\mu}\right| < \frac{1}{2}$ (strong pairing), the phase is trivial: it does not exhibit edge modes and has a unique ground state (independent of boundary conditions). These two phases cannot be connected whilst preserving an energy gap, which indeed vanishes for $\left|\frac{t}{\mu}\right| = \frac{1}{2}$ [136]. In the limit $\mu \to 0$ the edge mode is identified with the unpaired Majorana fermion γ_1, which does not appear in the Hamiltonian (2.44).

---

[34] This latter feature makes it a toy model for p-wave superconductivity in one dimension.

String order parameter and topological order

Whilst such topological order cannot be probed by local order parameters, it can be identified with nonlocal ones. If we define the semi-infinite string operators

$$\mathcal{S}_j^{\text{triv}} = (-1)^{\cdots+n_{j-2}+n_{j-1}} = \prod_{k<j} (i\tilde{\gamma}_k \gamma_k) \tag{2.48}$$

$$\mathcal{S}_j^{\text{top}} = (-1)^{\cdots+n_{j-2}+n_{j-1}}(c_j^\dagger + c_j) = \left(\prod_{k<j} (i\tilde{\gamma}_k \gamma_k)\right)\gamma_j, \tag{2.49}$$

then it can be shown that the trivial phase has long-range order in

$$\lim_{|i-j|\to\infty} \left|\langle \mathcal{S}_i^{\text{triv}} \mathcal{S}_j^{\text{triv}} \rangle\right| \neq 0, \tag{2.50}$$

whereas the topological phase has long-range order in

$$\lim_{|i-j|\to\infty} \left|\langle \mathcal{S}_i^{\text{top}} \mathcal{S}_j^{\text{top}} \rangle\right| \neq 0. \tag{2.51}$$

The discrete invariant distinguishing these two cases is the charge of the string order parameter under fermion parity: $P\mathcal{S}^{\text{triv}}P = \mathcal{S}^{\text{triv}}$ whereas $P\mathcal{S}^{\text{top}}P = -\mathcal{S}^{\text{top}}$. Indeed, it can be argued that having long-range order in a string order parameter that is odd under P is sufficient to deduce the existence of zero-energy Majorana modes in the presence of boundaries.

It is sometimes said that instead of having strict topological order, the Kitaev chain is a symmetry-protected topological (SPT) phase, in this case protected by the fermion parity symmetry P. Indeed, it naturally fits into the general SPT framework (as is also evidenced by the fact that the bulk order parameter has a string consisting of the protecting symmetry, which is a common theme for SPT phases). However, it is important to keep in mind that it is impossible to break fermion parity symmetry whilst preserving locality; it is thus an automatic symmetry of any fermionic system.

Jordan-Wigner transformation and the transverse-field Ising model

Long before the topological properties of Hamiltonian (2.44) were fully appreciated by Kitaev, this model was known as the JW dual of the transverse-field Ising chain (TFIM) [138], given by the following spin-1/2 Hamiltonian:

$$H_{\text{TFIM}} = -t\sum_i \tau_i^x \tau_{i+1}^x + \frac{\mu}{2}\sum_i \tau_i^z. \tag{2.52}$$

Here the JW transformation is defined by

$$\tau_j^x = (-1)^{\sum_{k<j} n_k}\gamma_j \qquad \text{and} \qquad \tau_j^z = 2n_j - 1 = i\tilde{\gamma}_j\gamma_j, \tag{2.53}$$

where $n_j = c_j^\dagger c_j$ denotes the number operator, which indeed maps Eq. (2.44) to Eq. (2.52). Since this transformation is non-local, it can drastically alter the physics of the system. In this case, we see that it maps the topological phase to a symmetry-breaking phase, with the topological string order parameter $\mathcal{S}^{\mathrm{top}}$ becoming the local Ising order parameter. The JW transformation is a unitary map for open boundaries, and indeed, for this geometry both the topological Kitaev chain and the Ising phase have a twofold ground state degeneracy. However, for periodic boundary conditions, Eq. (2.53) would generate an additional non-local term, which looks unnatural in the spin chain language. In absence of this unnatural term, H in Eq. (2.44) and H_{TFIM} are not unitarily equivalent, the former having a unique ground state (in the topological phase) whereas the latter is still twofold degenerate due to symmetry-breaking.

2.3.2 The Gauged Kitaev chain

The Hamiltonian for the gauged Kitaev chain is promptly obtained by following the general principles outlined in section 2.1. It reads

$$\begin{aligned} H &= -t\sum_j \left(c_j^\dagger - c_j\right) \sigma^z_{j+1/2} \left(c_{j+1}^\dagger + c_{j+1}\right) - \mu \sum_j \left(c_j^\dagger c_j - \frac{1}{2}\right) - h\sum_j \sigma^x_{j+1/2} \\ &= i\,t \sum_j \tilde{\gamma}_j\, \sigma^z_{j+1/2} \gamma_{j+1} + \frac{i\,\mu}{2}\sum_j \tilde{\gamma}_j\, \gamma_j - h\sum_j \sigma^x_{j+1/2}, \end{aligned} \tag{2.54}$$

with the Gauss law

$$G_j = \sigma^x_{j-1/2}\,(-1)^{n_j}\,\sigma^x_{j+1/2} = \sigma^x_{j-1/2}\; i\tilde{\gamma}_j\gamma_j\,\sigma^x_{j+1/2} = +1. \tag{2.55}$$

Except for the absence of a global $U(1)$ symmetry, similar considerations to the ones following Eq. (2.19) apply: unitary transformations can toggle the signs of either h or t, so that one does not need to consider all cases separately. At $h = 0$ the model enjoys the global magnetic symmetry W given by Eq. (2.17) which, as we will see, in this section rises to a more prominent role. Since in the following we consider chains with boundaries, it is of paramount importance to keep in mind the considerations of section 2.1.2 concerning the fermionic parity. In the presence of boundaries, gauging the global P symmetry does not completely trivialize it, but makes it act on the edges of the system only as shown in Eq. (2.13). It is the interplay between the W and P symmetries that gives rise to novel and rich edge physics.

2.3.3 Bulk Phase diagram

We now elucidate the structure of the phase diagram of the gauged Kitaev chain as a function of the two dimensionless parameters t/μ and h/μ. This can be obtained numerically by computing the ground state of (2.54) directly, or we can use the fact that this model is dual to the Ising chain in a transverse and longitudinal field for which the phase diagram is known.[35] The results are shown in Fig. 2.11.

---

[35] This local duality is remarkable and is the subject of Chapter 5. In our original paper the two points of view are intertwined, while here we focus on the fermionic LGT perspective exclusively.

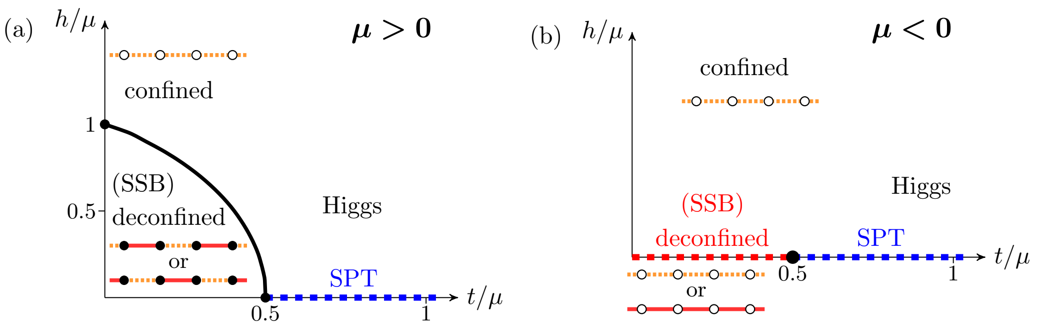

Figure 2.11: Phase diagram of the gauged Kitaev chain (2.54) for $\mu > 0$ (a) and $\mu < 0$ (b). In the absence of vortexes ($h = 0$), the system enjoys magnetic symmetry, protecting an SPT order in the Higgs phase (highlighted by a dashed blue line) as explained in section 2.3.4. For $h \neq 0$, the Higgs and confined regimes are adiabatically connected. For $\mu > 0$ the solid black line denotes Ising criticality. For $\mu < 0$ the degeneracy of the two symmetry broken ground states is immediately lifted by the longitudinal field, and $\mathbb{Z}_2$ charges are confined for any $h > 0$.

The deconfined phase

The physics of the model is readily understood in the limits $\mu \pm \infty$, where all quantum fluctuations are suppressed and full and zero particle occupancy are forced respectively. As a consequence of the Gauss law, this imposes antiferromagnetic and ferromagnetic order on the $\mathbb{Z}_2$ gauge fields respectively. This phase of the model can therefore be labeled as SSB, since it breaks spontaneously the magnetic symmetry W.[36] However, in the gauge theory language, this is better understood as the deconfined phase. Indeed, there are deconfined gauge invariant fermionic domain wall excitations

$$D_j = \left(\prod_{k<j} \sigma^z_{k+1/2} \right) \sigma^x_{j-1/2} \gamma_j \tag{2.56}$$

which are allowed to spread dynamically without string tension.[37] While in the absence of a $\mathbb{Z}_2$ electric field the cases $\mu > 0$ and $\mu < 0$ can mapped into each other, they are in general not equivalent. At finite h, the antiferromagnetic order is robust while the ferromagnetic one is immediately destroyed by the perturbation, which explains why for $\mu > 0$ one observes a finite deconfined region of the phase diagram characterized by SSB. Another way of understanding why the deconfined phase at $\mu > 0$ is stable to $h \neq 0$ is the realization that the true instanton operator is $(-1)^j \sigma^x_{j+1/2}$, which would indeed immediately lead to confinement. Since our Hamiltonian has translation symmetry, this operator cannot be generated. In other words the presence of additional crystalline symmetries prevents us from the usual confinement mechanism, which is similar to what was studied by Lai and

---

[36] To be precise, in the antiferromagnetic case the translational symmetry of the Hamiltonian is also spontaneously broken. This is exactly what differentiates the cases $\mu > 0$ and $\mu < 0$.

[37] As a matter of fact, deconfinement of domain wall excitations is a characteristic of all one dimensional SSB phases.

Motrunich in a spin liquid ladder [69]. More generally, having monopoles which carry non-trivial charge under crystalline symmetries is also key to many known instances of deconfined quantum criticality [139].

The Higgs phase

If we only look at the bulk physics, there is just one other phase in the gauge theory, namely the Higgs phase. While we have learned that for large values of h the $\mathbb{Z}_2$ charged fermionic matter undergoes confinement, in this model this regime does not form a different phase: the Higgs and confined phases are smoothly connected.[38] Physically, the Higgs phase is signaled by charge condensations in the ground state. In other words, we require that there is long range order in the domain wall operators (2.56) defined above, i.e. that

$$\lim_{|i-j|\to\infty} \langle D_i D_j \rangle \neq 0. \tag{2.57}$$

For $\mu > 0$ the two phases are separated by a critical line described by an Ising CFT, while for $\mu < 0$ there is only an isolated quantum critical point.

2.3.4 Edge physics: the Higgs phase is an SPT

As promised at the beginning of this section, we now consider what happens in the presence of boundaries.[39] In the phase diagram of Fig. 2.11 we claim that at $h = 0$ the Higgs phase is an SPT. We now justify this statement.

Construction of the edge modes

The SPT phase is protected by the magnetic symmetry

$$W = \prod_{i=0}^{L} \sigma^z_{i+1/2} \tag{2.58}$$

and by the fermionic parity symmetry which, as a consequence of gauging, acts as

$$P = \sigma^x_{1/2}\sigma^x_{L+1/2} \tag{2.59}$$

which means that it is localized at the edge. Let us consider the left edge for concreteness. The particular form of the P symmetry is related to the fact that for open boundary conditions the Majorana fermion γ_1 does not appear in any t-term of the Hamiltonian (2.54). Indeed, a suitable modification would be the inclusion of the gauge invariant edge term $-t\sigma^z_{1/2}\gamma_1$ which is not invariant under P, but this is fermionic and cannot appear in a local Hamiltonian. The left symmetry operator $\sigma^x_{1/2}$ anticommutes with W. The presence of two anticommuting symmetries already implies a twofold degeneracy of the ground state,[40] but this is not necessarily related to topology or edge physics. As a matter of fact, in the deconfined phase this is just another manifestation of spontaneous symmetry breaking. In the Higgs phase, however, we know that the ground state in the bulk is unique and therefore we expect this degeneracy to manifest itself at the boundaries. In fact, there is a second commuting edge operator defined by

---

[38] We will see another example of this in section 4.2.1, this time in two dimensions.

[39] We remind the reader that, as explained in section 2.1, we choose that both the left and the right boundaries terminate with links.

[40] In fact, for this fine-tuned Hamiltonian, we see that the degeneracy applies to the whole spectrum; we say this is a *strong* edge mode in the sense of Ref. [140].

$$\gamma_l = \sigma^y_{1/2}\gamma_1 - \frac{\mu}{2t}\,\sigma^z_{1/2}\gamma_1\tilde{\gamma}_1\sigma^y_{3/2}\gamma_2 + \left(-\frac{\mu}{2t}\right)^2 \sigma^z_{1/2}\gamma_1\tilde{\gamma}_1\sigma^z_{3/2}\gamma_2\tilde{\gamma}_2\sigma^y_{5/2}\gamma_3 + \cdots \tag{2.60}$$

A careful computation shows that

$$[\gamma_l, H] = O\left(\left(-\frac{\mu}{2t}\right)^L\right) \tag{2.61}$$

i.e., γ_l is an exponentially-localized fermionic zero-energy mode (with an exponentially-small finite-size energy splitting) in the Higgs phase ($|\mu| < 2t$). In conclusion, in the Higgs phase at $h = 0$, the left edge has two localized edge mode operators that commute with the Hamiltonian but anticommute with one another, γ_l and $\sigma^x_{1/2}$, giving us a localized twofold ground state degeneracy at the left edge. Fermion parity P prevents us from adding γ_l to the Hamiltonian, and magnetic symmetry W prevents us from adding $X_{1/2}$; the edge qubit is thus protected! Arguing similarly at the right edge, we conclude that the open chain has four-fold ground state degeneracy with an exponentially-small finite-size energy splitting. To be more precise, the four-dimensional ground state manifold is formed by a pair of two strictly degenerate eigenstates which are separated by an exponentially-small energy gap.

The derivation above should also make clear that any finite h destroys the edge modes. Indeed, for $h \neq 0$ the magnetic symmetry is explicitly broken and cannot protect the SPT phase.

Symmetry fractionalization

We demonstrated the existence and stability of the edge mode constructively. However, the reader might wonder why they are there in the first place. While in the above discussion they appeared as if by magic, we can interpret them as naturally arising from the notion of symmetry fractionalization which explains all SPT phases (for a review, see e.g. Ref. [141]). More precisely, we can interpret the two edge mode operators $\sigma^x_{1/2}$ and γ_l as encoding the effective symmetry action of P and W on the boundary, respectively. Since it is already clear how the P symmetry localizes at the boundaries, we only need to inspect W. For convenience, let us work in the fixed point limit $\mu \to 0$, such that the Majorana edge operator is just $\gamma_l = \sigma^y_{1/2}\gamma_1$, see Eq. (2.60). In the same limit all the terms in the Hamiltonian commute, which means that in the ground state

$$-i\tilde{\gamma}_j\sigma^z_{j+1/2}\gamma_{j+1} = 1 \qquad 0 < j < L. \tag{2.62}$$

With this in mind we can rewrite W as

$$\begin{aligned} W &= \sigma^z_{1/2}\sigma^z_{3/2}\ldots\sigma^z_{L+1/2} \propto \sigma^z_{1/2}\tilde{\gamma}_1\gamma_2\tilde{\gamma}_2\gamma_3\cdots\tilde{\gamma}_{L-1}\gamma_{L-1}\tilde{\gamma}_L\sigma^z_{L+1/2} \\ &= \sigma^z_{1/2}\gamma_1\, P\,\gamma_L\sigma^z_{L+1/2} \;=\; \left(\sigma^y_{1/2}\gamma_1\right)\left(\gamma_L\sigma^y_{L+1/2}\right) \;=\; \gamma_l\,\gamma_r \end{aligned} \tag{2.63}$$

which shows that at the fixed point this symmetry also fractionalizes. This way, we have derived our two edge mode operators from symmetry principles. In the latter derivation (for W), we made our lives simple by working in the fixed-point limit of the Higgs phase. However, the idea that one can effectively write $W \approx W_l W_r$ (where W_l and W_r only act near the boundary with an exponentially small tail into the bulk) is applicable to any gapped phase of matter that does not break the symmetry. This can either be derived using the matrix product state formalism, or more physically using the idea that $W \approx 1$ for periodic boundary conditions and the fact that the state has a finite correlation length (for a more detailed discussion, see Ref. [141]). The fact that $PW_lP = -W_l$ means that the magnetic and fermion parity $\mathbb{Z}_2$ symmetries are realized projectively on the edge. This discrete property of W_l cannot change as long as it is well-defined, i.e., as long as the system remains gapped and symmetric. This gives us a discrete SPT invariant, putting the system in the same phase of matter as a stack of *two* Kitaev chains, protected by the fermion parity of a *single* chain. In fact, in section 2.3.5 this relationship will become very apparent.

The fact that the Higgs phase is a non-trivial SPT phase can also be detected in the bulk, e.g., by using string order parameters. This perspective shows that it is in fact inevitable: from concatenating Gauss laws, we see that the ground state has long-range order in

$$\left\langle \sigma^x_{i-1/2} (-1)^{\sum_{i \leq k \leq j} n_k} \sigma^x_{j+1/2} \right\rangle = 1. \tag{2.64}$$

This can be interpreted as a string order parameter for the fermion parity symmetry, whose endpoint operator is odd under the magnetic symmetry. Since this is an automatic consequence of the Gauss law, we see that *any magnetic-symmetry-preserving phase in the gauge theory must be a non-trivial SPT phase!* This more general perspective is worked out in greater detail (e.g., in higher dimensions) in an upcoming work [142]. Equivalently, we can look at the string order parameter associated to the magnetic symmetry W. This is in fact given by the domain wall operator (2.56), and again, we see that its endpoint operator is charged under P, signifying a non-trivial topological phase of matter. Given that this is unavoidable (indeed, we cannot realize the trivial phase in our gauge theory), one might wonder whether it remains meaningful to think of it as non-trivial. The fact that it has protected edge modes is the most clear-cut way of seeing that this is indeed meaningful. In fact, one can think of the 'vacuum' on the outside of the system as being a truly trivial phase, as distinct from the Higgs phase. We will be able to make this point more explicit using gentle gauging in section 2.3.5.

Before addressing the effects of turning on $h \neq 0$, let us note that while the γ_l edge mode operator (2.60) delocalizes as we approach the Ising criticality to the deconfined phase, the other edge mode operator, $X_{1/2}$, remains. This means that the critical system with open boundaries exhibits exact twofold degeneracy of the energy spectrum, whereas this does not occur for periodic boundary conditions. (If one tunes beyond the critical point, this becomes the twofold symmetry-breaking degeneracy.) In particular, the critical ground state thus forms a topologically non-trivial gapless phase in the sense of Refs. [143, 144]—where the Ising criticality for the $\mathbb{Z}_2$ magnetic symmetry W is enriched by the fermionic parity symmetry P.

2.3.5 Gentle gauging

What we discussed until now shows that gauging is a drastic operation which radically changes the physics of the Kitaev chain. Despite this, one could ask whether the Kitaev model and its gauged counterpart can both emerge from a unified framework, where one can study the phase transition separating them. In addition, in section 2.3.4 we saw that the Higgs phase is topologically non-trivial with respect to the $\mathbb{Z}_2^f \times \mathbb{Z}_2$ symmetry. This might seem unusual, given that fermion parity is gauged—the catch of course being that in the presence of a boundary this global symmetry actually survives gauging. To get a different perspective on this subtlety, it is valuable to see this SPT phase arise in an emergent gauge theory, where the Gauss law is not hardwired into the Hilbert space but is merely energetically implemented such that the fermion parity is truly a symmetry in the Hilbert space, even in the bulk.[41]

To this purpose, consider the following Hamiltonian that acts in the unconstrained Hilbert space that includes link and site variables

$$H = \sum_j \left(it\tilde{\gamma}_j \sigma^z_{j+1/2} \gamma_{j+1} + i\frac{\mu}{2}\tilde{\gamma}_j\gamma_j - h\sigma^x_{j+1/2} - iK\sigma^x_{j-1/2}\tilde{\gamma}_j\gamma_j\sigma^x_{j+1/2} - \frac{t^2}{K}\sigma^z_{i+1/2} \right) \tag{2.65}$$

with a new parameter $K \geq 0$. In the limit $K \to 0$, this model essentially reduces to the Kitaev chain (2.44): although the Hilbert space still contains degrees of freedom on the links, due to the last term in the Hamiltonian these are frozen to $\sigma^z = +1$ and thus completely decouple from the fermions. On the other hand, as $K \to \infty$ the next-to-last term in the Hamiltonian enforces a large energetic penalty to every state that does not satisfy the Gauss law. Hence in this limit, at energies much below the energy scale K, we recover the gauged model (2.54). For intermediate values of K, the Hamiltonian (2.65) interpolates between these two limiting regimes. We refer to this procedure as a *gentle gauging*.

Quantum phase diagram and exact dualities in the absence of vortices

At $h = 0$ the model (2.65) enjoys a global $\mathbb{Z}_2^f \times \mathbb{Z}_2$ symmetry, generated by the fermionic parity and Wilson loop operators

$$P = \prod_j \left(i\tilde{\gamma}_j\gamma_j \right) \qquad\qquad W = \prod_j \sigma^z_{j+1/2} \tag{2.66}$$

We expect the phases of the gently gauged model to be classified in terms of these two symmetries.

We investigate the quantum phase diagram as a function of two dimensionless parameters μ/t and K/t restricted to the quadrant $\mu, t \geq 0$, since at $h = 0$ the other regions are related by a unitary transformation. In addition to the two limits $K = 0$ and $K = \infty$ described above, the behavior of the model can also be understood exactly in the limit $\mu \to \infty$. In this case the fermionic bands are fully occupied: hopping and particle number fluctuations are therefore impossible, and the local fermion parity $i\tilde{\gamma}_i\gamma_i = -1$ everywhere. In that limit the Hamiltonian (2.65) at $h = 0$ reduces to

---

[41] We point out that this is the most realistic perspective if the gauged Kitaev model is implemented on a quantum simulator, where violations of the Gauss law are expected and -to some extent- controllable [145–149].

$$H = \sum_j K\sigma^x_{j-1/2}\sigma^x_{j+1/2} - \frac{t^2}{K}\sigma^z_{j+1/2} \tag{2.67}$$

which is the TFIM (with the link variables being the degrees of freedom), exhibiting a phase transition from a disordered to the SSB phase at $K/t = 1$. For small K, this is the same trivial phase as we encountered in the Kitaev chain (2.44), whereas for large $K \to \infty$, the symmetry-breaking phase becomes the deconfined phase of the gauge theory discussed in section 2.3.3. Since this critical point corresponds to an Ising-type transition involving the gauge variables only, we expect it to be connected by a critical line to the point $\mu/t = 2$, $K = \infty$ where, as we have seen, an analogous transition takes place. This singles out a whole region in the top-right corner of the μ-K plane (see Fig. 2.12) in which the system is in the symmetry broken phase of the link magnetization $\mathbb{Z}_2$ symmetry. On the other hand, we know that at $\mu/t = 2$, $K = 0$ another critical point exists, this time corresponding to the purely fermionic topological phase transition of the ungauged Kitaev chain. It remains therefore to determine the fate of this transition at a finite coupling K.

As a first step towards fully mapping out the quantum phase diagram of the gently gauged model, one can apply a non-local transformation to the Hamiltonian (2.65). We introduce $\mathbb{Z}_2$ gauge-invariant Majorana operators on sites

$$\eta_{2i+1} = \left(\prod_{k<i}\sigma^z_{k+1/2}\right)\gamma_i, \qquad \tilde{\eta}_{2i+1} = \left(\prod_{k<i}\sigma^z_{k+1/2}\right)\tilde{\gamma}_i \tag{2.68}$$

and also a new set of Majorana operators on links through the “hybrid" Jordan-Wigner transformation

$$\eta_{2i} = \left(\prod_{k<i}\sigma^z_{k+1/2}e^{i\pi n_{k+1}}\right)\sigma^x_{i+1/2}, \qquad \tilde{\eta}_{2i} = \left(\prod_{k<i}\sigma^z_{k+1/2}e^{i\pi n_{k+1}}\right)\sigma^y_{i+1/2}. \tag{2.69}$$

In terms of these, the model (2.65) takes the form

$$H = \underbrace{i\sum_j\left(t\,\tilde{\eta}_{2j-1}\eta_{2j+1} + \frac{\mu}{2}\,\tilde{\eta}_{2j+1}\eta_{2j+1}\right)}_{H_1}\underbrace{-i\sum_j\left(-K\,\tilde{\eta}_{2j}\eta_{2j+2} + \frac{t^2}{K}\,\tilde{\eta}_{2j}\eta_{2j}\right)}_{H_2}. \tag{2.70}$$

These are just two decoupled Kitaev chains governed by the Hamiltonians H_1 and H_2, whose phase diagram depends only on μ/t and K/t, respectively. For any value of K, the Hamiltonian H_1 is critical at $|\mu/t| = 2$. Conversely, the Hamiltonian H_2 is critical at $|K/t| = 1$ for any value of μ. As a result, the phase diagram in the positive μ-K quadrant is divided into four rectangular regions by these two critical lines, as illustrated in Fig 2.12. Besides, as a consequence of the well known

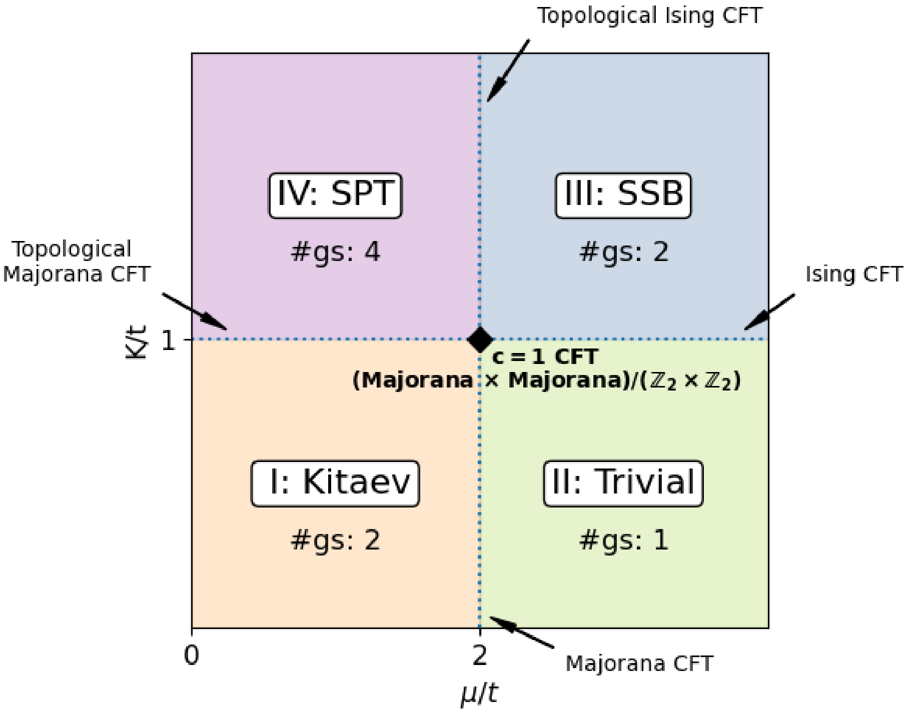

Figure 2.12: The phase diagram for the Hamiltonian (2.65) at $h = 0$. The transition lines are straight, as a consequence of two exact dualities explained in the main text. The intersection point (solid) corresponds to a conformal field theory with central charge $c = 1$. Ground state degeneracy in open chain geometry for each phase is also presented. The limit $K \to 0$ corresponds to the ordinary Kitaev chain (2.44) whereas $K \to +\infty$ is the gauged Kitaev chain (2.54) studied in section 2.3.

dualities of the Kitaev chains, each region can be exactly mapped onto one of the other three.

While the analysis above allows us to correctly identify the phase boundaries, we need to refer to the original model (2.65) to understand the nature of the four discovered phases.[42] In phases I and II ($K < t$) the link spin fields form a trivial paramagnet, while the fermionic sector is smoothly connected to the pure Kitaev chain limit ($K = 0$) which undergoes a topological-to-trivial phase transition as μ/t is varied. Therefore, we label phase I as “Kitaev" and phase II as “Trivial". On the other hand, the nature of phase III can be inferred from the limit $\mu \to \infty$ governed by the Hamiltonian (2.67). For $K > t$ its ground state forms an Ising antiferromagnet, and therefore we refer to this phase as “Spontaneously Symmetry Broken (SSB)". As for phase IV, its SPT nature in the gauge limit $K \to \infty$ was proved in section 2.3.4. This fermionic SPT belongs to the same class as a stack of two Kitaev chains, which can be shown as follows.[43] Consider the limiting case

---

[42] Under a non-local transformations, the physics of a quantum phase is generically modified. The paradigmatic example is the duality between the Kitaev chain and the TFIM, reviewed in section 2.3.1

[43] We emphasize that this is not guaranteed by Eq. (2.70), since the mapping (2.68)-(2.69)

$\mu = 0$, $K \gg t$, where we have the stabilizer code

$$H = \sum_j \left(it\tilde{\gamma}_j \sigma^z_{j+1/2} \gamma_{j+1} - iK\sigma^x_{j-1/2} \tilde{\gamma}_j \gamma_j \sigma^x_{j+1/2} \right). \tag{2.71}$$

Let us define the following Majorana modes, obtained from the original Majorana and link variables through a *local* transformation:

$$\begin{aligned} \eta_{j,A} &= \gamma_j, \\ \tilde{\eta}_{j,A} &= \tilde{\gamma}_j \sigma^z_{j+1/2}, \\ \eta_{j,B} &= \tilde{\gamma}_j \sigma^x_{j+1/2}, \\ \tilde{\eta}_{j,B} &= \tilde{\gamma}_j \sigma^y_{j+1/2}. \end{aligned} \tag{2.72}$$

Using these new variables, the Hamiltonian (2.71) reads

$$H = \sum_j \left(it\tilde{\eta}_{j,A}\eta_{j+1,A} - K(i\tilde{\eta}_{j,A}\eta_{j+1,A})(i\tilde{\eta}_{j,B}\eta_{j+1,B}) \right). \tag{2.73}$$

Despite being an interacting Hamiltonian, its ground state is a free-fermion state. Indeed, using the fact that $i\tilde{\eta}_{j,A}\eta_{j+1,A}$ is a local integral of motion, it is easy to see that for $K > 0$ the ground state does not change along the following path parametrized by λ:

$$H = \sum_j \left(it\tilde{\eta}_{j,A}\eta_{j+1,A} - (1-\lambda)K(i\tilde{\eta}_{j,A}\eta_{j+1,A})(i\tilde{\eta}_{j,B}\eta_{j+1,B}) + i\lambda\tilde{\eta}_{j,B}\eta_{j+1,B} \right). \tag{2.74}$$

While for $\lambda = 0$ this is the same as Eq. (2.73), for $\lambda = 1$ the Hamiltonian describes a stack of two Kitaev chains. Its ground state corresponds to an SPT phase protected either by complex conjugation, or by the $\mathbb{Z}_2^f \times \mathbb{Z}_2^f$ group of fermionic parities of each chain.

We have thus completely mapped the quantum phase diagram of the Hamiltonian (2.65) at $h = 0$, and the result is shown in Fig. 2.12. There are four distinct phases that are classified in terms of the global $\mathbb{Z}_2^f \times \mathbb{Z}_2$ symmetry of the model. The phases are separated by the two straight transition lines $K/t = 1$ and $\mu/t = 2$. The boundaries between different phases are critical. While all (except the multicritical point) are conformal field theories (CFTs) with central charge $c = 1/2$, they are all distinct. In particular, two are fermionic and two are bosonic: the two transitions out of the Kitaev phase are Majorana CFTs whereas the two transitions out of the Ising phase are Ising CFTs. Moreover, the two Majorana CFTs are topologically distinct: in the sense of Ref. [144] they are symmetry-enriched such that the transition between the Kitaev phase and the SPT phase is itself topologically non-trivial (with protected edge modes). Similarly, the Ising CFT between the SSB and SPT phases is also topologically non-trivial. These four critical lines meet at a multicritical point which is a CFT with central

---

involves a non-local transformation.

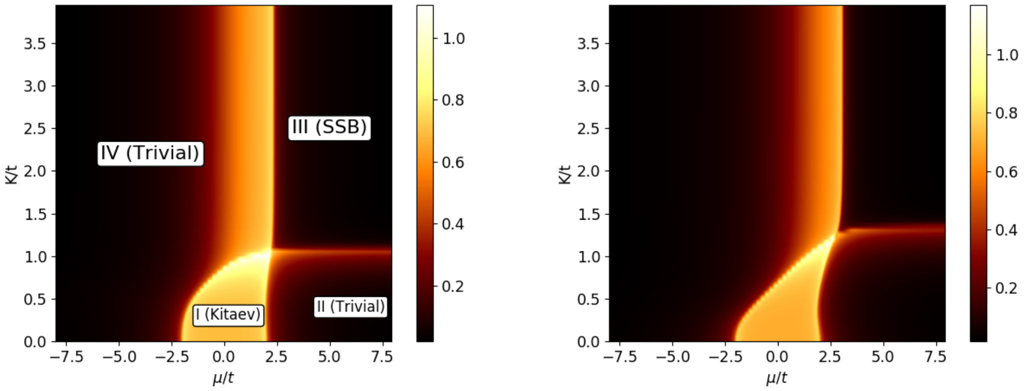

Figure 2.13: Half-chain entanglement entropy for a system described by the Hamiltonian (2.65) with $h = 1$ (left) and $h = 2$ (right). Results are obtained using DMRG for a chain of length $L = 100$. Phases are labeled as in section 2.3.5, except that the phase IV is not SPT anymore, but becomes trivial here.

charge $c = 1$. It can be identified[44] with the field theory labeled S_2 in Fig. 2 of Ref. [73].[45]

Quantum phase diagram in the presence of vortices

In the presence of vortices ($h > 0$) the magnetic symmetry generated by $W = \prod_i \sigma^z_{i+1/2}$ is explicitly broken. Since our understanding of the quantum phases of the gently gauge model at $h = 0$ in Sec. 2.3.5 relied on such symmetry being present, we anticipate qualitative differences once a finite h is turned on.

The physics of the Kitaev (I) and trivial (II) phases is essentially unchanged. This is clear from the fact that in the $K \to 0$ limit the h-term is negligible compared to the last term of the Hamiltonian (2.65), and moreover the fermion parity symmetry that characterizes the ordinary Kitaev chain is still present.

The fate of the symmetry broken phase (III) depends on the sign of the chemical potential. This is clear from our discussion in Sec. 2.3, where we showed that at $K \to \infty$ the problem is governed by the asymptotic TLFIM Hamiltonian (5.13), whose Ising coupling is determined by the chemical potential. As explained in section 2.3.3, the Ising symmetry broken phase survives at finite longitudinal field only in the antiferromagnetic case. Therefore, we need to discuss the ferromagnetic ($\mu < 0$) and antiferromagnetic ($\mu > 0$) regimes separately. In the former case, the phase III becomes a trivial paramagnet with no ground state degeneracy as soon as a finite h is introduced. In the latter case, SSB phase is still present at $h \neq 0$, but the nature of SSB is modified compared to the $h = 0$ problem. We note that one can the reach same conclusions about phase III at $h \neq 0$ by examining a different limit of the Hamiltonian (2.65), where $\mu \to \pm\infty$ but the coupling K is finite. Here we get a different asymptotic TLFIM

---

[44] There are only three points in Fig. 2 of Ref. [73] that can be related to free fermions. One is the Dirac CFT, but this cannot be perturbed into an Ising CFT; another is the stack of a Majorana CFT and an Ising CFT, but in the phase diagram in Fig. 2.12 the Majorana CFTs make a 90° turn at the multicritical point, rather than being a straight line. By exclusion, we are dealing with the third option, the S_2 theory.

[45] Note that the transformation (2.70) maps the $c = 1$ multicritical point into a standard Dirac CFT, but this mapping is *non-local.*

$$H_{\mu=\pm\infty} = \sum_j \left(\pm K\, \sigma^x_{j-1/2}\sigma^x_{j+1/2} - \frac{t^2}{K}\sigma^z_{j+1/2} - h\sigma^x_{j+1/2} \right), \tag{2.75}$$

where the sign of the Ising term is still determined by the sign of the chemical potential μ.

Finally, we consider phase IV: the absence of the $\mathbb{Z}_2$ magnetic symmetry destroys the SPT order and lifts the ground state degeneracy completely. We are left with another trivial phase.

The complete quantum phase diagram at $h \neq 0$ was mapped out numerically and is shown in Fig. 2.13. For $\mu < 0$ there are only two regions: the Kitaev phase (I) is separated from a single trivial phase (IV) by the Majorana critical line. The case $\mu > 0$ is more interesting, as we still find four distinct quantum phases. Since phases II and IV are now both trivial, it is natural to ask why they are not connected. In other words, we want to understand why the special $c = 1$ critical point that separates them at $h = 0$ still survives at a finite h. In order to answer this question, we consider at first the large h limit: $h \gg t$, K, t^2/K, μ. In that regime we can replace $\sigma^x \to 1$, $\sigma^z \to 0$ and the Hamiltonian (2.65) takes the simple form

$$H_{h=\infty} = i\left(\frac{\mu}{2} - K\right)\sum_j \tilde{\gamma}_j\gamma_j = \left(\frac{\mu}{2} - K\right)\sum_j (1 - 2n_j), \tag{2.76}$$

i.e. the fermionic sites are either completely occupied or completely empty depending on the sign of the prefactor. Remarkably, these are two distinct phases in the presence of translation symmetry. To see this, one can consider the string order parameter for fermion parity symmetry. Considering that it is an (unbreakable) symmetry, there will be long-range order of $\langle \mathcal{O}_i P_{i+1} \cdots P_{j-2}P_{j-1}\mathcal{O}_j \rangle$ for some appropriate choice of endpoint operator $\mathcal{O}_j$. Moreover, since parity is a $\mathbb{Z}_2$ symmetry, the momentum of this endpoint operator can only[46] be 0 or π. We thus have a discrete invariant. Moreover, the two fixed-point limits discussed above (where every site is empty or fully-occupied) realize both cases. They must thus be separated by a quantum critical point. We can think about these states as defining two distinct symmetry protected trivial (SPt) states [150] protected by the fermion parity $\mathbb{Z}_2^f$ symmetry and translation symmetry.

In the region of parameters specified above, one can use perturbation theory to find corrections to the simple Hamiltonian (2.76). We have to consider virtual processes induced by the full Hamiltonian (2.65), that move the states away and then back into the low-energy $h \to \infty$ Hilbert space, where $\sigma^x = 1$, $\sigma^z = 0$. At second order, we have one such process where one link is first flipped by the first term of the Hamiltonian (2.65) and then flipped back by the last term, or vice

---

[46] The endpoint operator of the square of the symmetry is the square of the endpoint operator. Since the endpoint operator of the trivial string has zero momentum, the momentum of the original endpoint operator has to satisfy $2k \equiv 0 \mod 2\pi$.

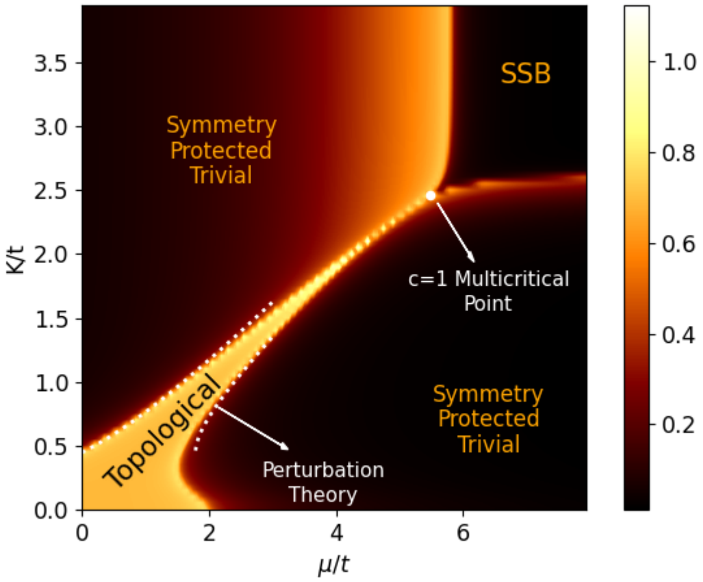

Figure 2.14: Numerical results for the half-chain entanglement entropy at $h/t = 5$. The white dotted lines are the analytical results from perturbation theory at large h, see Eq. (2.78). This approximation is valid for $t^2/h \ll K \ll h$ and $\mu \ll h$, where it reproduces correctly the phase boundaries. However, it cannot be used to infer that the critical lines converge into a $c = 1$ multicritical point.

versa. This gives a hopping contribution leading to the following effective fermionic Hamiltonian

$$H_{eff} = i\left(\frac{\mu}{2} - K\right)\sum_j \tilde{\gamma}_j\gamma_j - i\frac{t^3}{Kh}\sum_j \tilde{\gamma}_j\gamma_{j+1}. \tag{2.77}$$

This is a Kitaev chain, which is critical when

$$\frac{\mu}{2} - K = \pm\frac{t^3}{Kh}. \tag{2.78}$$

For a fixed h, the two positive solutions of this quadratic equation in the coupling K give critical lines $K^+(\mu, t)$ and $K^-(\mu, t)$ which separate the topological Kitaev phase I from the trivial phases II and IV. As shown in Fig. 2.14, these lines agree well with our numerical results in the region of parameters described above, where perturbation theory is applicable. At $\mu = 0$, the transition happens for $K^* = (t^3/h)^{1/2}$. The two transition lines converge to each other without touching for large values of μ. This provides additional evidence that the two trivial phases are indeed separated. Note however that the critical point with $c = 1$, where the topological region ends, lies outside the range $h \gg t$, K, t^2/K, μ for which Eq. (2.77) is a valid approximation. Therefore the critical point cannot be located with this method.

Chapter 3

Emergent integrability and extended constraints

One of the recurring themes in our investigation of one dimensional systems is the appearance of integrable constrained models. From the gauge-theory point of view, this can be understood from the fact that we consider spinless fermionic matter, that for large values of the confining potential binds into dimers. Such extended objects occupy at least two lattice sites and cannot overlap because of the exclusion principle, *de facto* enforcing a blockade that is reminiscent -for instance- of the physics of Rydberg atoms arrays [80, 118]. Surprisingly, similar physics arises in a particular limit of the Ising model in a tilted field. While in the presence of a longitudinal field the Ising model does not have a purely fermionic dual,[1] it can be locally mapped to a $\mathbb{Z}_2$ lattice gauge theory, i.e. the gauged Kitaev chain studied in section 2.3. This is part of a beautiful web of dualities, that will be explored in detail in Ch. 5.

Structure

This chapter is dedicated to a particular class of integrable models with extended constraint, studied first by Alcaraz and Bariev (AB). Due to its significance for our research, in section 3.1 we provide an extensive introduction to the AB model, which includes novel results about its hydrodynamics and thermodynamics. In section 3.2 we give an account of how this model emerges in the context of $\mathbb{Z}_2$ lattice gauge theories for large values of the $\mathbb{Z}_2$ electric coupling. This extends the results obtained in section 2.2.3 to more complicated cases, where constraints with longer range are generated. In section 3.3 we derive how the AB model describes a particular integrable sector of the Ising chain in a tilted field, and we apply the results of section 3.1 to investigate transport under different partitioning protocols. We also take a small detour from the main subject of this chapter by discussing the physics of non-integrable sectors of the perturbative effective model.

---

[1] The longitudinal field corresponds to a non-local operator under the Jordan-Wigner transformation.

3.1 The Alcaraz-Bariev model

In this section we review the physics of the constrained XXZ chain, first investigated by Alcaraz and Bariev [126]. Similarly to its unconstrained counterpart, the model is dual to hopping fermions with density-density interactions under a Jordan-Wigner transformation. Here, however, we will stick to the spin language. Some details of the Bethe Ansatz solution, which are also relevant to section 3.3, are discussed in appendix C, while here we focus on presenting the most relevant definitions and results. The reader can find much needed background information on Bethe Ansatz and generalized hydrodynamics in the references [151–153].

3.1.1 The model

The Hamiltonian of the Alcaraz-Bariev model reads [126]:

$$H_{AB} = -\frac{1}{2}\sum_i P_l \left(\sigma_i^x \sigma_{i+1}^x + \sigma_i^y \sigma_{i+1}^y + \Delta \sigma_i^z \sigma_{i+l+1}^z - g\sigma_i^z\right) P_l, \tag{3.1}$$

where P_l is a projector that forbids the presence of two up-spins at a distance that is smaller or equal to l lattice spacings. Unsurprisingly, for $l = 0$ we recover the familiar XXZ chain, so that all the results obtained here can be seen as a generalization of the former. In our convention the "vacuum" is given by the state $|0\rangle = |\downarrow\downarrow \dots\rangle$, while a spin up (magnon) can be interpreted as a particle. The Hamiltonian conserves the "magnon number" charge

$$\hat{n}_{mag} = \sum_i \frac{1 + \sigma_i^z}{2}, \tag{3.2}$$

with the external field g playing the role of a chemical potential. Due to the constraint, one can only accommodate a magnon every $l + 1$ sites, so that the maximum filling that can be achieved is

$$\rho_{max} = \frac{1}{1 + l}. \tag{3.3}$$

The "half filling", correspondingly, is defined as

$$\rho_{half} = \frac{1}{2 + l}, \tag{3.4}$$

i.e. the filling for which only half of the *available* sites are occupied. Similarly to the XXZ chain, the Alcaraz-Bariev model is integrable and can be solved analytically with the coordinate Bethe ansatz. As detailed in appendix C, the AB model can be seen as an XXZ chain in a reduced, density dependent volume. Intuitively, we can imagine that each magnon is in fact a larger object that does not simply occupy a single site, but rather extends over all the l sites forbidden by the constraint. As a consequence, the magnon density naturally enters results for critical exponents and other observables. Remarkably, the Hamiltonian (3.1) at $\Delta = 1/2$ is known to be a supersymmetric model [154, 155], which can be realized in a Rydberg-based quantum simulator [156].

Conformal dimensions

In conformal field theories, one is interested among other things in calculating the conformal dimensions δ of primary operators $\mathcal{O}$, i.e. the exponent that governs the power law decay

$$\langle \mathcal{O}_{x_1} \mathcal{O}_{x_2} \rangle \propto \frac{1}{|x_1 - x_2|^{2\delta}} \tag{3.5}$$

of correlators. We focus here on the field with lowest conformal dimension, which we denote by $\mathcal{O}_{1,0}$ and corresponds to the lattice operator σ^+[2] This will be the only relevant operator in our discussion, as it is related to single particle creation. At $\Delta = 0$, this has a density dependent conformal dimension

$$\delta_{1,0} = \frac{1}{4(1 - l\rho)^2}. \tag{3.6}$$

For $\Delta \neq 0$, this is modified through the introduction of the density-dependent parameter η_{ρ_B}:

$$\delta_{1,0} = \frac{1}{(1 - \rho_B)^2 \, \eta_{\rho_B}^2}, \tag{3.7}$$

where η_{ρ_B} can be obtained by solving a system of integral equations derived in [126, 157]. In particular, when $\Delta = -\cosh(\lambda) < -1$ the equations to solve are

$$1 = \eta(U) + \frac{1}{2\pi} \int_{-U_0}^{U_0} \frac{\sinh(2\lambda)\eta(U')}{\cosh(2\lambda) - \cos(U - U')} dU', \tag{3.8}$$

$$Q(U) = \frac{1}{2\pi} \frac{\sinh\lambda}{\cosh\lambda - \cos U} - \frac{1}{2\pi} \int_{-U_0}^{U_0} \frac{\sinh(2\lambda) Q(U')}{\cosh(2\lambda) - \cos(U - U')} dU', \tag{3.9}$$

$$\int_{-U_0}^{U_0} Q(U) dU = \begin{cases} \frac{\rho_B}{1-\rho_B}, & 0 \leq \rho_B \leq \frac{1}{3}, \\ \frac{1-2\rho_B}{1-\rho_B}, & \frac{1}{3} \leq \rho_B \leq \frac{1}{2}, \end{cases} \tag{3.10}$$

where U_0 in Eq. (3.8) is determined by solving Eqs. (3.9) and (3.10). Finally, the parameter η_{ρ_B} that appears in Eq. (3.7) can now be obtained by evaluating the function $\eta(U)$ at $U = U_0$. For $-1 < \Delta < 1$, instead, one uses the parametrization $\Delta = -\cos\gamma$ and obtains similar equations, with the hyperbolic functions replaced by their trigonometric counterparts. An application of these results is the exact curve in Fig. 2.5, which is obtained by solving numerically the equations above for different values of ρ.

3.1.2 Transport in the Alcaraz-Bariev model

As the Alcaraz-Bariev model is a close relative of the XXZ spin chain, it inherits most of its integrable structure, further enriched by the constraint. For this reason, we will often refer to the methods that apply to the unconstrained XXZ chain. We briefly review these methods in Appendix C, but more comprehensive accounts can be find in the dedicated literature [151, 153]. While the original papers [126, 157, 158] addressed the equilibrium thermodynamics, transport and hydrodynamics of the AB model at arbitrary Δ are tackled in [159].

---

[2] In the notation of Appendix B this corresponds to the vertex operator $e^{n\phi + m\theta}$ with $n = 1$ and $m = 0$.

Being integrable, the AB model possesses an extensive number of quasi-local conserved quantities [160], with striking consequences on its non-equilibrium features, hindering thermalization [161] and featuring ballistic transport [162]. As we saw, the AB Hilbert space is formed by multiparticle magnonic asymptotic states, which correspond to isolated spin-ups in a background of spin-downs. These can be labeled by the set of rapidities $\{\lambda_j\}_{j=1}^N$, which generalize the momenta of non-interacting systems. The fundamental property that makes integrable systems so special is that multiparticle scattering events can be factorized in two-body scattering processes, the latter fully described by the scattering phase $\Theta(\lambda, \lambda')$.[3] The scattering phase of the AB model and of the XXZ spin chain are intimately connected [126]

$$\Theta(\lambda, \lambda') = l\, p(\lambda) - l\, p(\lambda') + \Theta^{XXZ}(\lambda - \lambda'), \tag{3.11}$$

with $p(\lambda)$ the momentum of the magnon.[4] On a finite chain, the allowed rapidities are quantized, similarly to the momenta of non-interacting models. However, the interactions couple the rapidities through the highly non-linear Bethe equations [151], which explicitly depend on Θ. Being non-linear, the Bethe equations are difficult to solve. In the zero density limit, where the size of the system $L \to \infty$ while keeping the particle number N fixed, the solutions of the Bethe equations form groups of rapidities sharing the same real part, but shifted in the imaginary direction. These special solutions are called strings and are determined by the zeroes and poles of the scattering matrix $e^{i\Theta(\lambda,\lambda')}$ [151] and are readily interpreted as bound states of magnons. Since the factor $e^{il(p(\lambda)-p(\lambda'))}$ does not have zeroes or poles, in the AB scattering matrix these are entirely determined by the XXZ scattering matrix. Hence the two models share the same pattern of strings.

Strings in unconstrained and constrained XXZ chains

As stated above, strings can be identified as solutions of the Bethe equations in the zero-density limit. The string hypothesis [151], however, claims the persistence of strings even in the thermodynamic limit ($L \to \infty$, $N/L = n$ fixed). Within the Thermodynamic Bethe Ansatz (TBA) approach [151], one opts for a coarse-grained description of the Bethe equations, defining the so called root densities $\rho_j(\lambda)$, one for each string, where λ parametrizes the (real) center of the string. Then, $L\rho_j(\lambda)\,\mathrm{d}\lambda$ is interpreted as the number of solutions of the j^{th} string within the interval $[\lambda, \lambda + \mathrm{d}\lambda]$. The interactions affect the occupancy, hence the need of introducing the total root density $\rho_j^t(\lambda) \geq \rho_j(\lambda)$ representing full occupancy. The root densities fully determine the equilibrium thermodynamics and homogeneous non-equilibrium steady states [160, 170, 171].

Since the AB and XXZ models are closely related, it is worth to address properly the string hypothesis in the latter. The string classification in the XXZ chain [151] is recapped in Appendix C.1. The structure of XXZ strings greatly depends on the parameter Δ: in particular, for $|\Delta| \geq 1$ the string hypothesis, strictly speaking, does not cover the entire phase space. The thermodynamics of the strings built on the all-spin-up reference state covers only states up to half filling $0 < n < 1/2$, with n being the density of flipped spins. In the XXZ model, one circumvents this limitation by using the reflection symmetry $S_j^z \to -S_j^z$ and building the string hypothesis on the symmetric all-spin-down reference state. The two descriptions together cover the whole phase space and, in addition to the root densities, one introduces the magnetization sign $\mathfrak{f} = \pm 1$ to specify the sector. In the case $|\Delta| < 1$, the string hypothesis covers all magnetization sectors and $\mathfrak{f}$ is not needed.

---

[3] The scattering matrix is given by $S(\lambda, \lambda') = e^{i\Theta(\lambda,\lambda')}$.

[4] We point out that the relation resembles the celebrated $T\bar{T}$ deformation, see [163–169] and references therein.

In the AB model the constraint shifts the half-filling point to the value $1/(2+l)$ and, moreover, it breaks the spin reflection symmetry. In Ref. [126] the Bethe equations of the AB model in all sectors have been mapped onto the corresponding equations for the XXZ chain in a reduced magnetization-dependent volume. This approach is reviewed in Appendix C.2. Building on these ideas, one can determine the thermodynamics of the AB model at a generic filling, which is described by the same set of root densities as the XXZ spin chain. For the reasons just explained, above half filling these cannot be interpreted as strings anymore. However, for the sake of retaining a standard notation, we will still refer to these root densities as strings. In addition, for $|\Delta| > 1$ one needs an extra bit of information $\mathfrak{f} = \pm 1$ that distinguishes the regions below and above half filling, respectively.

When addressing thermodynamics and transport, it is crucial to know the amount of magnetization carried by each string. Within the ordinary string hypothesis, this is simply the number of magnons belonging to the same bound state. In the XXZ case, one has

$$m_j^{XXZ} = \mathfrak{f} |m_j^{XXZ}|, \tag{3.12}$$

with $|m_j^{XXZ}|$ a $\mathfrak{f}-$independent integer. On the other hand, in the AB model we find an explicitly $\mathfrak{f}-$dependent magnetization

$$m_j = [1 + l(1-\mathfrak{f})/2]^{-1} m_j^{XXZ}. \tag{3.13}$$

We observe that for $\mathfrak{f} = -1$ (needed if $|\Delta| > 1$) the string magnetization m_j becomes fractional! This signals the lack of microscopic interpretation of the root density as a bound state of magnons. The non-trivial $\mathfrak{f}-$dependence extends from the magnetization to thermodynamic observables. To see that we consider the TBA string scattering phase $\Theta_{j,j'}(\lambda, \lambda')$ that, whenever the string hypothesis holds, is obtained from $\Theta(\lambda, \lambda')$ summing over the constituents of the string [151]. In all sectors it can be written as

$$\Theta_{j,j'}(\lambda, \lambda') = l\, p_j(\lambda) m_{j'} - l\, m_j p_{j'}(\lambda') + \Theta_{j,j'}^{XXZ}(\lambda - \lambda')\,. \tag{3.14}$$

The appearance of the magnetization m_j makes $\Theta_{j,j'}$ explicitly $\mathfrak{f}-$dependent. In addition, $\mathfrak{f}$ renormalizes the total root density

$$2\pi \sigma_j \rho_j^t = (\partial_\lambda p_j)^{\mathrm{dr}} (1 + l(1-\mathfrak{f})/2)^{-1}, \tag{3.15}$$

where σ_j is the string parity and the standard definition of dressing is

$$(\partial_\lambda p_j)^{\mathrm{dr}} = \partial_\lambda p_j - \sum_{j'} \int \frac{\mathrm{d}\lambda}{2\pi} \partial_\lambda \Theta_{j,j'}(\lambda, \lambda') \vartheta_{j'}(\lambda') \sigma_{j'} (\partial_{\lambda'} p_{j'})^{\mathrm{dr}}, \tag{3.16}$$

with $\vartheta_j = \rho_j/\rho_j^t$ being the filling fraction. With these caveats, one can recover the full equilibrium thermodynamics by standard methods and move on towards discussing hydrodynamics.

Hydrodynamics of the AB model

Let us imagine that the system, still governed by the homogeneous AB Hamiltonian, features a long wavelength inhomogeneity in the state. In the limit of weak inhomogeneities, one can invoke local relaxation to weakly space-time dependent root densities. This is the idea behind the Generalized Hydrodynamics (GHD) [172, 173], which in its simplest form describes the convective expansion of particles

$$\partial_t \rho_j(\lambda) + \partial_x [v_j^{\mathrm{eff}}(\lambda) \rho_j(\lambda)] = 0 \tag{3.17}$$

or, equivalently,

$$\partial_t \vartheta_j(\lambda) + v_j^{\mathrm{eff}}(\lambda) \partial_x \vartheta_j(\lambda) = 0 \tag{3.18}$$

with $\vartheta_j = \rho_j/\rho_j^t$ being called the filling fraction.[5] The effective velocity

$$v_j^{\mathrm{eff}}(\lambda) = (\partial_\lambda \epsilon_j(\lambda))^{\mathrm{dr}} / (2\pi \sigma_j \rho_j^t(\lambda)), \tag{3.19}$$

depends on the state due to interactions, making the equation non-linear. Above, ϵ_j is the energy carried by the string. It is worth mentioning that, in contrast to the AB model, in most integrable systems the identity

$$2\pi \sigma_j \rho_j^t = (\partial_\lambda p_j)^{\mathrm{dr}} \tag{3.20}$$

holds, leading to the alternative more intuitive definition

$$v_j^{\mathrm{eff}}(\lambda) = (\partial_\lambda \epsilon_j)^{\mathrm{dr}} / (\partial_\lambda p_j)^{\mathrm{dr}} \tag{3.21}$$

that was originally reported in Refs. [172, 173]. However, in a recent rigorous proof [174–176], Eq. (3.19) naturally emerges from the calculations. To the extent of our knowledge, this is the only model with this feature. In the case with $|\Delta| > 1$, the continuity equation $\partial_t n + \partial_x j_n = 0$, with

$$n = (1 - \mathfrak{f})/(2 + l(1 - \mathfrak{f}))^{-1} + \sum_j \int \mathrm{d}\lambda m_j \rho_j(\lambda) \tag{3.22}$$

and

$$j_n = \sum_j \int \mathrm{d}\lambda v_j^{\mathrm{eff}}(\lambda) m_j \rho_j(\lambda), \tag{3.23}$$

closes the hydrodynamic equations giving a further condition on $\mathfrak{f}$, similarly to the XXZ model [177].

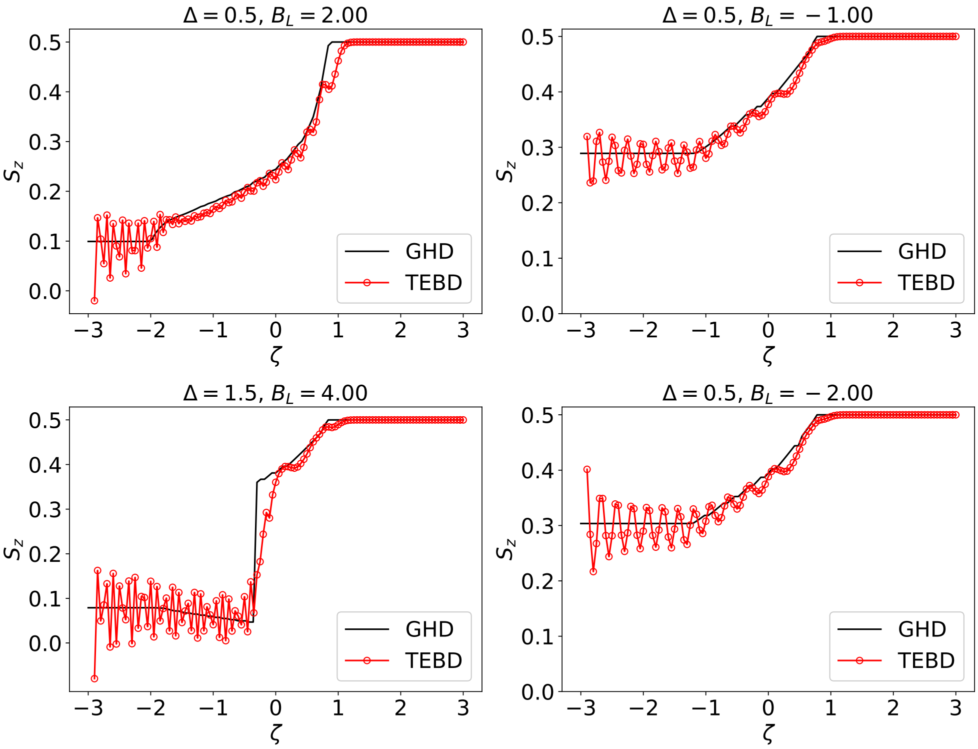

Figure 3.1: Comparison between TEBD numerical simulations of partitioning protocols in the Alcaraz Bariev and the exact hydrodynamic solution. We initialize the state in two halves $|\mathrm{GS}_{\langle Z\rangle}\rangle \otimes |\downarrow\downarrow\downarrow\ldots\rangle$ with $|\mathrm{GS}_{\langle Z\rangle}$ the ground state at fixed magnetization. In practice, $|\mathrm{GS}_{\langle Z\rangle}\rangle$ can be obtained by applying an external magnetic field in the z direction (B_L in the figure). The same method is used also to obtain the desired matrix product state state in the microscopic simulations. Notice the sharp jump for $\Delta = 1.5$, since states above and below half filling are connected.

The partitioning protocol

Transport is best studied by defining a partition protocol, that prescribes how the left and right halves of a chain are initialized. Time evolution of this inhomogeneous initial state probes important properties of the system, showing for instance that integrable systems exhibit ballistic transport. The partitioning protocol is best addressed by means of the hydrodynamic equations in the form (3.18). In this protocol, the two halves are initialized in two homogeneous states

$$\vartheta_j(\lambda)\Big|_{t=0,x} = \theta(x)[\vartheta_j(\lambda)]_R + \theta(-x)[\vartheta_j(\lambda)]_L \tag{3.24}$$

with $\theta(x)$ the Heaviside theta function $\theta(x > 0) = 1$ and zero otherwise. The left and right fillings $[\vartheta_j(\lambda)]_{L,R}$ are the initial conditions and must be given as an input. In our case, we probed filling fractions belonging to a class of thermal states. Due to the appearance of only first derivatives in the hydrodynamic equation, signaling

---

[5] The equivalence between (3.17) and (3.18) is non trivial.

the ballistic transport, the solution of Eq. (3.18) with these initial condition is scale-invariant. Namely, for $t > 0$ the filling is not an independent function of time and space, but a function of their ratio. We define the ray $\zeta = x/t$ and Eq. (3.18) admits the solution [172, 173]

$$\vartheta_j(\lambda) = \theta(\zeta - v_j^{\text{eff}}(\lambda))[\vartheta_j(\lambda)]_R + \theta(v_j^{\text{eff}}(\lambda) - \zeta)[\vartheta_j(\lambda)]_L \tag{3.25}$$

where the $\zeta-$dependence of $v_j^{\text{eff}}(\lambda)$ is left implicit. Since v^{eff} depends on the state through the dressing, the above solution is only implicit and cannot be further analytically simplified. However, very simple recursive numerical schemes guarantee fast convergence: first, one finds an initial Ansatz for $\vartheta_j(\lambda)$ ignoring the dressing in the effective velocities in Eq. (3.25). Then, the filling fraction is used to recalculate v^{eff} and the procedure is iterated until convergence is reached, which usually happens after only few steps. In the case where the two halves are initialized in opposite magnetic sectors, one must supplement Eq. (3.25) with the proper equation for the sign $\mathfrak{f}$ [177]. Imposing spin conservation $\partial_t n + \partial_x j_n = 0$ in the scaling form, one readily obtains an equation similar to (3.25)

$$\mathfrak{f} = \theta(\zeta - \bar{v})\mathfrak{f}_R + \theta(\bar{v} - \zeta)\mathfrak{f}_L \tag{3.26}$$

with $\mathfrak{f}_{R,L}$ set by the initial conditions and

$$\bar{v} = \left(\sum_j \int \mathrm{d}\lambda\, m_j v_j^{\text{eff}}(\lambda)\rho_j(\lambda)\right)\left(\frac{1}{2+l} - \sum_j \int \mathrm{d}\lambda m_j \rho_j(\lambda)\right)^{-1}. \tag{3.27}$$

In Fig. 3.1 we provide checks of the hydrodynamic solution against the TEBD numerical simulation of the Alcaraz-Bariev model, finding excellent agreement as expected. To this purpose, one adopts a partitioning protocol where the right half of the chain is initialized to the ferromagnetic state $|\uparrow\uparrow\uparrow\dots\rangle$ while the left half is in a state where the filling of magnons is either below or above one half. This is done both for $\Delta < 1$ and $\Delta > 1$. In the latter case, when sectors below and above half filing are connected, the profile at large times exhibits a sharp jump. This is readily understood: at $t = 0$, the $\mathfrak{f}(x)$ profile is a step function and due to discreteness of $\mathfrak{f}$, GHD cannot smoothen its profile, but will only move the position of the jump.[6]

Further examples of the validity of the GHD solution are provided in section 3.3, where the Alcaraz-Bariev model emerges as effective theory for an integrable sector of the Ising model in a weakly tilted field.

3.2 Constrained XXZ chain from $\mathbb{Z}_2$ lattice gauge theories

The aim of this section is to give an account of how the Alcaraz-Bariev model emerges naturally in the context of $\mathbb{Z}_2$ lattice gauge theories. The bulk of the work was already done in section 2.2.3, where we have shown how the AB model can be obtained as the large h limit of the $\mathbb{Z}_2$ LGT with Hamiltonian

---

[6] A similar behavior is observed in the magnetization of the XXZ chain [177], but in the AB model $\mathfrak{f}$ affects the whole set of TBA equations. As a result, non-analyticity is found also in the profiles of other conserved charges.

$$H = -t \sum_i \left(c_i^\dagger \sigma^z_{i+\frac{1}{2}} c_{i+1} + h.c. \right) - h \sum_i \sigma^x_{i+\frac{1}{2}}, \tag{3.28}$$

in the "even" Gauss' law sector

$$\sigma^x_{i-\frac{1}{2}} (-1)^n \sigma^x_{i+\frac{1}{2}} = 1. \tag{3.29}$$

The AB model (3.1) appears by applying second order perturbation theory at large h to the sector of the model that consists of isolated mesons only. Physically, this effective theory captures the physics of particles (magnons) corresponding to length-one dimers in the microscopic theory. As a result of Pauli's principle, the dimers are hardcore bosons which are also not allowed to occupy neighboring sites: the effective theory in this regime therefore has a constrained Hilbert space. Adopting the usual identification of hardcore bosonic particles with magnons[7], we obtain as an effective model the Hamiltonian (3.1) with $\Delta = 1$, with an overall prefactor t^2/h that sets the energy scale.

3.2.1 AB model from constrained hole dynamics at large h

It is instructive to see how the same result can be obtained from the theory describing the behavior of holes in the model (3.28). While this does not lead to new physics[8], it gives insight into the correlated hopping of holes. This was first investigated by Bariev [178], who demonstrated its integrable nature which was explored further in [179–181]. To this purpose, we first define the dimer creation and annihilation operators in terms of the hole operators (2.26):

$$b^\dagger_{i+1/2} = h_i h_{i+1} \qquad b_{i+1/2} = -h_i^\dagger h_{i+1}^\dagger. \tag{3.30}$$

Dimers do not behave strictly like bosons because of the following commutation relation on neighboring sites:

$$[b_{i-1/2}, b^\dagger_{i+1/2}] = -h^\dagger_{i-1} h_{i+1}, \tag{3.31}$$

which indicates that the Hilbert space is constrained. Again, the reason is simply that since the dimers are made of single-component fermions, they cannot simultaneously occupy neighboring links. In the limit of strong string tension, the dynamics of holes in this sector is governed by the effective Hamiltonian

$$\mathcal{H}_{\text{eff}} = -t_{\text{eff}} \sum_i (h^\dagger_{i-1}(1 - n_i^h) h_{i+1} + \text{h.c.}) + U_{\text{eff}} \sum_i n_i^h n_{i+1}^h \tag{3.32}$$

with $U_{\text{eff}} = t^2/h = 2t_{\text{eff}}$. The correlated hopping term describes the fact that a hole always hops by two sites, which corresponds to the hopping of a dimer. By using the definitions above and the commutation relation (3.31), it is straightforward to show that the hopping term can be rewritten in terms of dimers as

---

[7] Here represented by spin-ups in a spin-down background.

[8] The hole description is complementary to the description in terms of particles.

$$H_{\text{hop}} = -t_{\text{eff}} \sum_i P_1 (b^\dagger_{i+1/2} b_{i-1/2} + \text{ h.c. }) P_1, \tag{3.33}$$

where P_1 denotes a projector that inhibits multiple dimer occupation of any link of the lattice and simultaneous occupation of dimers on neighbouring links.

As for the interaction term, we note that on a closed chain the number of the nearest-neighbour holes is complementary to the number of the next-to-nearest dimers. Given that, the nearest neighbour repulsion between the holes can be rewritten as the next-nearest neighbour repulsion between the dimers and we obtain once again the effective AB model with $l = 1$ and $\Delta = 1$.

3.2.2 Extended constraints from density-density repulsive interactions

The Hamiltonian (3.28) can be extended to include repulsive interactions between fermions. Starting with the case of nearest-neighbor interactions, we can write

$$H_1 = H_0 + V_1 \sum_i n^f_i n^f_{i+1} \tag{3.34}$$

where V_1 is a positive coefficient that, for our purposes, can be assumed to be of order t. In the large h limit such term gives a first order contribution to the next-nearest neighbor repulsion between dimers, that results directly from the repulsion between neighboring fermions belonging to different dimers. Therefore the strength of the repulsion is modified: $U_B \to U_B + V_1 \gg U_B$, since $V_1 \approx t \gg t^2/h$. In the AB language, one obtains a constrained XXZ chain with $\Delta \gg 1$. For generic l the maximum filling consistent with the constraint is $\rho_{max} = 1/(l+1)$. If $\rho < \rho_{half}$ the strong repulsion $\Delta \gg 1$ enforces energetically an extended next-nearest neighbor constraint, so that effectively one recovers an AB model with $l = 2$ and a next-to-next-nearest neighbor asymmetry $\Delta_2 = 0$. If $\rho > \rho_{half}$, on the other hand, this is not possible since the extended constraint is not compatible with the number of particles. An example of this is the upper left corner of the phase diagram in Fig. 2.8(a). There the repulsion is small enough to be in the perturbative regime, but it can still be tuned to large enough values compared to the emergent energy scale t^2/h. For this reason, the exponent governing the decay of dimer-dimer correlators is found to converge to the one of a AB model with $l = 2$ and $\Delta = 0$ as $h/t \to \infty$.

The argument can be easily extended to longer range repulsive interactions: the Hamiltonian

$$H_n = H_0 + V_1 \sum_i n^f_i n^f_{i+1} + V_2 \sum_i n^f_i n^f_{i+2} + \cdots + V_n \sum_i n^f_i n^f_{i+n} \tag{3.35}$$

has as large h limit an AB model with $l = n + 1$ and $\Delta_{n+1} = 0$, provided that the filling satisfies $\rho < \frac{1}{n+2}$ and all the interactions strengths $V_m \approx t$.

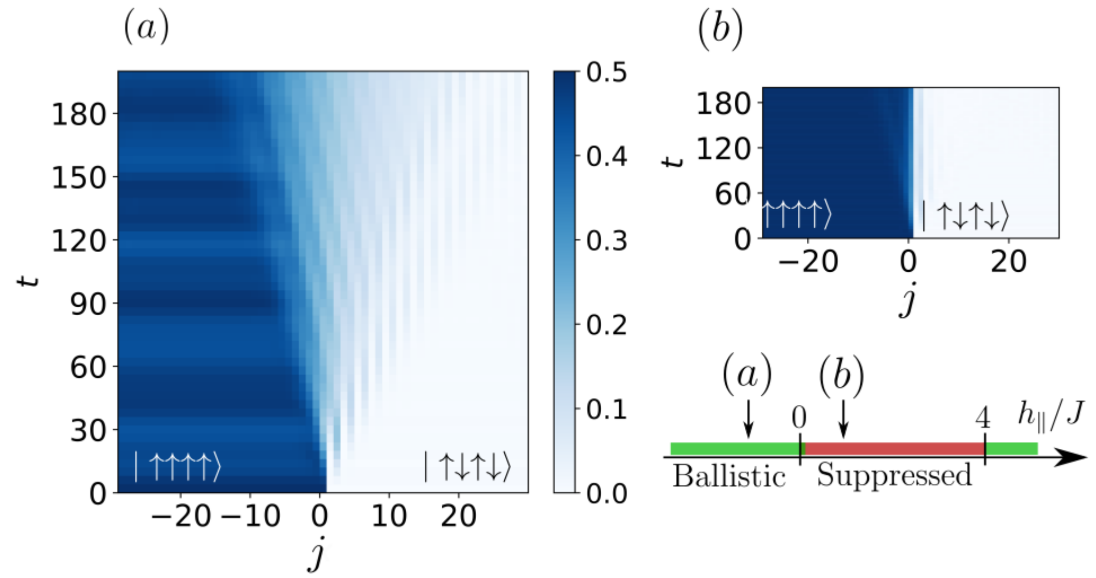

Figure 3.2: Magnetization profiles $\langle S_j^z \rangle$ in the Ising chain at $J = 1$ and $h_\perp = 0.2$ initialized by joining the ferromagnetic and Neel states. (a) For $h_\parallel = -0.7$ we observe ballistic transport with a characteristic lightcone. (b) For $h_\parallel = 0.7$ we find strong suppression of spin transport. TEBD simulations are done for a chain of length $L = 80$. The peculiar transport is captured by the emergent integrable dynamics governed by the Hamiltonian (3.52), see main text for discussion.

3.3 Constrained XXZ chain as a limit of the tilted-field Ising model

So far we have explored how constrained models can emerge from $\mathbb{Z}_2$ lattice gauge theories in the limit of large electric fields. Here we take a different path and show how the constrained XXZ chain appears in a different (although somewhat related) scenario, i.e. as a limit of the familiar Ising model in the presence of a longitudinal field.[9] This is at first sight surprising, since it is well known that the longitudinal field breaks the integrability of the TFIM, apparently in contrast with the emergence of an integrable sector described by the Alcaraz-Bariev model. Evidence for this unexpected behavior comes from a direct numerical inspection of the model. With the help of Time Evolving Block Decimation (TEBD) [183, 184], one can investigate transport in the Ising chain in a tilted magnetic field, which is described by the Hamiltonian

$$H = -J \sum_i Z_i Z_{i+1} - h_\parallel \sum_i Z_i - h_\perp \sum_i X_i, \tag{3.36}$$

---

[9] This can be related to $\mathbb{Z}_2$ LGT in two inequivalent ways. Firstly, as shown in Chapter 5, a local mapping transforms the gauged Kitaev chain studied in section 2.3 into a TLFI model. Secondly, the Ising model can be reformulated as a gauge theory by artificially extending its Hilbert space and imposing a Gauss law [182]. For the sake of simplicity, we will not indulge on this perspective any further.

where X_i and Z_i denote the Pauli matrices at site i. To study transport, we adopt a partitioning protocol [185] where one initializes the state in two different halves $|\Psi\rangle = |\Psi_L\rangle \otimes |\Psi_R\rangle$ and then lets the system evolve with the homogeneous Hamiltonian. To obtain the results displayed in Fig. 3.2 (a) $|\Psi_L\rangle$ and $|\Psi_R\rangle$ are chosen to be the Neel and ferromagnetic state respectively, and we focus on the regime where the transverse field is weak. While the Hamiltonian (3.36) is known to be non-integrable for generic values of the parameters, our analysis unveils persistent ballistic transport typical of integrable models [172, 173], in contrast with the naively expected diffusion. With this choice of initial states, it is also evident how transport strongly depends on the longitudinal field and the Ising coupling, with a lightcone suppression whenever $0 < h_{\parallel}/J < 4$, as displayed in Fig. 3.2 (b). As we will see in the following, this can be ascribed to the appearance of a peculiar integrable model.

3.3.1 Effective Hamiltonian from perturbation theory

In order to gain an analytical understanding of the bizarre phenomenology displayed above, let us consider the Ising chain (3.36) in the regime where the transverse field $h_\perp$ is much smaller than the two generic (but incommensurate) couplings J and $h_\parallel$. To set up a perturbative expansion, the Hamiltonian (3.36) is split into the classical Z-dependent part H_0 (the Ising and longitudinal field terms) and the transverse field perturbation. Since $[H_0, Z_i] = 0$, the Hamiltonian H_0 has an extensive number of symmetries and trivially splits in the Z-basis into 2^L independent blocks. Notwithstanding, its energy spectrum is organized into degenerate multiplets characterized only by a pair of emergent $U(1)$ quantum charges: the magnon number

$$N = \sum_i \frac{1 - Z_i}{2}. \tag{3.37}$$

and the domain wall number

$$D = \sum_i \frac{1 - Z_i Z_{i+1}}{2}. \tag{3.38}$$

By construction, N and D are both simultaneously preserved by the effective perturbative dynamics. The transverse field perturbation changes the number of magnons and, as we will verify explicitly, can contribute only at even orders of the degenerate perturbation theory.

Computation of the effective Hamiltonian

Employing the Schrieffer-Wolff transformation [125, 186] we now construct the second-order effective perturbative Hamiltonian. While H_0 trivially preserves the number of magnons N and the number of domain walls D, the perturbation $V = -h_\perp \sum_i X_i$ changes them. We eliminate transitions that do not conserve N and D order by order in $h_\perp$ by performing a unitary transformation of the

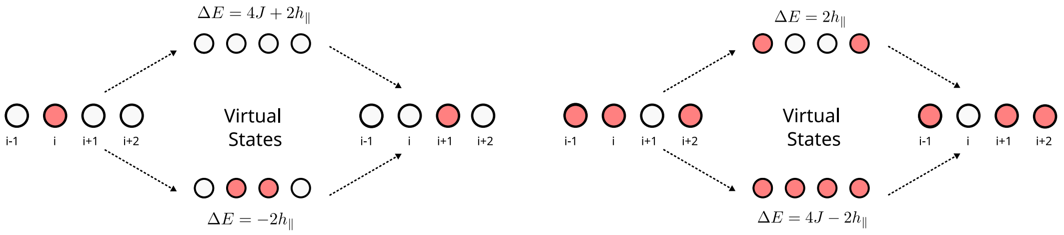
$\Delta E = 4J + 2h_{\parallel}$
Virtual States
$\Delta E = -2h_{\parallel}$
i-1
i
i+1
i+2
$\Delta E = 2h_{\parallel}$
Virtual States
$\Delta E = 4J - 2h_{\parallel}$

Figure 3.3: Virtual second-order processes that give rise to the nearest-neighbor spin exchange. To ensure domain wall conservation, magnons can hop only if the surrounding sites are both empty (left) or both occupied (right).

Hamiltonian

$$H_{eff} = e^{S} H e^{-S} = H + [S, H] + \frac{1}{2}[S,[S,H]] + \dots, \tag{3.39}$$

where the anti-Hermitian operator S is organized in the power series $S = \sum_{n=1}^{\infty} S^{(n)}$ in the transverse field coupling $h_{\perp}$. As a result, the expansion of the effective Hamiltonian in $h_{\perp}$ reads

$$H_{eff} = H_0 + \underbrace{\left([S^{(1)}, H_0] + V\right)}_{H^{(1)}_{eff}} + \underbrace{\left([S^{(2)}, H_0] + [S^{(1)}, V] + \frac{1}{2}[S^{(1)},[S^{(1)}, H_0]]\right)}_{H^{(2)}_{eff}} + \dots . \tag{3.40}$$

Now the terms $S^{(n)}$ are chosen such that up to the n-th order in the perturbation coupling $h_{\perp}$ the effective Hamiltonian operates exclusively within the degenerate subspaces of the Hamiltonian H_0. Mathematically, one has

$$[H^{(n)}_{eff}, \mathcal{P}_{N,D}] = 0, \tag{3.41}$$

i.e. the n^{th} order contribution to effective Hamiltonian $H^{(n)}_{eff}$ commutes with every operator $\mathcal{P}_{N,D}$ that projects on the Hilbert subspace with N magnons and D domain walls. Since V changes the number of magnons, it is purely off-diagonal. Hence, the linear order Hamiltonian $H^{(1)}_{eff}$ vanishes

$$H^{(1)}_{eff} = \mathcal{P}_{N,D} V \mathcal{P}_{N,D} = 0. \tag{3.42}$$

To quadratic order, the effective Hamiltonian is

$$\begin{aligned} H^{(2)}_{eff} &= \mathcal{P}_{N,D}\left(\left[S^{(1)}, V\right] + \frac{1}{2}\left[S^{(1)}, \left[S^{(1)}, H_0\right]\right]\right)\mathcal{P}_{N,D} \\ &= \mathcal{P}_{N,D} V \frac{1 - \mathcal{P}_{N,D}}{E^{(0)}_{N,D} - H_0} V \mathcal{P}_{N,D}, \end{aligned} \tag{3.43}$$

where $E^{(0)}_{N,D}$ is the unperturbed energy of the degenerate manifold with N magnons and D domain walls. As illustrated in Fig. 3.3, at second order in $h_{\perp}$, a nearest-

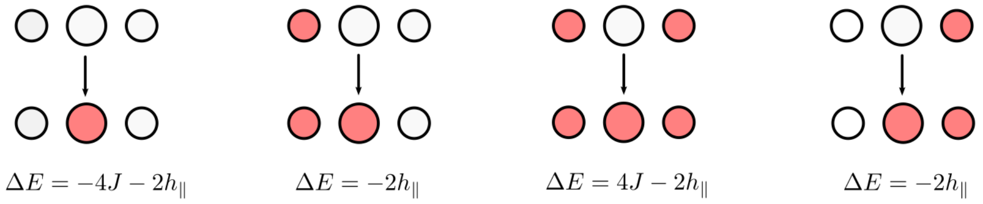
$\Delta E = -4J - 2h_\parallel$
$\Delta E = -2h_\parallel$
$\Delta E = 4J - 2h_\parallel$
$\Delta E = -2h_\parallel$

Figure 3.4: After flipping the middle spin from up to down, a virtual state is obtained whose energy differs by ΔE from the energy of the original configuration.

neighbor spin-exchange term is generated

$$\begin{aligned} H^{(2)}_{eff,se} = &-\frac{h_\perp^2 J}{h_\parallel(h_\parallel + 2J)} \sum_j \mathcal{P}^+_{j-1,j+2} \left(S^+_j S^-_{j+1} + h.c.\right) \\ &- \frac{h_\perp^2 J}{h_\parallel(h_\parallel - 2J)} \sum_j \mathcal{P}^-_{j-1,j+2} \left(S^+_j S^-_{j+1} + h.c.\right) \end{aligned} \tag{3.44}$$

where $S^\pm_j = (X_j \pm iY_j)/2$ is the creation/annihilation spin 1/2 operator on the site j. The operators

$$\mathcal{P}^\pm_{i,j} = \frac{1 \pm (Z_i + Z_j) + Z_i Z_j}{4} \tag{3.45}$$

are projectors on spin up-up and down-down pair states, respectively. Notably, any longer-range spin exchange vanishes because all virtual processes exactly cancel each other in that case. By taking a closer look at Eq. (3.44), one realizes that domain wall conservation enforces a peculiar form of the nearest-neighbor exchange term. This involves a projector which ensures that the two outer spins (surrounding the hopping pair) point in the same direction. Similar type of hopping have been discussed in [179–181, 187].

Having established the form of the spin exchange, we now turn to the interaction terms. To this end, we take into account all second-order processes where first a spin is flipped by the perturbation $V = -h_\perp \sum_i X_i$ and next the very same spin is flipped back again. The energy of the intermediate virtual state depends on the two surrounding spins, as illustrated in Fig. 3.4. We find that all these processes generate the following effective Hamiltonian

$$H^{(2)}_{eff,int} = -\frac{h_\perp^2 J^2}{h_\parallel \alpha} \sum_j Z_{j-1} Z_j Z_{j+1} + \frac{h_\perp^2 J}{\alpha} \sum_j Z_j Z_{j+1} - \frac{h_\perp^2 (h_\parallel^2 - 2J^2)}{2 h_\parallel \alpha} \sum_j Z_j, \tag{3.46}$$

where $\alpha = h_\parallel^2 - 4J^2$. We observe that a three-spin interaction term is generated by the second-order perturbation theory. Moreover, the Ising and longitudinal terms, present in the unperturbed Hamiltonian H_0, acquire small perturbative shifts.

Putting now the spin-exchange (3.44) and the interaction (3.46) contributions together, we arrive at the complete second-order Hamiltonian

$$\begin{aligned} H^{(2)}_{eff} = &- \sum_{s=\pm 1} t_s \sum_j \mathcal{P}^s_{j-1,j+2} \left(S^+_j S^-_{j+1} + h.c. \right) \\ &- g \sum_j Z_{j-1} Z_j Z_{j+1} - \delta J \sum_j Z_j Z_{j+1} - \delta h_\parallel \sum_j Z_j, \end{aligned} \tag{3.47}$$

where we have defined the spin-exchange coupling

$$t_s = \frac{h_\perp^2 h_\parallel^{-1} J}{h_\parallel + 2sJ}, \tag{3.48}$$

the induced three-spin coupling

$$g = \frac{h_\perp^2 h_\parallel^{-1} J^2}{\alpha} \tag{3.49}$$

and the shifts of the Ising and longitudinal couplings

$$\delta J = -\frac{h_\perp^2 J}{\alpha} \qquad \delta h_\parallel = \frac{h_\perp^2 h_\parallel^{-1} (h_\parallel^2 - 2J^2)}{2\alpha} \quad . \tag{3.50}$$

with $\alpha = h_\parallel^2 - 4J^2$. This effective Hamiltonian agrees with a previous derivation [188], while related studied are contained in [187, 189].

Corrections beyond second order

Having established a complete effective model at second order in perturbation theory, it is now natural to wonder what is left behind by not including higher order corrections. While these additional terms can be explicitly computed by moving to the next order in the Schrieffer-Wolff transformation, the calculation is lengthy and beyond the scope of this analysis. Hence, we limit ourselves to characterize the scaling. As already mentioned the perturbation induced by the transverse field changes the number of magnons, hence only even orders in the perturbation theory can contribute. Therefore, the next-to-leading order correction to the effective Hamiltonian scales as $\mathcal{O}(h_\perp^4)$. Furthermore, additional contributions emerge due to the fact that the spin degrees of freedom appearing in Eq.(3.46) are in the Schriffer-Wolff rotated basis. Rotating back to the original spin degrees of freedom, the Pauli matrices get $\propto h_\perp^2$ corrections which ultimately result in further $\mathcal{O}(h_\perp^4)$ corrections to Eq. (3.46). Given that, at short times, generic observables acquire corrections that grow linearly in time $\mathcal{O}(t h_\perp^4)$. However, notice that as $h_\perp$ is taken smaller, also the overall energy scale of the effective model is reduced as $h_\perp^2$. Therefore, for practical purposes one wishes to express the corrections in the limit of small $h_\perp$, while keeping constant the timescale in energy-units of the effective model

$$t_{eff} = \mathcal{J} t \propto t h_\perp^2, \qquad \mathcal{J} = \frac{2 h_\perp^2 h_\parallel^{-1} J}{h_\parallel + 2J}. \tag{3.51}$$

Following this reasoning, corrections beyond the second order approximation are expected to scale as $\mathcal{O}(t_{eff}\, h_\perp^2)$ at small times, as we indeed observe in Fig. 3.5.

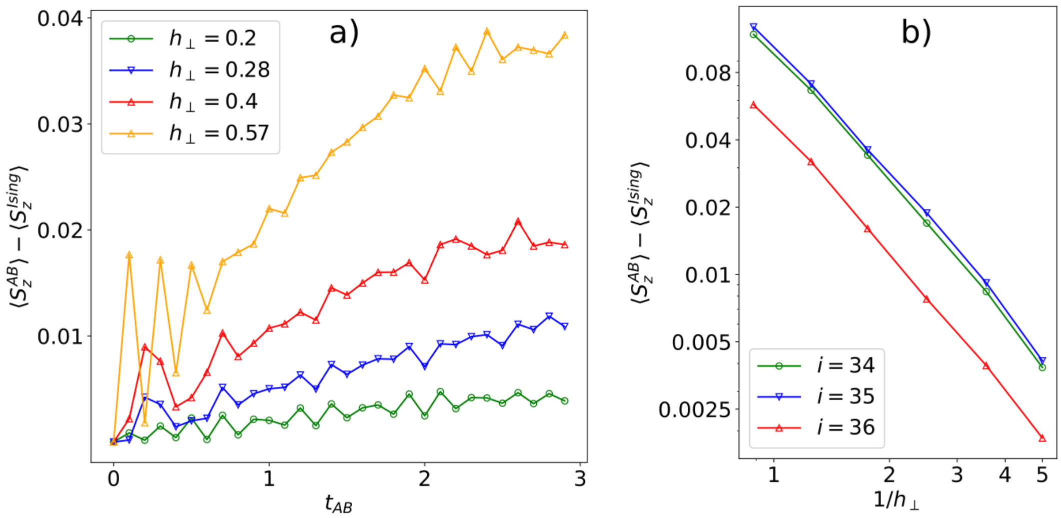

Figure 3.5: We analyze systematically the discrepancy between the Ising model and the effective Alcaraz-Bariev Hamiltonian derived with second order perturbation theory. For this purpose, we consider a partitioning protocol on a chain of 80 sites, where the first half of the chain $1 \leq i \leq 40$ is initialized in a Neel state, while the rest $40 < i \leq 80$ is in a fully polarized state. (a) At site $i = 36$ (i.e. four sites left of the junction), the discrepancy in $\langle S_z \rangle$ between the Alcaraz-Bariev and Ising prediction grows approximately linearly on the Alcaraz-Bariev time scale t_{AB}. Similar behavior is observed at other sites on the chain. (b) At fixed value of the AB time $t_{AB} = 3$, we study the convergence in $h_\perp$ at different points of the chain in the proximity of the junction. We show that the magnetization $\langle S_z \rangle$ converges as a power-law in $h_\perp$ to the value predicted by the effective AB model. A fit of the deviation is compatible with the expected $\propto h_\perp^2$ behavior.

3.3.2 Integrable transport of isolated magnons

Up to this point we were able to derive an effective Hamiltonian that governs the behaviour of the system for small values of the transverse coupling $h_\perp$. This model, however, is generically non integrable and cannot yet explain the ballistic transport observed numerically.

Since both D and N are conserved by the perturbative dynamics, however, we can consider a sector with N isolated magnons in the spin-up background. In this case D is fixed to $2N$ and pairs of magnons cannot appear next to each other. The spin exchange term then acquires the more familiar form $S_j^x S_{j+1}^x + S_j^y S_{j+1}^y$, but with the inclusion of a projector $\mathcal{P}_1$ that enforces the constraint. As for the three-spins term in Eq. (3.47), it gives an energy shift to configurations where magnons are only one site apart form each other and can therefore be written as a NNN interaction $S_{i-1}^z S_{i+1}^z$.

With this considerations in mind, the second-order Hamiltonian (3.47) in this

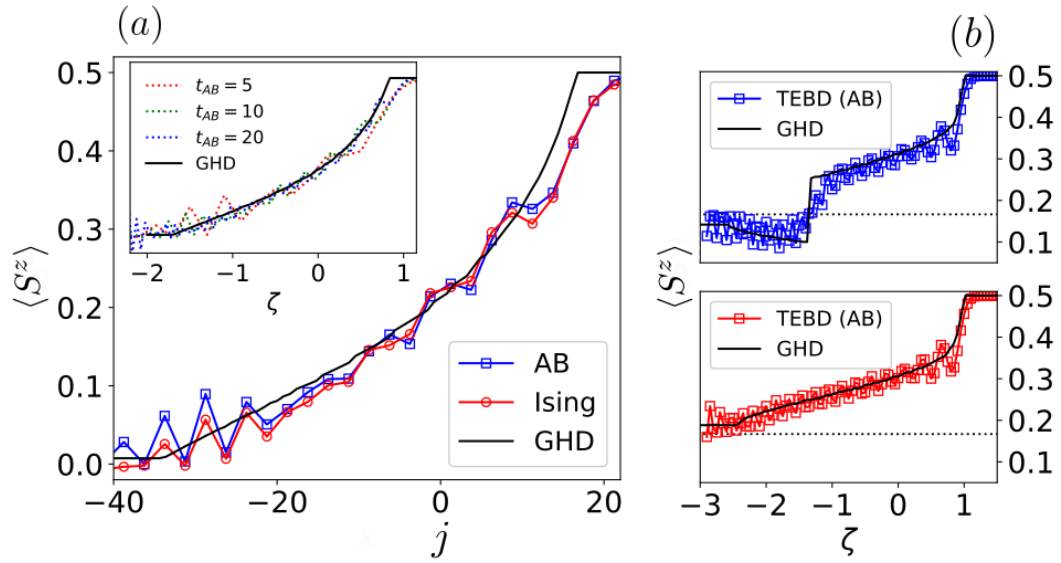

Figure 3.6: (a) The magnetization profile of a chain of length $L = 80$ evolved with TEBD from $|\text{Neel}\rangle \otimes |\text{ferro}\rangle$ at large time (measured in the AB units $[\mathcal{J}^{-1}]$) $t_{\text{AB}} = 20$ approaches the GHD prediction. For the Ising model we choose parameters $h_\perp = 0.5$, $h_\parallel = 6$ and $J = 1$, corresponding to $\Delta = 0.5$ in the AB model. In the inset, we show the collapse of the AB simulations on the GHD analytical prediction. (b) To highlight magnetization jumps in $|\Delta| > 1$ (precisely, $\Delta = 1.5, \mathcal{J} = -1$), we consider the partitioning from $|\text{GS}_{\langle Z\rangle}\rangle \otimes |\text{ferro}\rangle$ with $|\text{GS}_{\langle Z\rangle}\rangle$ the ground state of the AB model in the sector at fixed magnetization $\langle Z\rangle$ for a chain of length $L = 120$. For the left-side magnetization being below (top) and above (bottom) the half-filling dotted line, the profile exhibits qualitatively different behaviour.

sector reduces to

$$H^{(2)}_{eff} \to -\mathcal{J} \sum_j \mathcal{P}_1 \left(S^x_j S^x_{j+1} + S^y_j S^y_{j+1} + \Delta S^z_j S^z_{j+2} \right) \mathcal{P}_1, \tag{3.52}$$

where the projector $\mathcal{P}_1$ prohibits two spin-down magnons to occupy neighbouring sites. As promised at the beginning of this section, Eq. (3.52) is once again the Alcaraz-Bariev model, this time emerging as an integrable limit of the tilted field Ising chain. This of course explains the ballistic transport observed in Fig. 3.2. We note that while in the AB models derived in section 3.2 the anisotropy was strictly fixed by the parameters of the original models, here it can be tuned by changing the dimensionless ratio $h_\parallel / J^{10}$:

$$\Delta = \frac{2J}{h_\parallel - 2J}. \tag{3.53}$$

The inverse of the coupling $\mathcal{J} = 2t_+$, on the other hand, defines the slow time scale associated with hopping of the isolated magnons.

---

[10] Provided that the perturbative regime is not abandoned.

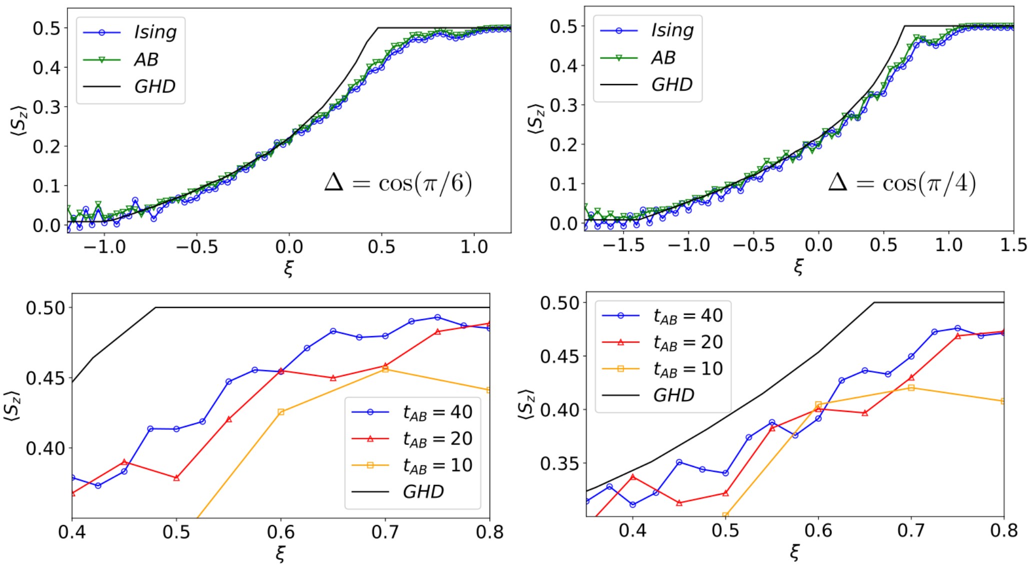

Figure 3.7: Here we provide further evidence that the Alcaraz-Bariev model gives an effective description of the Ising model in the limit of weak transverse field. Due to its integrability, at large times we can compare expectation values of observables to the ones predicted by the Generalized Hydrodynamics. We consider partitioning protocols where the left half is initialized in the Neel state, while the right half is a fully polarized state. We consider two different values of the AB interaction parameter Δ. In the upper panels, we show that the expectation values $\langle S_z \rangle$ at a large time $t_{AB} = 30$ in the Ising and AB models match with very good agreement for $h_\perp = 0.5$, and approach the GHD curve. A deviation from the hydrodynamic prediction is evident, but this is a finite-time effect. In the lower panels, we zoom on the region where the mismatch is more evident and show that for large times the curves slowly converge to the GHD (only the AB prediction is shown).

In section 3.1.2 we reviewed how the problem of transport in the Alcaraz-Bariev model is solved by means of the generalized hydrodynamics (GHD). After a short transient the profile of local observables becomes scale-invariant [172, 173], i.e.

$$\langle \mathcal{O}(t, x) \rangle = F[x/t]$$

and curves at different times collapse when plotted as a function of the ray $\zeta = x/t$. In general, if one starts from an initial state with only isolated magnons the Ising chain agrees with the underlying AB description (up to a time scale $t \sim h_\perp^{-4}$) and supports ballistic transport. Whenever the initial root density of the two halves is known, GHD provides an exact solution of the partitioning protocol as explained in section 3.1.2. Further evidence of the validity of our analysis is presented in figures 3.6 and 3.7, where the magnetization $\langle S_z \rangle$ is computed at large times for different values of the microscopic parameters and compared with the effective description and with the GHD solution.

For $|\Delta| \geq 1$, i.e. $0 \leq h_\parallel / J \leq 4$, the magnetization sign $\mathfrak{f}$ is responsible of sharp jumps whenever states from the two different magnetization sectors are joined. We

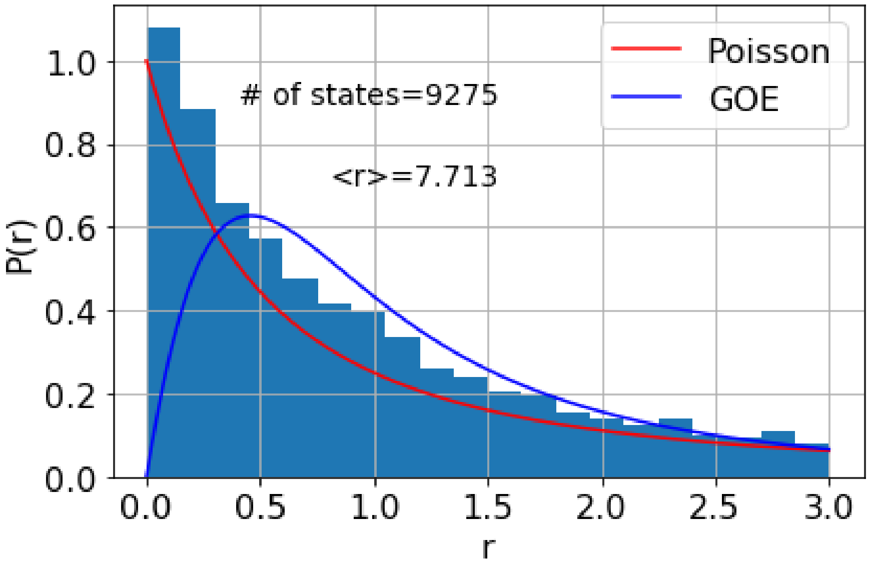

Figure 3.8: The distribution $P(r)$ of the ratios r of consecutive level spacings of the second-order effective Hamiltonian (3.47) in the sector with $N_m = 5$ isolated magnons on a closed chain of length $L = 40$ in the momentum sector with $k = 7 \times 2\pi/L$. The Ising couplings that fix all parameters of the effective model are $J = 1.17$, $h_{||} = 0.91$ and $h_{\perp} = 0.0291$.

provided a short explanation of this fact in section 3.1.2. An extreme example of this is precisely the one presented at the beginning of this section in Fig. 3.2(b): for $|\Delta| \geq 1$, the Neel state and the ferromagnetic states have the exactly same trivial root density $\rho_j(\lambda) = 0$, but differ in the sign of $\mathfrak{f}$. Hence, any smooth dependence of the profile is suppressed and only the jump, that is pinned at the origin, remains. In this case, transport is inhibited.

3.3.3 Beyond isolated magnons

While the focus of this chapter is on emergent integrable models, it is worth to take a small detour and explore sectors of the Hilbert space other than the one which contains isolated magnons exclusively. We first want to check that these are generically not integrable. This can be done explicitly by performing an energy levels statistics analysis [190, 191].

Level spacing statistics analysis

Let us start by showing how the method works for the integrable sector described in section 3.3.2. On a closed chain of length $L = 40$ we compute numerically the energy spectrum of the sector populated with $N_m = 5$ isolated magnons with momentum $k = 7 \times 2\pi/L$. Instead of looking directly at the energy level spacings, we follow ideas from [190, 191] and compute the ratios of consecutive level spacings

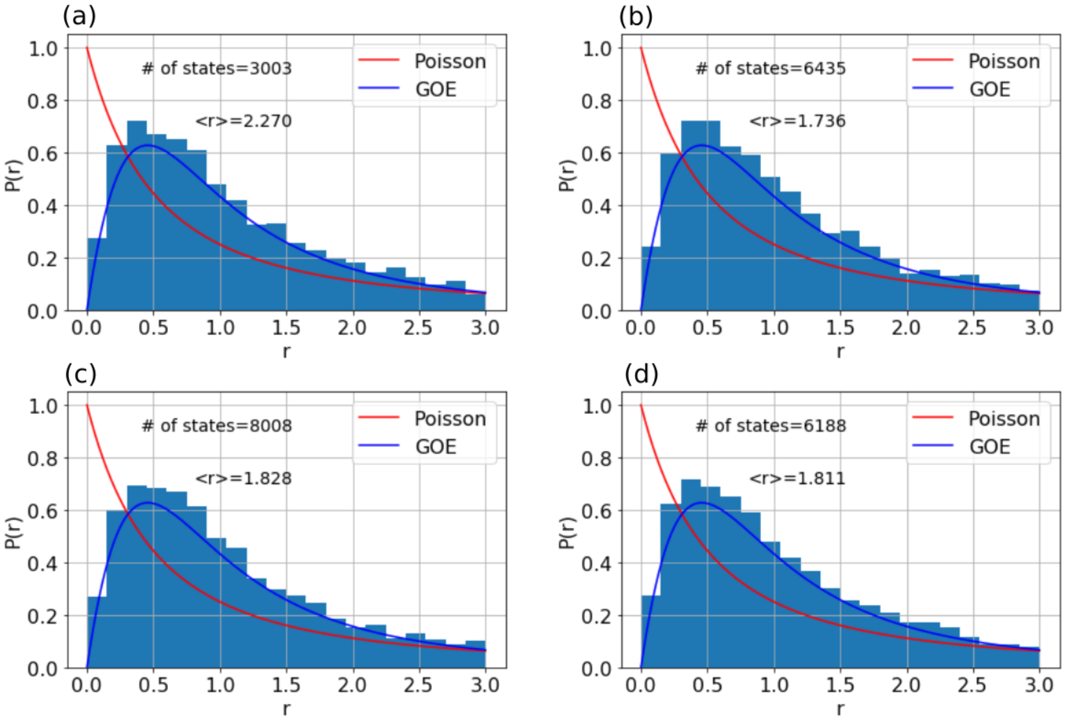

Figure 3.9: The distribution $P(r)$ of the ratios r of consecutive level spacings of the second-order effective Hamiltonian (3.47) in the sector with $N_m = 10$ magnons including one (a) dimer, (b) trimer, (c) tetramer and (d) pentamer on a closed chain of length $L = 25$ in the momentum sector with $k = 7 \times 2\pi/L$. The Ising couplings that fix all parameters of the effective model are $J = 1.17$, $h_{\|} = 0.91$ and $h_{\perp} = 0.0291$.

$$r_n = \frac{E_{n+1} - E_n}{E_n - E_{n-1}}. \tag{3.54}$$

The resulting distribution $P(r)$, plotted in Fig. (3.8), agrees with

$$P(r) = \frac{1}{(1+r)^2}, \tag{3.55}$$

which one gets if the energy levels are completely random (the Poisson distribution) [191]. As a result, our numerics is consistent with integrability of the sectors consisting of isolated magnons exclusively, which was proven in the previous section.

We turn now to sectors with clusters. In particular, we consider closed chains of length $L = 25$ with $N_m = 10$ magnons, among which there is one cluster of sizes two, three, four and five, respectively. The resulting distributions of $P(r)$ are plotted in Fig. 3.9. The fact that they all plummet at low r suggests that the energy levels repel, implying that these sectors are not integrable. The curves that we found are indeed compatible with the Gaussian orthogonal ensemble which characterizes the level statistics of non-integrable models [191].

Number of independent frozen states

One simple consequence of the peculiar hopping term in (3.47) is that clustered magnons in an homogeneous background cannot move, because any hopping would break domain-wall number conservation. Therefore, the perturbative model (3.47) must support a large number of immobile (frozen) quantum states that contain clusters of magnons. Let us quantify this statement. The number F_l of independent frozen states of size $l \gg 1$ scales exponentially according to the Fibonacci constraint, i.e., $F_l \sim \varphi^l$, where φ is the golden ratio [187]. Here we demonstrate that on a closed chain of a length $L \gg 1$ when expressed in the Z-basis the Hamiltonian (3.47) splits into a large number of independent blocks which grows exponentially with the system size. Following ideas from [187], we start from the observation that each independent sector can be labelled by a reference configuration

$$\underbrace{\boxed{\text{frozen state}}}_{L-2k}\underbrace{\boxed{\uparrow\downarrow\uparrow\downarrow\cdots\uparrow\downarrow}}_{2k}. \tag{3.56}$$

The frozen state is constructed out of clusters of magnons, but does not contain isolated magnons. The form of the kinetic term in the effective Hamiltonian (3.47) ensures that in the absence of isolated magnons these clusters are immobile. The number of independent frozen states of a length l follows the Fibonacci recurrence $F_{l+1} = F_l + F_{l-1}$ and thus for $l \gg 1$ the number F_l grows exponentially as φ^l [187], where $\varphi = (1+\sqrt{5})/2$ is the golden ratio. To estimate the total number B_L of independent blocks of the Hamiltonian (3.47), we compute the number of frozen states which can fit into the chain of length $L \gg 1$

$$B_L = \sum_{k=0}^{L/2} F_{L-2k} \approx \sum_{k=0}^{L/2} \varphi^{L-2k} = \varphi^L \sum_{k=0}^{L/2} \varphi^{2k} \approx \varphi^L \frac{1}{1-\varphi^{-2}} = \varphi^{L+1}. \tag{3.57}$$

Such exponential growth is parametrically larger than the $O(L^2)$ scaling expected purely from the two $U(1)$ emergent symmetries. A similar pattern of fragmentation of the Hilbert space was discovered in spin models in the strict confinement regime [187].

Late time dynamics of clusters

As just mentioned, within leading order perturbation theory clusters are frozen when isolated [11] and do not contribute to transport by themselves, but their mobility is activated by the scattering with a magnon. If the scattering is reflective, the cluster stands still, but if transmission occurs the cluster hops by two sites in the direction opposite to the traveling magnon. Therefore, one can relate the cluster displacement x with the total magnetization transported through it as $x = 2\delta S^z$. Given that, the cluster position reflects the local transport of spin and its fluctuations. At late times, a cluster of two magnons undergoes a biased random walk, hopping in the left and right directions with certain rates $R_{L,R}$ which depend on the interactions with the magnonic gas and being proportional to its density. As

---

[11] The hopping of an isolated cluster composed of ℓ magnons scales $\sim h_\perp^{2\ell}$.

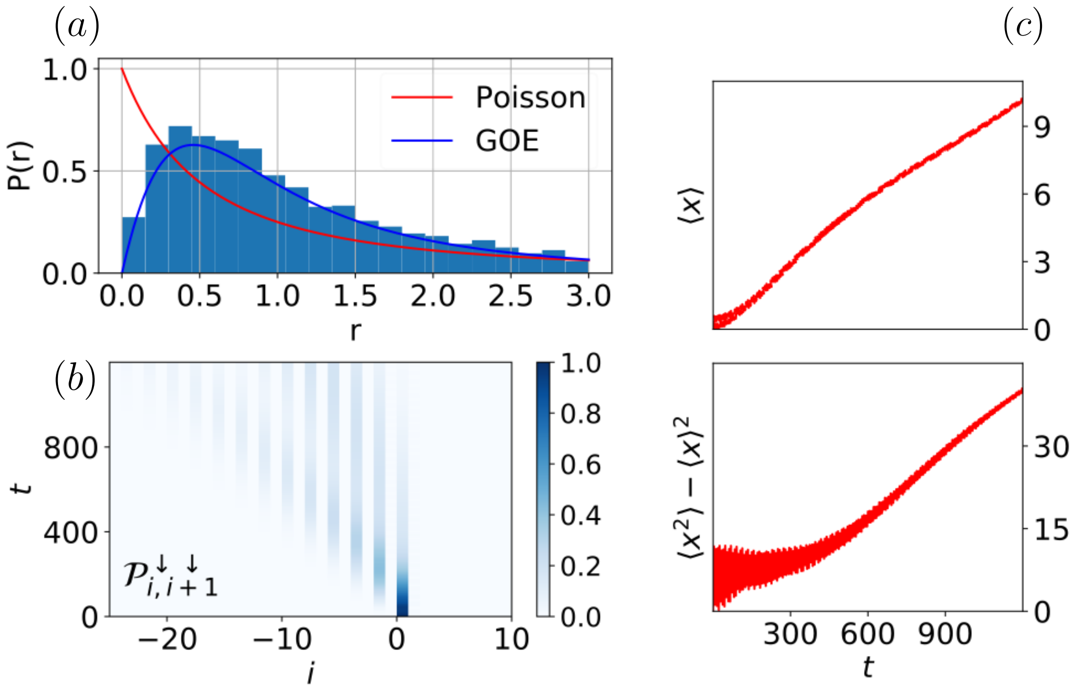

Figure 3.10: (a) The level statistics analysis shows compatibility with the Gaussian Orthongonal Ensamble, suggesting that the sector with a two-magnon cluster is not integrable. (b) A two-magnon cluster, initially at the center of a chain of length $L = 80$ bipartitioned into anti-ferromagnetic and ferromagnetic halves, can move to the left by virtue of the magnon-assisted hopping. We track its position by measuring the projector on two consecutive flipped spins $\mathcal{P}^{\downarrow\downarrow}_{i,i+1}$. (c) At large times, the position $\langle x\rangle$ and variance $\langle x^2\rangle - \langle x\rangle^2$ of the cluster evolve linearly in time, as described in the main text. The TEBD simulations for (b) and (c) are done with the Ising Hamiltonian with parameters corresponding to $\Delta = 0.5$ and $\mathcal{J} = -1$.

a result at late times the cluster experiences diffusion with a linear growth of the average position and variance, which we now proceed to demonstrate. Results are shown in Fig. 3.10(b) and 3.10(c). Since the methods of generalized hydrodynamics no longer apply, we develop a simple phenomenological description to capture the late time dynamics of the clusters. For concreteness, let us consider an initial inhomogeneous state in the form of a partitioning protocol $|\Psi_L\rangle \otimes |\Psi_r\rangle$ and, in addition, we place a cluster composed of two magnons at the origin. Clusters in isolation are static in perturbation theory, but the surrounding isolated magnons can activate their dynamics. A two-magnon cluster undergoes assisted hopping of two sites at once, mediated by the scattering with an isolated magnon. The case of a bigger cluster of length $L_c > 2$ is more complicated, since they can also decay into smaller clusters at intermediate stages, see Fig. 3.11. For the sake of simplicity, we focus here on the case $L_c = 2$ that cannot decay into smaller clusters.

We investigate activation of transport on the timescale where the effective perturbative Hamiltonian is valid. Far from the cluster, the dynamics is locally

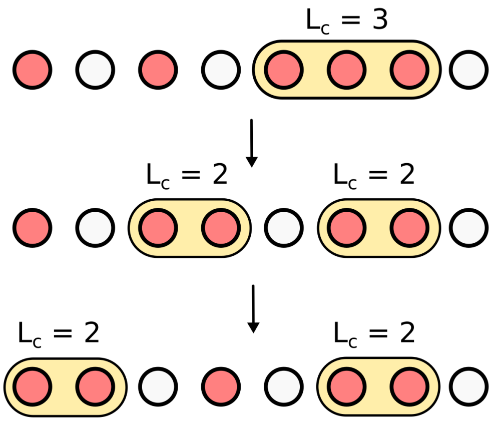

Figure 3.11: Decay of a three-magnon cluster in two clusters mediated by the interaction with surrounding isolated magnons.

integrable and can be rightfully assumed to be described by the GHD equation

$$\partial_t \rho_j + \partial_x (v_j^{\text{eff}} \rho_j) = 0. \tag{3.58}$$

In this perspective, the cluster plays the role of a *dynamical impurity* for the integrable excitations and sets the proper boundary conditions in the form of a generalized scattering matrix. Finding the exact boundary conditions is a challenging problem, since one needs to solve the non-integrable magnon-cluster scattering. Nevertheless, after a transient time, the cluster will be surrounded by a state that reached a local equilibrium, hence the interactions between the cluster and the surrounding magnons will remain constant in time. Let us consider the motion of the cluster in a semi-classical approximation, by denoting with $P_t(j)$ the probability of finding the cluster at a position j. At any time, the cluster can jump to the left by two sites with rate a R_L and to the right with a rate R_R. These rates originate from the interaction with the surrounding isolated magnons: their computation is a formidable task, but in the present calculation we will treat them as phenomenological parameters that are constant in time. Given that, one expects $P_t(j)$ to obey the difference equation

$$\partial_t P_t(j) = R_L P_t(j+2) + R_R P_t(j-2) - (R_L + R_R) P_t(j). \tag{3.59}$$

This equation can be easily solved by passing to the Fourier space

$$P_t(j) = \sum_{j'} G_{j-j'}(t) P_0(j') \qquad G_j = \int \frac{\mathrm{d}k}{2\pi} e^{ikj - tR_L(1-e^{i2k}) - tR_R(1-e^{-i2k})}\,. \tag{3.60}$$

At late times when $P_t(j)$ becomes a smooth function of j, we can replace discrete jumps with spatial derivatives. As a result, a a biased diffusive equation is obtained

$$\partial_t P_t(x) \simeq 2(R_L - R_R)\partial_j P_t(j) + 2(R_L + R_R)\partial_j^2 P_t(j) + \mathcal{O}(\partial_j^3 P)\,. \tag{3.61}$$

From this equation we find for the average displacement and its variance

$$\langle x \rangle = 2t(R_R - R_L) \qquad\qquad \langle x^2 \rangle - \langle x \rangle^2 = 4t(R_R + R_L) \tag{3.62}$$

respectively. Remarkably, the expressions for $\langle x \rangle$ and $\langle (x)^2 \rangle$ can be exactly recovered from the solution of Eq. (3.59), hence the linear growth of averaged position and variance is expected to emerge as soon as Eq. (3.59) is valid.

Chapter 4

$\mathbb{Z}_2$ gauge theories in two spatial dimensions

In this chapter we abandon the comfort of 1+1 dimensional space-time and adventure into the 2d world. The basic ideas behind $\mathbb{Z}_2$ gauge invariance in two dimensions are easy generalizations of their one-dimensional counterparts, discussed extensively in section 2.1. For this reason, we jump directly to some physically relevant models, introducing useful concepts and notation as we encounter them. Similarly to Chapter 2, our original results concern for the most part systems where the matter fields are spinless fermions. In two dimensions, however, even the pure gauge theory without any matter field is non-trivial and exhibits conceptually relevant features such as topological order and phase transitions that do not involve a Landau order parameter. Indeed, it is the interplay between the physics of the pure gauge sector and the matter fields that makes the models presented in this Chapter so intriguing.

Structure

To give a somewhat comprehensive account, we start in section 4.1 with a discussion of Franz Wegner's pure $\mathbb{Z}_2$ lattice gauge theory, that allows us to introduce the concepts of topological order and deconfinement. Before moving on to the original results, in section 4.2 we review some selected works that explore fundamental models which are of great relevance to our research. First we focus on the celebrated work of Fradkin and Shenker [39], which unveiled the phase diagram of lattice gauge theories in the presence or bosonic matter.[1] Then we treat the case of spinful fermionic matter, which was investigated for example in the works from Gazit et. al. [44, 45], which connect very naturally to our research. Section 4.3 contains the main original results of this chapter, which concern the intricate phase diagram of a model of spinless fermions with $U(1)$ particle number conservation coupled to $\mathbb{Z}_2$ gauge fields.

---

[1] Their famous paper contains very comprehensive results that go well beyond $\mathbb{Z}_2$ LGT, but to be coherent with our discussion we will focus on the $\mathbb{Z}_2$ case with Ising matter (i.e. hardcore bosons).

4.1 Pure $\mathbb{Z}_2$ lattice gauge theories

The quantum version of a $\mathbb{Z}_2$ lattice gauge theory is defined by the Hamiltonian

$$H = -J \sum_{\mathbf{r}*} \prod_{b \in \square_{\mathbf{r}*}} \sigma_b^z - h \sum_{\mathbf{r},\eta} \sigma^x_{\mathbf{r},\eta}. \tag{4.1}$$

complemented with a Gauss law

$$G_{\mathbf{r}} = \prod_{b \in +_{\mathbf{r}}} \sigma_b^x = \pm 1, \tag{4.2}$$

where we use $\mathbf{r} = (i_x, i_y)$ to label the sites of the lattice, $\eta = \hat{x}, \hat{y}$ denotes a unit lattice displacement and $\mathbf{r}^*$ the dual lattice formed by the centers of the plaquettes. Since star and plaquette operators are ubiquitous in two dimensional lattice gauge theories, we introduce here the standard notation

$$B_{\mathbf{r}^*} = \prod_{b \in \square_{\mathbf{r}*}} \sigma_b^z, \qquad A_{\mathbf{r}} = \prod_{b \in +_{\mathbf{r}}} \sigma_b^x. \tag{4.3}$$

Similar to the Gauss law in one dimension, Eq. (4.2) to be interpreted as a constraint on the "$\mathbb{Z}_2$-divergence" of the electric field. Since in this simplest case there are no dynamical matter fields that carry $\mathbb{Z}_2$ charge, the only sources of electric lines are the "static charges" associated with the sites where $G_{\mathbf{r}} = -1$. Different choices of the Gauss law lead to significantly different versions of the gauge theory. Below, we explore the most relevant ones.

4.1.1 Wegner's $\mathbb{Z}_2$ LGT and the toric code

This is the quantum version[2] of Wegner's original formulation of a $\mathbb{Z}_2$ LGT [30], and it corresponds to the choice $G_{\mathbf{r}} = +1$ everywhere. The gauge constraint forces all the star operators to take the value $+1$. Since at $h = 0$ only the plaquette terms appear in the Hamiltonian, and all of them need to be equal to $+1$ as well in order to minimize the energy, this is equivalent to finding the ground state of the Hamiltonian[3]

$$-\sum_{\mathbf{r}} A_{\mathbf{r}} - \sum_{\mathbf{r}*} B_{\mathbf{r}^*}. \tag{4.4}$$

This is the well known toric code model introduced by Kitaev [37], which is indeed equivalent to our model at $h = 0$. The Hamiltonian (4.4) is an example of *stabilizer code*, i.e. a model where all the terms commute and can therefore be minimized independently. The ground state of Hamiltonian (4.4) can be written down exactly in the electric basis.[4] As the two terms in (4.4) commute, the ground state satisfies

$$A_{\mathbf{r}}|0\rangle = +1 \qquad \text{and} \qquad B_{\mathbf{r}^*}|0\rangle = +1, \qquad \forall \mathbf{r},\, \mathbf{r}^*. \tag{4.5}$$

---

[2] In the original paper of Franz Wegner the classical 3d version of the $\mathbb{Z}_2$ LGT emerges as the dual of the classical 3d Ising model on the square lattice. Below, we will present the quantum version of this duality. The 3d classical and 2d quantum models are related by the classical-quantum correspondence, which we do not review here.

[3] Since all stars and plaquettes commute, the relative value of the coefficients in front of the terms is inconsequential.

[4] I.e. the basis where σ^x is diagonal.

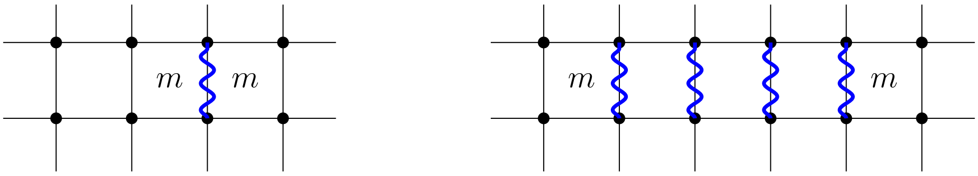

Figure 4.1: Finite t'Hooft lines, represented by blue wavy lines, create pairs of magnetic excitations at their ends. The plaquettes in between are unaffected, and so the energy cost of pairs of m particles is independent of their distance.

Since all the $A_{\mathbf{r}}$ operators need to evaluate to $+1$, an even number of electric lines must stick out of each site. On a closed manifold, this implies that each line cannot end on a site, but has to form a loop instead. The action of $B_{\mathbf{r}^*}$, on the other hand, flips the state of the $\mathbb{Z}_2$ electric field on all the links around a plaquette, with the effect of deforming loops without breaking them. In other words, the first term in Eq. (4.4) tells us that the ground state has to be formed by a superposition of all possible electric loops.[5] The second term, on the other hand, tells us that the superposition has to be equal weight, so that each term can be turned into another one by the action of plaquette operators. This limit corresponds to the deconfined regime of the lattice gauge theory, characterized by a perimeter-law decay of the Wilson loop operator[6]

$$W_{\mathcal{C}} = \prod_{l \in \mathcal{C}} \sigma_l^z, \tag{4.6}$$

where $\mathcal{C}$ is a closed contour. The deconfined regime is stable to the introduction of an h-perturbation, which causes an exponentially decaying attractive interaction between static charges [36]. This regime of the gauge theory is gapped, since the excitations are obtained by flipping plaquettes which comes with a finite energy cost. We refer to such excited states as *magnetic* or 'm' particles. We note the following important fact: the local gauge-invariant operator σ^x can only create pairs of excitations, since it changes the state of σ^z on a single link which is always shared by two plaquettes. Similarly any finite string of σ^x operators, as the one shown in Fig. 4.1, creates a pair of excitations at a certain distance from each other, with the same energy cost since even in this case only two plaquettes are flipped. We learn from this that the m particles are deconfined, in the sense that they can be brought far apart without increasing the energy of the system. A single magnetic excitation can only be created by the non local semi-infinite "t'Hooft line" operator

$$\tilde{W}_{\mathbf{r}*} = \prod_{l \in \gamma} \sigma^x, \tag{4.7}$$

where γ is an arbitrary semi-infinite line of parallel links, which we will take conventionally to be straight. An example is shown in Fig. 4.2.

In the large h regime, on the other hand, the ground state is a paramagnet with $\sigma^x = +1$ everywhere, which is consistent with the gauge constraint. This is the

---

[5] Loops are allowed to intersect, as at the intersection of two electric lines $\sigma^x = -1$ on all four links and the stars are positive.

[6] See the discussion in section 4.2.1 for details on how to detect confinement in $\mathbb{Z}_2$ lattice gauge theories.

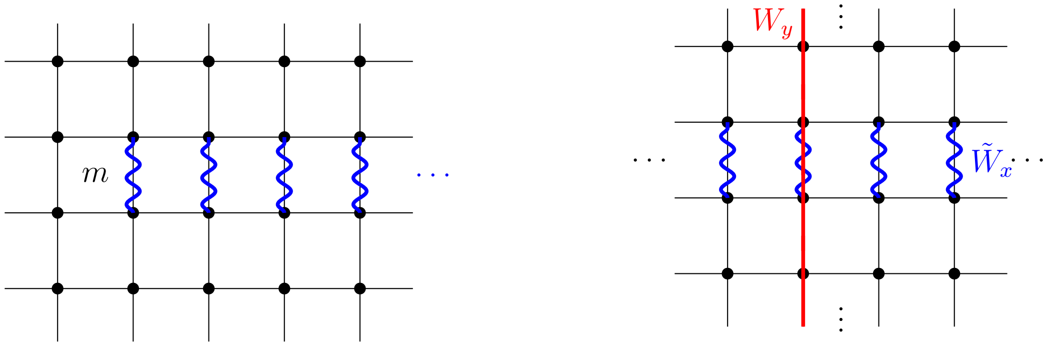

Figure 4.2: Left: the semi-infinite horizontal t'Hooft line $\tilde{W}_{\mathbf{r}^*}$, that creates a single m particle at its open end. The choice of the line is conventional since it can be deformed by applying the Gauss law. We always take it to be straight and going from left to right. Right: the horizontal t'Hooft loop $\tilde{W}_x$(blue) and the vertical Wilson loop W_y (red) on a torus, where the left-right and up-down edges are identified.

confined phase of the gauge theory, since the interaction potential between static charges grows linearly with their distance.[7] Here Wilson loops follow an area-law decay. It is easy to see that this phase is also gapped. Indeed, since the ground state is a paramagnet, the only possibility is to flip a certain number of spins, which comes with a finite energy cost. This can be done in a gauge invariant way only by flipping spins around a closed loop. Excitations are therefore "electric loops" where $\sigma^x = -1$ on each link, and they carry an amount of energy proportional to their length. The simplest excitation is the loop that encircles an elementary plaquette, which is created by the operator $B_{\mathbf{r}^*}$.

Duality with the 2d quantum Ising model

While the analysis above should clarify that the model (4.1) has two distinct phases, this can be shown in another very instructive way by mapping it to the two-dimensional quantum Ising model whose solution is known. To this purpose, we define the following operators on the dual lattice:

$$\mu^x_{\mathbf{r}*} = B_{\mathbf{r}*} \qquad\qquad \mu^z_{\mathbf{r}*} = \tilde{W}_{\mathbf{r}*}. \tag{4.8}$$

These are the plaquette and t'Hooft lines defined in Eq. (4.3) and (4.7). It is straightforward to verify that μ^x and μ^z, together with $\mu^y = \frac{i}{2}[\mu^x, \mu^z]$ satisfy the Pauli algebra and can be regarded as new spin one-half operators. Under this transformation, the plaquette operator obviously maps to μ^x. As for the electric term, if we take the definition of Fig. 4.2 for the t'Hooft line, we see that the product $\tilde{W}_{\mathbf{r}^*}\tilde{W}_{\mathbf{r}^*+\hat{x}}$ gives precisely σ^x on the vertical link between $\mathbf{r}^*$ and $\mathbf{r}^* + \hat{x}$, since the rest of the semi-infinite string cancels. For the horizontal links, we can take the product $\tilde{W}_{\mathbf{r}^*}\tilde{W}_{\mathbf{r}^*+\hat{y}}$. While in this case there is no immediate cancellation, we can insert the Gauss law $A_{\mathbf{r}} = +1$ at all sites between the semi-infinite strings. All σ^x operators square to one, except for the leftmost one on the horizontal link between $\mathbf{r}^*$ and $\mathbf{r}^* + \hat{y}$. Putting it all together, we obtain that

---

[7] This works as in one dimension: $\mathbb{Z}_2$ charges must be connected by electric lines, and each line has a cost proportional to its length.

$$H = -h \sum_{\langle \mathbf{r}^* \mathbf{r}^{*\prime} \rangle} \mu^z_{\mathbf{r}^*} \mu^z_{\mathbf{r}^{*\prime}} - J \sum_{\mathbf{r}^*} \mu^x_{\mathbf{r}^*}. \tag{4.9}$$

which is the Hamiltonian for the 2d Ising model. This is the two dimensional version of the Kramers-Wannier duality: the confined "paramagnetic" phase exhibits order in the domain wall operators μ^z, while the deconfined phase corresponds to alignment of the plaquette operators μ^x. While in one dimension the Ising model is self-dual, in two dimensions it maps to a lattice gauge theory! While this reveals that the model has two phases, the non-local character of the transformation hides some key features of the model, which we now explore.

Topological order

While the model in Eq. (4.9) exhibits spontaneous symmetry breaking for large values of h, the order parameter $\langle \mu^z \rangle$ is non local in the gauge theory language and cannot be used to classify the phases according to Landau's paradigm. The lack of a local order parameter means essentially that in order to characterize the model we have to resort to global properties. To this purpose, we put the system on a torus where the following non-local incontractible loops can be defined:

$$W_{x,y} = \prod_{l \in \mathcal{C}_{x,y}} \sigma^z_l \qquad\qquad \tilde{W}_{x,y} = \prod_{l \in \Gamma_{x,y}} \sigma^x_l \tag{4.10}$$

where $\mathcal{C}_{x,y}$ and $\Gamma_{x,y}$ are the closed loops around the horizontal and vertical directions of the torus defined in Fig. 4.2. We refer to W and $\tilde{W}$ as the Wilson (or magnetic) and t'Hooft (or electric) loops respectively.[8] At $h = 0$, i.e. in the Toric Code limit, both W and $\tilde{W}$ commute with the Hamiltonian and can be regarded as symmetries. Moreover, we have that

$$\{W_x, \tilde{W}_y\} = 0 \qquad\qquad \{W_y, \tilde{W}_x\} = 0 \tag{4.11}$$

since these pairs always share exactly one link, on which $\{\sigma^x_l, \sigma^z_l\} = 0$. All the other combinations commute. The presence of two pairs of anticommuting symmetries guarantees that the ground state of the system is 4-fold degenerate. In practice, this means that the construction of the ground state as a sum of electric loops outlined above is not unique. Indeed, the value on W_x and W_y is not fixed, and each ground state can be taken to be an eigenstate of the two Wilson loops, and is classified by the four possible combinations of their eigenvalues. Explicitly we define the four ground states as

$$|0\rangle \equiv |++\rangle \qquad |1\rangle \equiv |+-\rangle \qquad |2\rangle \equiv |-+\rangle \qquad |3\rangle \equiv |--\rangle, \tag{4.12}$$

---

[8] This terminology is quite generic and is used in other contexts to denote space-time loops as well. In the particular case of Hamiltonian $\mathbb{Z}_2$ LGT the more appropriate nomenclature is Wegner-Wilson/Wegner-t'Hooft, but we avoid this for brevity.

where the signs denote the eigenvalues of W_x and W_y. The t'Hooft loop can then be used to toggle between them:

$$\tilde{W}_x|0\rangle = |1\rangle \qquad \tilde{W}_y|0\rangle = |2\rangle \qquad \tilde{W}_x\tilde{W}_y|0\rangle = |3\rangle. \tag{4.13}$$

At finite h the Wilson loop is not a symmetry anymore, and so the degeneracy is lifted. However, since the different states can only be connected by the action of the non local $\tilde{W}$ operators, the mixing is exponentially small in the size of the torus: $\Delta E \propto h^L$. This is because a string of σ^x operators of length L can only be generated at order L in perturbation theory. The ground state degeneracy on the torus is therefore robust in the thermodynamic limit, and it persists up until the critical point where the perturbative expansion ceases to converge. We note that while the construction above is done for the torus, one is free to consider topologically non-trivial surfaces of higher genus. In that case there are more non-contractible loops and the ground state degeneracy is larger. For a surface of genus g, the number of ground states is given by

$$N_{GS} = 4^g. \tag{4.14}$$

This particular quantum phase of matter, characterized by ground state degeneracy on the torus and by the presence of anyonic excitations, is said to exhibit *topological order*.

Anyons in the toric code

Anyonic excitations are a peculiarity of two dimensional systems, where particles are not restricted to be fermionic or bosonic [192–194]. This rich subject goes beyond the scope of this thesis, and here we merely scratch the surface by identifying the simple anyons that show up in the toric code.[9] The first one is the "magnetic particle" m that we already encountered, corresponding to a defect $B_{\mathbf{r}^*} = -1$. The second one is the "electric particle" e, corresponding to a defect $A_{\mathbf{r}} = -1$. Both can only be created in pairs at the end of t'Hooft and Wilson lines respectively.[10] It can be verified by performing the braiding operation explicitly that while e and m are bosons with respect to themselves, they are fermions with respect to each other [195, 196]. This is not consistent with them being fermions or bosons, hence the need to extend the concept to anyons. An e and an m particle can be combined into a third anyon, often denoted by ψ. Since braiding two ψ particles involves exchanging e and m, the operation gives a minus sign and therefore ψ can be regarded as a fermion.

Field theoretical perspective

We show here how to develop a field theoretical understanding of the phase transition that occurs in the even $\mathbb{Z}_2$ LGT. This describes the condensation of

---

[9] These are an example of abelian anyons, meaning that they gain a phase upon braiding but they do not "mix" with each other. We will not discuss non-abelian anyons.

[10] In the $\mathbb{Z}_2$ gauge theory, the e particle has to be seen as a static charge corresponding to a defect in the Gauss law and not as an excitation.

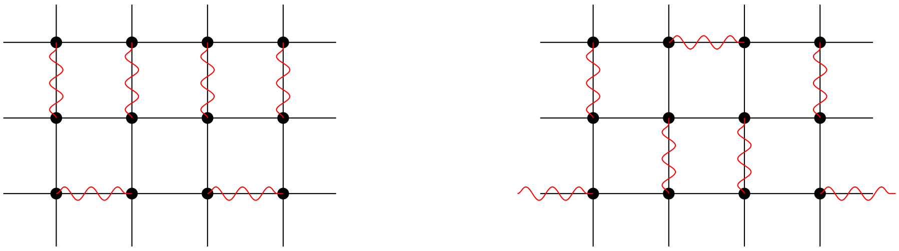

Figure 4.3: Examples of dimer configurations that form the ground state of the odd $\mathbb{Z}_2$ lattice gauge theory in the $h \to \infty$ limit. Each site hosts a static $\mathbb{Z}_2$ charge, which is connected to another charge by an electric line of unit length.

visons, which marks the topological phase transition. The visons can be seen as hopping particles, that move from one plaquette to the other under the effect of the electric term. A single vison costs an amount of energy equal to $2J$, while the h term is responsible for a dispersion. At first order in h, this is given by a simple cosine band:

$$\epsilon^{v}_{\mathbf{k}} = 2J - 2h\left(\cos k_x + \cos k_y\right). \tag{4.15}$$

As h is increased the gap diminishes as expected, but since higher order corrections kick in it is not possible to find the precise location of the transition point by simply looking at where the gap closes. By exploiting the duality with the Ising model described above, it is easy to write down a continuum theory in the vicinity of the critical point. Indeed, in equation (4.8) we have defined the vison creation operator to be the Ising spin μ^z in the dual formulation. Therefore, the transition can be described by the familiar ϕ^4 field theory which is employed for the Ising model. In this case, the ordered phase corresponds to the confined regime, where visons condense and the non-local domain wall operators acquire a non-zero expectation value. The potential takes the form

$$V(\phi) = -\lambda_2\,\phi^2 + \lambda_4\,\phi^4 \tag{4.16}$$

where the “mass” λ_2 changes sign at the transition, triggering vison condensation. The critical theory belongs to the Ising* universality class, which differs from the usual Ising CFT in that only operators which are even under the $\mathbb{Z}_2$ transformation $\phi \to -\phi$ are allowed.[11]

4.1.2 Odd $\mathbb{Z}_2$ LGT

The odd $\mathbb{Z}_2$ lattice gauge theory corresponds to the choice $G_i = -1$ everywhere. In other words, each site hosts a static charge which acts as a source of $\mathbb{Z}_2$ electric lines. In this case, no closed electric loops are possible since an odd number of lines needs to stick out of each site. Similarly to its even counterpart, this $\mathbb{Z}_2$ LGT can be mapped to an Ising model through (4.8). The different sign of the Gauss law, however, results in a flipped sign for some of the Ising couplings leading to the so-called fully-frustrated transverse field Ising model (FFTFIM) [197].

---

[11] Indeed, we have identified ϕ with the vison creation operator, but the creation of an odd number of visons is not allowed in this model.

In the $h = 0$ limit the ground state can be constructed in analogy with the toric code, with the difference that this time we have to consider the superposition of all possible (intersecting) electric lines that connect all possible pairs of sites. This still corresponds to the deconfined phase of the gauge theory. Deep in the confined phase, on the other hand, the physics of the problems becomes significantly more intricate compared to its even counterpart. In this limit, it is clear that a gauge invariant state that minimizes the electric term is formed by connecting pairs of neighboring sites with electric lines of length one. However, this can be done in a number of ways, leading to a huge ground state degeneracy for $J = 0$. A finite J lifts this degeneracy, but which state wins the energetic competition is a complicated and partially unresolved problem. The results presented in [197] indicate that the columnar order is privileged.

Field theoretical perspective

We have seen that the large h limit of the odd $\mathbb{Z}_2$ lattice gauge theory is far from trivial. This shows up in the field theory description of the model close to criticality. As a starting point, we take once more the dispersion relation for the visons. In this case, a careful analysis shows that the visons effectively hop in a "π-flux", resulting in two energy bands with degenerate minima located at $\mathbf{k} = (0, 0)$ and $\mathbf{k} = (0, \pi)$ [198, 199]. When the gap closes, then, the relevant physics is captured by the two real scalar fields ϕ_1 and ϕ_2 which represent visons at the minima. A critical theory can be written down by identifying correctly the symmetries of the problem, to narrow down the amount of terms that can appear in the Lagrangian. Under one-site translations and $\pi/2$ rotations, which are symmetries of the lattice problem, the fields transform as follows:

$$\begin{aligned} T_x : \quad & \phi_1 \to \phi_2 & \phi_2 \to \phi_1 \\ T_y : \quad & \phi_1 \to \phi_1 & \phi_2 \to -\phi_2 \\ R_{\pi/2} : \quad & \phi_1 \to \frac{1}{\sqrt{2}}(\phi_1 + \phi_2) & \phi_2 \to \frac{1}{\sqrt{2}}(\phi_1 - \phi_2)\,. \end{aligned} \tag{4.17}$$

These operations generate the non-abelian dihedral group D_8, which constrains the form of the critical theory. It is more practical to combine ϕ_1 and ϕ_2 into a single complex field

$$\Phi = e^{-i\pi/8}(\phi_1 + i\phi_2)\,, \tag{4.18}$$

which under the operations (4.17) transforms as

$$T_x : \Phi \to e^{i\pi/4}\Phi^*, \qquad T_y : \Phi \to e^{-i\pi/4}\Phi^*, \qquad R_{\pi/2} : \Phi \to \Phi^*. \tag{4.19}$$

A Lagrangian for the complex field Φ that respects the D_8 symmetry is

$$\mathcal{L} = |\partial_\mu \Phi|^2 + \lambda_2|\Phi|^2 + \lambda_4|\Phi|^4 + \lambda_8\left(\Phi^8 + \Phi^{*8}\right). \tag{4.20}$$

The phase diagram of the model near criticality is governed by the sign of λ_2, which triggers spontaneous symmetry breaking. For $\lambda_2 > 0$ we are in the deconfined phase, where the Φ field is gapped. For $\lambda_2 < 0$ and $\lambda_8 = 0$ the potential has the typical Mexican-hat shape and we are in the symmetry broken phase. A finite λ_8 deforms the potential, with the sign determining the position of the minima along the "edge" of the hat. Different signs of λ_8 favour one of the two possible orders (columnar and plaquette) that compete in the confined phase [198, 199]. As for the transition point, here the λ_8 term is an irrelevant perturbation, and the critical theory is the XY^* Wilson-Fisher CFT, where the star denotes the exclusion of operators that are odd under the $\mathbb{Z}_2$ symmetry.

4.2 Coupling to matter fields: notable examples

In this section, we take a short detour to review some important work that inspired our research. In doing so, we introduce a number of useful concepts which will be recurrent in the rest of the chapter. Due to the significant amount of research that has been carried out on $\mathbb{Z}_2$ lattice gauge theories and related models in a variety of contexts, it is not easy to choose some particular model on which to focus. We refer to simplicity as a guiding principle, and we single out two theories which are especially notable for containing a limited amount of ingredients and still exhibiting the features we are most interested in. First, we consider an example featuring (hardcore) bosonic matter. This is studied in a famous paper by Fradkin and Shenker, together with other bosonic models with generic gauge groups and higher dimensionality. Subsequently, we turn to fermionic matter and give an account of results from Gazit et al. concerning an interacting theory of spinful fermions and $\mathbb{Z}_2$ gauge fields. Their findings, which are supported by extensive sign-problem free quantum-Monte Carlo simulations, include exotic phases where superfluid order coexists with deconfined gauge excitations and a very unusual critical theory at the quantum critical point.

4.2.1 Ising matter

Frankin and Shenker studied in great generality models where a bosonic Higgs field couples to gauge theories on a lattice [39]. Here we focus on the simplest case, where the gauge group is $\mathbb{Z}_2$ and the Higgs field takes the form of an Ising spin. The Hamiltonian that describes Ising matter coupled to $\mathbb{Z}_2$ gauge fields is given by

$$H = -\frac{1}{\lambda}\sum_{\mathbf{r}} \tau^z_{\mathbf{r}} - J\sum_{\mathbf{r}^*} B_{\mathbf{r}^*} - \lambda \sum_{\mathbf{r},\eta} \tau^x_{\mathbf{r}}\sigma^z_{\mathbf{r},\eta}\tau^x_{\mathbf{r}+\eta} - h\sum_{\mathbf{r},\eta}\sigma^x_{\mathbf{r},\eta}, \tag{4.21}$$

where the gauge fields are defined on the links as usual, while the matter fields on the sites consist of an additional set of Pauli matrices $\{\tau^x, \tau^y, \tau^z\}$. For the couplings, we stick to the same notation as the previous section for the pure gauge sector, while in the matter sector we introduce the interaction strength λ. The coupling of the two matter terms in the Hamiltonian are chosen so that the pure $\mathbb{Z}_2$ LGT is properly recovered. Indeed, as $\lambda \to 0$, the coupling vanishes while the "chemical potential" blows up pushing all the matter excitations high up in the spectrum. This minimal coupling between the matter and gauge fields is chosen so that the model is invariant under the local transformation generated by

$$G_{\mathbf{r}} = A_{\mathbf{r}}\tau^z_{\mathbf{r}}, \tag{4.22}$$

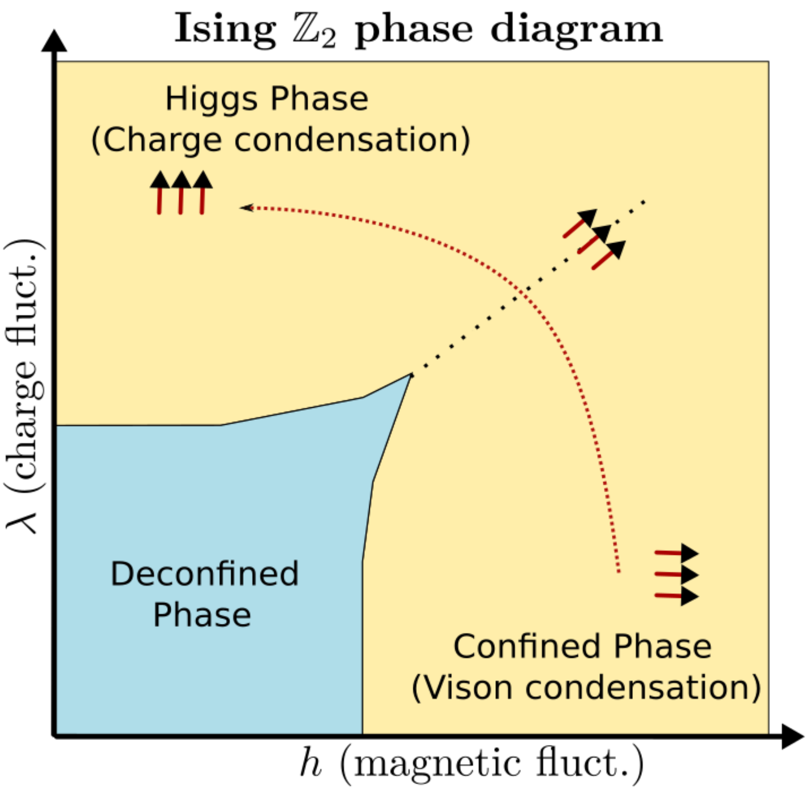
Ising $\mathbb{Z}_2$ phase diagram
Higgs Phase
(Charge condensation)
Deconfined
Phase
Confined Phase
(Vison condensation)
λ (charge fluct.)
h (magnetic fluct.)

Figure 4.4: Quantum phase diagram of the Fradkin-Shenker model given in Eq. (4.21).

which plays the role of the Gauss law. This modification accounts for the fact that the matter fields, being $\mathbb{Z}_2$ charged, can act as dynamical sources for electric lines.[12] As usual, we define the physical Hilbert space by the condition $G_{\mathbf{r}} = +1$ everywhere.

Deconfined phase

In the limit where both the Ising coupling λ and the electric field strength h vanish, we end up in the deconfined phase of the $\mathbb{Z}_2$ lattice gauge theory. This can be verified explicitly by resolving the Gauss law to replace the first term in equation (4.21) with a star operator. The spectrum of the theory is of course modified by the presence of matter fields. In particular, there are now bound states. They consist of open electric strings with $\mathbb{Z}_2$ charged endpoints, created by the operator

$$\mathcal{O}^E_{\mathbf{r}_i,\mathbf{r}_f} = \tau^x_{\mathbf{r}_i}\left(\prod_{\mathbf{r}_i<\mathbf{r}<\mathbf{r}_f}\sigma^z_{\mathbf{r}}\right)\tau^x_{\mathbf{r}_f}. \tag{4.23}$$

---

[12] Compare with the pure $\mathbb{Z}_2$ LGT, where the only sources are "defects" in the Gauss law $G_{\mathbf{r}} = -1$.

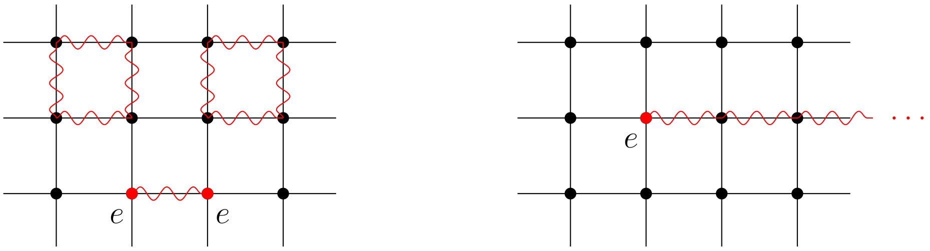

Figure 4.5: Left: elementary excitations in the confined phase of the $\mathbb{Z}_2$ LGT with Ising matter Eq. (4.21). Apart from the electric loops, also present in the absence of matter fields, there are tightly confined bound states of e-particles. Right: A single e particle always carries around an infinite electric string. In the deconfined phase, long strings are allowed to proliferate and the particle can move freely.

In the deconfined phase such strings proliferate, in the same fashion as the electric loops of the pure $\mathbb{Z}_2$ model. We can also think to stretch the electric string in (4.23) all the way to infinity. In this case, a single deconfined "electric" particle is created.[13] At finite λ the deconfined phase is stable, and it still exhibits topological order despite the fact that now the t'Hooft loop does not commute with the Hamiltonian. Indeed, the matter fields are massive, with a gap of order λ^{-1} and can be integrated our resulting in a renormalization of the gauge coupling [36]. Their only effect on the phase diagram is therefore to shift the location h_c of the QCP corresponding to the confinement transition. When J is finite and $h = 0$, the system is forced into the 0-flux phase, and by fixing the gauge we can set $\sigma^z = +1$ on each link.[14] We are left with a transverse field Ising model in the matter variables, which exhibits an Ising phase transition at a certain critical point $\lambda = \lambda_c$. The two single points can be connected, so that a whole deconfined region of the phase diagram is singled out.

Confined and Higgs phases

When the charge fluctuations are suppressed and the electric term dominates, on the other hand, we fall into the confined phase. At $\lambda = 0$ the matter fields are infinitely massive, and do not modify the large h regime of the gauge theory in any way. For small but finite λ bound states of Ising matter appear in the spectrum. Since long electric strings are energetically penalized, dynamical charges are confined and this regime is smoothly connected with confined phase of the pure $\mathbb{Z}_2$ LGT. The limit where $\lambda \to \infty$, finally, corresponds to the Higgs phase of a gauge theory in the sense that charges are condensed in the ground state. To see this we note that in this regime each term $\tau^x \sigma^z \tau^x$ in the Hamiltonian is pinned to $+1$. If we concatenate them by taking products on neighboring links, we obtain exactly the operator $\mathcal{O}^E$ in Eq. (4.23). This proves that there is long range order:

$$\lim_{|\mathbf{r}_i - \mathbf{r}_f|} \langle \mathcal{O}^E_{\mathbf{r}_i,\mathbf{r}_f} \rangle \neq 0. \tag{4.24}$$

---

[13] This corresponds to the e anyon of the toric code, which in the pure $\mathbb{Z}_2$ LGT could only appear as a defect in the Gauss law.

[14] See section 4.3.2 for a gauge invariant argument.

Fradkin and Shenker proved that, surprisingly, the Higgs and confined regimes do not form different phases: these seemingly opposite regimes can be smoothly connected following a path in parameter space along which the spectrum evolves analytically. We are left with a phase diagram with only two regions.[15]

Self-duality of the model

In this particular model, matter and gauge fields can be disentangled by choosing an appropriate gauge. Everywhere except on the lines $\lambda = 0$ and $h = 0$, we can impose that $\tau^x = +1$ when acting on the physical states [36]. Provided that the Gauss law (4.22) is also enforced, one gets

$$H = -\frac{1}{\lambda}\sum_{\mathbf{r}} A_{\mathbf{r}} - J\sum_{\mathbf{r}^*} B_{\mathbf{r}^*} - \lambda\sum_{\mathbf{r},\eta}\sigma^z_{\mathbf{r},\eta} - h\sum_{\mathbf{r},\eta}\sigma^x_{\mathbf{r},\eta}, \tag{4.25}$$

which describes a toric-code model in two external fields. In particular this reveals why the Higgs and confined phases are smoothly connected: if $\lambda = \rho\cos\theta$ and $h = \rho\sin\theta$, then for $\rho \to \infty$, the ground state is a product state describing a paramagnet pointing in a coupling-dependent direction:

$$|\psi\rangle = \otimes_l \left(\cos(\theta/2)\left|\uparrow\right\rangle_l + \sin(\theta/2)\left|\downarrow\right\rangle_l\right). \tag{4.26}$$

Eq. (4.25) enjoys a self duality that amounts to exchanging the roles of the star and plaquette operators and redefining the couplings accordingly. Indeed, the links of the original lattice (identified by their midpoints) formed by sites are the same as the links of the dual lattice formed by the plaquettes, but the roles of stars and plaquettes are exchanged.

Detecting confinement

While we saw that the presence of matter fields does not substantially alter the physics of the confined phase for small values of λ, it affects the way we can detect confinement. We mentioned in section 4.1 that the two phases of the pure $\mathbb{Z}_2$ gauge theory can be told apart by looking at the behavior of the Wilson loop operator (4.6): a Wilson loop W_Γ defined on a closed contour Γ decays exponentially following a perimeter law in the deconfined phase, and an area law in the confined phase. To understand why this does not work anymore in the presence of dynamical charges, let us sketch first how the area law behavior comes into play. As $h \to \infty$, we can do perturbation theory in J/h starting from the unperturbed paramagnetic ground state $|0\rangle = |\uparrow\uparrow\uparrow\ldots\rangle$ with $\sigma^x = 1$ everywhere. Let us call

$$|\Gamma\rangle = W_\Gamma|0\rangle \tag{4.27}$$

the state obtained by acting with an arbitrary Wilson loop Γ on the ground state. It is clear that $|\Gamma\rangle$, where the state of the electric field is flipped on the L links in

---

[15] In general, whether the Higgs and confined phases are connected or not depends on whether the Higgs field is in the fundamental representation of the gauge group or not. In our case we do not have a choice, since $\mathbb{Z}_2$ has only one representation.

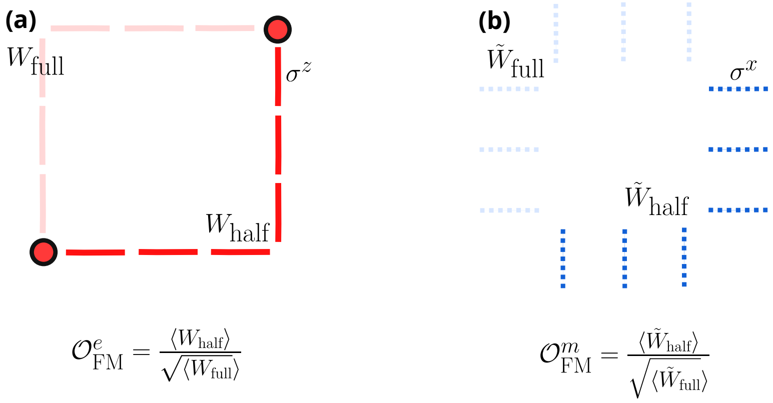
(a)
W_{full}
σ^z
W_{half}
$\mathcal{O}^e_{\text{FM}} = \frac{\langle W_{\text{half}} \rangle}{\sqrt{\langle W_{\text{full}} \rangle}}$
(b)
$\tilde{W}_{\text{full}}$
σ^x
$\tilde{W}_{\text{half}}$
$\mathcal{O}^m_{\text{FM}} = \frac{\langle \tilde{W}_{\text{half}} \rangle}{\sqrt{\langle \tilde{W}_{\text{full}} \rangle}}$

Figure 4.6: Definitions of the electric (a) and magnetic (b) Fredenhagen-Marcu order parameters, as in Eq. (4.28) and (4.29).

Γ, is orthogonal to the unperturbed ground state. To have a non-zero perturbative contribution to the expectation value we need to find a virtual state that overlaps with $|\Gamma\rangle$ by acting on the ground state with the plaquette operator. This is obtained at order N in perturbation theory, where N is the number of plaquettes encircled by the Wilson loop. Indeed, the product of all such plaquettes give exactly W_Γ.[16] This proves that $\langle W_\Gamma \rangle \propto J^N$ with N growing as the area enclosed by the loop.

In the presence of matter fields, however, there is another perturbative process in λ/h that contributes to the expectation value and becomes dominant for larger loops. We have seen above that electric strings with $\mathbb{Z}_2$ charged endpoints (see Eq. (4.23)) can be created by concatenating the $\tau^x \sigma^z \tau^x$ terms in the Hamiltonian. If we multiply them along the closed circuit Γ, even the endpoints cancel and we are left once more with a Wilson loop W_Γ. Therefore the state $|\Gamma\rangle$ can now be obtained at order L in perturbation theory, where L is the number of links in Γ. This grows as the perimeter of the loop. It is clear that for large enough loops $N \gg L$, and a perimeter law decay $\langle W_\Gamma \rangle \propto \lambda^L$ is expected. In this case, the expectation value of the Wilson loop does not reliably identify the two phases of the gauge theory.

To our luck, a suitable modification of the Wilson loop exists. This is given by the Fredenhagen-Marcu operator, which acts as an order parameter for the confined phase. It is defined by

$$\mathcal{O}_e^{FM} = \frac{\langle W_{1/2} \rangle}{\sqrt{\langle W \rangle}} \tag{4.28}$$

where $W_{1/2}$ denotes an open Wilson line of half the length of the closed loop W terminating with $\mathbb{Z}_2$ charged operators[17] to ensure gauge invariance. The subscript e reminds us that the "electric" string in the numerator measures condensation of the e-particles - much like the one in Eq. (4.24). A careful calculation shows that dividing by the square root of the full Wilson loop eliminates the L dependence form perimeter law in the confined phase, so that here $\mathcal{O}_e^{FM} \to$ *const*. In the deconfined phase on the other hand $\mathcal{O}_e^{FM} \to 0$, which makes it a proper non-local string order parameter. With this perspective in mind, it is natural to define a dual "magnetic" order parameter in terms of magnetic strings. Contrary to $\mathcal{O}_e^{FM}$, this new operator detects the transition due to the condensation of magnetic particles [200]. A proper definition is

---

[16] This is the $\mathbb{Z}_2$ equivalent of Stokes' theorem.

[17] In this case, the endpoint operator is τ^x.

$$\mathcal{O}_m^{FM} = \frac{\langle \tilde{W}_{1/2} \rangle}{\sqrt{\langle \tilde{W} \rangle}}, \tag{4.29}$$

where $\tilde{W}$ and $\tilde{W}_{1/2}$ denote closed and open t'Hooft lines (see Eq. (4.7)) respectively. Note that compared to the electric parameter, here there is no need for $\mathbb{Z}_2$ charged endpoints, as the open t'Hooft line creates pairs of m particles at its ends by itself. In the case of the Fradkin-Shenker model the two order parameters can be used interchangeably, since there is no distinction between Higgs and confined phases. In practice, the electric one is more suitable to detect the Higgs regime (condensation of e particles and confinement of visons), while the magnetic one is preferred in the regime where e particles are confined and visons condense [200].

4.2.2 Spinful fermionic matter

We now turn our attention to models that feature fermionic matter fields. Here we focus on a system that was investigated by Gazit et al. [44, 45] where spinful fermions interacts with $\mathbb{Z}_2$ gauge fields. From the methodological point of view, this model is relevant because it allows for sign-problem free Quantum Monte Carlo (QMC) simulations. Observables can be computed for finite systems of relatively large size, so that the thermodynamic and zero-temperature limit can be reliably extracted. Physically, its phase diagram exhibits a number of interesting features that are a consequence of the the interplay between gauge fields and fermions. In reviewing these phases, we will have a first glance at how the presence of dynamic fermionic particles modifies a pure $\mathbb{Z}_2$ LGT. As usual, fermions live on the sites of the lattice, while gauge fields are on the links.[18] The model reads

$$H = H_f + H_{\mathbb{Z}_2}, \tag{4.30}$$

where the fermion Hamiltonian is

$$H_f = -t \sum_{\mathbf{r},\eta,\sigma} \left(c^\dagger_{\mathbf{r},\sigma} \sigma^z_{\mathbf{r},\eta} c_{\mathbf{r}+\eta,\sigma} + \text{h.c.} \right) - \mu \sum_{\mathbf{r},\sigma} c^\dagger_{\mathbf{r},\sigma} c_{\mathbf{r},\sigma} \tag{4.31}$$

with $\sigma = \pm$ labeling up and down spins, and the gauge theory Hamiltonian is the same as usual, e.g. Eq. (4.1). As in one dimension, fermions are minimally coupled to $\mathbb{Z}_2$ gauge fields through an appropriate version of the Peierls substitution. The Gauss law for this model is

---

[18] For a pictorial representation, the reader can refer to Fig. 4.9, which represents a system that is identical up to the fact that fermions are spinless.

$$G_{\mathbf{r}} = (-1)^{n_{\mathbf{r}}} \prod_{b \in +_{\mathbf{r}}} \sigma_b^x, \tag{4.32}$$

where $n_{\mathbf{r}} = c^\dagger_{\mathbf{r},\uparrow} c_{\mathbf{r},\uparrow} + c^\dagger_{\mathbf{r},\downarrow} c_{\mathbf{r},\downarrow}$ counts the total number of fermions at site $\mathbf{r}$. The meaning of this is that in a $\mathbb{Z}_2$ gauge theory it is the parity of charge carriers at each site that determines whether the site is a source of electric lines.[19] Importantly this model enjoys a global $U(1)$ symmetry, corresponding to a conservation of the total particle number. We can therefore consider sectors with different numbers of fermions independently. At $\mu = 0$ the Hamiltonian (4.32) exhibits a particle hole symmetry

$$c_{\mathbf{r},\sigma} \to (-1)^{\mathbf{r}} c^\dagger_{\mathbf{r},\sigma} \tag{4.33}$$

where $(-1)^{\mathbf{r}} = (-1)^{i_x + i_y}$.

This can be combined with the aforementioned $U(1)$ symmetry to obtain and enhanced $SU(2)$ “pseudospin” symmetry, generated by

$$P^+_{\mathbf{r}} = (-1)^{\mathbf{r}} c^\dagger_{\mathbf{r},\uparrow} c^\dagger_{\mathbf{r},\downarrow} \qquad P^-_{\mathbf{r}} = (-1)^{\mathbf{r}} c_{\mathbf{r},\uparrow} c_{\mathbf{r},\downarrow} \qquad P^z_{\mathbf{r}} = \frac{n_{\mathbf{r}\uparrow} + n_{\mathbf{r}\downarrow} - 1}{2}. \tag{4.34}$$

This rotates superfluid order into charge density wave order. Moreover, particle hole symmetry acting on one of the spin species only leaves the Hamiltonian invariant, but changes the sign of the Gauss law. Therefore it realizes an exact mapping between the odd and even sectors of the $\mathbb{Z}_2$ gauge theory. In the following, we always refer to the even case. We now outline the half-filling phase diagram, which is depicted in Fig. 4.7.

The deconfined-BCS phase

For $J \gg h, t$, all $\mathbb{Z}_2$ charges are deconfined. As $t \to 0$, fermions play the role of static charges for the pure $\mathbb{Z}_2$ LGT. As in the Ising theory discussed above, we expect a small finite hopping not to modify the physics of the gauge sector, but rather to shift the point of the confinement transition. For small non-zero h the $\mathbb{Z}_2$ electric field mediates weak attractive interactions between charges [36]. This causes a Cooper instability of the Fermi surface, which leads to a BCS ground state where the global $U(1)$ symmetry of the model is spontaneously broken. This is enriched by the presence of deconfined $\mathbb{Z}_2$ excitations, and so the phase is labeled SF* to distinguish it from a conventional superfluid. As a consequence of the additional $SU(2)$ symmetry at $\mu = 0$, the superfluid order parameter can be rotated into a charge-density wave (CDW) one, so that this phase can be characterized in either way.

The confined-BEC phase

As h is increased, the system enters the confined phase. Here pairs of $\mathbb{Z}_2$ charges with opposite spin are bound into on-site bosonic molecules $|\uparrow\downarrow\rangle$. This guaran-

---

[19] This is of course true even in the spinless cases studied e.g. in sections 2.2 and 4.3. In such models, however, this fact is hidden as there can be at most one fermion per site, and parity is in one-to-one correspondence with particle number.

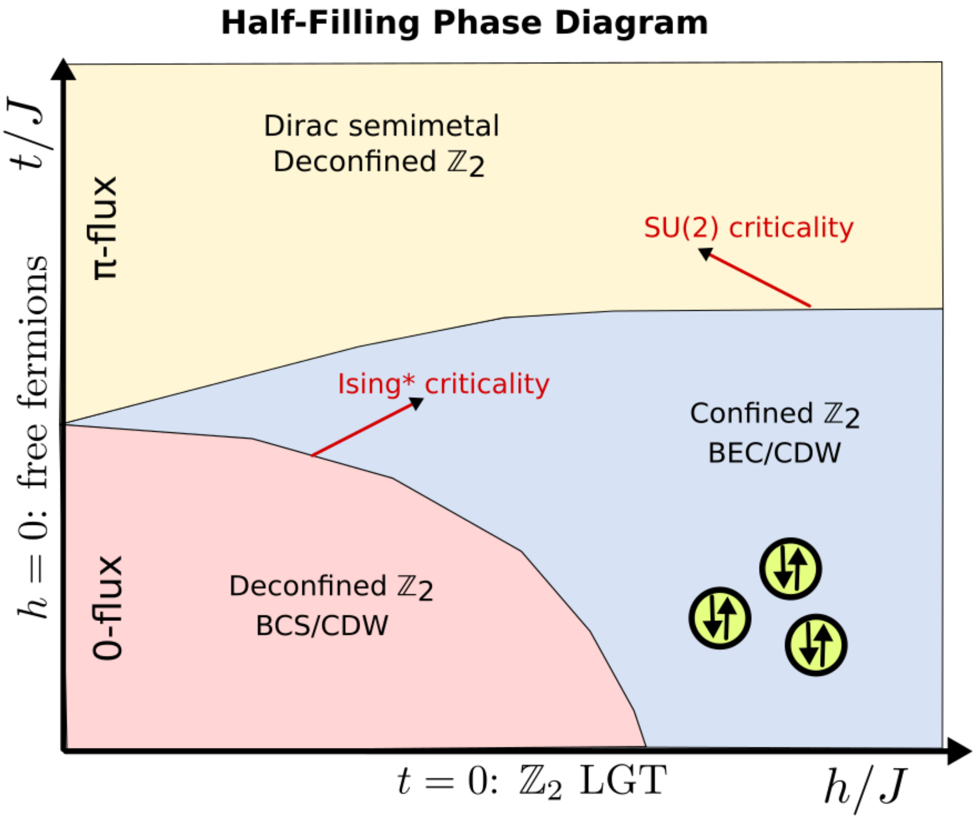
Half-Filling Phase Diagram
t/J
$h = 0$: free fermions
π-flux
0-flux
Dirac semimetal
Deconfined $\mathbb{Z}_2$
SU(2) criticality
Ising* criticality
Confined $\mathbb{Z}_2$
BEC/CDW
Deconfined $\mathbb{Z}_2$
BCS/CDW
$t = 0$: $\mathbb{Z}_2$ LGT
h/J

Figure 4.7: Schematic quantum phase diagram of the Hamiltonian (4.35) at half-filling. The axes $t = 0$ and $h = 0$ correspond to the pure $\mathbb{Z}_2$ LGT and free fermions respectively.

tees that there is no source of $\mathbb{Z}_2$ electric lines, and all the links can be in the energetically preferred state $\sigma^x = +1$ while still respecting the Gauss law. Perturbative corrections induce hopping and repulsion between the bosonic molecules. Intuitively, as h is increased the attraction between particles with opposite spins changes from strong to weak and the fermionic sector of the model experiences a typical BCS-BEC crossover. As above, the global $U(1)$ symmetry is spontaneously broken. Moreover, superfluid order and CDW order are degenerate with each other.

The deconfined-Dirac phase

To conclude, we analyze the regime where the hopping t is dominant. At $h = 0$ and in the absence of a strong plaquette term that forces the system into a 0-flux phase, the preferred configuration of fluxes is determined by the energetics of hopping fermions. At half filling, this actually favors a π flux, a result known as Lieb's theorem.[20] The corresponding free-fermions band structure exhibits two Dirac cones. As the density of states is vanishing at half filling (the Fermi surface reduces to two points), the ground state is stable to the introduction of finite h and there is no pairing. The entire large-t limit corresponds to a Dirac semi-metal.

---

[20] This is discussed further in section 4.3.2 for the case of spinless fermions, which is entirely equivalent in the absence of h. There we also present numerical results for the competition between J and t on a small cylinder.

Critical lines

Having justified the three regimes of the phase diagram of Fig. 4.7, let us see how they are connected. Along the line $h = 0$ there is a single critical point, corresponding to a transition from large to small Fermi surface which is not related to translational symmetry breaking. At small finite h, following vertical lines we encounter two transitions: the different deconfined phases are separated by a confined region. While this may sound counterintuitive, it is explained by the fact that increasing t generates a progressively larger negative correction to the plaquette term, so that effectively the ratio h/J grows leading to a confinement transition. As the negative effective J becomes dominant we are back into a plaquette dominated phase, this time the deconfined-Dirac one. For large enough h, only the confinement transition from the Dirac semi-metal to the BEC phase occurs. This is actually the most interesting one, as the two apparently independent phenomena of confinement and SSB of the global $U(1)$ symmetry happen simultaneously. The exotic quantum criticality associated with this transition was studied further in [45]. There it was shown that it can be described by an emergent non-abelian $SU(2)$ gauge theory with a matrix Higgs field. It was also proven that the two transitions can be split by introducing appropriate repulsive interactions, showing on the other hand that in this set up the exotic quantum critical point extends to a whole line.

4.3 $\mathbb{Z}_2$ lattice gauge theory with spinless fermionic matter

We now introduce the model to which the rest of this chapter is dedicated, i.e. a $\mathbb{Z}_2$ lattice gauge theory with spinless fermionic matter. The Hamiltonian of the model is the spinless version of the one reviewed in the previous section, which we rewrite once more for completeness.

$$H = H_f + H_{\mathbb{Z}_2}, \tag{4.35}$$

where the fermion Hamiltonian is

$$H_f = -t\sum_{\mathbf{r},\eta}\left(c^\dagger_{\mathbf{r}}\sigma^z_{\mathbf{r},\eta}c_{\mathbf{r}+\eta} + \text{h.c.}\right) - \mu\sum_{\mathbf{r}} c^\dagger_{\mathbf{r}}c_{\mathbf{r}} \tag{4.36}$$

and the gauge theory Hamiltonian

$$H_{\mathbb{Z}_2} = -J\sum_{\mathbf{r}*}\prod_{b\in\square_{\mathbf{r}*}}\sigma^z_b - h\sum_{\mathbf{r},\eta}\sigma^x_{\mathbf{r},\eta}. \tag{4.37}$$

Compared to the spinful case, the model at hand is deceptively simpler. Indeed, it enjoys less symmetries and lacks an interplay between spin and charge degrees of freedom. However the absence of spin, combined with the Gauss law, sets the stage for the emergence of a number of interesting and exotic behaviors. Firstly, spinless fermions are often associated with the possibility of p-wave superconductivity. Indeed, since the $\mathbb{Z}_2$ electric field mediates weak attractive interactions between fermions at small h, a Cooper instability that leads to triplet pairing is not unlikely. Secondly, similarly to 1d, the large h limit of a model with single-component fermions has to be an effective theory of dimers and therefore much richer compared to the spinful case.

From the technical point of view this model -to the best of our knowledge- cannot be studied with quantum Monte Carlo techniques. In particular the approach used in [44, 45] relied on the fact that at $\mu = 0$ the fermionic determinants coming from the two different spin species combine to give a positive definite weight, which is obviously not the case here. Still at half-filling, the sign problem is not present if the Gauss law is not enforced. This possibility is explored in [48], where it is found that the absolute ground state lies in the "staggered" gauge sector with the checkerboard Gauss law $G_\mathbf{r} = (-1)^\mathbf{r}$.

The goal of the rest of this section is to unveil the intricate phase diagram of the Hamiltonian (4.37). After giving an account of the symmetries of the model we consider various simple limits, which help understanding what happens at the boundaries of the phase diagram. We then try to connect these different regions by exploring more challenging regimes, with a particular focus on large h physics and half filling. The main results of this section are displayed in Fig. 4.8.

4.3.1 Symmetries of the model

Since we want to analyze this model in great detail, we give here a precise and self-contained account of all the symmetries.[21] Let us start with the gauge "symmetry". The Gauss law reflects the fact that fermions are a dynamical source of $\mathbb{Z}_2$ electric lines:

$$G_\mathbf{r} = (-1)^{n_\mathbf{r}} \prod_{b \in +_\mathbf{r}} \sigma_b^x = (-1)^{n_\mathbf{r}} A_\mathbf{r}. \tag{4.38}$$

In the rest of this chapter we will work in the sector where $G_\mathbf{r} = 1$ for all sites, which corresponds to the gauge theory with no background $\mathbb{Z}_2$ charges. In other words, the Hamiltonian (4.35) must be diagonalized under the local constraint $G_\mathbf{r} = 1$. We note that the "pure" even and odd $\mathbb{Z}_2$ lattice gauge theories are obtained as limits when the lattice is empty or fully filled, as under these conditions the matter fields are frozen and the Gauss law reduces to $A_\mathbf{r} = \pm 1$. We refer the reader to section 4.1 for an account of these models.

The gauge invariance comes from taking the global fermion parity symmetry

$$\Pi = \prod_\mathbf{r} (-1)^{n_\mathbf{r}} \tag{4.39}$$

and making it local with the help of new degrees of freedom. As already discussed in Chapter 2 for the one-dimensional case, this procedure usually trivializes the global symmetry, it the sense that it restricts it to a single sector. Indeed, when

---

[21] This partially overlaps with the discussion of section 4.2, but it does not hurt to have everything in one place.

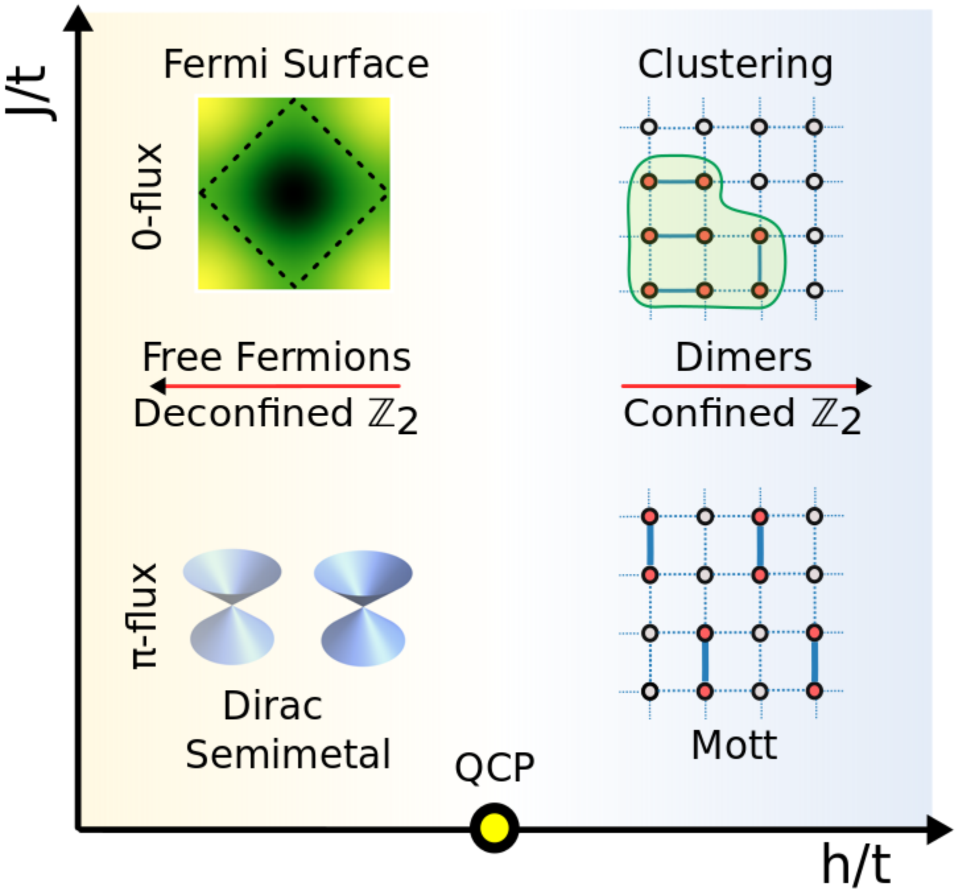

Figure 4.8: Schematic quantum phase diagram at half-filling: At a weak magnetic coupling there are two phases– the deconfined Dirac semimetal emerging in the π-flux $\mathbb{Z}_2$ gauge field background and the staggered confined Mott insulator. There is evidence that the two phases are separated by a single quantum critical point. On the other hand, in the regime $J \gg t$ we find a deconfined Fermi surface and a confined clustered phase. Away from the zero-tension regime, the Fermi surface is expected to have a BCS instability towards a p-wave paired superfluid state.

the model is defined on a closed surface such as a torus, the fermion number must be necessarily even[22], i.e., the physical Hilbert space contains only states with even fermion parity. On the other hand, in the presence of boundaries the situation is more subtle and the fate of the global fermion parity $\mathbb{Z}_2$ symmetry depends on how the Gauss law is implemented at the edge. For example, if the lattice terminates everywhere with links, the global fermion parity survives gauging and acts on the boundary links [113]. After taking a product of the Gauss law constraints over all sites, one finds

$$\Pi = \prod_{b \in \mathrm{edge}} \sigma_b^x, \tag{4.40}$$

which is the gauge-invariant t'Hooft loop operator of the $\mathbb{Z}_2$ gauge theory traversing

---

[22] This follows immediately from taking a product of the generators $G_{\mathbf{r}}$ over all sites of the lattice.

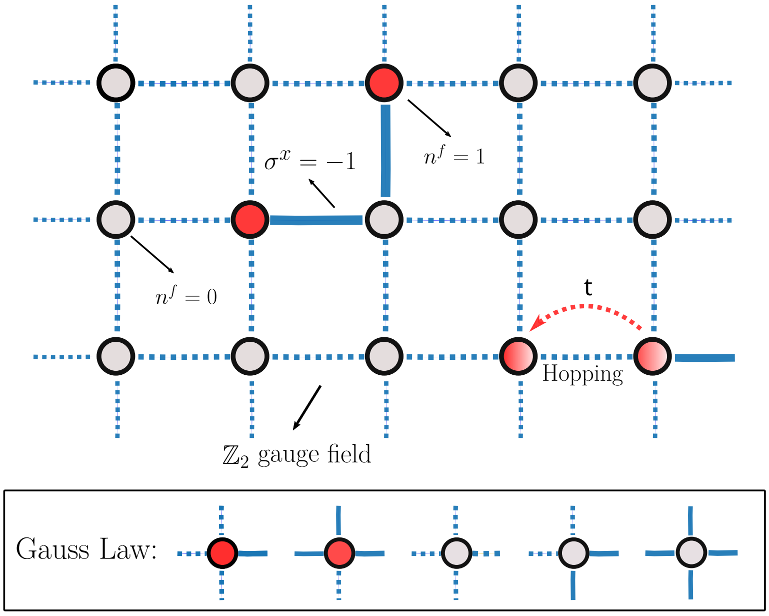

Figure 4.9: Illustration of the model. Matter degrees of freedom live on the sites of the lattice, while gauge fields are defined on the links. Fermions (red dots) must be connected by the electric lines $\sigma^x = -1$ (solid blue lines). In the panel below, we show the states of the local Hilbert space which satisfy the Gauss law $G_i = +1$. Occupied sites are sources to an odd number of $\mathbb{Z}_2$ electric lines.

the boundary. In this case both even and odd fermion numbers are allowed in the physical Hilbert space, but the symmetry operator is localized at the boundary.

Analogously to the spinful case studied in the previous section, this Hamiltonian is invariant under a global $U(1)$ symmetry that acts only on the fermionic degrees of freedom as $c_\mathbf{r} \to e^{i\alpha} c_\mathbf{r}$. One can thus introduce the associated $U(1)$ chemical potential μ to tune the fermionic density $n_\mathbf{r} = c^\dagger_\mathbf{r} c_\mathbf{r}$ in the ground state. Equivalently, one can focus on a sector with a given particle number and restrict the study to that particular sector. The particle-hole transformation (4.33) is to be restricted to a single species of fermions. While the hopping term in the Hamiltonian (4.36) commutes with this transformation, the chemical potential term anti-commutes with it. One thus might naively conclude that the problem is particle-hole symmetric at $\mu = 0$. However under this transformation the Gauss law changes sign $G_\mathbf{r} \to -G_\mathbf{r}$ and the even $\mathbb{Z}_2$ gauge theory ($G_\mathbf{r} = 1$) transforms onto the odd gauge theory($G_\mathbf{r} = -1$), where a static $\mathbb{Z}_2$ charge occupies every lattice site. As a result, the particle-hole transformation is not a symmetry, but relates the even and odd $\mathbb{Z}_2$ gauge theories at chemical potentials μ and $-\mu$, respectively.

As for the discrete symmetries, the Hamiltonian is invariant under one-site translations in both directions and under the D_4 point group transformations. In addition, both the Hamiltonian and the Gauss law are invariant under the following anti-unitary transformation

$$c_\mathbf{r} \to c_\mathbf{r}, \quad \sigma^x_{\mathbf{r},\eta} \to \sigma^x_{\mathbf{r},\eta}, \quad \sigma^y_{\mathbf{r},\eta} \to -\sigma^y_{\mathbf{r},\eta}, \quad \sigma^z_{\mathbf{r},\eta} \to \sigma^z_{\mathbf{r},\eta} \tag{4.41}$$

which realizes time-reversal symmetry in this model. Additionally, the energy spectrum is symmetric under $t \to -t$ since the two cases are related via the unitary transformation generated by $\prod_{\mathbf{r},\eta} \sigma^x_{\mathbf{r},\eta}$. Similarly, the unitary transformation $\prod_{\mathbf{r},\eta} \sigma^z_{\mathbf{r},\eta}$ flips the sign of the parameter h. As a result, henceforth we will consider only the regime $t, h \geq 0$.

To conclude, we point out that at $h = 0$ the model enjoys an additional *magnetic* symmetry, much like the pure $\mathbb{Z}_2$ lattice gauge theory studied in section 4.1. In this case the Hamiltonian commutes with gauge-invariant Wilson operators

$$W_{closed} = \prod_{b \in \text{loop}} \sigma^z_b,$$

where the product is taken over links forming a closed loop.[23] As a result, the model enjoys an additional global symmetry. Since this symmetry is generated by operators acting on co-dimension one manifolds, this is usually referred to as a one-form symmetry. Higher-form symmetries play an increasingly relevant role in the classification of quantum many-body systems, paving the way for a generalized Landau paradigm which is valid for all equilibrium phases of matter[201]. An example is that gauged fermion parity in a system with a symmetric ground state under the magnetic one-form symmetry implies symmetry-protected topological (SPT) order [142]. This can be seen as a higher dimensional extension of the concepts introduced in section 2.3.4. On the other hand, spontaneous symmetry breaking of the magnetic one-form symmetry leads to topological order [201, 202].

4.3.2 Free fermions in a static $\mathbb{Z}_2$ gauge field at $h \to 0$

Let us consider first the limit of vanishing $\mathbb{Z}_2$ electric fields, i.e. $h = 0$. We start by showing how the Hamiltonian can be expressed in terms of gauge invariant fermions and $\mathbb{Z}_2$ fluxes through a process of string-attachment.

Gauge invariant construction of the free-fermions Hamiltonian.

Consider the non-local operator [49]

$$f_{\mathbf{r}} = c_{\mathbf{r}} \, \Sigma^z_{\mathbf{r}} \tag{4.42}$$

where $\Sigma^z_{\mathbf{r}}$ is a semi-infinite string of σ^z operators that starts at site $\mathbf{r}$, but is otherwise arbitrary. The operator $f_{\mathbf{r}}$ defined above is gauge invariant, i.e. $G_{\mathbf{r}'} f_{\mathbf{r}} G^{-1}_{\mathbf{r}'} = f_{\mathbf{r}}$ for any choice of sites $\mathbf{r}$ and $\mathbf{r}'$ and for any choice of the string $\Sigma^z_{\mathbf{r}}$. The fermionic part of the Hamiltonian can now be rewritten as

$$H_f = -t \sum_{\mathbf{r},\eta} \left(f^\dagger_{\mathbf{r}} \bar{B}_{\mathbf{r},\eta} f_{\mathbf{r}+\eta} + \text{h.c.} \right) - \mu \sum_{\mathbf{r}} f^\dagger_{\mathbf{r}} f_{\mathbf{r}}, \tag{4.43}$$

where $\bar{B}_{\mathbf{r},\eta}$ are $\mathbb{Z}_2$ gauge-invariant parameters that can have values ± 1[49]. One possible convention is to choose horizontal strings that extend to the right of the given fermionic site. In this case one has $\bar{B}_{\mathbf{r},\eta} = 1$ on the horizontal links, while

---

[23] On an open lattice terminating with links, gauge-invariant Wilson lines ending on the boundary also commute with the Hamiltonian.

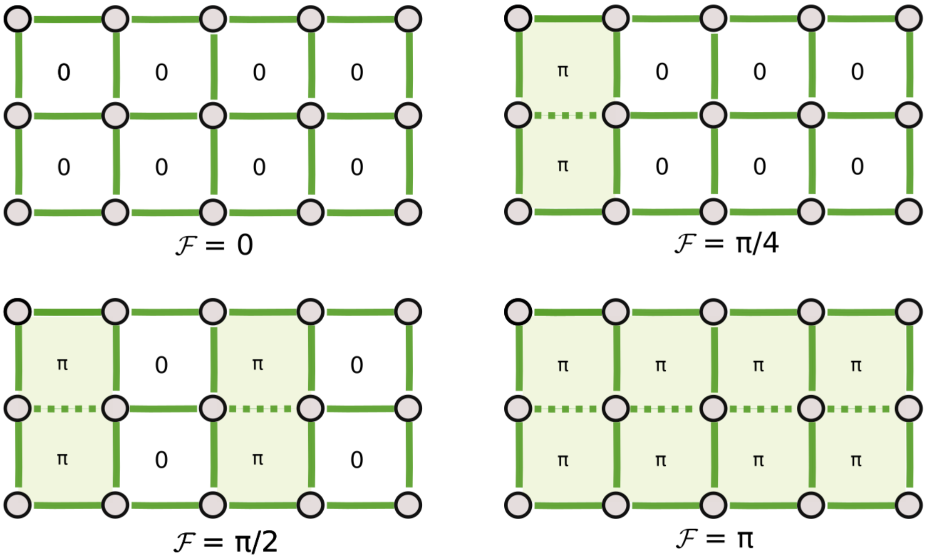

Figure 4.10: Example of hopping configurations that realize vertical stripes of π-flux plaquettes. The dashed lines denote links with $B_{ij} = -1$ and $\mathcal{F}$ represents the average $\mathbb{Z}_2$ flux.

on the vertical links it is possible to express $\bar{B}_{\mathbf{r},\eta}$ in terms of an infinite horizontal product of magnetic plaquette operators

$$\bar{B}_{\mathbf{r},\hat{y}} = \prod_{n\geq 1} B_{\mathbf{r}^*+n\hat{x}}.$$

Importantly, the product of $\bar{B}_{\mathbf{r},\eta}$ around a plaquette is the same as the the product of the gauge field σ^z around the same plaquette:

$$\prod_{b\in\square_{\mathbf{r}^*}} \bar{B}_b = \prod_{b\in\square_{\mathbf{r}^*}} \sigma^z_b.$$

Thus the gauge theory Hamiltonian (4.37) at $h = 0$ reduces to

$$H_{\mathbb{Z}_2} = -J\sum_{\mathbf{r}*} \prod_{b\in\square_{\mathbf{r}^*}} \bar{B}_b. \tag{4.44}$$

We have therefore rewritten our problem in terms of free $\mathbb{Z}_2$ gauge-invariant fermions $f_{\mathbf{r}}$ in a background configuration of the fields $\bar{B}_{\mathbf{r},\eta}$, which determine a certain pattern of static $\mathbb{Z}_2$ fluxes.[24]

Flux phases at half filling

The absolute ground state of this model can be found by solving the free fermion problem in different flux sectors and then choosing the one which minimizes the

---

[24] It is worth noting that the attachment of a string $S^z_{\mathbf{r}}$ that defines non-local gauge invariant fermions fixes the $\mathbb{Z}_2$ gauge redundancy. However, the arbitrariness in the form of this string leads to a new form of redundancy, under which both the fermions $f_{\mathbf{r}}$ and the parameters $B_{\mathbf{r},\eta}$ transform non-trivially.

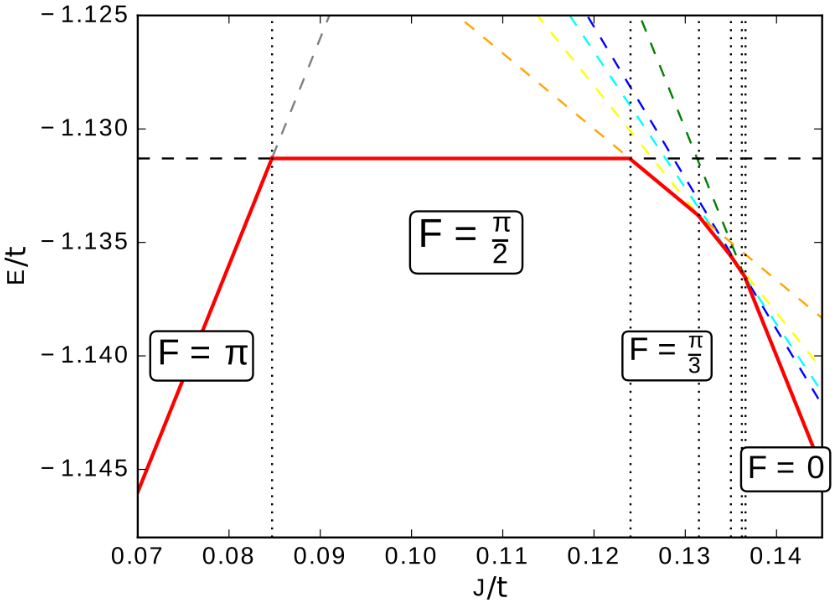

Figure 4.11: Ground state energy (red) and its average flux $\mathcal{F}$ as a function of J/t on a cylinder with $L_y = 2$. Dashed lines denote energies of configurations with different $\mathbb{Z}_2$ fluxes.

Hamiltonian $H_f + H_{\mathbb{Z}_2}$ [47, 49]. The half filling case $\mu = 0$ is particularly interesting: Lieb's theorem predicts that at $J = 0$ a π-flux configuration is energetically favorable [203]. In this case, the free-fermion band structure exhibits two Dirac cones at $(k_x, k_y) = (\pm\pi/2, \pi/2)$[25]. Any state with a different flux configuration has an energy gap that does not vanish even in the thermodynamic limit, and therefore plaquette excitations always cost a finite amount of energy. In summary, in this phase, $\mathbb{Z}_2$ charged fermions form gapless deconfined Dirac excitations, while the $\mathbb{Z}_2$ gauge fields are in the topologically ordered phase. This is the same phase of matter as the one depicted in yellow in the diagram of Fig. 4.7 for the spinful fermions.

On the other hand, for $J \gg t$ a zero-flux state is preferred, since every flipped plaquette comes with a large energetic penalty. The transition from a π-flux phase at small J to a zero-flux phase at large J can happen either sharply or through a series of intermediate configurations. Since each plaquette operator commutes with the Hamiltonian in this regime and thus can only take the values ± 1, such intermediate configurations must necessarily break translational invariance. In this case, the average flux over the extended unit cell takes fractional values (in units of π), as illustrated in Fig 4.10. As a concrete example, in Fig. 4.11 we provide numerical results for the transition between the π-flux and zero-flux limits on a thin cylinder with circumference $L_y = 2$. In this case, a number of intermediate flux phases appears as the dimensionless ratio J/t is tuned. Within each flux phase,

---

[25] We note that even away from half-filling a π-flux phase can always be obtained by choosing J to be negative and sufficiently large.

L_y	χ	$S_f + S_{\mathbb{Z}_2}$	S	Rel. Error
2	400	1.03972	1,03972	0.00
4	1000	3.04080	3.03225	$\approx 0.28\%$
6	2000	5.05664	4.93008	$\approx 2.5\%$

Table 4.1: Comparison between the entanglement entropy of our model at $J = h = 0$ at half filling with the predicted result $S = S_f + S_{\mathbb{Z}_2}$. The entropy S_f for hopping fermions in the π-flux background is computed numerically with iDMRG, with an error that is negligible compared to the one of S. The gauge contribution $S_{\mathbb{Z}_2} = (L_y - 1)\log 2$.

the ground state energy per unit cell is a linear function of J, and is given by

$$E_{gs}(J) = E^{\mathcal{F}} - J\langle \mathcal{P} \rangle, \tag{4.45}$$

where $E^{\mathcal{F}}$ is the ground state energy of free fermions in the flux-background $\mathcal{F}$ and $\langle \mathcal{P} \rangle$ is the average value of the plaquette operator within the extended unit cell. The competition between the two terms determines the most favorable configuration of $\mathbb{Z}_2$ fluxes[26].

Although for larger cylinders the computation of the ground state becomes numerically challenging, our analysis suggests that as L_y is increased the intermediate phases occupy a progressively smaller region of parameter space. In the thermodynamic limit we expect a sharp transition between the π-flux and the 0-flux phase, in agreement with the QMC results of [44], corresponding to the $h = 0$ line of Fig. 4.7. The interesting pattern emerging in Fig. 4.11 is therefore a peculiarity of small cylinders and has to be regarded as an example of quasi-1d phenomenology. This simple concrete example may be studied in cold atom based quantum simulators, where the implementation of $\mathbb{Z}_2$ lattice gauge theories on ladders and small cylinders is within reach [102].

Entanglement entropy and topological order

Deep in the deconfined phase of the $\mathbb{Z}_2$ gauge theory (toric code limit) the entanglement entropy under a bipartition into two half-infinite cylinders is given by

$$S_{\mathbb{Z}_2} = (L_y - 1)\log 2 \tag{4.46}$$

with the size-independent *topological entanglement entropy* γ being equal to $-\log 2$ [196]. Moreover, as argued above, at $h = 0$ and half-filling we expect a π-flux phase with a pair of deconfined Dirac fermions carrying $\mathbb{Z}_2$ charge, as long as $J \ll t$ (including the case $J \leq 0$). The entanglement entropy of such system is expected to split

$$S = S_f + S_{\mathbb{Z}_2}, \tag{4.47}$$

---

[26] In principle, this decomposition of the ground state energy E_{gs} allows to solve the problem analytically. However this involves a cumbersome task of calculating the fermionic band structure for a potentially infinite number of flux configurations $\mathcal{F}$.

with S_f being the entanglement entropy of free fermions hopping in the π-flux background. Numerical results confirm the prediction (4.47). Technically, in the thermodynamic limit the entropy S_f is unbounded because spinless fermions in a π-flux background form two Dirac cones that are at neutrality point at half filling. On the other hand, in a cylinder geometry quantization of momentum in the y-direction implies the existence of a finite size gap and the resulting entanglement entropy S_f is therefore finite[27]. In Table 4.1 we show that the formula (4.47) works very well for cylinders of size up to $L_y = 6$. This is a clear signature of a topologically ordered Dirac semimetal phase around half filling at $J \ll t$.

4.3.3 Quantum dimers at $h \to \infty$

If the coupling h is large, the electric strings become energetically expensive and isolated fermions are immobile [204]. At low energies they must form meson-like dimer states, where pairs of fermions are connected by a unit-length electric string. The dimers can be defined on links of the lattice and are created by the gauge-invariant operators $c^\dagger_{\mathbf{r}} \sigma^z_{\mathbf{r},\eta} c^\dagger_{\mathbf{r}+\eta}$. Due to the Pauli exclusion principle, any two links that share a site cannot simultaneously host dimers. The large h limit can be systematically constructed by starting from the classical Hamiltonian

$$\begin{aligned} H_0 &= -h \sum_{\mathbf{r},\eta} \sigma^x_{\mathbf{r},\eta} - \mu \sum_{\mathbf{r}} c^\dagger_{\mathbf{r}} c_{\mathbf{r}} \\ &= -h \sum_{\mathbf{r},\eta} \sigma^x_{\mathbf{r},\eta} - \frac{\mu}{2} \sum_{\mathbf{r}} \Big(1 - \prod_{b \in +_{\mathbf{r}}} \sigma^x_b\Big), \end{aligned} \tag{4.48}$$

where in the second line the Gauss law (4.38) was used. By tuning the chemical potential $\mu \sim h$ one can induce a finite density of dimers in the ground state. All the states with a fixed number of dimers have the same energy, and therefore the spectrum of H_0 is highly degenerate. For a fixed number of fermions the first excited states contain a single meson of length two. This is separated from the ground state by the gap $2h$. We now treat the remaining terms in the Hamiltonian as small perturbations and obtain and effective model that governs the dynamics of length one mesons.

First order perturbation theory: resonating dimers, Hilbert space fragmentation and clustering

At first order in degenerate perturbation theory, only the plaquette term

$$H_P = -J \sum_{\mathbf{r}*} \prod_{b \in \square_{\mathbf{r}*}} \sigma^z_b \tag{4.49}$$

contributes. Whenever an elementary plaquette is fully occupied with fermions this term induces transitions between two electric string configurations, as illustrated

---

[27] To be more precise, for a given L_y, whether a gap is present or not depends on the boundary conditions chosen for the fermions (periodic or antiperiodic). The latter can be interpreted as a the presence of a π flux threading the cylinder. As detailed in Appendix D, we observe that one of the two sectors remains gapless while the other one is gapped. Numerical results show that the absolute ground state always belongs to the gapped sector.

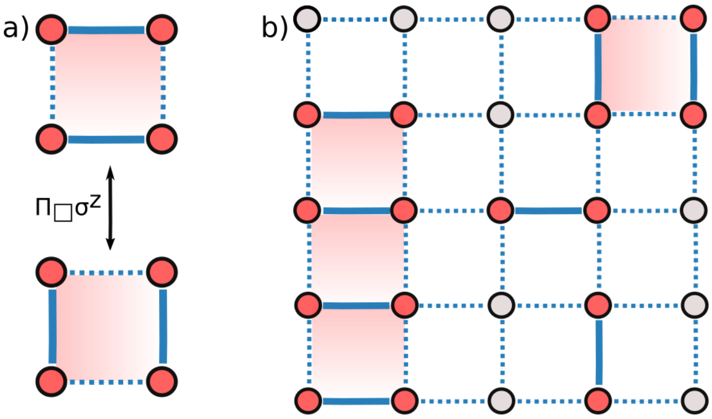

Figure 4.12: (a) Electric string transitions induced by the magnetic term on a plaquette that is fully occupied with fermions. (b) An example of quantum dimer configuration at partial filling. Highlighted in red are plaquettes fully filled with fermions, where the purely kinetic Rokhsar-Kivelson Hamiltonian resonates electric strings. On the other hand, isolated dimers are not affected by the magnetic term.

in Fig. 4.12a. Generically this results in a short-range attractive interaction of strength J between the dimers which is independent of the sign of J. At full filling, achieved at $\mu \gg h$, the problem reduces to the close-packed, purely kinetic Rokhsar-Kivelson quantum dimer model [205]

$$H_d = -J \sum \left(| \,\mid\;\;\mid\, \rangle \langle \,=\, | + \text{h.c.} \right) . \tag{4.50}$$

The ground state of this Hamiltonian is deeply in the confined regime of the odd $\mathbb{Z}_2$ gauge theory described in section 4.1.2. This shows how the large-μ and large-h limits of the phase diagram are connected.

At partial filling of fermions, the first-order effective Hamiltonian only resonates electric strings on islands of plaquettes that are fully occupied by fermions, but does not act on isolated dimers, see Fig 4.12b. For this reason, configurations where fermions are grouped in clusters are energetically favored. To study this in more detail, the perimeter of dimer arrangements in several disconnected sectors on a 5×5 lattice populated with four dimers can be computed numerically. The perimeter is a conserved quantity that is defined as shown in Fig. 4.14a and 4.14b. We find that a compact packing is preferred, i.e., the absolute ground state has the lowest perimeter, see Fig. 4.14 (c).

The full Hilbert space of the quantum dimer (4.50) model splits into many disconnected sectors. The logarithmic plot in Fig. 4.13 shows the number of these sectors as a function of dimer number for several different lattice sizes. The presence of an exponential number of disconnected subsectors originates from the $\mathbb{Z}_2$ gauge invariance of the original lattice gauge theory. Indeed, since we consider here the case with $t = 0$, the fermions are completely frozen and thus the problem reduces to a pure $\mathbb{Z}_2$ gauge theory in a background of static gauge charges. By construction, the resulting $\mathbb{Z}_2$ gauge invariant theory has an extensive number

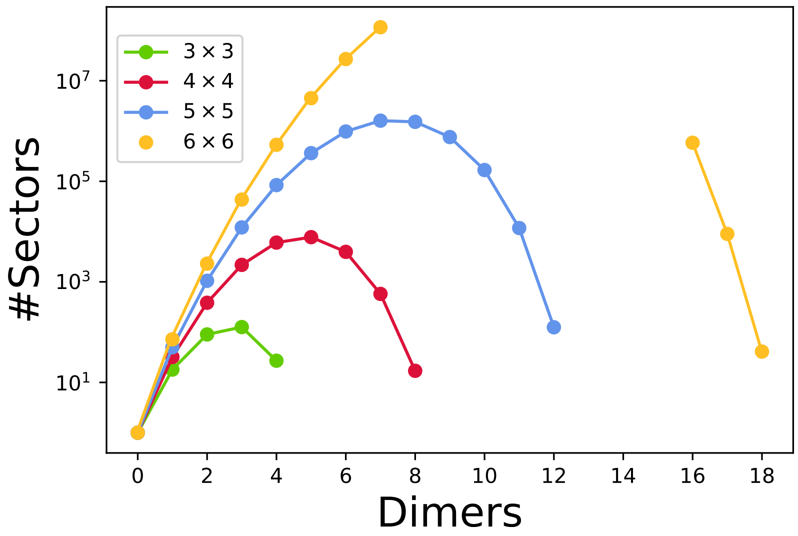

Figure 4.13: The number of disconnected subsectors of the Hilbert space as a function of the number of dimers for four different system sizes.

of local conservation laws and thus its Hamiltonian cannot connect subsectors characterized by different configurations of $\mathbb{Z}_2$ background charges. Similar physics arises in the strict confinement limit of the one-dimensional version of this lattice gauge theory studied in [187]. The phenomenon discussed here appears to be qualitatively different to the Hilbert space fragmentation introduced in [206, 207] in the context of dipole-conserving one-dimensional models. While in our case *local* $\mathbb{Z}_2$ gauge invariance is responsible for the fracture of the Hilbert space, what ensures the Hilbert space fragmentation of [206, 207] are *non-local* statistically localized integrals of motions that were introduced in [208].

Second order perturbation theory and the dimer-Mott state

The fermion hopping term in the Hamiltonian starts to contribute only at second order in perturbation theory, where it generates anisotropic short-range dimer hopping processes and repulsive interactions. An exact expression for the effective Hamiltonian can be obtained formally by employing the Schrieffer-Wolff transformation. Physically, the origin of these terms can be understood in complete analogy with their one-dimensional counterpart, where the same perturbation theory scheme is used. Therefore, we refer the reader to section 2.2.3 for more details. The hopping term has the following expression:

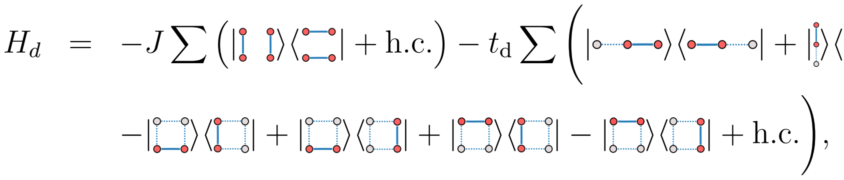

(4.51)

where t_d is of order t^2/h. The relative signs between the hopping processes stem from a careful consideration of fermionic statistics. From the equation above,

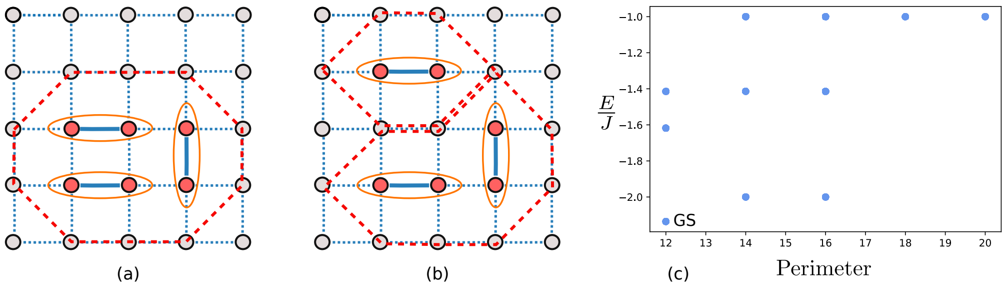

Figure 4.14: Zero fermionic hopping: (a) and (b) The perimeter is defined as the number of sites surrounding the dimers. The red dashed lines are the boundaries. Whenever a site lies on more than one boundary we count it again. Thus the perimeter in (a) is 10, while the perimeter in (b) is 15. (c) Four dimers on a 5×5 lattice: The lowest energy of each sector is plotted together with its perimeter. We observe that the ground state of the Hamiltonian has the smallest perimeter.

we learn that dimers cannot hop in the direction perpendicular to the electric string and thus exhibit restricted mobility. Contrary to dipoles in some theories of fractons [209, 210], where restricted mobility follows from symmetries, here it is imposed energetically.

In addition, second order processes give rise to short-range repulsive interactions between dimers. The energy scale of this effect is of order t^2/h, and so it is generally overshadowed by the first-order attraction of strength J discussed above. At $J = 0$ and when the density of dimers is significant, however, the repulsion is important and needs to be taken into account. In particular, at commensurate fillings it can potentially stabilize a Mott-insulating state of dimers. At half filling the staggered Mott pattern shown in Fig. 4.15 is a natural candidate, since this arrangement minimizes the inter-dimer repulsion. Whether this prediction is correct or not can be tested by obtaining the ground state wave function on cylinders of circumference up to $L_y = 8$ using iDMRG. The results for the fermion density, shown in Fig. 4.15, confirm that the guess is indeed correct up to the largest system size that we could probe. The Mott gap can be estimated by tuning the chemical potential away from the value $\mu = h$ until the filling deviates from 1/2. By doing this, we find that the gap decreases as h is increased, and at large h it is proportional to the emergent energy scale t^2/h, as shown in Fig. 4.15c.

Cluster dynamics

Second order perturbation theory can also be used to study how clusters slowly move by hopping all the dimers that form them, once a finite t is introduced. For a cluster composed of n_d dimers, this process is of the order t^{2n_d}, which leads to an extremely small energy-level splitting. We first study the physics of the smallest cluster. Specifically, we perform an exact diagonalization calculation for two dimers on a periodic 8×8 lattice. In Fig. 4.16a the degenerate energy levels of the lowest band have been resolved into momentum eigenstates with wave numbers $\boldsymbol{k} = (2\pi n/L, 2\pi m/L)$, where $n, m = 0, \ldots, L-1$. The ground state has zero momentum. Qualitatively, we observe that the band resembles a simple

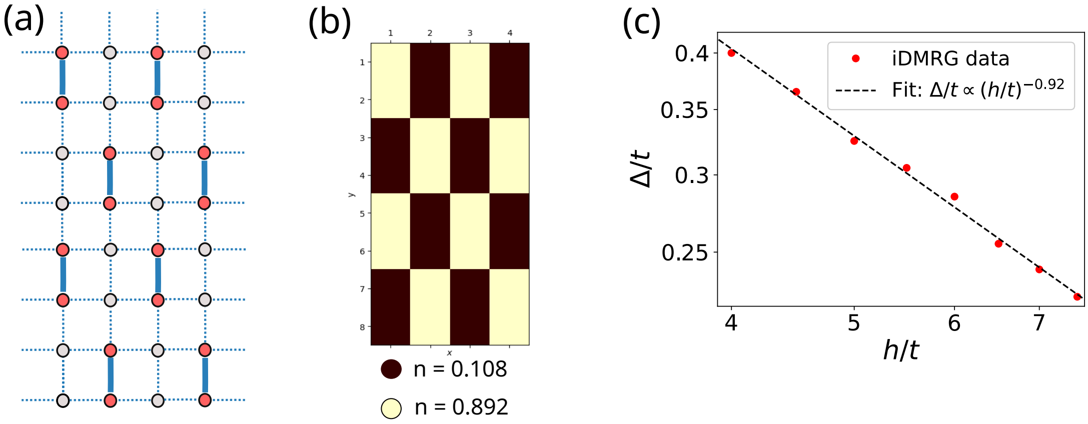

Figure 4.15: (a) Schematic illustration of a staggered dimer Mott state at half filling. For each dimer, the six sites directly next to it are empty, minimizing the energy penalty due to the repulsion between different dimers. (b) iDMRG results for the local fermion density on a cylinder of circumference $L_y = 8$ at $h/t = \mu/t = 4$ and $J = 0$. The arrangement of fermions into a staggered pattern of dimers is clearly visible. (c) Mott gap as a function of h. For large values of h the gap scales approximately as t^2/h, consistent with the second order perturbation theory emergent energy scale.

cosine band of an elementary particle hopping on a square lattice. Consistent with expectations from perturbation theory, we find that the bandwidth scales as t_d^2/J as $t_\mathrm{d} \to 0$.

Then, in order to explore the hopping of larger clusters, we numerically diagonalize a system of three dimers on a periodic 7×7 lattice, see Fig.4.16b. Here the excited levels are measured from the respective ground state at a given value of t_d, i.e. the plot shows the energy differences

$$\Delta E \equiv E_i(t_\mathrm{d}) - E_0(t_\mathrm{d}).$$

At finite t_d the ground state is 4-fold degenerate, with momentum wavevectors $\boldsymbol{k} = (0, \pm 6\pi/7), (\pm 6\pi/7, 0)$. Due to the four-fold rotation symmetry of the lattice some excited states retain their 4-fold or 8-fold degeneracy. The four ground states together with the lowest 45 excitations make up the first energy band. The same figure also shows a power-law fit to the lowest and highest excitation of the first and second band as a function of t_d/J. The second band has an energy dependence that scales as $(t_\mathrm{d}/J)^3$. This is consistent with our expectation that the bandwidth of a cluster composed of n_d dimers should scale as $\propto t_\mathrm{d}^{n_\mathrm{d}}$ in the limit $t_\mathrm{d} \to 0$. In contrast, the energies in the lowest band scale for $t_\mathrm{d} \ll J$ as the power-law $(t_\mathrm{d}/J)^4$.

Immobile excitations

Having looked into the physics of extended clusters, let us now calculate the band structure for a single dimer. Since the dimers live on links, each unit cell of the square lattice can be occupied by either a horizontal or a vertical dimer, resulting in two energy bands. We denote the creation operators of the horizontal and

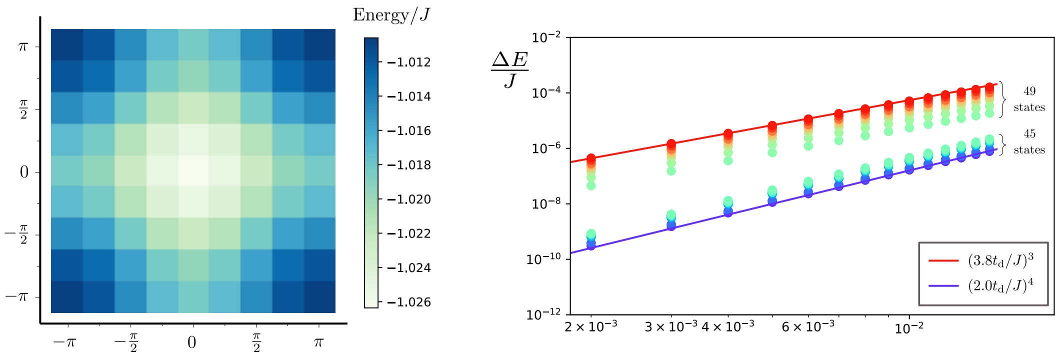

(a) (b)

Figure 4.16: Finite fermionic hopping: (a) Excitation energies of the lowest band of the Hamiltonian (4.51) with $t_\mathrm{d} = 0.05J$ on an 8×8 lattice with the cluster composed of two dimers, plotted in the first Brillouin zone. The ground state (center) is a zero momentum eigenstate. (b) Double logarithmic plot of the lowest two bands of excitation energies of the Hamiltonian (4.51), after subtracting the ground state energy, on a 7×7 lattice for a cluster composed of three dimers. The excitation energies of the two lowest bands grow as $\propto t_\mathrm{d}^4/J^3$ and $\propto t_\mathrm{d}^3/J^2$ for $t_\mathrm{d} \ll J$.

vertical states in the unit cell at site $\mathbf{r}$ by the operators $c^\dagger_\mathbf{r}$ and $d^\dagger_\mathbf{r}$, respectively. The dimensionless Hamiltonian takes the form

$$\begin{aligned} H/t_\mathrm{d} = \; & -\textstyle\sum_{\boldsymbol{r}} \left[-d^\dagger(\boldsymbol{r}) + d^\dagger(\boldsymbol{r}+\hat{x}) + d^\dagger(\boldsymbol{r}-\hat{y}) - d^\dagger(\boldsymbol{r}+\hat{x}-\hat{y})\right] c(\boldsymbol{r}) + \text{h.c.} \\ & -\textstyle\sum_{\boldsymbol{r}} c^\dagger(\boldsymbol{r}+\hat{x})c(\boldsymbol{r}) + \text{h.c.} - \sum_{\boldsymbol{r}} d^\dagger(\boldsymbol{r}+\hat{y})d(\boldsymbol{r}) + \text{h.c.} \end{aligned} \tag{4.52}$$

After Fourier transforming and diagonalizing, one obtains the two energy bands. The lowest band

$$\epsilon^{(1)}_{\boldsymbol{k}} = -2t_\mathrm{d}, \tag{4.53}$$

is flat, implying a macroscopic ground state degeneracy. The second band has cosine dispersion

$$\epsilon^{(2)}_{\boldsymbol{k}} = 2t_\mathrm{d}\left(1 - \cos k_x - \cos k_y\right). \tag{4.54}$$

The flatness of the lower band has striking consequences. To start, it implies that it is possible to create localized immobile excitations. We can construct such a frozen excitation explicitly as the following linear combination of the four dimer states around a single plaquette

$$F^\dagger_\mathbf{r} \equiv \frac{1}{2}\left[d^\dagger_\mathbf{r} - d^\dagger_{\mathbf{r}+\hat{x}} - c^\dagger_\mathbf{r} + c^\dagger_{\mathbf{r}+\hat{y}}\right]. \tag{4.55}$$

The state $|\psi(\boldsymbol{r})\rangle \equiv F^\dagger_\mathbf{r}|0\rangle$ created by this operator can be represented visually as

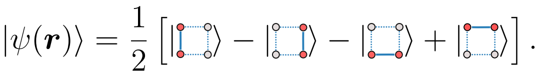

(4.56)

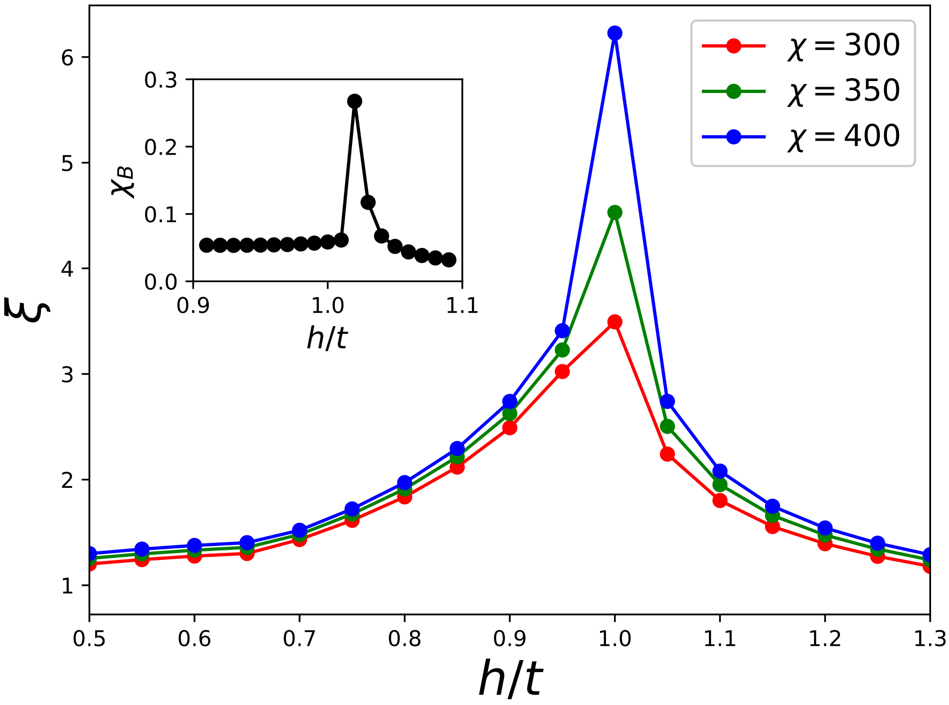

Figure 4.17: Correlation length ξ as a function of the electric coupling h, calculated with iDMRG on a cylinder with circumference $L_y = 4$ for $J = 0$. The system is kept at half filling by setting $\mu = h$. The peak in the correlation length is a signature of a quantum phase transition between a topologically ordered π-flux Dirac phase and a translational symmetry-breaking staggered Mott phase of dimers. The inset shows the magnetic susceptibility χ_B that exhibits a peak at the transition.

When the Hamiltonian acts on this state, the relative signs of its hopping terms, which have their origin in fermionic statistics, lead to a cancellation of hopping processes that would move the dimer away from the plaquette. Thus the dimer remains localized on this plaquette forever. As a consequence, it is possible to write down a many-body frozen state by creating well-separated frozen plaquette excitations. Since these dimers do not spread, they cannot interact and thereby are exact eigenstates of the Hamiltonian.

4.3.4 Half filling phase diagram and exotic quantum criticality

Given what we have learned so far, we can now combine our knowledge to understand the half-filling phase diagram of Hamiltonian (4.35) at $J = 0$.

At large h the ground state exhibits a “dimer-Mott” pattern that breaks translational symmetry spontaneously, as shown in Fig. 4.15. As the dimers are formed by tightly bound fermionic particles, which are the carriers of $\mathbb{Z}_2$ charge, the gauge sector lies in the confined phase. In the opposite limit $h \to 0$, the free Dirac fermions coexist with topologically ordered deconfined $\mathbb{Z}_2$ gauge fields. Analogously to the spinful case reviewed in section 4.2.2, at half filling the Fermi surface reduces to a point and the fermionic density of states vanishes. For this reason, turning on a weak attraction between particles is not enough to cause a Cooper instability, and we expect the "deconfined-Dirac" phase to be stable even at finite h, away from the free fermions point. Since these two limits are so radically different, it is natural to expect one or more quantum phase transitions as h is tuned from small to large values.

Numerical evidence for a transition is gathered by performing iDMRG simulations. On a cylinder of finite L_y both these phases are gapped[28], but a gap closing must occur at the transition point. This can be detected for instance by looking for peaks in the correlation length ξ, which is shown in Fig. 4.17. Such results suggest that a single transition occurs. Further analysis of the numerical data shows that at the transition point both confinement of the gauge fields and spontaneous breaking of the translational symmetry occur simultaneously. In the gauge sector, this is signaled by a peak in the $\mathbb{Z}_2$ magnetic susceptibility

$$\chi_B = \partial\overline{\langle P_{\mathbf{r}^*}\rangle}/\partial h, \tag{4.57}$$

where $P_{\mathbf{r}^*}$ is the plaquette operator (5.42) and the overbar denotes the average over a unit cell. This peak is shown in the inset of Fig. 4.17. The nature of this transition is of great interest, as it is not clear *a priori* and somewhat surprising that confinement of $\mathbb{Z}_2$ charges and SSB happen simultaneously. Such phenomenology reminds us of the transition between the deconfined-Dirac and confined-BEC phases studied in [45] and reviewed in section 4.2.2. There, confinement was also accompanied by the breaking of a global symmetry, $U(1)$ particle number conservation, leading to a very exotic type of quantum criticality. A more rigorous study of the transition in our system is deferred to a future work.

---

[28] See Appendix D for details about fermions in a π flux on the cylinder.

Chapter 5

$\mathbb{Z}_2$ gauge theories with spinless fermionic matter as spin $1/2$ systems

This chapter is devoted to a special feature of $\mathbb{Z}_2$ lattice gauge theories with spinless fermionic matter, namely the fact that they can be mapped *locally* to models of *gauge invariant* spins - in any dimension. This is remarkable for a number of reasons:

- The mapping unveils the fact that[1] the Hilbert space of the bulk of the system is essentially bosonic in nature. A basis is formed by spins constructed from states with two neighboring fermions.
- The spin model is defined directly in a physical, reduced Hilbert space where the Gauss law is automatically satisfied. The mapping is valid for any choice of $G_i = \pm 1$, with different choices only differing in the signs of some operators. From the computational point of view, the size of the Hilbert space is reduced, with significant advantages. As an example, in a 2d LGT on the square lattice with N sites there are 2^{3N} degrees of freedom, as a unit cell is formed by a site and two links. The dual model consists of link variables only, and so its Hilbert space has dimension 2^{2N}.
- Spin systems are generally regarded as easier to study numerically compared to fermions, and a wider array of techniques is available. Many numerical methods (e.g. DMRG and related MPS algorithms) convert fermions to spins using the Jordan-Wigner transformation, which introduces non-local couplings. A direct study of the spin system avoids this intermediate step.
- Local mappings present less subtleties, and do not change the characterization of the physics of the system as much as non-local ones. For example, the Kitaev and Ising chains are dual under the non-local Jordan-Wigner transformation, but the physical description of the corresponding phases differs substantially.
- In order to find numerically (e.g. with DMRG) the ground state of the system in the appropriate gauge sector the original Hamiltonian must be

---

[1] At least for the even case $G_i = +1$, on which we focus.

minimized while adding a term that energetically penalizes states belonging to the other sectors. This introduces errors and an additional convergence parameter. Working with a model which is already in the desired sector, devoid of any gauge redundancy, avoids this problem entirely.

While in this chapter we emphasize the simplicity and convenience of this specific mapping for for gauge theories with spinless fermionic matter and $\mathbb{Z}_2$ gauge fields, similar ideas are present in the literature. The construction of [211, 212] is very general and shows how to trade fermionic matter with hardcore bosons in generic gauge theories by constructing an appropriate unitary transformation. Related two-dimensional bosonization mappings were introduced in [52, 213–217]. In the latter case, one starts with a two-dimensional (ungauged) fermionic problem and maps it onto a $\mathbb{Z}_2$-gauged spin 1/2 model. Here on the other hand, our starting point is the gauged fermionic theory which maps to an unconstrained spin model.

Structure

This chapter is structured as follows: the two main sections 5.1 and 5.2 are dedicated to the mapping in one and two dimensions respectively. They develop in the same way, by first introducing the new gauge invariant variables and then discussing how relevant observables and Hamiltonians transform under the mapping. Along the way, we have the opportunity to restate and reinterpret some of the results of the previous chapters in terms of spin models.

5.1 The mapping in one dimension

The goal of this section is to understand how to map one-dimensional $\mathbb{Z}_2$ gauge models to systems of gauge invariant spins. To this purpose, one first introduces new gauge-invariant spin 1/2 degrees of freedom and then uses the Gauss law explicitly to write any operator of the original theory in this new language.

5.1.1 Gauge invariant spins

As a first step, we introduce Majorana variables

$$\gamma_i = c_i^\dagger + c_i, \qquad \tilde{\gamma}_i = i(c_i^\dagger - c_i) \tag{5.1}$$

or, conversely,

$$c_i = \frac{\gamma_i + i\tilde{\gamma}_i}{2}, \qquad c_i^\dagger = \frac{\gamma_i - i\tilde{\gamma}_i}{2}, \tag{5.2}$$

which satisfy the hermiticity condition $\gamma_i^\dagger = \gamma_i$ and the anticommutation relations

$$\{\gamma_i, \gamma_j\} = 2\delta_{ij}, \qquad \{\tilde{\gamma}_i, \tilde{\gamma}_j\} = 2\delta_{ij}, \qquad \{\gamma_i, \tilde{\gamma}_j\} = 0. \tag{5.3}$$

As a reference for the following we also remind that the local fermion parity can be expressed as

$$\Pi_i = (-1)^{n_i^f} = i\tilde{\gamma}_i\gamma_i, \tag{5.4}$$

and for spinless fermions is in one-to-one correspondence with the density, i.e. $\Pi_i = 1 - 2n_i^f$. We now define the following operators which satisfy the Pauli algebra, and can therefore be regarded as new spin 1/2 variables:

$$\begin{aligned} X_{i,i+1} &= \sigma^x_{i+1/2} \\ Y_{i,i+1} &= -i\tilde{\gamma}_i \sigma^y_{i+1/2} \gamma_{i+1} \\ Z_{i,i+1} &= -i\tilde{\gamma}_i \sigma^z_{i+1/2} \gamma_{i+1}. \end{aligned} \tag{5.5}$$

The properties of the Majorana operators ensure that the new variables in Eq. (5.5) square to the identity and follow the appropriate (anti)commutation relations. We see that Eq. (5.5) is a local transformation that defines a new link variable for each site-link-site triplet. In other words, sites are removed from the physical space which is halved in size, consisting now of links exclusively. In order for this to be of any use, of course, we need to be able to express all the observables of the gauge theory in terms of these new spins, and not just some gauge-invariant Majorana bilinears. Let's see how this works.

5.1.2 Mapping of Hamiltonians

We now show how typical Hamiltonians look after the mapping. Since equation (5.5) is expressed in terms of Majorana operators, we will focus on those and comment later on what they correspond in terms of c-fermions. The mapping uses explicitly the Gauss law, and therefore it has a different form in each sector of the gauge theory. Here we focus on the sector $G_i = 1$, where

$$\Pi_i = \sigma^x_{i-1/2}\,\sigma^x_{i+1/2} = X_{i-1/2}\,X_{i+1/2}. \tag{5.6}$$

The derivations below, in any case, generalize readily to arbitrary sectors by taking appropriate care of the minus signs that pop up along the way.

Mapping of density-dependent terms

We start with the fermion density $n_i^f = c_i^\dagger c_i$, which is mapped using the Gauss law only:

$$n_i^f = \frac{1+\Pi_i}{2} = \frac{1 + X_{i-1/2}\,X_{i+1/2}}{2}. \tag{5.7}$$

This means that any "chemical potential" term maps into an Ising-type interaction. Moreover, we learn that the particle number now corresponds to the number of domain walls. In the same fashion, any kind of density-density interaction is mapped through the Gauss law. For example, a nearest neighbor interaction gives

$$n_i^f n_{i+1}^f = \frac{1 + X_{i-1/2}\,X_{i+1/2}}{2}\,\frac{1 + X_{i+1/2}\,X_{i+3/2}}{2} = \frac{\Big(1 + X_{i-1/2}X_{i+1/2} + X_{i+1/2}X_{i+3/2} + X_{i-1/2}X_{i+3/2}\Big)}{4}$$

where we have used that on the central link $X^2 = I$ to simplify the last term.

Mapping of fermion bilinears

The bilinear $-i\tilde{\gamma}_i\sigma^z_{i+1/2}\gamma_{i+1}$ maps trivially to $Z_{i+1/2}$ under (5.5). This is exactly what appears in the gauged Kitaev chain (2.54), which indeed takes a very simple form under the mapping. The bilinear $-i\gamma_i\sigma^z_{i+1/2}\tilde{\gamma}_{i+1}$, on the other hand, requires some more work and needs resolving the Gauss law to be mapped: one gets

$$\begin{aligned}
&- i\gamma_i\sigma^z_{i+1/2}\tilde{\gamma}_{i+1} = -i\,\underbrace{\tilde{\gamma}_i\tilde{\gamma}_i}_{=I}\,\gamma_i\sigma^z_{i+1/2}\tilde{\gamma}_{i+1}\,\underbrace{\gamma_{i+1}\gamma_{i+1}}_{=I} = \\
&\underbrace{-i\tilde{\gamma}_i\sigma^z_{i+1/2}\gamma_{i+1}}_{=Z_{i+1/2}}\,\Pi_i\Pi_{i+1} = -Z_{i+1/2}X_{i-1/2}X_{i+1/2}\,X_{i+1/2}X_{i+3/2} = \\
&- X_{i-1/2}\,Z_{i+1/2}\,X_{i+3/2}
\end{aligned} \tag{5.8}$$

which is the stabilizer of the cluster model, a spin 1/2 chain with $\mathbb{Z}_2 \times \mathbb{Z}_2$ symmetry [218–220].

Mapping of generic quadratic Hamiltonians

The quadratic part of any generic Hamiltonian where fermions are coupled to $\mathbb{Z}_2$ gauge fields reads

$$\begin{aligned}
H_G = &- t\sum_i \left(\hat{c}_i^\dagger\,\sigma^z_{i+\frac{1}{2}}\,\hat{c}_{i+1} + h.c\right) - \Delta\sum_i \left(\hat{c}_i^\dagger\,\sigma^z_{i+\frac{1}{2}}\,\hat{c}_{i+1}^\dagger + h.c\right) = \\
&i(t+\Delta)\sum_i \left(\tilde{\gamma}_i\sigma^z_{i+\frac{1}{2}}\,\gamma_{i+1}\right) - i(t-\Delta)\sum_i \left(\gamma_i\sigma^z_{i+\frac{1}{2}}\,\tilde{\gamma}_{i+1}\right)
\end{aligned} \tag{5.9}$$

where we have separated the contributions of the two Majorana bilinears to make quick use of the expressions derived above. This maps to

$$H = -(t+\Delta)\sum_i Z_{i+1/2} - (t-\Delta)\sum_i X_{i-1/2}Z_{i+1/2}X_{i+3/2}. \tag{5.10}$$

Density density interactions can easily be included as explained above (See Eq. (5.7) and below). Besides, any electric term involving one or more factors of σ^x maps trivially, since σ^x remains unchanged under the transformation (5.5). More complicated terms that describe e.g. pair-pair interactions can be accounted for as well, but we will not treat them here.

5.1.3 Notable examples

As notable applications of the mapping (5.5), we consider the two relevant cases corresponding to the models discussed in Ch. 2.

The U(1) conserving model

For the particle-number conserving model (2.19), we need to set $\Delta = 0$ in (5.10) so that the pairing term vanishes. We obtain

$$H = -\frac{t}{2}\sum_i Z_{i+1/2} - X_{i-1/2}Z_{i+1/2}X_{i+3/2} \tag{5.11}$$

which is the Hamiltonian of the cluster model in an external field. Despite the slightly unusual appearance, it can be shown that this corresponds indeed to free fermions with a global $U(1)$ symmetry[2], with all the caveats explained in section 2.2.1. The conservation of particle number in the original model corresponds here to conservation of domain walls, i.e.

$$[H, Q] = 0, \qquad Q = \sum_i \frac{1 - X_{i-1/2} X_{i+1/2}}{4}. \tag{5.12}$$

Indeed, it is instructive to notice that the term $Z_{i+1/2}(1 - X_{i-1/2} X_{i+3/2})$ is nothing but a hopping, since it flips a spin (in the X basis) only if the two neighboring spins point in opposite directions, i.e. if it belongs to the boundary of a domain wall. To conclude, we note that the dimers that emerge naturally in the large h limit studied in section (2.2.3) are simply isolated magnons in the spin language.

Gauged Kitaev chain

As mentioned already at the beginning of section 2.3.3, the $\mathbb{Z}_2$ gauged Kitaev chain maps to the Ising model in a transverse and longitudinal field.[3]. All we need to do to obtain this result is to set $\Delta = t$ in Eq. (5.10) and add the "chemical potential" and electric terms: we obtain

$$H = \frac{\mu}{2} \sum_j X_{j-1/2} X_{j+1/2} - t \sum_j Z_{j+1/2} - h \sum_j X_{j+1/2}. \tag{5.13}$$

This allows us to reinterpret the physical results of section 2.3 from a different perspective and unveil some intriguing dualities. Let us focus first on the line $h = 0$, where non-trivial edge physics appears. Here we have a transverse field Ising model (TFIM), which makes manifest that the deconfined (large μ) phase is characterized by spontaneous symmetry breaking. The first subtlety arises in the Higgs phase. In the large t limit the ground state of (5.13) is a trivial paramagnet, apparently in contrast with our claim that this regime hosts a non-trivial SPT. The puzzle is solved if we remember that under the mapping (5.5) Z is a composite object so that the ground state, expressed in the original variables, carries non-trivial entanglement.

The reader might be confused by the following fact: while the gauged Kitaev chain is found to be *locally* equivalent to the TFIM, this is also the Jordan-Wigner (JW) dual of the *ungauged* Kitaev chain. So what is happening? Are the two models equivalent? The answer is that they are definitely not: indeed, if we compare the Hamiltonian (5.13) with the JW dual (2.53) found in section 2.3, we find that the roles of the parameters are swapped! Let us clarify these relationships, with the help of the diagram in Fig. 5.1. Starting from the Kitaev chain (2.44) we see that gauging fermion parity symmetry leads to a symmetry-breaking deconfined

---

[2] From the "cluster model" perspective, the external field drives the system out of the SPT phase. At the value corresponding to (5.11), we are exactly at the gapless critical point that it is known to correspond to free fermions.

[3] Among other things, this creates interesting connections with the ideas presented in section 3.3

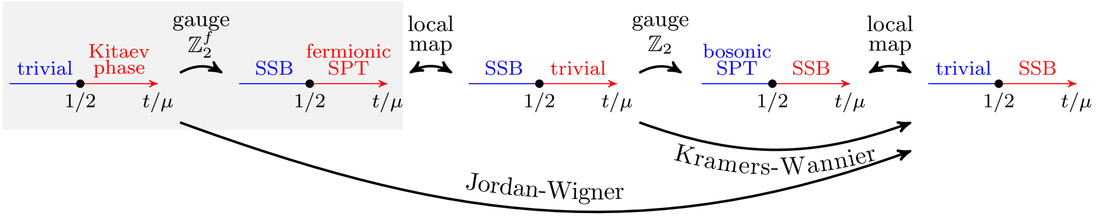

Figure 5.1: Relations between the gauged and ungauged Kitaev chains and Ising models for $h = 0$. The Kitaev chain (left) can be gauged as explained in section 2.3. The resulting Hamiltonian is identified with a TFIM (center) through a *local* transformation. Yet a different TFIM (right) can be obtained either as the Jordan-Wigner dual of the original Kitaev chain, or as the Kramers-Wannier dual of the aforementioned Ising model (i.e., of the gauged Kitaev chain).

phase, and a symmetry-protected topological Higgs phase. Morever, the latter has fermionic edge modes and is thus a fermionic SPT phase. This is summarized in the gray box in Fig. 5.1. Moreover, a local change of variables (5.5) maps the latter SPT phase to a trivial product state, which is summarized by the second black arrow in Fig. 5.1. We discussed how this Ising chain has a magnetic $\mathbb{Z}_2$ symmetry for $h = 0$. In principle, this symmetry could also be gauged. Similar to before, we find that the trivial phase maps to a symmetry-breaking phase, and the other phase maps to a (now bosonic) SPT phase, as shown in Fig. 5.1. Again, a local change of variables can trivialize the latter. In effect, this ends up swapping the trivial and symmetry-breaking phases of the Ising chain, being equivalent to a Kramers-Wannier transformation. As summarized in Fig. 5.1, concatenating all these transformations is effectively equivalent to the Jordan-Wigner transformation encountered in section 2.3.1. These relationships between gauging and the Jordan-Wigner and Kramers-Wannier transformations have been pointed out before in the continuum [221] and on the lattice [72]. However, in these cases, the subtlety of the local mappings was not addressed and the SPT phases were overlooked.

To conclude, we take a look at how the edge properties of this system translate to the spin language. Since the mapping is local, we expect the mapped system to retain all the topological properties of the gauge theory.[4] As we choose that the chain ends with links on both sides, the Gauss law does not require a modification at the edge but the mapping does. In particular, we cannot define new gauge invariant Y and Z spin 1/2 operators on the first and last links, and instead we need

$$\begin{aligned} Y_{1/2} &= \sigma^y_{1/2}\gamma_1, & Z_{1/2} &= \sigma^z_{1/2}\gamma_1; \\ Y_{L+1/2} &= \tilde{\gamma}_L\sigma^y_{L+1/2}, & Z_{L+1/2} &= \tilde{\gamma}_L\sigma^z_{L+1/2}. \end{aligned} \tag{5.14}$$

These are fermionic operators, and therefore cannot appear in the Hamiltonian. This corroborates our intuition that while in the bulk the Hilbert space of a $\mathbb{Z}_2$ LGT coupled to spinless fermions is bosonic, at the boundaries it maintains its fermionic character. Moreover, in the fixed point limit $\mu \to 0$ the Majorana edge operators (2.60) take the simple form

---

[4] The only caveat being, as explained above, that the Z and Y operators are composite objects in the original variables.

$$\gamma_l = Y_{1/2} \qquad\qquad \gamma_{L+1/2} = Y_{L+1/2} \tag{5.15}$$

and the W and Π symmetries fractionalize as

$$W = Y_{1/2}Y_{L+1/2} \qquad\qquad \Pi = X_{1/2}X_{L+1/2}. \tag{5.16}$$

Note that the form of the Π symmetry is consistent with the fact that $Z_{1/2}$ and $Z_{L+1/2}$ are not present in the Hamiltonian.

5.1.4 Constrained Hilbert space and emergent PXP model

We present here an interesting result that was originally derived in the context of the gauged Kitaev chain (2.54), but is best understood in the spin language. In order to gain insight on the competition between the confined and deconfined phases of the gauge theory, let us set $t = 0$ in Eq. (5.13). We obtain

$$H = \frac{\mu}{2}\sum_j X_{j-1/2}X_{j+1/2} - h\sum_j X_{j+1/2}. \tag{5.17}$$

This can be seen as a classical model, since it is diagonal in the X basis. It is useful to rewrite it (up to a global constant) as

$$H = 2\mu\sum_j \mathcal{P}_{j-1/2}\mathcal{P}_{j+1/2} + (\mu - h)\sum_j X_{j+1/2} \quad \text{with } \mathcal{P}_{j-1/2} := \frac{1 - X_{j-1/2}}{2}. \tag{5.18}$$

The operator $\mathcal{P}_{j-1/2}$ is a projector onto a down spin. Hence, if $\mu = h$ (such that the second term disappears), the first term energetically punishes all states where two neighboring spins point down. These degenerate ground states span a Hilbert space without a tensor product structure, with a number of states asymptotically given by ϕ^N, where $\phi = (1 + \sqrt{5})/2$ is the golden ratio[5], as made well-known by recent studies of the Rydberg chain [222–225]. As soon as we perturb $\mu > h$, the system naturally prefers a maximal number of spins to point down. Given that we have to satisfy the aforementioned constraint at low energies, the two possible ground states are the antiferromagnetic states $|+-+-\rangle$ and $|-+-+\rangle$. As observed for instance in section 2.2.4, the breaking of transitional symmetry is directly related to deconfinement, in agreement with the phase diagram that we derived. If instead $\mu < h$, the ground state is given by $|++++\rangle$, leading to confinement.

Starting from the degenerate point ($\mu = h$), it is also interesting to consider the effect of turning on $t \neq 0$. This term brings us out of the low-energy Hilbert space, but at leading order in t, we have the projected Hamiltonian

$$H_{\text{eff}} = 2\mu\sum_j \mathcal{P}_{j-1/2}\mathcal{P}_{j+1/2} - t\sum_j \mathcal{P}_{j-1/2}Z_{j+1/2}\mathcal{P}_{j+3/2}. \tag{5.19}$$

---

[5] This follows from the observation that on a finite chain of length L the number of states in the Hilbert space of the model is given by the Fibonacci number F_L.

This can be recognized as the celebrated PXP model with its quantum scars [77, 226]. This is indeed known to have an Ising transition for $\mu - h \approx 0.7t$ [227, 228], or in other words, $h/\mu \approx 1 - 0.7\, t/\mu$, which sets the slope of the solid black line in Fig. 2.11(a) as it emerges from the vertical axis, agreeing with our numerical phase diagram.

We note that the effective constrained Hilbert space has a nice interpretation in terms of the original gauge theory (2.54): at the point $\mu = h,\ t = 0$, the energy cost of a pair of neighboring fermions (a dimer) is zero since the cost of flipping one electric string, as required by gauge-invariance, is exactly compensated by the gain due to the chemical potential μ. In this language, the constrained Hilbert space is formed by all possible degenerate configurations of dimers of unit length. At small t, the physics of these dimers is governed by the PXP model.

5.1.5 Mapping of Ising matter

In this section we show a strictly related mapping for gauged Ising matter and apply it to the simple example of the gauged Ising chain. We take this occasion to adventure out of the $\{G_i = 1\}$ sector, and explore the case where the Gauss law follows a staggered pattern of different forms.

Gauge invariant spins

The Hilbert space for $\mathbb{Z}_2$ gauged Ising matter consists of sites and links, both hosting spin 1/2 degrees of freedom. We denote the Ising matter fields on the sites by τ and the link fields by σ. The Gauss law for this system reads

$$G_i = \sigma^x_{i-1/2}\tau^z_i\sigma^x_{i+1/2} = q_i \tag{5.20}$$

where $q_i = \pm 1$. We introduce[6] the gauge invariant spins

$$X_{j+1/2} = \sigma^x_{j+1/2}, \qquad Y_{j+1/2} = \tau^x_j\sigma^y_{j+1/2}\tau^x_{j+1}, \qquad Z_{j+1/2} = \tau^x_i\sigma^z_{j+1/2}\tau^x_{j+1} \tag{5.21}$$

that live on the links.

Examples of the mapping

Let's see now how typical terms map to these new variables:

- As usual, the "chemical potential" term τ^z is taken care of by the Gauss law:

  $$\tau^z_i = q_i\,\sigma^x_{i-1/2}\sigma^x_{i+1/2} = q_i\,X_{i-1/2}X_{i+1/2}, \tag{5.22}$$

  i.e. it maps to an Ising coupling whose sign depends on the presence of a static charge q_i on the site between the two links in the original gauge theory.

---

[6] Here we abuse the notation that we already employed for the fermionic case. Since the present subsection is entirely self contained, we think that this will not be confusing.

- The "gauged Ising" term maps directly to a transverse field:

$$\tau_i^x \sigma^z_{j+1/2} \tau^x_{j+1} = Z_{j+1/2}. \tag{5.23}$$

  This is consistent with what we observed in the previous section when mapping the Kitaev chain[7], i.e. that the mapping remarkably does not require the explicit use of the Gauss law.

- A term of the form $\tau_i^y \sigma^z_{i+1/2} \tau^y_{+1}$, encountered for example in the gauged XY chain, requires some more work:

$$\begin{aligned} \tau_i^y \sigma^z_{j+1/2} \tau^y_{i+1} &= \tau_i^z \tau_i^x \sigma^z_{i+1/2} \tau^x_{i+1} \tau^z_{i+1} = \\ &= q_i \, q_{i+1/2} \, X_{i-1/2} X_{i+1/2} Z_{i+1/2} \, X_{i+1/2} X_{i+3/2} = \\ &= q_i \, q_{i+1/2} \, X_{i-1/2} \, Z_{i+1/2} \, X_{i+3/2} \end{aligned} \tag{5.24}$$

  which is the cluster term encountered already in the mapping of generic quadratic fermionic Hamiltonians. The sign of this term depends on the distribution of static charges. In particular, it is positive if all background charges are positive or negative, but it turns negative if they are in a staggered pattern.

Mapping of the gauged Ising model

The Hamiltonian of the gauged Ising model reads:

$$H = -J \sum_j \tau_j^x \sigma^z_{j+1/2} \tau^x_{j+1} - f \sum_j \tau_j^z - h \sum_j \sigma^x_{j+1/2}. \tag{5.25}$$

Following the prescriptions above, this is mapped straightforwardly to the new gauge-invariant spins. In particular, it is easy to keep track of an arbitrary distribution of background charges and carry out the mapping in an arbitrary gauge sector. The new Hamiltonian is

$$H = -f \sum_j q_j X_{j-1/2} X_{j+1/2} - J \sum_j Z_{j+1/2} - h \sum_j X_{j+1/2}, \tag{5.26}$$

which describes an Ising model in a tilted field whose coupling are ferromagnetic or antiferromagnetic on different pairs of sites depending on the gauge sector that one considers.

Such models can be cast into a more familiar form by applying a global unitary that transfers the alternating sign to the longitudinal field. Let us concentrate on the case where the background charges are staggered: $q_j = (-1)^j$. Here the appropriate unitary transformation is

$$U = ZZIIZZIIZZII\ldots, \tag{5.27}$$

---

[7] Which is the Jordan-Wigner dual of the transverse-field Ising model.

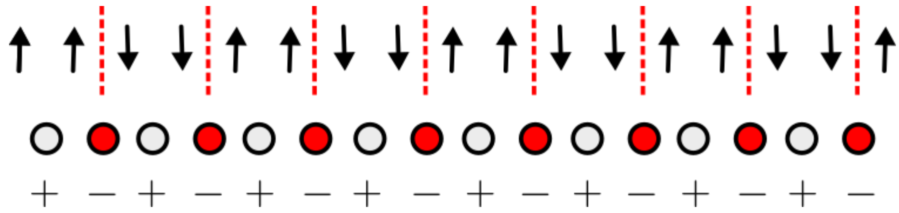

Figure 5.2: A strong longitudinal field that changes sign every two sites aligns the spins (in the X-basis) as shown by the black arrows. The domain walls (red dashed lines) corresponds to $\mathbb{Z}_2$ charged particles of the gauge theory (red dots). These are placed every second site, neutralizing the static background charges ($-$) so that all electric strings are expelled from the ground state.

that sends $X_j \to (-1)^{j(j+1)/2} X_j$. One gets

$$\begin{aligned} H &= -f \sum_j (-1)^j (-1)^{j(j+1)/2} (-1)^{(j+1)(j+2)/2} X_j X_{j+1} \\ &\quad - J \sum_j Z_j - h \sum_j (-1)^{j(j+1)/2} X_j \\ &= f \sum_j X_j X_{j+1} - J \sum_j Z_j - h \sum_j (-1)^{j(j+1)/2} X_j \end{aligned}$$

which describes an Ising model with longitudinal field that changes sign every two sites. Physically, this can be understood as follows: in the large h regime, we want to eliminate the energetically expensive $\mathbb{Z}_2$ electric strings from the ground state. In our case, where the background charge are staggered, this can be done by placing neutralizing Ising matter $\tau^z = +1$ on every second site. But under the mapping $\mathbb{Z}_2$ charges correspond to domain walls: in this regime the longitudinal field dominates and forces exactly one domain wall every second site, giving the correct physical picture. This is illustrated in Fig. 5.2.

Edge modes of the gauged Ising chain

To conclude this section, we go back to the uniform Gauss law $G_i = +1$ and consider the edge physics of the gauged Ising chain, operating directly in the spin language. At $h = 0$, the model exhibits symmetry-protected *bosonic* edge modes in the Higgs phase. One can construct these modes in the following way: on an open chain of length L which starts and ends with links the definition of the gauge-invariant spins (5.21) cannot be applied to the outer left and right links, but instead we define

$$\begin{aligned} &X_{1/2} = \sigma^x_{1/2}, && Y_{1/2} = \sigma^y_{1/2}\tau^x_1, && Z_{1/2} = \sigma^z_{1/2}\tau^x_1; \\ &X_{L+1/2} = \sigma^x_{L+1/2}, && Y_{L+1/2} = \tau^x_L \sigma^y_{L+1/2}, && Z_{L+1/2} = \tau^x_L \sigma^z_{L+1/2}. \end{aligned} \tag{5.28}$$

In contrast to the gauged Kitaev chain, all edge gauge-invariant operators are bosonic and thus a priori can appear as individual terms in the Hamiltonian of an open chain. At $h = 0$, however, the model enjoys the magnetic symmetry $W = \prod_j \sigma^z_{j+1/2} = Q \prod_j Z_{j+1/2}$. As a result, all edge terms (5.28) are ruled out

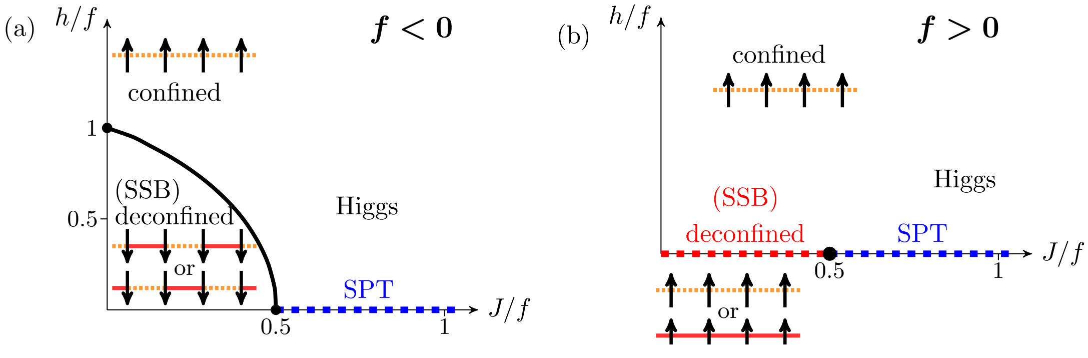

Figure 5.3: Phase diagram of the gauged TFIM (5.25) for $f < 0$ and $f > 0$, respectively. In absence of vortices ($h = 0$), the system enjoys the magnetic symmetry $W = \prod_j \sigma^z_{j+1/2}$, protecting the SPT order in the Higgs phase (highlighted by dashed blue line). For $h \neq 0$, the Higgs and confined regimes are adiabatically connected. For $f < 0$ the solid black line denotes Ising criticality, which is stabilized due the translation-breaking nature of the antiferromagnetic phase.

by symmetries. In particular, the Ising symmetry prohibits the edge Y and Z operators to appear in the Hamiltonian, while the magnetic symmetry does not allow X and Y. As a result, at $h = 0$ the open chain Hamiltonian is

$$H = -f \sum_{j=1}^{L} X_{j-1/2} X_{j+1/2} - J \sum_{j=1}^{L-1} Z_{j+1/2}. \tag{5.29}$$

We will now identify two edge operators localized near the left boundary that commute with this Hamiltonian. First, we have $X_l = X_{1/2}$. In addition, the operator

$$Y_l = Y_{1/2} + \frac{f}{J} Z_{1/2} Y_{3/2} + \frac{f^2}{J^2} Z_{1/2} Z_{3/2} Y_{5/2} + \dots \tag{5.30}$$

also commutes with the Hamiltonian (5.29) and is exponentially localized near the left boundary in the Higgs phase, where $|f| < J$. The presence of two anti-commuting localized edge operators X_l and Y_l ensures two-fold ground state degeneracy associated with the left boundary. Since similar arguments apply also to the right edge, the total degeneracy of the ground state manifold on an open chain is four-fold with exponentially small corrections in system size L. The existence and stability of this degeneracy originates from fractionalization of the Ising and magnetic symmetries. In particular, the two $\mathbb{Z}_2$ symmetries anti-commute with each other at each edge and thus are realized projectively at the boundary.

5.2 The mapping in two dimensions

We now extend the ideas presented in section 5.1 to two dimensions, and show how models with $\mathbb{Z}_2$ gauge fields and spinless fermionic matter can be mapped onto spin one-half models through a local transformation. The general reasoning behind the mapping is the same as in one dimension, i.e. one constructs gauge invariant spins from Majorana and link operators. We reckon that the deep reason why this is possible is that the Hilbert space of the model is effectively bosonic, since gauge invariant states are formed by pairs of fermions connected by electric strings.[8] The generalization is however not straightforward, since tricks are needed in order to keep track of the fermionic statistics which in 2d has a significantly more relevant impact.

5.2.1 Gauge invariant spins

As in 1d, we first introduce the Majorana operators

$$\gamma_{\mathbf{r}} = c_{\mathbf{r}}^{\dagger} + c_{\mathbf{r}}, \qquad \tilde{\gamma}_{\mathbf{r}} = i(c_{\mathbf{r}}^{\dagger} - c_{\mathbf{r}}). \tag{5.31}$$

In terms of these variables the Gauss law reads

$$i\tilde{\gamma}_{\mathbf{r}}\gamma_{\mathbf{r}} = \prod_{b\in +_{\mathbf{r}}} \sigma_b^x. \tag{5.32}$$

Out of the original $\mathbb{Z}_2$ gauge fields and Majorana variables, it is possible to construct new gauge-invariant Pauli operators as follows

$$\begin{aligned} X_{\mathbf{r},\eta} &= \sigma_{\mathbf{r},\eta}^x, \\ Z_{\mathbf{r},\hat{x}} &= -i\tilde{\gamma}_{\mathbf{r}}\sigma_{\mathbf{r},\hat{x}}^z\gamma_{\mathbf{r}+\hat{x}}\sigma_{\mathbf{r}+\hat{x},-\hat{y}}^x, \\ Z_{\mathbf{r},\hat{y}} &= -i\tilde{\gamma}_{\mathbf{r}}\sigma_{\mathbf{r},\hat{y}}^z\gamma_{\mathbf{r}+\hat{y}}\sigma_{\mathbf{r},\hat{x}}^x. \end{aligned} \tag{5.33}$$

Note that, compared to the one-dimensional case, the factors σ^x in the definition of $Z_{\mathbf{r},\eta}$ are needed to ensure that the new spin operators not only satisfy the Pauli algebra on a given link, but also always commute on neighboring links. We also point out that this choice is not unique: different arrangements of σ^x are possible, including non-symmetric ones where two factors of σ^x appear in the definition of $Z_{\mathbf{r},\hat{x}}$, but no σ^x is needed for $Z_{\mathbf{r},\hat{y}}$ (or vice-versa). It is worth mentioning that such kind of mapping is possible in any dimension, generically requiring some factors of σ^x in the definition of $Z_{\mathbf{r},\eta}$ on properly chosen neighboring links. The only exception is one spatial dimension, where no extra operators σ^x are needed [70, 113, 229, 230].

5.2.2 Mapping of Hamiltonians

Let's now see how different terms of typical Hamiltonians transform under the mapping (5.33).

Fermion bilinears

We start with Majorana bilinears, which can be used to express hopping and pairing terms alike. Under (5.33), the horizontal and vertical bilinears where $\tilde{\gamma}$

---

[8] Again, this is true for the relevant case $G_i = +1$ everywhere.

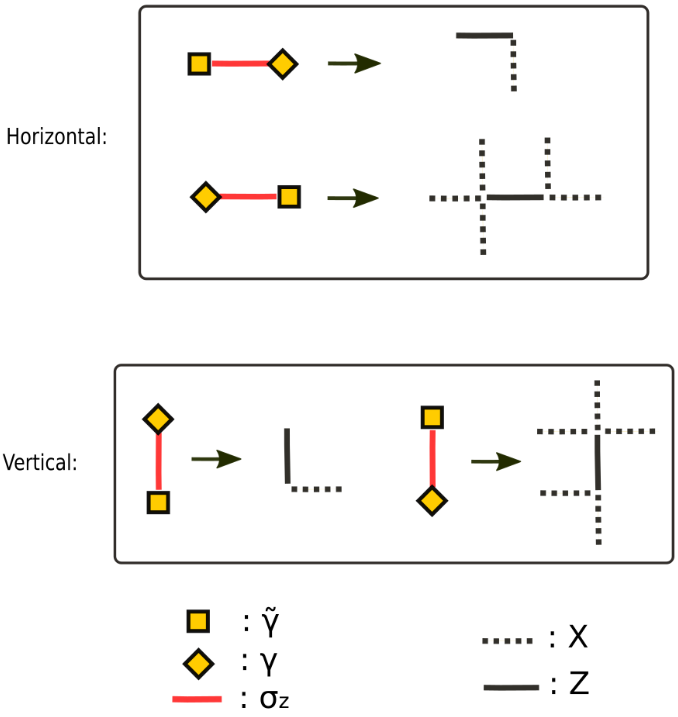

Figure 5.4: Illustration of the hopping terms under the mapping (5.33) for horizontal and vertical links.

appears on the left and lower site respectively can be immediately rewritten as

$$\begin{aligned} i\tilde{\gamma}_{\mathbf{r}}\sigma^z_{\mathbf{r},\hat{x}}\gamma_{\mathbf{r}+\hat{x}} &= -Z_{\mathbf{r},\hat{x}}\,X_{\mathbf{r}+\hat{x},-\hat{y}}, \\ i\tilde{\gamma}_{\mathbf{r}}\sigma^z_{\mathbf{r},\hat{y}}\gamma_{\mathbf{r}+\hat{y}} &= -Z_{\mathbf{r},\hat{y}}\,X_{\mathbf{r},\hat{x}}. \end{aligned}$$

When the roles of $\tilde{\gamma}$ and γ are swapped, however, a straightforward mapping is not possible and one needs to use the Gauss law.[9] Since all operators are understood to act only on states in the physical Hilbert space, the identity can be inserted on the right of each expression in the form $\mathbf{1} = G_{\mathbf{r}_1}\dots G_{\mathbf{r}_k}$. This can be done for an arbitrary choice of sites $\mathbf{r}_1,\dots\mathbf{r}_k$ because the Gauss law is enforced on every site independently. Hence on horizontal links one has

$$\begin{aligned} i\gamma_{\mathbf{r}}\sigma^z_{\mathbf{r},\hat{x}}\tilde{\gamma}_{\mathbf{r}+\hat{x}} &= i\gamma_{\mathbf{r}}\sigma^z_{\mathbf{r},\hat{x}}\tilde{\gamma}_{\mathbf{r}+\hat{x}}G_{\mathbf{r}}G_{\mathbf{r}+\hat{x}} \\ &= i\tilde{\gamma}_{\mathbf{r}}\sigma^z_{\mathbf{r},\hat{x}}\gamma_{\mathbf{r}+\hat{x}}\prod_{b\in+_{\mathbf{r}}}X_b\prod_{b'\in+_{\mathbf{r}+\hat{x}}}X_{b'} \\ &= -Z_{\mathbf{r},\hat{x}}\prod_{\mu\in\{l\}}X_{\mathbf{r},\mu}, \end{aligned}$$

where the last product is over a set of five X operators on the links determined by the displacements $\{-\hat{x}, 2\hat{x}, \hat{y}, -\hat{y}, \hat{x}+\hat{y}\}$. A similar arguments applies to the vertical links. The result is shown pictorially in Fig. 5.4. With these results in mind, the hopping term

---

[9] This is entirely equivalent to what is done in 1d, but we repeat the argument for completeness.

$$-\left(c^{\dagger}_{\mathbf{r}}\sigma^{z}_{\mathbf{r},\eta}c_{\mathbf{r}+\eta}+\text{h.c.}\right)=\frac{1}{2}\left(i\tilde{\gamma}_{\mathbf{r}}\sigma^{z}_{\mathbf{r},\eta}\gamma_{\mathbf{r}+\eta}-i\gamma_{\mathbf{r}}\sigma^{z}_{\mathbf{r},\eta}\tilde{\gamma}_{\mathbf{r}+\eta}\right). \tag{5.34}$$

that appears in Hamiltonian (4.35) can be readily expressed in terms of spins. On horizontal links one gets

$$-\underbrace{\frac{1}{2}\left(1-\prod_{b\in+_{\mathbf{r}}}X_b\prod_{b'\in+_{\mathbf{r}+\hat{x}}}X_{b'}\right)}_{\mathcal{P}_{\mathbf{r},\hat{x}}}Z_{\mathbf{r},\hat{x}}\,X_{\mathbf{r}+\hat{x},-\hat{y}}, \tag{5.35}$$

and analogously for the vertical hopping we find

$$-\underbrace{\frac{1}{2}\left(1-\prod_{b\in+_{\mathbf{r}}}X_b\prod_{b'\in+_{\mathbf{r}+\hat{y}}}X_{b'}\right)}_{\mathcal{P}_{\mathbf{r},\hat{y}}}Z_{\mathbf{r},\hat{y}}\,X_{\mathbf{r},\hat{x}}. \tag{5.36}$$

This compact form has a nice interpretation in terms of the original fermionic theory: due to the Gauss law the factor $\mathcal{P}_{\mathbf{r},\hat{\eta}}$ is a projector that annihilates all states with equal fermion parity on sites $\mathbf{r}$ and $\mathbf{r}+\hat{\eta}$. This means that the hopping is only possible if one of the sites hosts a fermion particle and the other one does not, as it should be to avoid double occupancy or creation of pairs of particles out of the vacuum. A generic linear combination of the two Majorana bilinears does not have this property, and would correspond to a $U(1)$ non-conserving fermionic model with anomalous terms of the form $c^{\dagger}_{\mathbf{r}}\sigma^{z}_{\mathbf{r},\eta}c^{\dagger}_{\mathbf{r}+\eta}+\text{h.c.}$ Physically, in the spin formulation the operator Z is responsible for the hopping process, as it swaps the fermion parities on the two neighboring sites. The operators X, on the other hand, keep track of the fact that the hopping particles are fermions. This can be seen explicitly by exchanging two identical particles and verifying that in the process the statistical phase of π is acquired, as we now proceed to explain.

An excursus: Fermionic statistics in the spin language

Having expressed the hopping in terms of spin degrees of freedom only, it is natural to ask how the statistics of the original constituents is taken into account after the mapping. In the original formulation of Sec. 4.3, the σ^z operator in the hopping term of the Hamiltonian (4.36) assigns a phase of 0 or π to the hopping amplitude of the fermion, depending on the state of the gauge field on that link. When a fermion is carried all the way around a closed loop $\mathcal{C}$, it picks up the Aharonov-Bohm phase given by the operator $e^{i\hat{\Phi}}=\prod_{\mathcal{C}}\sigma^z$. This is related by Stokes' theorem to the total $\mathbb{Z}_2$ magnetic flux piercing the surface enclosed by $\mathcal{C}$.

Here we show how the hopping operators (5.35) and (5.36) encode in the gauge-invariant spin formulation the fermionic statistics of the $\mathbb{Z}_2$ charges. In general, one expects that after an exchange of two identical $\mathbb{Z}_2$-charged fermionic particles the initial state evolves as

$$|\psi_0\rangle\longrightarrow e^{i(\alpha+\hat{\Phi})}|\psi_0\rangle, \tag{5.37}$$

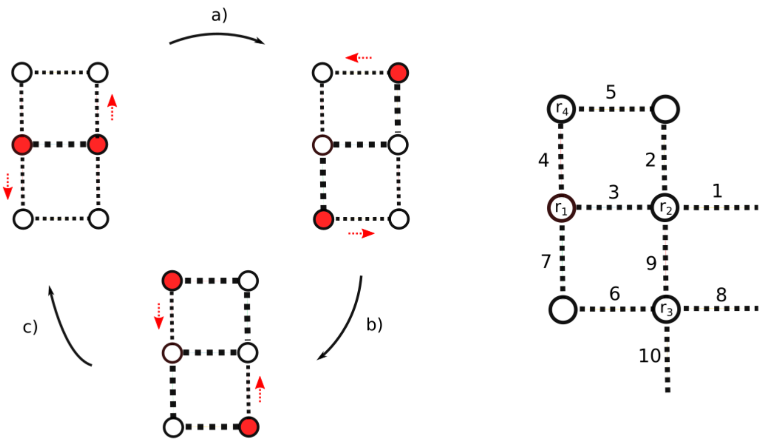

Figure 5.5: Left: The positions of two identical $\mathbb{Z}_2$ charges (red blobs) are exchanged by successively applying the hopping operators (5.35) and (5.36). Right: the notation adopted in Eq. (5.38).

where $\alpha = \pi$ is the fermion statistical phase while $\hat{\Phi}$ is the operator that measures the phase acquired due to the magnetic flux as explained above.

For a generic initial state of two neighboring particles, the braiding process shown in Fig. 5.5 can be represented as the action of a braiding operator $\mathcal{B}$ constructed by combining the appropriate hoppings (5.35) and (5.36): $|\psi_0\rangle \longrightarrow \mathcal{B}\,|\psi_0\rangle$. Following the notation of Fig. 5.5 for the labeling of the relevant links and sites, one has

$$\begin{aligned}\mathcal{B} &= Z_9X_8\, Z_4X_3\, Z_6X_{10}\, Z_5X_2\, Z_7X_6\, Z_2X_1 \\ &= -Z_9Z_4Z_6Z_5Z_7Z_2\, X_8X_3X_{10}X_2X_6X_1 \\ &= -\tilde{P}_{\mathbf{r}_3}\tilde{P}_{\mathbf{r}_2}A_{\mathbf{r}_3}A_{\mathbf{r}_2},\end{aligned} \tag{5.38}$$

where $\tilde{P}_{\mathbf{r}}$ denotes a plaquette operator of Z spins (not of σ^z!) at the top left of site $\mathbf{r}$, while $A_{\mathbf{r}} = \prod_{b\in+_{\mathbf{r}}} X_b$ is the star operator. To isolate the contribution from the $\mathbb{Z}_2$ flux, we express $\tilde{P}$ in terms of the operators X and σ^z by inverting Eq. (5.42). We get

$$\mathcal{B} = -\left(\prod_{\mathcal{C}} \sigma^z\right) A_{\mathbf{r}_1}A_{\mathbf{r}_2}A_{\mathbf{r}_3}A_{\mathbf{r}_4} = -\prod_{\mathcal{C}} \sigma^z, \tag{5.39}$$

where in the last step we have used the fact that $A_{\mathbf{r}_1} = A_{\mathbf{r}_2} = -1$ and $A_{\mathbf{r}_3} = A_{\mathbf{r}_4} = 1$ for the state $|\psi_0\rangle$. This completes the proof: besides the Bohm-Aharonov phase, an extra minus sign manifests the fermionic nature of the $\mathbb{Z}_2$ charges of the original gauge theory.

Density dependent terms

The inclusion of terms that depend only on combinations of fermion densities on different sites is straightforward. Indeed, the Gauss law yields immediately

$$n_{\mathbf{r}} = \frac{1 - \prod_{b\in+_{\mathbf{r}}} X}{2}, \tag{5.40}$$

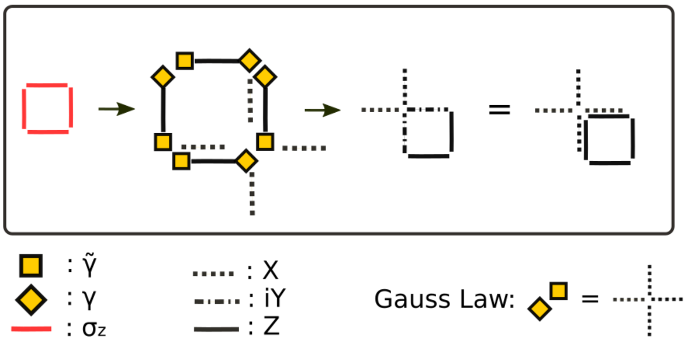

Figure 5.6: Elementary plaquette $P_{\mathbf{r}^*} = \prod_{b\in\Box_{\mathbf{r}*}} \sigma_b^z$ under the mapping (5.33). When two γ ($\tilde\gamma$) appear on the same site, they square to one. On the other hand, when γ and $\tilde\gamma$ appear, instead, they can be replaced with a star operator as a consequence of the Gauss law.

and so up to a constant the number operator maps onto a star. Similarly, more complicated terms amount to taking appropriate product of (5.40). A relevant example are nearest-neighbor, next-nearest-neighbor and next-next-nearest-neighbor interactions.

Plaquette term

To map the plaquette term we need once more to combine the mapping (5.33) with the Gauss law. Each σ_z transforms into a combination of Z, X and Majorana operators. When taking the product of σ_z operators around an elementary plaquette, the Majorana operators on two out of the four vertices square to one, while on the remaining vertices one is left with the product of the Majorana operators γ and $\tilde\gamma$. Such a product can be replaced with a star operator as a consequence of the Gauss law (5.32), leading eventually to the six-spins term

$$P_{\mathbf{r}^*} = \prod_{b\in\Box_{\mathbf{r}*}} \sigma_b^z = -Z_{\mathbf{r},\hat{x}} Z_{\mathbf{r}+\hat{x},\hat{y}} Y_{\mathbf{r},\hat{y}} Y_{\mathbf{r}+\hat{y},\hat{x}} X_{\mathbf{r}+\hat{y},-\hat{x}} X_{\mathbf{r}+\hat{y},\hat{y}}. \tag{5.41}$$

The procedure is outlined in Fig. 5.6. We note the following interesting fact: Eq. (5.41) can also be written as

$$P_{\mathbf{r}^*} = \prod_{b\in\Box_{\mathbf{r}*}} Z \prod_{b\in+_{\mathbf{r}}} X, \tag{5.42}$$

where here $\mathbf{r}^*$ labels the square of the dual lattice on the bottom-right of the vertex $\mathbf{r}$. The elementary plaquette operator $P_{\mathbf{r}^*}$ of the original model (4.35) maps onto the plaquette-star composite operator in the spin formulation.

Complete mapping of Hamiltonian (4.35)

Combining everything together, the full Hamiltonian (4.35) of the $\mathbb{Z}_2$ lattice gauge theory coupled to spinless fermions maps onto the following local spin one-half model

$$\begin{aligned}H =& - t \sum_{\mathbf{r}} \left(Z_{\mathbf{r},\hat{x}}\, X_{\mathbf{r}+\hat{x},-\hat{y}}\, \mathcal{P}_{\mathbf{r},\hat{x}} + Z_{\mathbf{r},\hat{y}}\, X_{\mathbf{r},\hat{x}}\, \mathcal{P}_{\mathbf{r},\hat{y}}\right)\\ &- \frac{\mu}{2} \sum_{\mathbf{r}} \left(1 - \prod_{b\in +_{\mathbf{r}}} X_b\right)\\ &- J \sum_{\mathbf{r}^*} \prod_{b\in \square_{\mathbf{r}*}} Z \prod_{b\in +_{\mathbf{r}}} X - h \sum_{\mathbf{r},\eta} X_{\mathbf{r},\eta}\end{aligned}$$

with the projectors $\mathcal{P}_{\mathbf{r},\hat{x}}$, $\mathcal{P}_{\mathbf{r},\hat{y}}$ defined in Eqs. (5.35) and (5.36). The time-reversal symmetry (4.41) is realized as complex conjugation

$$X_{\mathbf{r},\eta} \to X_{\mathbf{r},\eta}, \qquad Y_{\mathbf{r},\eta} \to -Y_{\mathbf{r},\eta}, \qquad Z_{\mathbf{r},\eta} \to Z_{\mathbf{r},\eta}. \tag{5.43}$$

Notice moreover that in the spin formulation the $U(1)$ particle number symmetry is not onsite.

5.2.3 Mapping of observables

Let's now take a look at how some important observables transform under the mapping.

Dimer operators

To express the gauge-invariant dimer operator

$$b^\dagger_{\mathbf{r},\eta} = c^\dagger_{\mathbf{r}} \sigma_{\mathbf{r},\eta} c^\dagger_{\mathbf{r}+\eta} \tag{5.44}$$

in terms of spin operators, let us first rewrite it in terms of the Majoranas:

$$\begin{aligned}b^\dagger_{\mathbf{r},\eta} =& \frac{1}{4}(\gamma_{\mathbf{r}} - i\tilde{\gamma}_{\mathbf{r}})\sigma^z_{\mathbf{r},\eta}(\gamma_{\mathbf{r}+\eta} - i\tilde{\gamma}_{\mathbf{r}+\eta})\\ =& \frac{-i}{4}\left(\tilde{\gamma}_{\mathbf{r}}\sigma^z_{\mathbf{r},\eta}\gamma_{\mathbf{r}+\eta} + \gamma_{\mathbf{r}}\sigma^z_{\mathbf{r},\eta}\tilde{\gamma}_{\mathbf{r}+\eta}\right) + \frac{1}{4}\left(\gamma_{\mathbf{r}}\sigma^z_{\mathbf{r},\eta}\gamma_{\mathbf{r}+\eta} - \tilde{\gamma}_{\mathbf{r}}\sigma^z_{\mathbf{r},\eta}\tilde{\gamma}_{\mathbf{r}+\eta}\right).\end{aligned} \tag{5.45}$$

Using our calculation of the hopping part of the Hamiltonian from Sec. 5.2.2, we find that the first bracketed summand above is just

$$\begin{aligned}\eta = \hat{x}: &\qquad \frac{1}{2} Z_{\mathbf{r},\hat{x}}\, X_{\mathbf{r}+\hat{x},-\hat{y}}\, \tilde{\mathcal{P}}_{\mathbf{r},\hat{x}},\\ \eta = \hat{y}: &\qquad \frac{1}{2} Z_{\mathbf{r},\hat{y}}\, X_{\mathbf{r},\hat{x}}\, \tilde{\mathcal{P}}_{\mathbf{r},\hat{y}},\end{aligned} \tag{5.46}$$

where we introduced

$$\tilde{\mathcal{P}}_{\mathbf{r},\hat{\eta}} = \frac{1}{2}\left(1 + \prod_{b\in +_{\mathbf{r}}} X_b \prod_{b'\in +_{\mathbf{r}+\eta}} X_{b'}\right) \tag{5.47}$$

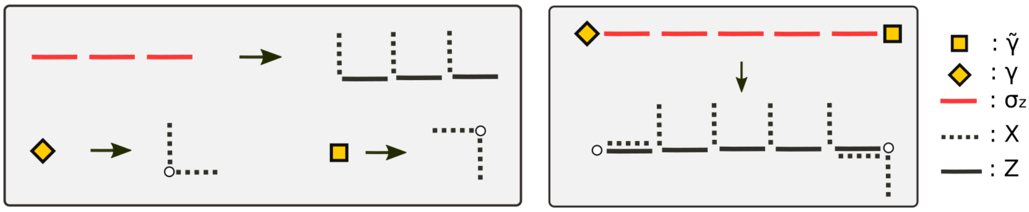

Figure 5.7: Left panel displays expressions for the Wilson line and endpoint fermionic operators in terms of gauge invariant spin variables using the mapping (5.33). From such building blocks one can construct all fermionic two-point functions. As an example, the mapping of the correlator $\tilde{\gamma}\,\sigma^z \ldots \gamma$ is shown in the right panel.

which annihilates states with opposite fermion parity on sites $\mathbf{r}$ and $\mathbf{r}+\eta$. The spin representation of the second bracketed summand in Eq. (5.45) can be computed by using the Gauss law, we find

$$\begin{aligned}
\frac{1}{4}\left(\gamma_{\mathbf{r}}\sigma^z_{\mathbf{r},\hat{x}}\gamma_{\mathbf{r}+\hat{x}} - \tilde{\gamma}_{\mathbf{r}}\sigma^z_{\mathbf{r},\hat{x}}\tilde{\gamma}_{\mathbf{r}+\hat{x}}\right) &= \frac{i}{2}Y_{\mathbf{r},\hat{x}}X_{\mathbf{r}+\hat{x},\hat{x}}X_{\mathbf{r}+\hat{x},\hat{y}}\tilde{\mathcal{P}}_{\mathbf{r},\hat{x}},\\
\frac{1}{4}\left(\gamma_{\mathbf{r}}\sigma^z_{\mathbf{r},\hat{y}}\gamma_{\mathbf{r}+\hat{y}} - \tilde{\gamma}_{\mathbf{r}}\sigma^z_{\mathbf{r},\hat{y}}\tilde{\gamma}_{\mathbf{r}+\hat{y}}\right) &= \frac{i}{2}Y_{\mathbf{r},\hat{y}}X_{\mathbf{r},-\hat{x}}X_{\mathbf{r},-\hat{y}}\tilde{\mathcal{P}}_{\mathbf{r},\hat{x}}.
\end{aligned} \tag{5.48}$$

Combining everything together we write the dimer creation operators in the spin language

$$\begin{aligned}
b^\dagger_{\mathbf{r},\hat{x}} &= \frac{1}{2}\Big(Z_{\mathbf{r},\hat{x}}\,X_{\mathbf{r}+\hat{x},-\hat{y}} + iY_{\mathbf{r},\hat{x}}X_{\mathbf{r}+\hat{x},\hat{x}}X_{\mathbf{r}+\hat{x},\hat{y}}\Big)\,\tilde{\mathcal{P}}_{\mathbf{r},\hat{x}} = Z_{\mathbf{r},\hat{x}}\,X_{\mathbf{r}+\hat{x},-\hat{y}}\Pi_{\mathbf{r},\hat{x}},\\
b^\dagger_{\mathbf{r},\hat{y}} &= \frac{1}{2}\Big(Z_{\mathbf{r},\hat{y}}\,X_{\mathbf{r},\hat{x}} + iY_{\mathbf{r},\hat{y}}X_{\mathbf{r},-\hat{x}}X_{\mathbf{r},-\hat{y}}\Big)\,\tilde{\mathcal{P}}_{\mathbf{r},\hat{y}} = Z_{\mathbf{r},\hat{y}}\,X_{\mathbf{r},\hat{x}}\Pi_{\mathbf{r},\hat{y}},
\end{aligned} \tag{5.49}$$

where

$$\Pi_{\mathbf{r},\eta} = \frac{1}{4}\Big(1 + \prod_{b\in+_{\mathbf{r}}} X_b + \prod_{b'\in+_{\mathbf{r}+\eta}} X_{b'} + \prod_{b\in+_{\mathbf{r}}} X_b \prod_{b'\in+_{\mathbf{r}+\eta}} X_{b'}\Big) \tag{5.50}$$

is a projector on simultaneously unoccupied sites $\mathbf{r}$ and $\mathbf{r}+\eta$. The annihilation operators of dimers can be obtained by hermitian conjugation

$$\begin{aligned}
b_{\mathbf{r},\hat{x}} &= Z_{\mathbf{r},\hat{x}}\,X_{\mathbf{r}+\hat{x},-\hat{y}}\tilde{\Pi}_{\mathbf{r},\hat{x}},\\
b_{\mathbf{r},\hat{y}} &= Z_{\mathbf{r},\hat{y}}\,X_{\mathbf{r},\hat{x}}\tilde{\Pi}_{\mathbf{r},\hat{y}},
\end{aligned} \tag{5.51}$$

where

$$\tilde{\Pi}_{\mathbf{r},\eta} = \frac{1}{4}\Big(1 - \prod_{b\in+_{\mathbf{r}}} X_b - \prod_{b'\in+_{\mathbf{r}+\eta}} X_{b'} + \prod_{b\in+_{\mathbf{r}}} X_b \prod_{b'\in+_{\mathbf{r}+\eta}} X_{b'}\Big) \tag{5.52}$$

is a projector on simultaneously occupied sites $\mathbf{r}$ and $\mathbf{r}+\eta$.

Fermion-fermion correlators

We consider here the gauge-invariant fermion-fermion correlator

$$\langle f^\dagger_{\mathbf{r}} f_{\mathbf{r}'}\rangle = \langle c^\dagger_{\mathbf{r}} \prod_{b\in l} \sigma^z_b c_{\mathbf{r}'}\rangle \tag{5.53}$$

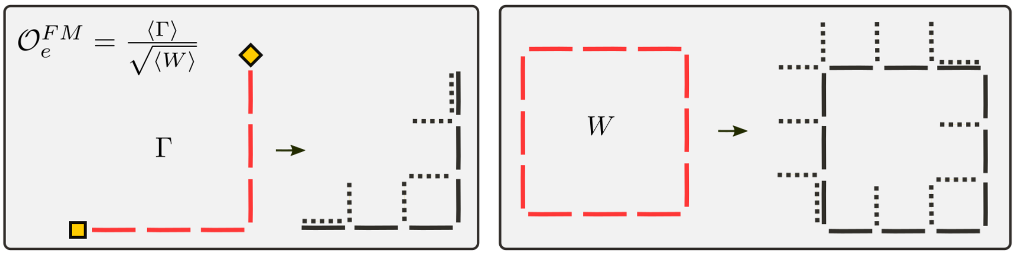
$\mathcal{O}_e^{FM} = \frac{\langle\Gamma\rangle}{\sqrt{\langle W\rangle}}$
Γ
W

Figure 5.8: Mapping of the Wilson line with Majorana endpoints (left) and of the Wilson loop (right). The electric Fredenhagen-Marcu order parameter can be expressed in terms of the expectation values of these two operators.

For concreteness, we take sites $\mathbf{r}$ and $\mathbf{r}'$ which are separated in the x direction, such that the Wilson line l connecting them is straight and horizontal. Let us see first how an infinite Wilson line transforms, without worrying about the endpoints. To use the mapping (5.33), we insert at each site crossed by the Wilson line the identity operator in the form $I = \gamma^2\tilde{\gamma}^2$. One then gets

$$\prod_{b\in l}\sigma^z_b = \dots\tilde{\gamma}_{\mathbf{r}_1}\underbrace{\tilde{\gamma}_{\mathbf{r}_1}\sigma^z_{\mathbf{r}_1,\hat{x}}\gamma_{\mathbf{r}_2}}_{iZ_{\mathbf{r}_1,\hat{x}}X_{\mathbf{r}_2,-\hat{y}}}\ \underbrace{\gamma_{\mathbf{r}_2}\tilde{\gamma}_{\mathbf{r}_2}}_{iS_{\mathbf{r}_2}}\tilde{\gamma}_{\mathbf{r}_2}\dots \tag{5.54}$$

where $S_{\mathbf{r}_i}$ is the star operator at site $\mathbf{r}_i$. The X operators on horizontal and lower vertical links square to one, so for the infinite Wilson line the mapping takes the simple form

$$\sigma^z_{\mathbf{r},\hat{x}} \longrightarrow Z_{\mathbf{r},\hat{x}}\,X_{\mathbf{r},\hat{y}}. \tag{5.55}$$

As for the endpoints, where fermions reside, not all the X operators cancel and therefore the mapping needs to be complemented with the following rules

$$\begin{aligned}\gamma_{\mathbf{r}} &\longrightarrow X_{\mathbf{r},-\hat{x}}\,X_{\mathbf{r},-\hat{y}},\\ \tilde{\gamma}_{\mathbf{r}} &\longrightarrow X_{\mathbf{r},\hat{x}}\,X_{\mathbf{r},\hat{y}}.\end{aligned}$$

From these building blocks one can easily reconstruct all fermionic two-point functions. An example is given in Fig. 5.7.

Fredenhagen-Marcu order parameters

In chapter 4 we have introduced and motivated the Fredenhagen-Marcu order parameters which are used to detect a confinement transition in the presence of matter fields. The "magnetic" parameter $\mathcal{O}_m^{FM}$ that detects the condensation of m-particles (visons) is defined entirely in terms the gauge invariant σ^x, and therefore it transforms trivially under the mapping. The "electric" order parameter $\mathcal{O}_e^{FM}$, on the other hand, requires some work. For the numerator, we choose for convenience γ and $\tilde{\gamma}$ as $\mathbb{Z}_2$ charged endpoints. Since this is nothing but a fermion-fermion correlator we adapt the results obtained above, taking extra care to keep track of what happens at the corner. Similarly, the results for the Wilson loop are an easy generalization of what we already derived, the only subtleties coming from the extra σ^x operators at the corners. The results for a 3×3 loop are shown in Fig. 5.8.

Chapter 6

Conclusions and outlook

This thesis aims at giving a comprehensive account of recent results in the field of $\mathbb{Z}_2$ lattice gauge theories. To do this in an effective and pedagogical way, we introduce the reader to relevant concepts such as gauge invariance, topological order and deconfinement. In the introduction, we provide context by first discussing the development of gauge theories throughout the 20th century, and then zooming in on the condensed matter theory applications which are most connected to our research work. The original results contained in this thesis can be grouped in the following way:

- **Confinement in 1d $\mathbb{Z}_2$ LGT:** The results of section 2.2 (See in particular subsections 2.2.2 and 2.2.4) show that in a simple model of spinless fermions coupled to $\mathbb{Z}_2$ gauge fields the elementary constituents are confined into mesonic dimers as soon as the $\mathbb{Z}_2$ electric field is turned on. Single holes in a fully filled background are instead deconfined. Among our results, these are the ones that can find more immediate experimental applications. The model can be simulated using existing ultracold atoms platforms, and the predicted doubling in the period of Friedel oscillations is easy to observe in this setup.

- **Edge physics of the gauged Kitaev chain:** In section 2.3 we derive a gauged version of the famous Kitaev chain. While the bulk phase diagram of the model is readily obtained thanks to a mapping to the TLFI model, we unveil intriguing aspects concerning the edge physics. We introduce the idea that the Higgs phase of a gauge theory is, in some appropriate sense, a symmetry protected topological phase (SPT). A procedure referred to as "gentle gauging" lets us look at this under a different perspective. Extension of these concepts to gauge theories in higher dimensions will be treated in an upcoming work. These ideas are related to a new trend in the classification of quantum phases of matter where higher-form symmetries play a prominent role.

- **Emergence of constrained integrable models from $\mathbb{Z}_2$ LGT:** We show that in the limit of large electric string tension the model studied in section 2.2 becomes integrable and is described by a constrained version of the

XXZ chain. This model, also known as Alcaraz-Bariev (AB), is reviewed systematically in section 3.1, which includes novel results which fit into the theory of generalized hydrodynamics (GHD). In section 3.2 we show different instances where the AB model emerges from more complicated $\mathbb{Z}_2$ lattice gauge theories.

- **Integrable regime of the TLFI model:** Since it is well known that the Ising model can be expressed as a $\mathbb{Z}_2$ LGT, it is no surprise that emergent integrability appears in this context too. In section 3.3 we start directly from the TLFI model and show that in a certain regime the sector consisting of isolated magnons is captured by the AB effective Hamiltonian. As a consequence, the dynamics over long timescales is correctly captured by the GHD. In section 3.3.3 we extend the discussion to sectors including clusters of magnons whose effective Hamiltonian -in the same regime- is non-integrable. We find that such clusters exhibit restricted mobility and peculiar dynamics.
- **Quantum phase diagram of a 2d $\mathbb{Z}_2$ LGT:** After discussing related models in the literature, in section 4.3 we present a careful study of a two dimensional theory of spinless fermions coupled to $\mathbb{Z}_2$ gauge fields. We obtain several novel results. A perturbative analysis at generic filling reveals a phase where the elementary constituents cluster into extended object, which experience slow dynamics. At half filling we find, in two opposite limits, a Dirac deconfined phase and a state that exhibits a charge density wave pattern of dimers. Numerical results hint at a continuous transition between the two regimes, resulting in a highly unconventional quantum critical point that will be studied in greater detail in a future work.
- **Local mapping between $\mathbb{Z}_2$ LGT and spin $1/2$ models:** Chapter 5 of this thesis is dedicated entirely to a feature of $\mathbb{Z}_2$ LGT with Ising or spinless fermionic matter that we developed and employed extensively, namely the mapping between such models and spin 1/2 systems. While the mapping can be formulated in any dimension, we focus on the one and two dimensional cases. The mapping makes use of the Gauss law to operate directly in the physical Hilbert space, thus eliminating the redundant degrees of freedom of the system. We show how to map relevant Hamiltonian and observables, and point out some results which are best understood in terms of the spin models.

We believe that our results push forward the field of discrete lattice gauge theories in a number of different directions. Besides the concrete achievements listed above, our research connects to different communities, acting as a bridge between scientists in the fields of strongly correlated systems, integrability, high-energy theory and experiments on ultracold atoms in optical lattices. Each of these areas provides exciting opportunities for future studies. Ground state properties and dynamics of some deceivingly simple 1d systems can be probed in the most advanced cold atoms platforms, encouraging a closer synergy between theory and experiments. Significant advances in the study of two dimensional quantum system are expected to follow from the development of more and more refined tensor network techniques. Algorithms that are specifically tailored for $\mathbb{Z}_2$ gauge theories may provide unprecedented insight into many of the questions that are still unanswered.

Appendix

A Numerical Methods

As expected in any investigation of quantum many body systems, a substantial amount of our original results relies on numerical methods. These are used both to confirm the validity of analytical predictions, and to obtain entirely new insight into systems that cannot be treated otherwise. As the methods that we use are mostly standard, we refer to the literature for a comprehensive account of tensor network based methods [183, 231, 232] and exact diagonalization [233]. We outline here the aspects that are most relevant to our work.

A.1 DMRG

Density matrix renormalization group (DMRG), both in its finite and infinite forms [183, 234, 235], is the main method employed to achieve the numerical results presented throughout this thesis. It is used to obtain ground states of one-dimensional systems in the form of matrix product states (MPS) [236–239] using an efficient truncation system based on a parameter χ called *bond dimension*.[1] All our simulations are performed with the Python tensor network package TeNPy [184], which provides state-of-the-art algorithms for ground state search and time evolution and a convenient way to implement models and observables. On-site symmetries such as particle number and parity conservation are implemented efficiently, giving a great computational advantage.

While the algorithm works best for gapped systems, whose entanglement follows the area law [240], in practice current computational resources are sufficient to tackle gapless systems to a good accuracy. A significantly harder task is to adapt the algorithm to two dimensions. While this is in theory easy for finite systems, that can be mapped to 1d by simply ordering the lattice sites, the procedure introduces artificial long-range interactions that severely limit the performance of the algorithm. We usually consider “quasi 1d” systems whose y direction is periodic, i.e finite or infinite cylinders [241]. The entanglement of such systems grows exponentially with the size of the circumference, which make reaching the thermodynamic limit by finite size scaling an often insurmountable obstacle.

---

[1] The bond dimension χ is related to the maximum entanglement that can be captured by the MPS approximation of the quantum state.

Implementing the Gauss law

In simulating lattice gauge theories in their original formulations (see for example Hamiltonians 2.19 and 4.35), one faces the hurdle of implementing the gauge constraint. This is usually done energetically, by adding a large term to the Hamiltonian that penalizes the states which do not satisfy the Gauss law. While this works, it introduces a numerical error and one extra convergence parameter.[2] Fortunately, the mapping developed in chapter 5 comes to our rescue. Not only does the transformed Hamiltonian automatically incorporate the Gauss law: the Hilbert space of the new problem is also significantly smaller![3] Using the dual spin systems has one drawback: current DMRG implementations do not allow to conserve multi-site charges such as the number operator 5.40. For models with $U(1)$ charge conservation, this forces us to choose which feature we want to prioritize. While in general using the spin system and not conserving particle number is more efficient, the latter is a better choice when one needs to keep a given filling.[4] For instance, to derive the half-filling phase diagram of section 2.2.6 we preferred to use charge conservation, as keeping the gapless system at half filling at large h by tuning the chemical potential turned out to be a very inconvenient task.

Finite vs infinite DMRG

While finite DMRG has been used for almost 30 years and is an extremely well established method, iDMRG is more recent and requires some care to be applied correctly. In iDMRG, the thermodynamic limit in the x direction is extracted by obtaining the ground state MPS over a unit cell that represents the “center” of an infinite system. Choosing the appropriate unit cell, of length L_x, is of paramount importance. Small unit cells offer computational advantages, but are only able to capture states with periodicity up to L_x. It is therefore important to check the stability of the results for different unit cells to make sure that the ground state returned by the algorithm is not unphysical. For example, a Mott state of commensurability three (e.g. with a particle every three sites) can never be captured by choosing $L_x = 2$ or $L_x = 4$. Whenever possible, it is advisable to obtain preliminary results using the finite algorithm to have an initial understanding of the results, which can be used to choose the appropriate setup for the infinite algorithm. In the case of quasi-two dimensional systems, however, iDMRG is usually the only option available due to its much greater efficiency.

---

[2] I.e. at least in principle, one should run the algorithm for different large values of the energy penalty K, and extrapolate the results to $K \to \infty$. In practice, this is only done when a particularly large accuracy is required.

[3] Of course the two things are related, but we want to stress that the mapping solves two problems at once.

[4] When $U(1)$ conservation is not implemented, this requires to tune the chemical potential by trial and error for each choice of the other parameters, which under certain circumstances becomes a cumbersome task.

Correlation length

We emphasize here a feature of iDMRG that is used extensively in our research. The infinite algorithm allows to calculate through the so-called transfer matrix the correlation length ξ of the system. This corresponds to a length scale associated with the slowest-decaying correlations. In gapless systems quantum fluctuations occur over all length scales, and the correlation length is expected to diverge. This is particularly useful to detect a quantum critical point between gapped phases, corresponding to second-order phase transitions. Peaks in the correlation length, which increase as the algorithm is pushed to greater accuracy,[5] are a clear signature of quantum criticality that can be obtained without knowing further details about the system.[6] This is done for example in section 4.3 to detect the quantum critical point between the deconfined-Dirac and the dimer-Mott states.

Entanglement entropy scaling

In section 2.2 we studied a system that turned out to be gapless throughout the whole phase diagram.[7] For such systems the correlation length ξ is always a diverging quantity, and so it is not useful by itself. There is however another observable that is readily available within the MPS framework and divergent for gapless systems: the entanglement entropy S. The bond dimension regulates the maximum amount of entanglement that can be captured, while at the same time serving as an inverse energy cutoff. For this reason when simulations are performed for increasing χ, both S and ξ are expected to grow monotonically. In one spatial dimension, if the system is critical it can be described by a 2D CFT with central charge c. The three quantities are related by the important scaling equation [242]

$$S = \frac{c}{6} \log \xi + a \tag{A.1}$$

where a is a non-universal constant. This gives a means to probe the central charge of the system and thus the nature of the criticality. For instance, for the system in section 2.2 we found with this method $c = 1$, in agreement with the hypothesis that we are dealing with a Luttinger liquid described by the compact boson CFT. At points corresponding to 1d Ising criticality, on the other hand, one finds the result $c = 1/2$ (see for example the phase diagrams in section 2.3.5).

A.2 TEBD

TEBD [183, 184, 243] is another tensor network based method, implemented in TeNPy, which is used for time-evolution of MPS quantum states.[8] We employ it in section 3.3 to study the quantum dynamics of the TLFI and AB models, compare them and check that over large timescales they collapse onto the GHD solutions.

---

[5] This is done by increasing the bond dimension χ, which determines the entanglement-based truncation.

[6] E.g. one does not need to know which degrees of freedom are gapless.

[7] With the possible exception of a Mott state with infinitesimally small gap at large h and filling 2/3.

[8] There is also an imaginary time version which is used to obtain ground states, but it is in general less efficient than DMRG.

A.3 Exact Diagonalization

The 2d model of spinless fermions coupled to $\mathbb{Z}_2$ gauge fields studied in section 4.3 has three degrees of freedom per unit cell[9] in its original formulation, i.e. a local Hilbert space of size $2^3 = 8$. This means that on a 4×4 torus, which we regard as the minimum size to obtain useful physical insight, there are 48 two-level degrees of freedom, split between 32 spins (gauge fields) and 16 spinless fermions. Diagonalization of a Hamiltonian of size 2^{48}, even with sparse methods, is well beyond the most advanced computational capabilities. To our luck, is section 5.2 we have developed a mapping that casts the model to a system of gauge invariant spins living on the links of the lattice. Exact diagonalization of a system of 32 spins is possible, provided that enough symmetries are present. Since the system is defined on a torus, we have translational invariance in the x and y directions, which results in conservation of the quantized momenta k_x and k_y. Using the ED Python package QuSpin [244, 245], momentum conservation is readily implemented using standard techniques. However, it is crucial to exploit the global $U(1)$ particle number symmetry as well. The latter is not on-site in the spin model, as the number operator takes the form (5.40), and therefore more tricky to implement. We achieve this by using the advanced user_basis functionalities of QuSpin. Basis states of spin 1/2 systems can be put in correspondence with bit strings. In our case, we just need to choose an ordering for the 32 links, and then basis states are written in the X-basis (where the number operator is diagonal) with the correspondence $|1\rangle \leftrightarrow |\uparrow\rangle$ and $|0\rangle \leftrightarrow |\downarrow\rangle$. Then particle number is checked efficiently with bit-wise operations on the basis states, and the states with the desired filling can be filtered. This reduced basis, composed by states with a given filling and momenta, is small enough so that the Hamiltonian is diagonalizable with sparse methods.

B Luttinger liquids

In this Appendix we provide a quick summary of bosonization and Luttinger liquid theory. This has the main aim of clarifying our notation and justify some statements made in Chapter 2.

The Luttinger liquid theory states that the low energy physics of (almost) all one dimensional gapless systems is captured by the scalar field theory of a single compact boson ϕ. All the details concerning the interactions are absorbed into the renormalization of a single parameter K, the so called Luttinger parameter. We follow the notation from Sachdev's book [34], where the Hamiltonian takes the form

$$H_{LL} = \frac{1}{2\pi} \int dx d\tau \left[\frac{1}{K} (\nabla\phi)^2 + K(\nabla\theta)^2 \right]. \tag{A.2}$$

---

[9] An elementary unit cell is formed, in our convention, by a site and by the two links pointing to the right and upwards.

The field ϕ is related to the density by $\nabla\phi = \pi\rho(x)$, while $\nabla\theta$ is the conjugate momentum to ϕ. The corresponding Lagrangian is simply

$$S_{LL} = \frac{1}{2\pi K}\int dx d\tau (\partial^{\mu}\theta)(\partial_{\mu}\theta). \tag{A.3}$$

which corresponds to the compact boson CFT, where the Luttinger parameter K appears as the compactification radius. The free fermion point corresponds to $K = 1$, while different values of K signal the presence of interactions. In particular, $K < 1$ and $K > 1$ correspond to repulsive and attractive interactions respectively. One can imagine starting from a generic value of K, that corresponds to some microscopic model, and include arbitrary perturbations. Under the RG flow, these will either renormalize K or generate additional terms that are allowed by the symmetries of the problem. Since ϕ and θ are compact fields, the allowed terms must have the form $\cos(m\phi)$ and $\cos(m\theta)$ with $m \in \mathbb{N}$. Symmetry under one-site translations act on ϕ as

$$\phi \to \phi + k_F. \tag{A.4}$$

At half filling, for example, one has $k_F = \pi/2$ so that $\cos(4\phi)$ is invariant while $\cos(2\phi)$ is not invariant and forbidden by symmetry. A global $U(1)$ symmetry, on the other hand, acts as a shift on θ:

$$\theta \to \theta + \alpha. \tag{A.5}$$

Therefore if the $U(1)$ symmetry is to be preserved, i.e. in a particle number conserving model, all terms of the form $\cos(m\theta)$ are forbidden. Cosine perturbation can potentially open up a gap in the spectrum if they are RG-relevant. This depends on the value of K, as the scaling dimensions of $\cos(m\phi)$ and $\cos(m\theta)$ are $m^2/(4K)$ and $m^2K/4$ respectively. In particular, we note that at the free fermion point $K = 1$ the typical symmetry allowed mass term $\cos(4\phi)$ is not relevant, while a gap is opened by the $U(1)$ breaking perturbation $\sin(2\theta)$. This can be traced back to the usual pairing term in the microscopic theory.

C Details on integrability results and generalized hydrodynamics

In this section of the Appendix we provide some details about integrability of the constrained XXZ chain. Due to the technical character of the subject, the references given in the main text are essential to a full comprehension of how the problem is solved. We hope that reviewing the most salient aspects can help the reader follow the arguments in the main text.

C.1 Summary of XXZ thermodynamics

As stated, the treatment of the constrained XXZ chain (AB model) largely follows the logic of its unconstrained version. Therefore, we provide here a short summary of the XXZ thermodynamics on which the solution of the AB model is built.

For a more extended discussion, we refer to Ref. [151]. In particular, we provide expressions for the string parametrization, whose important role is briefly explained in section 3.1.2. The sectors with opposite interaction signs are unitary equivalent, hence as customary we focus on the regime $\Delta > 0$.

- The case $\Delta \geq 1$: The interaction is conveniently parametrized as $\Delta = \cosh\theta$, the string parametrization and scattering phases are

  $$p(\lambda) = -i \log\left[\frac{\sin(\lambda - i\theta/2)}{\sin(\lambda + i\theta/2)}\right], \qquad \Theta^{XXZ}(\lambda) = -i\log\left[-\frac{\sin(\lambda + i\theta)}{\sin(\lambda - i\theta)}\right]. \tag{A.6}$$

  In this sector, the system has infinitely many strings of species $j = \{1, 2, ...\}$ and the rapidities of the constituents of a string with real rapidity λ are obtained by shifting in the imaginary direction

  $$\lambda^{a,j} = \lambda + i\theta\frac{(j-1-2a)}{2}, \quad a = \{0, ..., j-1\}. \tag{A.7}$$

  The scattering phase is given by Eq. (3.14). In particular, one finds

  $$\partial_\lambda \Theta^{XXZ}_{j,j'}(\lambda) = (1-\delta_{j,j'})f_{|j-j'|}(\lambda) + f_{j+j'}(\lambda) + 2\sum_{s=1}^{\min(j,j')-1} f_{|j-j'|+2s}(\lambda) \tag{A.8}$$

  with

  $$f_j(\lambda) = \frac{1}{2\pi}\partial_\lambda p_j(\lambda) = \frac{1}{\pi}\frac{\sinh(j\theta)}{\cosh(j\theta) - \cos(2\lambda)} \tag{A.9}$$

  and $\epsilon_j(\lambda) = \mathcal{J}\pi\sinh\theta f_j(\lambda)$ and $|m_j^{XXZ}| = j$. In this sector, the parity of the string is always positive $\sigma_j = 1$ and the rapidities of the strings live within a finite domain $\lambda \in [-\pi/2, \pi/2]$. The choice of the magnetization sector $\mathfrak{f} = \pm 1$ only changes the sign of m_j^{XXZ} and nothing else.

- The case $0 < \Delta < 1$: With the parametrization $\Delta = \cos(\pi\gamma)$ one has

  $$p(\lambda) = -i\log\left[\frac{\sinh(\lambda + i\pi\gamma/2)}{\sinh(\lambda - i\pi\gamma/2)}\right], \qquad \Theta^{XXZ}(\lambda) = -i\log\left[\frac{\sinh(\lambda - i\pi\gamma/2)}{\sinh(\lambda + i\pi\gamma/2)}\right] \tag{A.10}$$

  The string content depends on the continued fraction representation of γ

  $$\gamma = \frac{1}{n_1 + \frac{1}{n_2 + ...}} \tag{A.11}$$

  where n_i are suitable positive integers and the total number of strings is $\sum_i n_i$. The constituents of a string of species j carry rapidities

  $$\lambda^{a,j} = \lambda + i\frac{\pi\gamma}{2}(m_j + 1 - 2a) + i\pi(1 - v_j)/4, \qquad a = \{1, .., m_j\}, \tag{A.12}$$

  where the real rapidity λ covers the entrire real axis $\lambda \in (-\infty, \infty)$. The value of the magnetization m_j, the parity σ_j and the parameter v_j depend on the continued fraction expansion (A.11). In the simplest case where one chooses $\gamma = 1/\ell$, one has ℓ strings and

$$m_j = j\,, \quad \sigma_j = 1\,, \quad v_j = 1\,, \quad j < \ell \qquad \text{and} \quad m_\ell = 1\,, \quad \sigma_\ell = -1\,, \quad v_\ell = -1. \tag{A.13}$$

For the general case, we refer to Ref. [151]. Finally, the string scattering data are

$$\begin{aligned} \partial_\lambda \Theta^{XXZ}_{j,j'}(\lambda) = (1-\delta_{m_j,m_{j'}})\, a^{v_j v_{j'}}_{|m_j-m_{j'}|}(\lambda) + a^{v_j v_{j'}}_{m_j+m_{j'}}(\lambda) + \\ + 2 \sum_{s=1}^{\min(m_j,m_{j'})-2} a^{v_j v_{j'}}_{|m_j-m_{j'}|+2s}(\lambda), \end{aligned} \tag{A.14}$$

where

$$a^y_x(\lambda) = \frac{y}{\pi} \frac{\sin(\pi\gamma x)}{\cos(2\lambda) - y\cos(\pi\gamma x)}$$

$$\frac{1}{2\pi}\partial_\lambda p_j(\lambda) = a^{v_j}_{m_j}(\lambda)\,, \quad \epsilon_j(\lambda) = \mathcal{J}\pi\sinh(\pi\gamma)\, a^{v_j}_{m_j}(\lambda). \tag{A.15}$$

C.2 The AB model as the XXZ chain in reduced volume

As argued, an important part of the treatment of the constrained XXZ chain consists in recasting the problem to the one of a regular (unconstrained) chain in reduced volume. This follows intuitively from the general arguments of section 3.1, but let's make the statement more precise. Without loss of generality, we assume N being odd and write the Bethe equations [126] as

$$e^{ik_j(L-TN)} = e^{-ilP} \prod_{\ell \neq j} e^{i\Theta^{XXZ}(k_j,k_\ell)}\,, \tag{A.16}$$

where we introduced $P = \sum_j k_j$. The above can be interpreted as the Bethe equations of a XXZ spin chain in a reduced volume $\tilde{L} = L - lN$ and with periodic boundary conditions twisted by the factor e^{-ilP}. This trick has already been noticed by Alcaraz and Bariev who used it to construct the coordinate Bethe Ansatz. We will now use this correspondence to address the thermodynamics and hydrodynamics of the AB model. In the rapidity parametrization, the density the local conserved charges $\hat{Q}$ (except for the magnetization to be discussed later) is

$$\tilde{L}^{-1}\langle\hat{Q}\rangle = \sum_j \int \mathrm{d}\lambda\, q_j(\lambda)\rho^{XXZ}_j(\lambda) \tag{A.17}$$

with $q_j(\lambda)$ being called the charge eigenvalue. We explicitly rewrite $\tilde{L} = L(1-ln)$ with n being the density of flipped spins. Hence, we can write

$$L^{-1}\langle\hat{Q}\rangle = \sum_j \int \mathrm{d}\lambda\, q_j(\lambda)(1-ln)\rho^{XXZ}_j(\lambda) = \sum_j \int \mathrm{d}\lambda\, q_j(\lambda)\rho_j(\lambda), \tag{A.18}$$

where we identified the rescaled XXZ root density with the root density of the AB model $\rho_j(\lambda) \equiv (1-ln)\rho^{XXZ}_j(\lambda)$. In the sectors where the string hypothesis of the

AB model is valid, this correspondence naturally emerges comparing the AB and rescaled XXZ thermodynamics. Now, we will assume its validity also beyond this case.

Let us now consider the magnetization that was ommited above: in the XXZ model at $|\Delta| \geq 1$ one needs to introduce the magnetization sign [177]

$$\tilde{L}^{-1}\langle S^z_j - 1\rangle = \frac{1-\mathfrak{f}}{2} + \sum_j \int \mathrm{d}\lambda \mathfrak{f} |m_j^{XXZ}| \rho_j^{XXZ}(\lambda). \tag{A.19}$$

Now, we rewrite $\tilde{L}^{-1}\langle S^z_j - 1\rangle = \tilde{L}^{-1}Ln = n(1-ln)^{-1}$ and solve the above for n

$$n = \frac{(1-\mathfrak{f})}{2+l(1-\mathfrak{f})} + \sum_j \int \mathrm{d}\lambda \frac{2\mathfrak{f}}{2+l(1-\mathfrak{f})} |m_j^{XXZ}| \rho_j(\lambda). \tag{A.20}$$

This leads to the natural identification $m_j \equiv (1 + l(1-\mathfrak{f})/2)^{-1} m_j^{XXZ}$ that we have already anticipated in the main text. The correspondence is then easily extended to the whole thermodynamics. In particular, the definition of the total root density

$$\sigma_j \rho^t_j(\lambda) = \frac{2}{2+l(1-\mathfrak{f})} \frac{\partial_\lambda p_j(\lambda)}{2\pi} - \sum_{j'} \int \frac{\mathrm{d}\lambda}{2\pi} \partial_\lambda \Theta_{j,j'}(\lambda,\lambda') \rho_{j'}(\lambda)\,, \tag{A.21}$$

where $\Theta_{j,j'}$ is defined in Eq. (3.14) is consistent with the expected rescaling $\rho^t_j(\lambda) \equiv (1-ln)[\rho^t_j]^{XXZ}(\lambda)$.

C.3 Thermal states in the presence of an external magnetic field

Finally, let us address the problem of constructing thermodynamics of thermal states in the presence of a magnetic field $e^{-\beta(H + B\sum_j S^z_j)}$, where β denotes the inverse temperature. These are the states to which the left and right halves of the chain are initialized in in section 3.3 to probe transport. By means of standard TBA techniques, the root densities of thermal states can be found solving the following integral equation

$$\varepsilon_j(\lambda) = \beta(\epsilon_j(\lambda) - Bm_j) - \sum_{j'} \int \frac{\mathrm{d}\lambda'}{2\pi} \partial_{\lambda'} \Theta_{j,j'}(\lambda,\lambda') \sigma_{j'} \log\left(1 + e^{-\varepsilon_{j'}(\lambda')}\right). \tag{A.22}$$

with $\rho_j(\lambda) = \rho^t_j(\lambda)(1+e^{\varepsilon_j(\lambda)})^{-1}$ and $\epsilon_j(\lambda)$ the energy of the string, which is the same as the XXZ spin chain. These TBA equations are consistent with first solving TBA equations in the XXZ spin chain in a reduced volume and then taking the proper rescaling afterwards. Notice that the ferromagnetic spin up state and Neel state are nothing else than ground states ($\beta \to \infty$) of the AB Hamiltonian with $B = -\infty$ and $B = +\infty$ respectively. Therefore, these states can be easily described with the above equation. The ferromagnetic spin up state is nothing else than the vacuum hence $\rho_j(\lambda) = 0$ (and $\mathfrak{f} = 1$ for $|\Delta| > 1$), the description of the Neel state depends on Δ. Indeed, if $|\Delta| < 1$ the associated root density is non-trivial, but whenever $|\Delta| > 1$ one gets again $\rho_j(\lambda) = 0$, but $\mathfrak{f} = -1$.

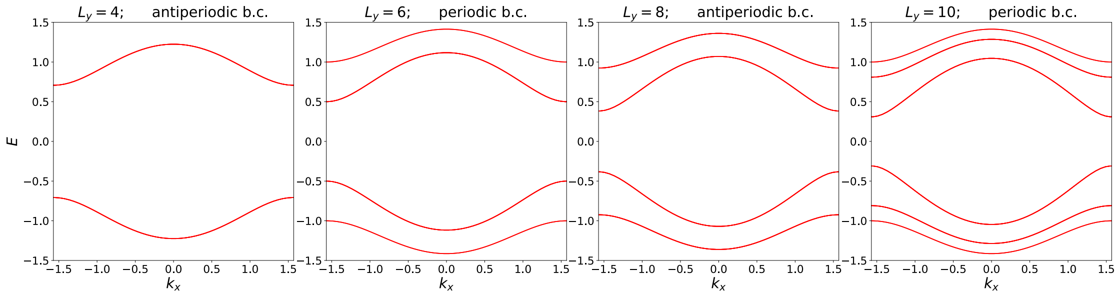

Figure 1: Band structures for the quasi-1d problem of hopping fermions in a π-flux on an infinite cylinder of circumference L_y. The quasi-1d band structure is obtained by intersecting the Dirac cones with the quantized momenta $\mathbf{k}_y$. As stated in the main text, if we take antiperiodic boundary conditions for $L_y = 0 \mod 4$ and periodic boundary conditions for $L_y = 2 \mod 4$, the system is gapped at half filling. Explicit integration of the energy bands up to the Fermi level shows that this configuration has the lowest energy.

D Free fermions on an infinite cylinder in a π flux.

We address here some details concerning the ground state of free fermions hopping in a π flux background on an infinite cylinder. This is relevant since our 2d iDMRG simulations, whose results are presented in Chapter 4, are performed in such geometry. As argued in section 4.3.2, at $h = 0$ the model (4.35) of spinless fermions coupled to $\mathbb{Z}_2$ gauge fields reduces to free fermions. However, there are some subtleties. The Hilbert space only includes states with even fermionic parity, but both periodic and antiperiodic boundary conditions are taken into account. This is similar to what happens in 1d, explained in section 4.3.2: at $h = 0$ the Wilson loop around the cylinder is an additional symmetry of the Hamiltonian. The two symmetry sectors $\langle W \rangle = \pm 1$ correspond to the two different choices of boundary conditions, as can be seen by fixing the gauge. Since the gauged model incorporates both sectors, the unbiased numerical algorithm will find the ground state corresponding to the choice of boundary conditions with the lowest energy. We are particularly interested in the π flux case. The band structure of this problem

$$E(\mathbf{k}) = \pm 2t\sqrt{\cos(k_x)^2 + \cos(k_y)^2} \tag{A.23}$$

is known to form a pair of Dirac cones. A finite circumference quantizes the momentum in the y direction, so that instead of having a full Dirac cone one gets a quasi-1d band structure, where the different bands are given by the intersection between the cone and the planes $\mathbf{k}_y = \{\tilde{\mathbf{k}}_y\}$. Here $\{\tilde{\mathbf{k}}_y\}$ denotes the set of allowed quantized momenta, which differs depending on the choice of boundary conditions. The problem of which choice of boundary conditions gives the lowest energy at half-filling can be solved analytically. For even size of the circumference L, we find the following interesting results: antiperiodic boundary conditions. win energetically if L is a multiple of 4 ($L = 4$, 8, 12 etc...), while periodic boundary conditions win otherwise ($L = 6$, 10 etc...). Moreover, the energetically favorable sector always gives a gapped ground state. This is of great help for our simulations, as MPS based methods are efficient only for gapped Hamiltonians.

Bibliography

[1] P. W. Anderson. More is different. *Science*, 177(4047):393–396, 1972.

[2] Michael E Peskin and Daniel V Schroeder. *An introduction to quantum field theory*. Westview, Boulder, CO, 1995. Includes exercises.

[3] Steven Weinberg. *The Quantum Theory of Fields, Volume 1: Foundations*. Cambridge University Press, 2005.

[4] Steven Weinberg. *The quantum theory of fields. Vol. 2: Modern applications*. 1996. Cambridge, UK: Univ. Pr. (1996) 489 p.

[5] Sean M Carroll. *Spacetime and geometry*. Cambridge University Press, 2019.

[6] J. Polchinski. *String theory. Vol. 1: An introduction to the bosonic string*. Cambridge Monographs on Mathematical Physics. Cambridge University Press, 12 2007.

[7] Carlo Rovelli and Francesca Vidotto. *Covariant Loop Quantum Gravity: An Elementary Introduction to Quantum Gravity and Spinfoam Theory*. Cambridge University Press, 2014.

[8] J D Jackson. *Classical electrodynamics*. Wiley, 1999.

[9] Hermann Von Weyl. Eine neue erweiterung der relativitätstheorie. *Annalen der Physik*, 364:101–133.

[10] Paul A. M. Dirac. Quantum theory of emission and absorption of radiation. *Proc. Roy. Soc. Lond. A*, 114:243, 1927.

[11] P. A. M. Dirac. Generalized hamiltonian dynamics. *Canadian Journal of Mathematics*, 2:129–148, 1950.

[12] R. P. Feynman. Space-time approach to non-relativistic quantum mechanics. *Rev. Mod. Phys.*, 20:367–387, Apr 1948.

[13] Julian Schwinger. Quantum electrodynamics. ii. vacuum polarization and self-energy. *Phys. Rev.*, 75:651–679, Feb 1949.

[14] S. Tomonaga. On a Relativistically Invariant Formulation of the Quantum Theory of Wave Fields*. *Progress of Theoretical Physics*, 1(2):27–42, 08 1946.

[15] F. J. Dyson. The radiation theories of Tomonaga, Schwinger, and Feynman. *Phys. Rev.*, 75:486–502, Feb 1949.

[16] E. Noether. Invariante variationsprobleme. *Nachrichten von der Gesellschaft der Wissenschaften zu Göttingen, Mathematisch-Physikalische Klasse*, 1918:235–257, 1918.

[17] C. N. Yang and R. L. Mills. Conservation of isotopic spin and isotopic gauge invariance. *Phys. Rev.*, 96:191–195, Oct 1954.

[18] F. Englert and R. Brout. Broken symmetry and the mass of gauge vector mesons. *Phys. Rev. Lett.*, 13:321–323, Aug 1964.

[19] Peter W. Higgs. Broken symmetries and the masses of gauge bosons. *Phys. Rev. Lett.*, 13:508–509, Oct 1964.

[20] G. S. Guralnik, C. R. Hagen, and T. W. B. Kibble. Global conservation laws and massless particles. *Phys. Rev. Lett.*, 13:585–587, Nov 1964.

[21] P. W. Anderson. Plasmons, gauge invariance, and mass. *Phys. Rev.*, 130:439–442, Apr 1963.

[22] David J. Gross and Frank Wilczek. Ultraviolet behavior of non-abelian gauge theories. *Phys. Rev. Lett.*, 30:1343–1346, Jun 1973.

[23] H. David Politzer. Reliable perturbative results for strong interactions? *Phys. Rev. Lett.*, 30:1346–1349, Jun 1973.

[24] John Kogut and Leonard Susskind. Hamiltonian formulation of Wilson's lattice gauge theories. *Phys. Rev. D*, 11:395–408, Jan 1975.

[25] John B. Kogut. An introduction to lattice gauge theory and spin systems. *Rev. Mod. Phys.*, 51:659–713, Oct 1979.

[26] Andreas S Kronfeld and /Fermilab. Twenty-first century lattice gauge theory: Results from the QCD Lagrangian.

[27] Workman R.L. et al. (Particle Data Group). Review of Particle Physics. *Progress of Theoretical and Experimental Physics*, 2022(8), 08 2022. 083C01.

[28] H.B. Nielsen and M. Ninomiya. Absence of neutrinos on a lattice: (i). proof by homotopy theory. *Nuclear Physics B*, 185(1):20–40, 1981.

[29] H.B. Nielsen and M. Ninomiya. Absence of neutrinos on a lattice: (ii). intuitive topological proof. *Nuclear Physics B*, 193(1):173–194, 1981.

[30] Franz J. Wegner. Duality in generalized Ising models and phase transitions without local order parameters. *Journal of Mathematical Physics*, 12(10):2259–2272, 1971.

[31] Lev Davidovich Landau. On the theory of phase transitions. I. *Phys. Z. Sowjet.*, 11:26, 1937.

[32] Alexander Altland and Ben D Simons. *Condensed matter field theory*. Cambridge University Press, 2010.

[33] X.G. Wen. *Quantum Field Theory of Many-Body Systems*. Oxford Graduate Texts. OUP Oxford, 2004.

[34] S Sachdev. *Quantum phase transitions*. Cambridge University Press, 2011.

[35] X. G. Wen. Vacuum degeneracy of chiral spin states in compactified space. *Phys. Rev. B*, 40:7387–7390, Oct 1989.

[36] E Fradkin. *Field Theories of Condensed Matter Physics*. Cambridge University Press, 2013.

[37] A.Yu. Kitaev. Fault-tolerant quantum computation by anyons. *Annals of Physics*, 303(1):2–30, 2003.

[38] X. G. Wen and A. Zee. Topological structures, universality classes, and statistics screening in the anyon superfluid. *Phys. Rev. B*, 44:274–284, Jul 1991.

[39] Eduardo Fradkin and Stephen H. Shenker. Phase diagrams of lattice gauge theories with Higgs fields. *Phys. Rev. D*, 19:3682–3697, Jun 1979.

[40] J. G. Bednorz and K. A. Müller. Possible high T_c superconductivity in the Ba$-$La$-$Cu$-$O system. *Zeitschrift für Physik B Condensed Matter*, 64(2):189–193, Jun 1986.

[41] Philip W Anderson. Twenty-five years of high-temperature superconductivity – a personal review. *Journal of Physics: Conference Series*, 449:012001, jul 2013.

[42] T. Senthil and Matthew P. A. Fisher. $\mathbb{Z}_2$ gauge theory of electron fractionalization in strongly correlated systems. *Phys. Rev. B*, 62:7850–7881, Sep 2000.

[43] Rahul Nandkishore, Max A. Metlitski, and T. Senthil. Orthogonal metals: The simplest non-Fermi liquids. *Phys. Rev. B*, 86:045128, Jul 2012.

[44] Snir Gazit, Mohit Randeria, and Ashvin Vishwanath. Emergent Dirac fermions and broken symmetries in confined and deconfined phases of $\mathbb{Z}_2$ gauge theories. *Nature Physics*, 13(5):484–490, 2017.

[45] Snir Gazit, Fakher F. Assaad, Subir Sachdev, Ashvin Vishwanath, and Chong Wang. Confinement transition of $\mathbb{Z}_2$ gauge theories coupled to massless fermions: Emergent quantum chromodynamics and $SO(5)$ symmetry. *Proceedings of the National Academy of Sciences*, 115(30):E6987–E6995, 2018.

[46] Snir Gazit, Fakher F Assaad, and Subir Sachdev. Fermi surface reconstruction without symmetry breaking. *Physical Review X*, 10(4):041057, 2020.

[47] Elio J. König, Piers Coleman, and Alexei M. Tsvelik. Soluble limit and criticality of fermions in $\mathbb{Z}_2$ gauge theories. *Phys. Rev. B*, 102:155143, Oct 2020.

[48] F. F. Assaad and Tarun Grover. Simple fermionic model of deconfined phases and phase transitions. *Phys. Rev. X*, 6:041049, Dec 2016.

[49] Christian Prosko, Shu-Ping Lee, and Joseph Maciejko. Simple $\mathbb{Z}_2$ lattice gauge theories at finite fermion density. *Phys. Rev. B*, 96:205104, Nov 2017.

[50] A. Smith, J. Knolle, D. L. Kovrizhin, and R. Moessner. Disorder-free localization. *Phys. Rev. Lett.*, 118:266601, Jun 2017.

[51] Daniel González-Cuadra, Luca Tagliacozzo, Maciej Lewenstein, and Alejandro Bermudez. Robust topological order in fermionic $\mathbb{Z}_2$ gauge theories: From Aharonov-Bohm instability to soliton-induced deconfinement. *Phys. Rev. X*, 10:041007, Oct 2020.

[52] Oscar Pozo, Peng Rao, Chuan Chen, and Inti Sodemann. Anatomy of $\mathbb{Z}_2$ fluxes in anyon Fermi liquids and Bose condensates. *Phys. Rev. B*, 103:035145, Jan 2021.

[53] Wolfram Brenig. Spinless fermions in a $\mathbb{Z}_2$ gauge theory on a triangular ladder. *Phys. Rev. B*, 105:245105, Jun 2022.

[54] Lukas Homeier, Annabelle Bohrdt, Simon Linsel, Eugene Demler, Jad C. Halimeh, and Fabian Grusdt. Quantum simulation of $\mathbb{Z}_2$ lattice gauge theories with dynamical matter from two-body interactions in $(2+1)$d. *arXiv:2205.08541*, 2022.

[55] Julian Schwinger. Gauge invariance and mass. ii. *Phys. Rev.*, 128:2425–2429, Dec 1962.

[56] J.H Lowenstein and J.A Swieca. Quantum electrodynamics in two dimensions. *Annals of Physics*, 68(1):172–195, 1971.

[57] A. Casher, J. Kogut, and Leonard Susskind. Vacuum polarization and the quark-parton puzzle. *Phys. Rev. Lett.*, 31:792–795, Sep 1973.

[58] G. 't Hooft. A two-dimensional model for mesons. *Nuclear Physics B*, 75(3):461–470, 1974.

[59] Sidney Coleman. More about the massive Schwinger model. *Annals of Physics*, 101(1):239–267, 1976.

[60] Curtis G. Callan, Nigel Coote, and David J. Gross. Two-dimensional yang-mills theory: A model of quark confinement. *Phys. Rev. D*, 13:1649–1669, Mar 1976.

[61] L.V. Belvedere, J.A. Swieca, K.D. Rothe, and B. Schroer. Generalized two-dimensional abelian gauge theories and confinement. *Nuclear Physics B*, 153:112–140, 1979.

[62] N.S Manton. The Schwinger model and its axial anomaly. *Annals of Physics*, 159(1):220–251, 1985.

[63] Edward Witten. On quantum gauge theories in two dimensions. *Communications in Mathematical Physics*, 141(1):153–209, 1991.

[64] Edward Witten. Two dimensional gauge theories revisited. *Journal of Geometry and Physics*, 9(4):303–368, 1992.

[65] David J. Gross and Washington Taylor. Two-dimensional QCD is a string theory. *Nuclear Physics B*, 400(1):181–208, 1993.

[66] Gregory Moore. Two-dimensional Yang-Mills theory and topological field theory. In S. D. Chatterji, editor, *Proceedings of the International Congress of Mathematicians*, pages 1292–1303, Basel, 1995. Birkhäuser Basel.

[67] T. Giamarchi. *Quantum Physics in One Dimension*. Clarendon Press, 2004.

[68] R. Moessner, S. L. Sondhi, and Eduardo Fradkin. Short-ranged resonating valence bond physics, quantum dimer models, and Ising gauge theories. *Phys. Rev. B*, 65:024504, Dec 2001.

[69] Hsin-Hua Lai and Olexei I. Motrunich. Majorana spin liquids on a two-leg ladder. *Phys. Rev. B*, 84:235148, Dec 2011.

[70] Umberto Borla, Ruben Verresen, Fabian Grusdt, and Sergej Moroz. Confined phases of one-dimensional spinless fermions coupled to $\mathbb{Z}_2$ gauge theory. *Phys. Rev. Lett.*, 124(12):120503, 2020.

[71] Fabian Grusdt and Lode Pollet. $\mathbb{Z}_2$ parton phases in the mixed-dimensional t-J_z model. *Physical Review Letters*, 125(25), dec 2020.

[72] Djordje Radicevic. Spin structures and exact dualities in low dimensions. *arXiv:1809.07757*, 2018.

[73] Andreas Karch, David Tong, and Carl Turner. A web of 2d dualities: $\mathbb{Z}_2$ gauge fields and Arf invariants. *SciPost Phys.*, 7:007, 2019.

[74] Shenghan Jiang and Olexei Motrunich. Ising ferromagnet to valence bond solid transition in a one-dimensional spin chain: Analogies to deconfined quantum critical points. *Phys. Rev. B*, 99:075103, Feb 2019.

[75] Adam Smith, Johannes Knolle, Roderich Moessner, and Dmitry L. Kovrizhin. Dynamical localization in $\mathbb{Z}_2$ lattice gauge theories. *Phys. Rev. B*, 97:245137, Jun 2018.

[76] C. J. Turner, A. A. Michailidis, D. A. Abanin, M. Serbyn, and Z. Papic. Weak ergodicity breaking from quantum many-body scars. *Nature Physics*, 14(7):745–749, 2018.

[77] C. J. Turner, A. A. Michailidis, D. A. Abanin, M. Serbyn, and Z. Papić. Quantum scarred eigenstates in a Rydberg atom chain: Entanglement, breakdown of thermalization, and stability to perturbations. *Phys. Rev. B*, 98:155134, Oct 2018.

[78] Sanjay Moudgalya, Stephan Rachel, B. Andrei Bernevig, and Nicolas Regnault. Exact excited states of nonintegrable models. *Phys. Rev. B*, 98:235155, Dec 2018.

[79] Sanjay Moudgalya, Nicolas Regnault, and B. Andrei Bernevig. Entanglement of exact excited states of Affleck-Kennedy-Lieb-Tasaki models: Exact results, many-body scars, and violation of the strong eigenstate thermalization hypothesis. *Phys. Rev. B*, 98:235156, Dec 2018.

[80] Cheng-Ju Lin and Olexei I. Motrunich. Exact quantum many-body scar states in the Rydberg-blockaded atom chain. *Phys. Rev. Lett.*, 122:173401, Apr 2019.

[81] Michael Schecter and Thomas Iadecola. Weak ergodicity breaking and quantum many-body scars in spin-1 XY magnets. *Phys. Rev. Lett.*, 123:147201, Oct 2019.

[82] Thomas Iadecola and Michael Schecter. Quantum many-body scar states with emergent kinetic constraints and finite-entanglement revivals. *Phys. Rev. B*, 101:024306, Jan 2020.

[83] Adith Sai Aramthottil, Utso Bhattacharya, Daniel González-Cuadra, Maciej Lewenstein, Luca Barbiero, and Jakub Zakrzewski. Scar states in deconfined $\mathbb{Z}_2$ lattice gauge theories. *Phys. Rev. B*, 106:L041101, Jul 2022.

[84] Alvise Bastianello, Umberto Borla, and Sergej Moroz. Fragmentation and emergent integrable transport in the weakly tilted ising chain. *Physical Review Letters*, 128(19), may 2022.

[85] N. Goldman, G. Juzeliūnas, P. Öhberg, and I. B. Spielman. Light-induced gauge fields for ultracold atoms. *Reports on Progress in Physics*, 77(12):126401, nov 2014.

[86] Erez Zohar, J. Ignacio Cirac, and Benni Reznik. Quantum simulations of lattice gauge theories using ultracold atoms in optical lattices. *Reports on Progress in Physics*, 79(1):014401, 2015.

[87] Mari Carmen Bañuls and Krzysztof Cichy. Review on novel methods for lattice gauge theories. *Reports on Progress in Physics*, 83(2):024401, jan 2020.

[88] Mari Carmen Bañuls, Rainer Blatt, Jacopo Catani, Alessio Celi, Juan Ignacio Cirac, Marcello Dalmonte, Leonardo Fallani, Karl Jansen, Maciej Lewenstein, Simone Montangero, Christine A. Muschik, Benni Reznik, Enrique Rico, Luca Tagliacozzo, Karel Van Acoleyen, Frank Verstraete, Uwe-Jens Wiese, Matthew Wingate, Jakub Zakrzewski, and Peter Zoller. Simulating lattice gauge theories within quantum technologies. *The European Physical Journal D*, 74(8):165, Aug 2020.

[89] Erez Zohar. Quantum simulation of lattice gauge theories in more than one space dimension—requirements, challenges and methods. *Philosophical Transactions of the Royal Society A: Mathematical, Physical and Engineering Sciences*, 380(2216), dec 2021.

[90] Ehud Altman, Kenneth R. Brown, Giuseppe Carleo, Lincoln D. Carr, Eugene Demler, Cheng Chin, Brian DeMarco, Sophia E. Economou, Mark A. Eriksson, Kai-Mei C. Fu, Markus Greiner, Kaden R.A. Hazzard, Randall G. Hulet, Alicia J. Kollár, Benjamin L. Lev, Mikhail D. Lukin, Ruichao Ma, Xiao Mi, Shashank Misra, Christopher Monroe, Kater Murch, Zaira Nazario, Kang-Kuen Ni, Andrew C. Potter, Pedram Roushan, Mark Saffman, Monika Schleier-Smith, Irfan Siddiqi, Raymond Simmonds, Meenakshi Singh, I.B. Spielman, Kristan Temme, David S. Weiss, Jelena Vučković, Vladan Vuletić, Jun Ye, and Martin Zwierlein. Quantum simulators: Architectures and opportunities. *PRX Quantum*, 2:017003, Feb 2021.

[91] I. M. Georgescu, S. Ashhab, and Franco Nori. Quantum simulation. *Rev. Mod. Phys.*, 86:153–185, Mar 2014.

[92] Immanuel Bloch, Jean Dalibard, and Wilhelm Zwerger. Many-body physics with ultracold gases. *Rev. Mod. Phys.*, 80:885–964, Jul 2008.

[93] Christian Gross and Immanuel Bloch. Quantum simulations with ultracold atoms in optical lattices. *Science*, 357(6355):995–1001, 2017.

[94] D. Jaksch, C. Bruder, J. I. Cirac, C. W. Gardiner, and P. Zoller. Cold bosonic atoms in optical lattices. *Physical Review Letters*, 81(15):3108–3111, oct 1998.

[95] Markus Greiner, Olaf Mandel, Tilman Esslinger, Theodor W. Hänsch, and Immanuel Bloch. Quantum phase transition from a superfluid to a Mott insulator in a gas of ultracold atoms. *Nature*, 415(6867):39–44, Jan 2002.

[96] M. Aidelsburger, M. Atala, M. Lohse, J. T. Barreiro, B. Paredes, and I. Bloch. Realization of the Hofstadter Hamiltonian with ultracold atoms in optical lattices. *Physical Review Letters*, 111(18), oct 2013.

[97] U.-J. Wiese. Ultracold quantum gases and lattice systems: quantum simulation of lattice gauge theories. *Annalen der Physik*, 525(10-11):777–796, 2013.

[98] Marcello Dalmonte and Simone Montangero. Lattice gauge theory simulations in the quantum information era. *Contemporary Physics*, 57(3):388–412, 2016.

[99] Alexander Mil, Torsten V. Zache, Apoorva Hegde, Andy Xia, Rohit P. Bhatt, Markus K. Oberthaler, Philipp Hauke, Jürgen Berges, and Fred Jendrzejewski. Realizing a scalable building block of a $U(1)$ gauge theory with cold atomic mixtures. 2019.

[100] Esteban A Martinez, Christine A Muschik, Philipp Schindler, Daniel Nigg, Alexander Erhard, Markus Heyl, Philipp Hauke, Marcello Dalmonte, Thomas Monz, Peter Zoller, et al. Real-time dynamics of lattice gauge theories with a few-qubit quantum computer. *Nature*, 534(7608):516, 2016.

[101] Christian Schweizer, Fabian Grusdt, Moritz Berngruber, Luca Barbiero, Eugene Demler, Nathan Goldman, Immanuel Bloch, and Monika Aidelsburger. Floquet approach to $\mathbb{Z}_2$ lattice gauge theories with ultracold atoms in optical lattices. *Nature Physics*, 15(11):1168–1173, sep 2019.

[102] Luca Barbiero, Christian Schweizer, Monika Aidelsburger, Eugene Demler, Nathan Goldman, and Fabian Grusdt. Coupling ultracold matter to dynamical gauge fields in optical lattices: From flux attachment to $\mathbb{Z}2$ lattice gauge theories. *Science advances*, 5(10):eaav7444, 2019.

[103] Frederik Görg, Kilian Sandholzer, Joaquín Minguzzi, Rémi Desbuquois, Michael Messer, and Tilman Esslinger. Realization of density-dependent peierls phases to engineer quantized gauge fields coupled to ultracold matter. *Nature Physics*, 15(11):1161–1167, 2019.

[104] Jad C. Halimeh, Lukas Homeier, Christian Schweizer, Monika Aidelsburger, Philipp Hauke, and Fabian Grusdt. Stabilizing lattice gauge theories through simplified local pseudogenerators. *Phys. Rev. Research*, 4:033120, Aug 2022.

[105] Lukas Homeier, Christian Schweizer, Monika Aidelsburger, Arkady Fedorov, and Fabian Grusdt. $\mathbb{Z}_2$ lattice gauge theories and Kitaev's toric code: A scheme for analog quantum simulation. *Phys. Rev. B*, 104:085138, Aug 2021.

[106] Mari Carmen Bañuls and Krzysztof Cichy. Review on novel methods for lattice gauge theories. *Reports on Progress in Physics*, 83(2):024401, 2020.

[107] N. Klco, E. F. Dumitrescu, A. J. McCaskey, T. D. Morris, R. C. Pooser, M. Sanz, E. Solano, P. Lougovski, and M. J. Savage. Quantum-classical computation of Schwinger model dynamics using quantum computers. *Phys. Rev. A*, 98:032331, Sep 2018.

[108] Erez Zohar, Alessandro Farace, Benni Reznik, and J. Ignacio Cirac. Digital quantum simulation of $\mathbb{Z}_2$ lattice gauge theories with dynamical fermionic matter. *Phys. Rev. Lett.*, 118:070501, Feb 2017.

[109] Luca Lumia, Pietro Torta, Glen B. Mbeng, Giuseppe E. Santoro, Elisa Ercolessi, Michele Burrello, and Matteo M. Wauters. Two-dimensional $\mathbb{Z}_2$ lattice gauge theory on a near-term quantum simulator: Variational quantum optimization, confinement, and topological order. *PRX Quantum*, 3:020320, Apr 2022.

[110] Reinis Irmejs, Mari Carmen Banuls, and Juan Ignacio Cirac. Quantum simulation of $\mathbb{Z}_2$ lattice gauge theory with minimal requirements. *arXiv:2206.08909*.

[111] Arata Yamamoto. Real-time simulation of (2+1)-dimensional lattice gauge theory on qubits. *Progress of Theoretical and Experimental Physics*, 2021(1), dec 2020.

[112] Xiaopeng Cui, Yu Shi, and Ji-Chong Yang. Circuit-based digital adiabatic quantum simulation and pseudoquantum simulation as new approaches to lattice gauge theory. *Journal of High Energy Physics*, 2020(8):1–35, 2020.

[113] Umberto Borla, Ruben Verresen, Jeet Shah, and Sergej Moroz. Gauging the kitaev chain. *SciPost Physics*, 10(6):148, 2021.

[114] Umberto Borla, Bhilahari Jeevanesan, Frank Pollmann, and Sergej Moroz. Quantum phases of two-dimensional $\mathbb{Z}_2$ gauge theory coupled to single-component fermion matter. *Physical Review B*, 105(7), feb 2022.

[115] Matjaž Kebrič, Umberto Borla, Ulrich Schollwöck, Sergej Moroz, Luca Barbiero, and Fabian Grusdt. Confinement induced frustration in a one-dimensional $\mathbb{Z}_2$ lattice gauge theory. *arXiv:2206.13487*.

[116] Aritra Das, Umberto Borla, and Sergej Moroz. Fractionalized holes in one-dimensional $\mathbb{Z}_2$ gauge theory coupled to fermion matter – deconfined dynamics and emergent integrability. *arXiv:2111.13205*, 2021.

[117] S Chandrasekharan and U.-J. Wiese. Quantum link models: A discrete approach to gauge theories. *Nuclear Physics B*, 492(1):455–471, 1997.

[118] Federica M. Surace, Paolo P. Mazza, Giuliano Giudici, Alessio Lerose, Andrea Gambassi, and Marcello Dalmonte. Lattice gauge theories and string dynamics in Rydberg atom quantum simulators. *Phys. Rev. X*, 10:021041, May 2020.

[119] D Banerjee, F-J Jiang, P Widmer, and U.-J. Wiese. The (2+1)d $U(1)$ quantum link model masquerading as deconfined criticality. *Journal of Statistical Mechanics: Theory and Experiment*, 2013(12):P12010, dec 2013.

[120] D. Banerjee, M. Dalmonte, M. Müller, E. Rico, P. Stebler, U.-J. Wiese, and P. Zoller. Atomic quantum simulation of dynamical gauge fields coupled to fermionic matter: From string breaking to evolution after a quench. *Physical Review Letters*, 109(17), oct 2012.

[121] S. Elitzur. Impossibility of spontaneously breaking local symmetries. *Phys. Rev. D*, 12:3978–3982, Dec 1975.

[122] N. W. Ashcroft and N. D. Mermin. *Solid State Physics*. Holt-Saunders, 1976.

[123] Sin-Itiro Tomonaga. Remarks on Bloch's Method of Sound Waves applied to Many-Fermion Problems. *Progress of Theoretical Physics*, 5(4):544–569, 07 1950.

[124] J. M. Luttinger. An exactly soluble model of a many-fermion system. *Journal of Mathematical Physics*, 4(9):1154–1162, 1963.

[125] J. R. Schrieffer and P. A. Wolff. Relation between the anderson and kondo Hamiltonians. *Phys. Rev.*, 149:491–492, Sep 1966.

[126] F.C. Alcaraz and R.Z. Bariev. An exactly solvable constrained XXZ chain. *arXiv:9904042*, 1999.

[127] Xun Jia, Arvind R Subramaniam, Ilya A Gruzberg, and Sudip Chakravarty. Entanglement entropy and multifractality at localization transitions. *Physical Review B*, 77(1):014208, 2008.

[128] E. Brezin and J. Zinn-Justin, editors. *Field Theory Methods and Quantum Critical Phenomena*, Les Houches 1988, Proceedings, Fields, strings and critical phenomena. North-Holland, North-Holland, 1988.

[129] Matjaž Kebrič, Luca Barbiero, Christian Reinmoser, Ulrich Schollwöck, and Fabian Grusdt. Confinement and mott transitions of dynamical charges in one-dimensional lattice gauge theories. *Phys. Rev. Lett.*, 127:167203, Oct 2021.

[130] Frank Pollmann, Ari M. Turner, Erez Berg, and Masaki Oshikawa. Entanglement spectrum of a topological phase in one dimension. *Phys. Rev. B*, 81:064439, Feb 2010.

[131] Lukasz Fidkowski and Alexei Kitaev. Topological phases of fermions in one dimension. *Phys. Rev. B*, 83:075103, Feb 2011.

[132] Xie Chen, Zheng-Cheng Gu, and Xiao-Gang Wen. Classification of gapped symmetric phases in one-dimensional spin systems. *Phys. Rev. B*, 83:035107, Jan 2011.

[133] Ari M. Turner, Frank Pollmann, and Erez Berg. Topological phases of one-dimensional fermions: An entanglement point of view. *Phys. Rev. B*, 83:075102, Feb 2011.

[134] Norbert Schuch, David Pérez-García, and Ignacio Cirac. Classifying quantum phases using matrix product states and projected entangled pair states. *Phys. Rev. B*, 84:165139, Oct 2011.

[135] B. van Heck, E. Cobanera, J. Ulrich, and F. Hassler. Thermal conductance as a probe of the nonlocal order parameter for a topological superconductor with gauge fluctuations. *Phys. Rev. B*, 89:165416, Apr 2014.

[136] A. Yu Kitaev. Unpaired majorana fermions in quantum wires. *Physics-Uspekhi*, 44(10S):131, 2001.

[137] Jason Alicea. New directions in the pursuit of Majorana fermions in solid state systems. *Rep. Prog. Phys.*, 75(7):076501, July 2012.

[138] T. D. Schultz, D. C. Mattis, and E. H. Lieb. Two-dimensional Ising model as a soluble problem of many fermions. *Rev. Mod. Phys.*, 36:856–871, Jul 1964.

[139] T Senthil, A Vishwanath, L Balents, S Sachdev, and MPA Fisher. Deconfined Quantum Critical points. *Science*, 303(March):457–461, 2004.

[140] Paul Fendley. Strong zero modes and eigenstate phase transitions in the XYZ/interacting majorana chain. *Journal of Physics A: Mathematical and Theoretical*, 49(30):30LT01, jun 2016.

[141] Ruben Verresen, Roderich Moessner, and Frank Pollmann. One-dimensional symmetry protected topological phases and their transitions. *Phys. Rev. B*, 96:165124, Oct 2017.

[142] Verresen et al. Higgs condensates are symmetry-protected topological phases. To appear, 2022.

[143] Thomas Scaffidi, Daniel E. Parker, and Romain Vasseur. Gapless symmetry-protected topological order. *Phys. Rev. X*, 7:041048, Nov 2017.

[144] Ruben Verresen, Ryan Thorngren, Nick G. Jones, and Frank Pollmann. Gapless topological phases and symmetry-enriched quantum criticality. *Physical Review X*, 11(4), dec 2021.

[145] Daniel González-Cuadra, Alexandre Dauphin, Przemysław R. Grzybowski, Paweł Wójcik, Maciej Lewenstein, and Alejandro Bermudez. Symmetry-breaking topological insulators in the $\mathbb{Z}_2$ Bose-Hubbard model. *Phys. Rev. B*, 99:045139, Jan 2019.

[146] Jad C. Halimeh and Philipp Hauke. Reliability of lattice gauge theories. *Phys. Rev. Lett.*, 125:030503, Jul 2020.

[147] Jad C Halimeh and Philipp Hauke. Staircase prethermalization and constrained dynamics in lattice gauge theories. *arXiv:2004.07248*, 2020.

[148] Jad C Halimeh, Valentin Kasper, and Philipp Hauke. Fate of lattice gauge theories under decoherence. *arXiv:2009.07848*, 2020.

[149] Zi-Yong Ge, Rui-Zhen Huang, Zi Yang Meng, and Heng Fan. Approximating lattice gauge theories on superconducting circuits: Quantum phase transition and quench dynamics. *arXiv:2009.13350*, 2020.

[150] Yohei Fuji, Frank Pollmann, and Masaki Oshikawa. Distinct trivial phases protected by a point-group symmetry in quantum spin chains. *Phys. Rev. Lett.*, 114:177204, May 2015.

[151] Minoru Takahashi. *Thermodynamics of one-dimensional solvable models*. Cambridge university press, 2005.

[152] Benjamin Doyon. Lecture notes on generalised hydrodynamics. *SciPost Physics Lecture Notes*, aug 2020.

[153] Fabio Franchini. *An Introduction to Integrable Techniques for One-Dimensional Quantum Systems*. Springer International Publishing, 2017.

[154] Paul Fendley, Kareljan Schoutens, and Jan de Boer. Lattice models with $\mathcal{N} = 2$ supersymmetry. *Phys. Rev. Lett.*, 90:120402, Mar 2003.

[155] Paul Fendley, Bernard Nienhuis, and Kareljan Schoutens. Lattice fermion models with supersymmetry. *Journal of Physics A: Mathematical and General*, 36(50):12399–12424, dec 2003.

[156] Jiří Minář, Bart van Voorden, and Kareljan Schoutens. Kink dynamics and quantum simulation of supersymmetric lattice Hamiltonians. *Phys. Rev. Lett.*, 128:050504, Feb 2022.

[157] I. N. Karnaukhov and A. A. Ovchinnikov. One-dimensional strongly interacting Luttinger liquid of lattice spinless fermions. *Europhysics Letters (EPL)*, 57(4):540–545, feb 2002.

[158] Francisco C Alcaraz and Matheus J Lazo. Exactly solvable interacting vertex models. *Journal of Statistical Mechanics: Theory and Experiment*, 2007(08):P08008–P08008, aug 2007.

[159] Alvise Bastianello, Bruno Bertini, Benjamin Doyon, and Romain Vasseur. Introduction to the special issue on emergent hydrodynamics in integrable many-body systems. *Journal of Statistical Mechanics: Theory and Experiment*, 2022(1):014001, jan 2022.

[160] Enej Ilievski, Marko Medenjak, Tomaž Prosen, and Lenart Zadnik. Quasilocal charges in integrable lattice systems. *Journal of Statistical Mechanics: Theory and Experiment*, 2016(6):064008, jun 2016.

[161] Marcos Rigol, Vanja Dunjko, Vladimir Yurovsky, and Maxim Olshanii. Relaxation in a completely integrable many-body quantum system: An ab initio study of the dynamics of the highly excited states of 1d lattice hard-core bosons. *Phys. Rev. Lett.*, 98:050405, Feb 2007.

[162] Jacopo De Nardis, Benjamin Doyon, Marko Medenjak, and Miłosz Panfil. Correlation functions and transport coefficients in generalised hydrodynamics. *Journal of Statistical Mechanics: Theory and Experiment*, 2022(1):014002, jan 2022.

[163] Alexander B. Zamolodchikov. Expectation value of composite field $t\bar{T}$ in two-dimensional quantum field theory, 2004.

[164] Yunfeng Jiang. $t\bar{T}$-deformed 1d bose gas, 2020.

[165] John Cardy and Benjamin Doyon. $t\bar{t}$ deformations and the width of fundamental particles, 2021.

[166] Benjamin Doyon, Joseph Durnin, and Takato Yoshimura. The space of integrable systems from generalised $t\bar{T}$-deformations, 2021.

[167] Marko Medenjak, Giuseppe Policastro, and Takato Yoshimura. Thermal transport in $t\overline{T}$-deformed conformal field theories: From integrability to holography. *Phys. Rev. D*, 103:066012, Mar 2021.

[168] Enrico Marchetto, Alessandro Sfondrini, and Zhou Yang. $t\overline{T}$ deformations and integrable spin chains. *Phys. Rev. Lett.*, 124:100601, Mar 2020.

[169] Balázs Pozsgay, Yunfeng Jiang, and Gábor Takács. $t\bar{T}$-deformation and long range spin chains. *Journal of High Energy Physics*, 2020(3):92, Mar 2020.

[170] Jean-Sébastien Caux and Fabian H. L. Essler. Time evolution of local observables after quenching to an integrable model. *Phys. Rev. Lett.*, 110:257203, Jun 2013.

[171] Jean-Sébastien Caux. The quench action. *Journal of Statistical Mechanics: Theory and Experiment*, 2016(6):064006, jun 2016.

[172] Olalla A. Castro-Alvaredo, Benjamin Doyon, and Takato Yoshimura. Emergent hydrodynamics in integrable quantum systems out of equilibrium. *Phys. Rev. X*, 6:041065, Dec 2016.

[173] Bruno Bertini, Mario Collura, Jacopo De Nardis, and Maurizio Fagotti. Transport in out-of-equilibrium XXZ chains: Exact profiles of charges and currents. *Phys. Rev. Lett.*, 117:207201, Nov 2016.

[174] Márton Borsi, Balázs Pozsgay, and Levente Pristyák. Current operators in Bethe Ansatz and generalized hydrodynamics: An exact quantum-classical correspondence. *Phys. Rev. X*, 10:011054, Mar 2020.

[175] Balázs Pozsgay. Algebraic construction of current operators in integrable spin chains. *Phys. Rev. Lett.*, 125:070602, Aug 2020.

[176] Márton Borsi, Balázs Pozsgay, and Levente Pristyák. Current operators in integrable models: a review. *Journal of Statistical Mechanics: Theory and Experiment*, 2021(9):094001, sep 2021.

[177] Lorenzo Piroli, Jacopo De Nardis, Mario Collura, Bruno Bertini, and Maurizio Fagotti. Transport in out-of-equilibrium XXZ chains: Nonballistic behavior and correlation functions. *Phys. Rev. B*, 96:115124, Sep 2017.

[178] R. Z. Bariev. Integrable model of interacting XY chains. *Journal of Physics A*, 24, 1991.

[179] Lenart Zadnik and Maurizio Fagotti. The Folded Spin-1/2 XXZ Model: I. Diagonalisation, Jamming, and Ground State Properties. *SciPost Phys. Core*, 4:10, 2021.

[180] Lenart Zadnik, Kemal Bidzhiev, and Maurizio Fagotti. The Folded Spin-1/2 XXZ Model: II. Thermodynamics and Hydrodynamics with a Minimal Set of Charges. *SciPost Phys.*, 10:99, 2021.

[181] Balázs Pozsgay, Tamás Gombor, Arthur Hutsalyuk, Yunfeng Jiang, Levente Pristyák, and Eric Vernier. Integrable spin chain with Hilbert space fragmentation and solvable real-time dynamics. *Phys. Rev. E*, 104:044106, Oct 2021.

[182] John McGreevy. Where do quantum field theories come from?, 2021.

[183] Ulrich Schollwöck. The density-matrix renormalization group in the age of matrix product states. *Annals of Physics*, 326(1):96–192, 2011. January 2011 Special Issue.

[184] Johannes Hauschild and Frank Pollmann. Efficient numerical simulations with tensor networks: Tensor Network Python (TeNPy). *SciPost Physics Lecture Notes*, 2018.

[185] Denis Bernard and Benjamin Doyon. Conformal field theory out of equilibrium: a review. *Journal of Statistical Mechanics: Theory and Experiment*, 2016(6):064005, jun 2016.

[186] Sergey Bravyi, David P. DiVincenzo, and Daniel Loss. Schrieffer–Wolff transformation for quantum many-body systems. *Annals of Physics*, 326(10):2793–2826, 2011.

[187] Zhi-Cheng Yang, Fangli Liu, Alexey V. Gorshkov, and Thomas Iadecola. Hilbert-space fragmentation from strict confinement. *Phys. Rev. Lett.*, 124:207602, May 2020.

[188] Cheng-Ju Lin and Olexei I. Motrunich. Quasiparticle explanation of the weak-thermalization regime under quench in a nonintegrable quantum spin chain. *Phys. Rev. A*, 95:023621, Feb 2017.

[189] P. I. Karpov, G.-Y. Zhu, M. P. Heller, and M. Heyl. Spatiotemporal dynamics of particle collisions in quantum spin chains. *Phys. Rev. Research*, 4:L032001, Jul 2022.

[190] Vadim Oganesyan and David A. Huse. Localization of interacting fermions at high temperature. *Phys. Rev. B*, 75:155111, Apr 2007.

[191] Y. Y. Atas, E. Bogomolny, O. Giraud, and G. Roux. Distribution of the ratio of consecutive level spacings in random matrix ensembles. *Phys. Rev. Lett.*, 110:084101, Feb 2013.

[192] J. M. Leinaas and J. Myrheim. On the theory of identical particles. *Il Nuovo Cimento B (1971-1996)*, 37(1):1–23, Jan 1977.

[193] Frank Wilczek. From electronics to anyonics. *Physics World*, 19(1):22–23, jan 2006.

[194] Frank Wilczek. Quantum mechanics of fractional-spin particles. *Phys. Rev. Lett.*, 49:957–959, Oct 1982.

[195] Alexei Kitaev and Chris Laumann. Topological phases and quantum computation. *arXiv:0904.2771*, 2009.

[196] Maria Hermanns. Entanglement in topological systems. *arXiv cond-mat/1702.01525*, 2017.

[197] Sandro Wenzel, Tommaso Coletta, Sergey E. Korshunov, and Frédéric Mila. Evidence for columnar order in the fully frustrated transverse field ising model on the square lattice. *Phys. Rev. Lett.*, 109:187202, Nov 2012.

[198] Subir Sachdev. Topological order, emergent gauge fields, and Fermi surface reconstruction. *Reports on Progress in Physics*, 82(1):014001, Nov 2018.

[199] Subir Sachdev. $\mathbb{Z}_2$ spin liquids, 2021.

[200] Ruben Verresen, Mikhail D. Lukin, and Ashvin Vishwanath. Prediction of toric code topological order from Rydberg blockade. *Phys. Rev. X*, 11:031005, Jul 2021.

[201] John McGreevy. Generalized symmetries in condensed matter, 2022.

[202] Xiao-Gang Wen. Emergent anomalous higher symmetries from topological order and from dynamical electromagnetic field in condensed matter systems. *Phys. Rev. B*, 99:205139, May 2019.

[203] Elliott H. Lieb. Flux phase of the half-filled band. *Phys. Rev. Lett.*, 73:2158–2161, Oct 1994.

[204] Shriya Pai and Michael Pretko. Fractons from confinement in one dimension. *Phys. Rev. Research*, 2:013094, Jan 2020.

[205] Daniel S. Rokhsar and Steven A. Kivelson. Superconductivity and the quantum hard-core dimer gas. *Phys. Rev. Lett.*, 61:2376–2379, Nov 1988.

[206] Pablo Sala, Tibor Rakovszky, Ruben Verresen, Michael Knap, and Frank Pollmann. Ergodicity breaking arising from hilbert space fragmentation in dipole-conserving Hamiltonians. *Phys. Rev. X*, 10:011047, Feb 2020.

[207] Vedika Khemani, Michael Hermele, and Rahul Nandkishore. Localization from hilbert space shattering: From theory to physical realizations. *Phys. Rev. B*, 101:174204, May 2020.

[208] Tibor Rakovszky, Pablo Sala, Ruben Verresen, Michael Knap, and Frank Pollmann. Statistical localization: From strong fragmentation to strong edge modes. *Phys. Rev. B*, 101:125126, Mar 2020.

[209] Rahul M. Nandkishore and Michael Hermele. Fractons. *Annual Review of Condensed Matter Physics*, 10(1):295–313, 2019.

[210] Michael Pretko, Xie Chen, and Yizhi You. Fracton phases of matter. *International Journal of Modern Physics A*, 35(06):2030003, 2020.

[211] Erez Zohar and J. Ignacio Cirac. Eliminating fermionic matter fields in lattice gauge theories. *Phys. Rev. B*, 98:075119, Aug 2018.

[212] Erez Zohar and J. Ignacio Cirac. Removing staggered fermionic matter in $U(N)$ and $SU(N)$ lattice gauge theories. *Phys. Rev. D*, 99:114511, Jun 2019.

[213] J Wosiek. A local representation for fermions on a lattice. *Acta Physica Polonica. Series B*, 13(7):543–552, 1982.

[214] Yu-An Chen, Anton Kapustin, and Djordje Radicevic. Exact bosonization in two spatial dimensions and a new class of lattice gauge theories. *Annals of Physics*, 393:234–253, 2018.

[215] A. Bochniak and B. Ruba. Bosonization based on Clifford algebras and its gauge theoretic interpretation. *Journal of High Energy Physics*, 2020(12), dec 2020.

[216] Nathanan Tantivasadakarn. Jordan-Wigner dualities for translation-invariant Hamiltonians in any dimension: Emergent fermions in fracton topological order. *Phys. Rev. Research*, 2:023353, Jun 2020.

[217] Peng Rao and Inti Sodemann. Theory of weak symmetry breaking of translations in $\mathbb{Z}_2$ topologically ordered states and its relation to topological superconductivity from an exact lattice $\mathbb{Z}_2$ charge-flux attachment. *Phys. Rev. Research*, 3:023120, May 2021.

[218] Masuo Suzuki. Relationship among Exactly Soluble Models of Critical Phenomena. I*): 2D Ising Model, Dimer Problem and the Generalized XY-Model. *Progress of Theoretical Physics*, 46(5):1337–1359, 11 1971.

[219] Robert Raussendorf and Hans J. Briegel. A one-way quantum computer. *Phys. Rev. Lett.*, 86:5188–5191, May 2001.

[220] W. Son, L. Amico, R. Fazio, A. Hamma, S. Pascazio, and V. Vedral. Quantum phase transition between cluster and antiferromagnetic states. *EPL (Europhysics Letters)*, 95(5):50001, aug 2011.

[221] Ryan Thorngren. Anomalies and bosonization. *Communications in Mathematical Physics*, 378(3):1775–1816, Sep 2020.

[222] M. D. Lukin, M. Fleischhauer, R. Cote, L. M. Duan, D. Jaksch, J. I. Cirac, and P. Zoller. Dipole blockade and quantum information processing in mesoscopic atomic ensembles. *Phys. Rev. Lett.*, 87:037901, Jun 2001.

[223] E. Urban, T. A. Johnson, T. Henage, L. Isenhower, D. D. Yavuz, T. G. Walker, and M. Saffman. Observation of Rydberg blockade between two atoms. *Nature Physics*, 5:110–114, February 2009.

[224] Alpha Gaëtan, Yevhen Miroshnychenko, Tatjana Wilk, Amodsen Chotia, Matthieu Viteau, Daniel Comparat, Pierre Pillet, Antoine Browaeys, and Philippe Grangier. Observation of collective excitation of two individual atoms in the Rydberg blockade regime. *Nature Physics*, 5:115–118, February 2009.

[225] Igor Lesanovsky and Hosho Katsura. Interacting fibonacci anyons in a Rydberg gas. *Phys. Rev. A*, 86:041601, Oct 2012.

[226] Christopher J. Turner, Alexios A. Michailidis, Dmitry A. Abanin, Maksym Serbyn, and Z. Papić. Weak ergodicity breaking from quantum many-body scars. *Nature Physics*, 14(7):745, 2018.

[227] Paul Fendley, K. Sengupta, and Subir Sachdev. Competing density-wave orders in a one-dimensional hard-boson model. *Phys. Rev. B*, 69:075106, Feb 2004.

[228] Natalia Chepiga and Frédéric Mila. Floating phase versus chiral transition in a 1d hard-boson model. *Phys. Rev. Lett.*, 122:017205, Jan 2019.

[229] Emilio Cobanera, Gerardo Ortiz, and Zohar Nussinov. Holographic symmetries and generalized order parameters for topological matter. *Phys. Rev. B*, 87:041105, Jan 2013.

[230] Djordje Radicevic. Spin structures and exact dualities in low dimensions. 2018.

[231] Steven R. White. Density-matrix algorithms for quantum renormalization groups. *Phys. Rev. B*, 48:10345–10356, Oct 1993.

[232] Román Orús. A practical introduction to tensor networks: Matrix product states and projected entangled pair states. *Annals of Physics*, 349:117–158, 2014.

[233] Anders W. Sandvik, Adolfo Avella, and Ferdinando Mancini. Computational studies of quantum spin systems. In *AIP Conference Proceedings*. AIP, 2010.

[234] Steven R. White. Density matrix formulation for quantum renormalization groups. *Phys. Rev. Lett.*, 69:2863–2866, Nov 1992.

[235] I. P. McCulloch. Infinite size density matrix renormalization group, revisited. 2008.

[236] M. Fannes, B. Nachtergaele, and R. F. Werner. Finitely correlated states on quantum spin chains. *Communications in Mathematical Physics*, 144(3):443–490, Mar 1992.

[237] M B Hastings. An area law for one-dimensional quantum systems. *Journal of Statistical Mechanics: Theory and Experiment*, 2007(08):P08024–P08024, aug 2007.

[238] Norbert Schuch, Michael M. Wolf, Frank Verstraete, and J. Ignacio Cirac. Entropy scaling and simulability by matrix product states. *Phys. Rev. Lett.*, 100:030504, Jan 2008.

[239] Daniel Gottesman and M B Hastings. Entanglement versus gap for one-dimensional spin systems. *New Journal of Physics*, 12(2):025002, feb 2010.

[240] Don N. Page. Average entropy of a subsystem. *Phys. Rev. Lett.*, 71:1291–1294, Aug 1993.

[241] Shoudan Liang and Hanbin Pang. Approximate diagonalization using the density matrix renormalization-group method: A two-dimensional-systems perspective. *Phys. Rev. B*, 49:9214–9217, Apr 1994.

[242] Pasquale Calabrese and John Cardy. Entanglement entropy and quantum field theory. *Journal of Statistical Mechanics: Theory and Experiment*, 2004(06):P06002, jun 2004.

[243] Guifré Vidal. Efficient simulation of one-dimensional quantum many-body systems. *Phys. Rev. Lett.*, 93:040502, Jul 2004.

[244] Phillip Weinberg and Marin Bukov. QuSpin: a Python Package for Dynamics and Exact Diagonalisation of Quantum Many Body Systems part I: spin chains. *SciPost Phys.*, 2:003, 2017.

[245] Phillip Weinberg and Marin Bukov. QuSpin: a Python Package for Dynamics and Exact Diagonalisation of Quantum Many Body Systems. Part II: bosons, fermions and higher spins. *SciPost Phys.*, 7:20, 2019.

Acknowledgements

Throughout my PhD I could count on the constant support of my advisor Sergej Moroz. His physical insight, relaxed attitude and enthusiasm have been of invaluable help during these years. Similarly, it was a pleasure to spend time at the faculty and share ideas with the numerous bright scientists in the groups of Frank Pollmann, Michael Knap, Johannes Knolle and Wilhelm Zwerger. Particular gratitude goes to my friends and office mates Claudio and Billa, who shared most of these five years with me. Among my collaborators, I want to thank in particular Alvise Bastianello, Fabian Grusdt and Ruben Verressen, for sharing their impressive knowledge with me. In the recent times I started fruitful projects with inspiring people like Snir Gazit, Erez Zohar and Luca Tagliacozzo, and I am sure that the future will bring even more exciting results. These years in Munich would not have been the same without my friends. I am therefore very grateful to my climbing buddies, to fellow physicists at MPQ, to the Italian crowd that always makes me feel at home, and to the bizarre people that do not belong to any of these groups. Despite the distance, I also cannot forget my long-time friends from Turin, the ones from Sweden and all those who are scattered around the world. To conclude I want to thank my parents, who valued my education above everything else, and Esther for making this eventful last year unforgettable.